The cellular functions of mammalian type II phosphatidylinositol 4-kinases

Ganiyu Olabanji Alli-Balogun

Division of Medicine

University College London

A thesis submitted in partial fulfilment of the requirements for the degree of Doctor of Philosophy

September 2017

Declaration

I confirm that the data presented in this thesis is my own. I confirm where information derived from other sources has been included, the source is acknowledged in the text.

_____

Ganiyu Olabanji Alli-Balogun

Dedication

This thesis is dedicated to the beautiful people of Nigeria, the world’s most populous black nation.

Acknowledgements

I would like to express my profound gratitude to everyone who contributed to the successful execution of this PhD project. I am grateful to the Federal Government of Nigeria for the award of the PRESSID scholarship.

I would like to thank my supervisor, Dr Shane Minogue, for giving me the great opportunity of working with him and for all the advice and support he has given me over the years. I would like to thank the members of the Lipid and Membrane Biology group for their help and support. Especially Dr Mark Waugh, for sharing his reagents and technical knowledge. My sincere appreciations go to Ruth Jacobs for providing recombinant lipid binding proteins and ensuring I don't run out of reagents.

I am grateful to our collaborators, Dr Janos Kriston-Vizi at the MRC laboratory for molecular cell biology (LMCB) and Dr Christina Gewinner at UCL translational research office (now at Astex Pharmaceuticals, Cambridge UK). I would also like to thank those who shared reagents with us: Prof Volker Haucke, Leibniz institute for molecular pharmacology, Berlin; Dr Mihaela Anitei, Technische Universität, Dresden; and Dr Gerald Hammond, University of Pittsburgh.

Special thanks to my mum for supporting my education to the highest level and for her continuous support over the years. My sincere appreciation to my siblings, Adebola and Omobolanle for their unending love, financial and moral support. Also to my late grandmother (who passed away two weeks before my viva) for being a wonderful guardian and teaching me things that can never be learnt in a classroom. I would like to thank the PRESSID team in the United Kingdom for encouraging and supporting me during my PhD. I would like to thank my best friend, the queen of my heart, Aisha for the unending love and support she has given me.

Gbogbo ogo ati ọpẹ fun Ọlọrun Olódùmarè.

Abstract

Type II phosphatidylinositol 4-kinases (PI4KIIs), PI4KIIα and PI4KIIβ, both catalyse phosphatidylinositol 4-phosphate (PI(4)P) synthesis and are implicated in the control of trafficking from the *trans*-Golgi network (TGN) and endosomal membranes. It has been suggested that these closely related isoforms perform redundant roles. This study addresses the issue of functional overlap, by studying the location of the PI(4)P pools synthesised by each isoform, the associated membrane trafficking routes and the functional consequences of loss of these PI4P pools.

The TGN localisations of PI4KIIα and PI4KIIβ could be distinguished by co-immunostaining with TGN markers syntaxin 6 and TGN46, indicating that the isoforms localise to separate TGN domains. In addition, depletion of PI4KII isoforms using small interfering RNA (siRNA) had differential effects on TGN pools of PI(4)P, with PI4KIIα loss significantly affecting a syntaxin 6 positive PI(4)P pool while PI4KIIβ depletion altered a TGN46 positive pool; thus indicating the synthesis of metabolically separate PI(4)P pools by these two isoforms. Depletion of either PI4KII isoform also impaired post-TGN traffic of cation independent mannose 6-phosphate receptor (CI-M6PR) and the endo-lysosomal traffic and degradation of the EGF receptor which is suggestive of overlapping roles for both isoforms in post-TGN traffic.

PI4KII gene silencing also had differential effects on the actin cytoskeleton. Loss of PI4KIIα led to increased stress fibre formation while PI4KIIβ depletion induced the formation of functional invadopodia containing membrane type I matrix metalloproteinase (MT1-MMP). This was accompanied by decreased colocalization of MT1-MMP with the endosomal markers Rab5 and Rab7 that control lysosomal trafficking and regulate surface levels of MT1-MMP. However, MT1-MMP showed increased colocalisation with Rab8, which mediates exocytic trafficking and pro-invasive activity of MT1-MMP. In addition, depletion of PI4KIIβ conferred a migratory phenotype on minimally invasive HeLa and MCF-7 cell lines. This cell phenotype was substantiated by oncogenomic database analyses

showing that loss of PI4KIIβ expression was a risk factor for numerous human carcinomas.

Table of Contents

List of Figures[1]

[1] High resolution images can be accessed on the CD-ROM attached with the hard copy.

List of Tables

Abbreviations

BSA	Bovine serum albumin
CDP	Cytidine diphosphate
CI-M6PR	Cation-independent mannose 6-phosphate receptor
DAG	Diacylglycerol
DMSO	Dimethyl sulphoxide
ECM	Extracellular matrix
EDTA	Ethylenediaminetetraacetic acid
EE	Early endosome
EEA1	Early endosome autoantigen 1
EGF	Epidermal growth factor
EGFP	Enhanced green fluorescent protein
EGFR	Epidermal growth factor receptor
EGTA	Ethylene-glycol-bis(β-aminoehtylether)-N,N,N’N’-tetraacetic acid
ERC	Endocytic recycling compartment
Erk	Extracellular-signal regulated kinases
FACS	Fluorescence activated cell sorting
FAPP	Four-phosphate adaptor proteins

FBS	Foetal bovine serum
FERM	Band 4.1/ezrin/radixin/moesin
FITC	Fluorescein isothiocyanate
FRAP	Fluorescent recovery after photobleaching
FYVE	Fab1p/YOTB/Vac1p/EEA1 homology
GAPDH	Glyceraldehyde 3-phosphate dehydrogenase
GBA	Glucoceribrosidase
GFP	Green fluorescent protein
GGA	Golgi-localised γ-ear containing ADP-ribosylation factor (Arf) binding proteins
GLUE	GRAM-like ubiquitin-binding in EAP45
GST	Glutathione S-transferase
HA	Haemagglutinin
HEPES	4-(2-hydroxyethyl)-1-piperazine ethanesulphonic acid
HMIT	Proton (H^+)-*myo*-inositol co-transporter
HSP	Heat shock protein
INPP	Inositol polyphosphate phosphatase
kDa	Kilodalton
LAMP-1	Lysosome associated membrane protein-1

LE	Late endosome
MAPK	Mitogen activated protein kinases
MMP	Matrix metalloproteinase
MOPS	3-(N-Morpholino)-propanesulphonic acid
MT1-MMP	Membrane type 1-matrix metalloproteinase
MTT	3-(4,5)-dimethylthiazo-2-yl)-2,5-diphenyl tetrazolium
MVB	Multi-vesicular body
NP-40	Nonylphenoxypolyethoxyethanol
NSF	N-ethyl maleimide (NEM) sensitive factor
NT	Non-targeting siRNA
OCRL	Oculocerebrorenal syndrome of Lowe
OSBP	Oxysterol binding protein
P4C	PI(4)P binding domain of SidC protein
PAGE	Polyacrylamide gel electrophoresis
PBS	Phosphate-buffered saline
PCR	Polymerase chain reaction
PDGF	Platelet derived growth factor
PH	Pleckstrin homology

PI	Phosphatidylinositol
PI(3)P	Phosphatidylinositol 3-phosphate
$PI(3,4)P_2$	Phosphatidylinositol 3,4-bisphosphate
$PI(3,4,5)P_3$	Phosphatidylinositol 3,4,5-trisphosphate
$PI(3,5)P_2$	Phosphatidylinositol 3,5-bisphosphate
PI(4)P	Phosphatidylinositol 4-phosphate
$PI(4,5)P_2$	Phosphatidylinositol 4,5-bisphosphate
$PI(5)P_2$	Phosphatidylinositol 5-phosphate
PI3K	Phosphatidylinositol 3-kinase
PI4KIIIα	Phosphatidylinositol 4-kinase IIIα
PI4KIIIβ	Phosphatidylinositol 4-kinase IIIβ
PI4KIIα	Phosphatidylinositol 4-kinase IIα
PI4KIIβ	Phosphatidylinositol 4-kinase IIβ
PIPES	Piperazine-N,N'-bis-(2-ethanesulphonic acid)
PKC	Protein kinase C
PLC	Phospholipase C
PMA	Phorbol 12-myristate 13-acetate
PTEN	Phosphatase and tensin homologue deleted on chromosome 10

PVDF	Polyvinylindenefluoride
PX	Phox homology
RIPA	Radio Immunoprecipitation assay
RNAi	RNA interference
SDS	Sodium dodecyl sulphate
SE	Sorting endosome
siRNA	Small interfering RNA
SMIT	Sodium-*myo*-inositol co-transporter
SNAP	Soluble NSF adaptor protein
SNARE	SNAP receptor
SNX	Sorting nexin
SOC	Super optimal broth with catabolite repression
TBS	Tris-buffered Saline
TBST	TBS+Tween 20
VAMP	Vesicle associated membrane protein
VSVG	Vesicular stomatitis virus G-protein

Chapter 1 Introduction

1.1 Phosphoinositides

Phosphoinositides (also called PI lipids) are phosphorylated derivatives of the glycerophospholipid phosphatidylinositol (PI), that are concentrated on membrane/cytosol interphases. They make up a small fraction of total cellular phospholipids but control nearly every aspect of cellular physiology. These lipids gained tremendous attention over four decades ago when they were identified as signalling molecules. PI lipids serve as pleiotropic regulators controlling organelle function via vesicular trafficking, membrane transport and control of entry (endocytosis) and exit (exocytosis) of cellular materials. Because of these many functions, perturbation of PI lipid metabolism often underlies disorders of clinical significance including several human cancers, diabetes and rare genetic disorders. In addition, membrane PI lipids are utilised by pathogens as a means of subverting the host's replicative machinery. There is an ever-growing list of functions attributable to this lipid class, and some of their modifying enzymes have been highlighted as targets of potent pharmacological agents. This lipid class maintain some form of uniqueness as the parent molecule, phosphatidylinositol (PI) serves as a rich target for phosphorylation at the cytoplasmic leaflet of biological membranes. The resulting phosphorylated derivatives can serve as docking sites for a myriad of proteins thereby altering their cellular localisation or conformation. This is the case for cytosolic proteins (e.g. signalling molecules) and peripheral membrane proteins that interact with PI lipids.

1.1.1 A brief history of PI lipids

An important link to the history of PI lipids can be traced to the discovery of inositol towards the end of the 19th century. Inositol was identified as a major component of the muscle and was described as a hexa-hydroxylcyclohexane (Reviewed by Balla, 2013). It was identified as a vital factor, particularly during the vitamin era where it described as a protective factor against hair loss and fatty liver in rodents (Holub, 1982). Inositol was first described as a

component of cellular membranes in *Mycobacterium* as part of the lipid phosphatidylinositolmannoside (Ballou and Lee, 1964).

The pioneering work by Jordi Folch in the 1940s constituted a major finding in phosphoinositide biology. He obtained an ethanol-insoluble phospholipid fraction from bovine brain containing an approximately equimolar mixture of phosphatidylinositol, phosphatidylinositol 4-phosphate (PI(4)P) and phosphatidylinositol 4,5-bisphosphate ($PI(4,5)P_2$). At that time, he postulated that the phosphate: inositol ratio was about 2:1 and assumed that this was one compound regarded as a diphosphoinositide (DPI; (Agranoff, 2009)). Early studies also revealed that acute radiolabelling of brain slices with ^{32}P increases radioactivity in phosphatidic acid (PA) and DPI (Dawson, 1954) . This was the first indication that phosphoinositides undergo constant turnover. Subsequent work by three different groups identified the structures derived upon metabolic labelling as mono-, di- and tri-phosphoinositides (MPI, DPI and TPI; (Hawthorne, 1955; Dittmer and Dawson, 1961; Tomlinson and Ballou, 1961)). The TPI from Dittmer and Dawson's study was ultimately proven to be $PI(4,5)P_2$ by Brown and Stewart in 1966 (Irvine, 2003).

Understanding the turnover of PI lipids was an important step in explaining the significance of ^{32}P incorporation into inositol. Initial work by Eugene Kennedy and colleagues had revealed that cytidine nucleotides were used to furnish head-groups to the DAG moiety during phosphatidylcholine and phosphatidylethanolamine synthesis. However, work by Bernard Agranoff revealed that this was not the case for phosphatidylinositol synthesis. During phosphatidylinositol synthesis, the lipid backbone itself is activated by a cytidine nucleotide as CDP-DAG. Paulus and Kennedy carried out the chemical synthesis of CDP-DAG and elucidated its biosynthetic steps in the microsomal fraction of chicken liver (Paulus and Kennedy, 1960). These findings were perfected by those of Agranoff and his graduate students at the University of Michigan using chicken embryo brain preparations while studies using the microsomal fraction of guinea pig brain indicated a preference for *myo*-inositol over other cyclitols in PI synthesis (Benjamins and Agranoff, 1969; Agranoff, 2009).

Lowell and Mabel Hokin demonstrated receptor-mediated turnover of PI lipids in 1953. They observed that cholinergic stimulation of enzyme secretion in pigeon pancreas slices induced incorporation of ^{32}P while radioactivity was lost in the RNA fraction following purification but was retained in what they referred to as "Junk". This "junk" was investigated and subsequently identified as an alkaline product of phospholipid hydrolysis. At that time, phospholipid analysis was an arduous task but the timely discovery by Dawson whose finding one year later permitted analysis of glycerophospholipids by deacylation and 2-dimensional separation of the hydrophilic glycerol backbone (Dawson, 1954). This permitted the Hokins to demonstrate that the inositol lipids and phosphatidic acid were responsible for increased ^{32}P radioactivity following cholinergic stimulation of pancreatic slices (Hokin, 1987). In addition, the Hokins also suggested that the primary response to agonist stimulation was an increased activity of a phosphoinositide specific phospholipase that catalysed hydrolysis of a PI lipid, producing DAG which was in turn converted to phosphatidic acid (PA) by the action of DAG kinase (DGK), which acquired ^{32}P and converted back to PI via a cytidine nucleotide step, thereby completing a cycle that was termed the "PI cycle" (Figure 1-1). Studies by the Hokins implicated PI lipids in agonist-mediated secretion but it was almost impossible at that time, to study their roles in other biochemical processes.

The biology of phosphoinositides has dramatically expanded in the last 20 years, particularly in the post-genomic era. Improvements in molecular biology techniques and gene sequencing methods have led to the discovery and characterisation of PI metabolising enzymes and identification of phosphorylated PIs.

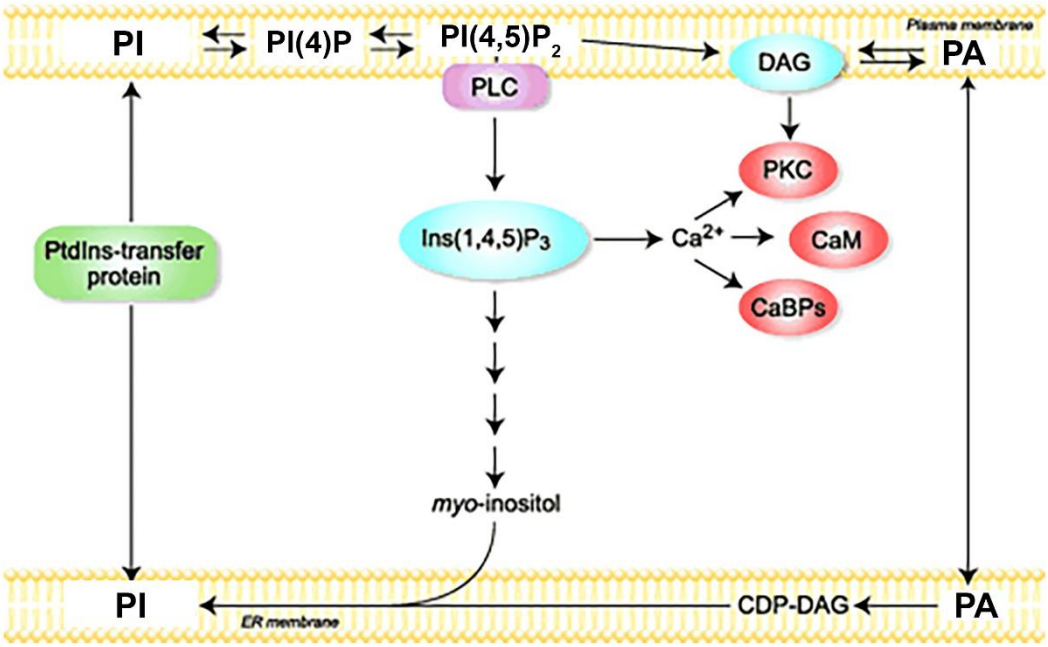

Figure 1-1. The PI cycle.

The PI cycle is triggered by agonist stimulated PLC activation resulting in the hydrolysis of $PI(4,5)P_2$ to DAG and $Ins(1,4,5)P_3$, second messenger molecules that stimulate calcium channels and PKC activity. DAG is converted to phosphatidic acid (PA) by a DAG kinase (DGK) while the other product, $Ins(1,4,5)P_3$ is sequentially dephosphorylated to yield *myo*-inositol. Both products are recycled on ER membranes where they are used for phosphatidylinositol (PI) synthesis. PI is transported to the plasma membrane via several mechanisms including transfer by phosphatidylinositol transport proteins (PITPs). At the PM, PI is sequentially phosphorylated to yield $PI(4,5)P_2$, making it available for PLC-mediated hydrolysis. Adapted from Balla, 2006.

1.2 Structure, metabolism and intracellular distribution

The parent molecule, phosphatidylinositol is synthesised on the membranes of endoplasmic reticula (Kim *et al.*, 2011) via condensation of CDP-diacylglycerol (CDP-DAG) with *myo*-inositol by a phosphatidylinositol synthase (Figure 1-2a). CDP-DAG is synthesised from CTP and phosphatidic acid in a reaction catalysed by CDP-DAG synthase (also known as CTP: phosphatidate cytidyl transferase). This enzyme localises to the outer surface of the ER (Ballas and Bell, 1981) but can also be found in the mitochondrial matrix where it furnishes CDP-DAG for cardiolipin (diphosphatidyl-glycerol) synthesis (Schlame and Haldar, 1993).

The other substrate for PI synthesis, *myo*-inositol moiety assumes a chair conformation in which five hydroxyls are in the equatorial conformation while one (position-2) assumes an axial conformation. This moiety was likened to a turtle by Bernard Agranoff (Agranoff, 2009) in which each hydroxyl except that on position 2- labelled in an anti-clockwise manner represents a flipper. The hydroxyl on position-2 represents the turtle's head and serves as the point of linkage to the phosphatidic acid backbone (Figure 1-2b). Mammalian cells meet their *myo*-inositol demands via three means: (1) de novo synthesis from glucose 6-phosphate (Seelan *et al.*, 2009) via D-inositol 3-phosphate (also called L-inositol 1-phosphate); (2) recycling *myo*-inositols generated from PLC mediated hydrolysis of phosphoinositides; (3) uptake from the cellular environment. Mammalian cells express three different proteins for inositol uptake: SMIT1 (Kwon *et al.*, 1991), SMIT2 (Coady *et al.*, 2002) and HMIT (Uldry *et al.*, 2001). SMIT1 and 2 are sodium/myo-inositol cotransporters that use a sodium gradient to transport myo-inositol into cells. Unlike SMIT1 which is highly expressed in renal medulla cells (Kwon *et al.*, 1991), SMIT2 has a wider tissue expression but has a lower affinity for myo-inositol (Balla, 2013). HMIT is a proton (H+)/myo-inositol cotransporter that has a lower affinity but a high capacity for myo-inositol and highly expressed in the brain (Uldry *et al.*, 2001).

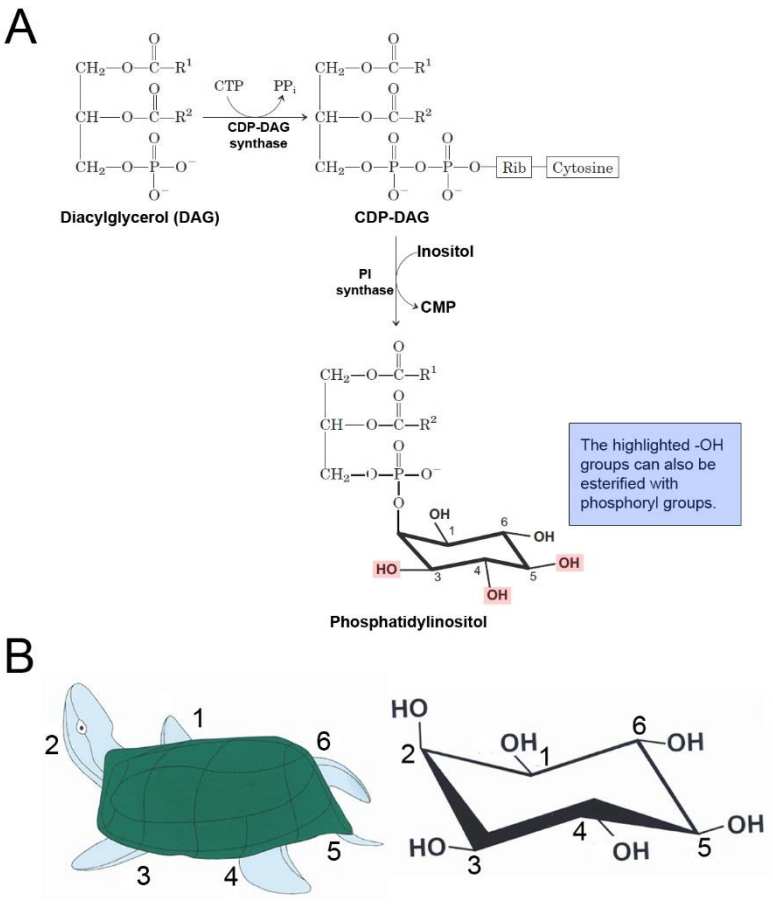

Figure 1-2. Synthesis of phosphatidylinositol in eukaryotes.

A. Phosphatidylinositol is generated from two substrates, CDP-DAG and inositol, in a reaction catalysed by a PI synthase. R^1 and R^2: Acyl chains of fatty acids esterified to the sn-1 and sn-2 positions of DAG. Rib: Ribose backbone of CDP (cytidine diphosphate), CTP: Cytidine triphosphate, CMP: Cytidine monophosphate. **B.** Agranoff's turtle depicting the orientation of hydroxyl groups in *myo*-inositiol.

Phosphatidylinositol is delivered to other cellular compartments via vesicular transport or by specific PI transport proteins (PITPs) (McDermott and Mousley, 2016). The hydroxyl groups can then be esterified with phosphoryl groups to form different phosphorylated derivatives via the activities of specific phosphatidylinositol kinases. The two fatty acyl chains of the DAG moiety anchor the PI molecule to membranes via hydrophobic interactions with other fatty acyl chains in the lipid bilayer while exposing the *myo*-inositol head group into polar region of the membrane bilayer. Here the exposed

phosphate groups of the *myo*-inositol head group serve as docking sites for membrane proteins including lipid transfer proteins and small GTPases (Godi *et al.*, 2004; Dickson *et al.*, 2016; Dong *et al.*, 2016). A striking feature of phosphoinositides is the enrichment in arachidonic acid at the sn-2 position of the parent molecule and majority of mammalian PI lipids exist in the 1-stearoyl-2-arachidonoyl form (Wenk *et al.*, 2003; Clark *et al.*, 2011; Hammond and Balla, 2014; Traynor-Kaplan *et al.*, 2017). Enzymes involved in PI turnover may display specificity for the forms of lipids esterified with arachidonic acid at the sn-2 position (Milne *et al.*, 2008; Lung *et al.*, 2009; Shulga *et al.*, 2011).

Reversible phosphorylation of the D-3, D-4 and D-5 hydroxyls of the *myo*-inositol moiety of PI results in the generation of seven distinct PI lipid species (Figure 1-3). Multiple isoforms of virtually all PI lipid modifying enzymes act upon the same substrate but generally do so in a compartmentalised manner, giving a partial explanation for non-redundancy despite that they catalyse the same biochemical reaction.

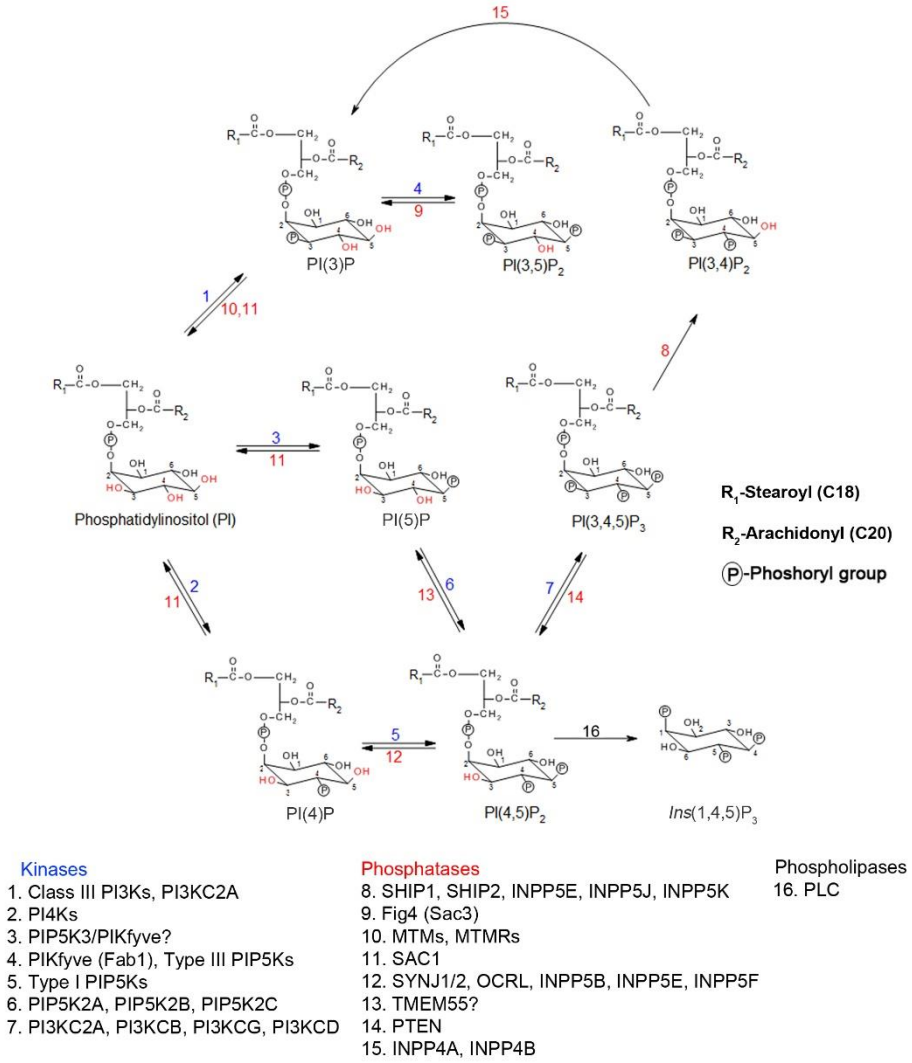

Figure 1-3. Pathways of phosphoinositide synthesis and degradation.

Phosphatidylinositol is phosphorylated and dephosphorylated by kinases and phosphatases, respectively. There are seven known PI lipids in eukaryotes which are: PI(4)P, PI(5)P, PI(3)P, PI(4,5)P_2, PI(3,5)P_2, PI(3,4)P_2 and PI(3,4,5)P_3. PI4Ks convert PI to PI(4)P which serves as a substrate for PIP 5-kinases (PIP5Ks) that convert it to PI(4,5)P_2. PI(4,5)P_2 can also be phosphorylated by PI 3-kinases to generate PI(3,4,5)P_3. PI(3)P can equally be modified to PI(3,5)P_2 by type PIKfyve, while all levels of all PI species are balanced through the actions of phosphatases which dephosphorylate specific phosphoryl groups. PI(4,5)P_2 can also be hydrolysed by PLC to generate inositol 1,4,5trisphosphate (Ins(1,4,5)P_3) and diacylglycerol(DAG).

PI lipids constitute a low percentage of the total number of phospholipids within the cell. Their concentrations have been estimated in different cells and tissues but these estimates show significant variations (Nasuhoglu *et al.*, 2002; Wenk *et al.*, 2003; Traynor-Kaplan *et al.*, 2017). Nonetheless, chromatographic analysis of resting mammalian cells showed that PI(4)P and PI(4,5)P_2 are the most abundant PI lipid species (Wenk *et al.*, 2003; Traynor-Kaplan *et al.*, 2017); however, lipid compositions exhibit tissue variation and are completely different in *Saccharomyces* and plants (Balla, 2013). PI lipids are metabolised by three main enzyme classes kinases, phosphatases and phospholipases that are recruited to specific subcellular membrane compartments in response to certain cellular signals which culminate in cellular responses including chemotaxis, cell adhesion and proliferation.

1.2.1 Phosphatidylinositol kinases (PI-kinases)

Phosphorylation of the *myo*-inositol head group can be attributed to two broad classes of enzymes: phosphatidylinositol kinases (PI-kinases) which utilise phosphatidylinositol as a substrate and phosphatidylinositolphosphate kinases (PIP-kinases) which have preference for PI's phosphorylated derivatives.

1.2.1.1 Phosphatidylinositol 4-kinases (PI4-kinases)

Phosphatidylinositol kinase activity was initially defined by Michell and colleagues as one that could transfer the γ-phosphoryl group of ^{32}P-Labelled ATP to phosphatidylinositol in membrane fractions and tissue extracts (Michell *et al.*, 1967). Two decades later, studies involving the use of cell and tissue extracts revealed that phosphatidylinositol kinase activity could be characterised into three types based on sensitivity to different inhibitors and migration in a sucrose gradient (Whitman *et al.*, 1987). These were described as the type I, II and III phosphatidylinositol kinases. The type I enzyme was later demonstrated to phosphorylate the D3 position of the myo-inositol moiety of phosphatidylinositol and is now referred to as phosphatidylinositol 3-kinase (PI3K). It is now known that each PI4K family (type II and II activities) comprises two isoforms: PI4KIIα, PI4KIIβ, PI4KIIIα and PI4KIIIβ.

Saccharomyces expresses three conserved PI4Ks: Stt4, Pik1 and Lsb6. Stt4 and Pik1 are the yeast orthologues of mammalian type III PI4K α and β isoforms, respectively while Lsb6 is the single type II PI4K in yeast. Both mammalian families catalyse PI(4)P synthesis but have characteristically different subcellular localisation, chemical sensitivities and structural architecture. PI4Ks are discussed in greater detail in section 1.3.

1.2.1.2 Class III phosphatidylinositol 3-kinases (PI3KC3)

It is not unusual to find this class of enzymes grouped along with other PI3K classes, but they are regarded as classical phosphatidylinositol kinases because of their specificity for PI and not its phosphorylated derivatives. The first PI3K to be cloned was Vps34 (Schu *et al.*, 1993), which was identified in yeast screens for studying sorting defects in *Saccharomyces cerevisiae* mutants, hence its name Vps (meaning, vacuolar protein sorting). The *C*-terminal region of this protein exhibits a high degree of sequence similarity with the 110 kDa catalytic subunit of mammalian type I PI3 kinase (Hiles *et al.*, 1992) and this similarity revealed that Vps34 is a PI3K (Schu *et al.*, 1993). Depletion of this enzyme deprives the cell of PI(3)P and therefore confirms it as the sole source of PI(3)P in yeast (Schu *et al.*, 1993; Stack and Emr, 1994). In addition, unlike class I and II PI3Ks of higher eukaryotes, it can only phosphorylate PI but not its phosphorylated derivatives (Schu *et al.*, 1993). Studies involving mutation or complete deletion of this protein in yeast show that cells have intact vacuoles with unaltered secretory pathways but exhibit defective cargo sorting. Loss of Vps34 function alters sorting of carboxypeptidase Y to the vacuole (Herman and Emr, 1990). Vps34 is also required for multivesicular body (MVB) function (Katzmann *et al.*, 2001; Babst *et al.*, 2002a, 2002b) and is also involved in the regulation of autophagy (Kihara *et al.*, 2001). Vps34 is regulated by the Ser/Thr kinase, Vps15 which stimulates its kinase activity and loss of Vps15 function results in changes in cellular behaviour that mirror Vps34 loss (Kihara *et al.*, 2001).

Mammalian Vps34 (also called hVps34) is a PI-specific PI3K or class III PI3K. Like its yeast orthologue, it also associates with an adaptor protein, p150.

hVps34 regulates endosomal sorting pathways and is recruited as a complex with p150 onto early endosomes (Nielsen *et al.*, 2000; Murray *et al.*, 2002) where it catalyses PI(3)P synthesis and recruits FYVE and PX domain bearing proteins (Gillooly *et al.*, 2000; Kanai *et al.*, 2001; Xu *et al.*, 2001). hVps34 also regulates autophagic pathways via an interaction with Beclin-1 which in turn associates with various regulators of autophagy and endocytosis (Zhong *et al.*, 2009). hVps34 is involved in mTOR activation, particularly during nutrient starvation (Byfield *et al.*, 2005). PI3Ks are sensitive to the compound, wortmannin (Wm) with the yeast Vps34 having the lowest sensitivity (Schu *et al.*, 1993). In addition, hVps34 is less sensitive to Wm (IC_{50}= 100-300 nM) than the class I PI3Ks (IC_{50}= 1-5 nM). Wortmannin inhibits PI3K activity via a covalent interaction with a *C*-terminal domain lysine residue that is conserved across all PI3K classes (Wymann *et al.*, 1996; Wymann, 2012).

1.2.2 Phosphatidylinositolphosphate kinases (PIPKs)

These were initially described as enzymes that phosphorylate the D5 position of the *myo*-inositol moiety of PI(4)P. Early studies identified membrane bound PIPK activities responsible for PI(4,5)P_2 synthesis in a PI signalling cycle (Bazenet *et al.*, 1990). Subsequently, two isoforms were characterised from erythrocyte membranes and classified as types I and II activities based on different biochemical properties (Boronenkov and Anderson, 1995; Loijens *et al.*, 1996; Anderson *et al.*, 1999). Type I activity was strongly stimulated by phosphatidic acid while type II activity was unable to make PI(4,5)P_2 from PI(4)P on native membranes but did so with PI(4)P on micellar preparations, albeit with a low activity (Bazenet *et al.*, 1990). Type II PIPKs were the first to be cloned (Boronenkov and Anderson, 1995; Divecha *et al.*, 1995). Subsequent cloning of type I PIPKs revealed a high degree of sequence homology between both isoforms, especially within the *C*-terminal catalytic domain (Loijens and Anderson, 1996; Anderson *et al.*, 1999). It was later discovered that type II PIPKs use PI(5)P as substrate and phosphorylates the D4 position of *myo*-inositol and that the initially reported 5-kinase activity was due to contamination of commercial PI(4)P preparations with PI(5)P (Rameh

et al., 1997b) therefore explaining its lack of activity against native membranes.

1.2.2.1 Type I PIPKs

In mammalian cells, type I PIPKs (PIPKIs) are encoded by three genes encoding PIPKIα, PIPKIβ and PIPKIγ. PIPKIγ has at least five different splice variants (Anderson *et al.*, 1999; Doughman *et al.*, 2003). They are widely expressed but display unique tissue distribution and cellular localisation. It is thus suggested that they synthesise functionally distinct pools of $PI(4,5)P_2$. The first yeast PIPK homologues to be identified were Mss4p and Fab1p (Yamamoto *et al.*, 1995; Desrivières *et al.*, 1998; Gary *et al.*, 1998; Homma *et al.*, 1998). Mss4p is required for actin organisation and membrane morphogenesis (Amatruda *et al.*, 1992; Audhya *et al.*, 2004) while Fab1p is required for maintaining vacuolar structure and function (Yamamoto *et al.*, 1995; Gary *et al.*, 1998). Fab1p was later reported to phosphorylate PI(3)P to $PI(3,5)P_2$ and like its mammalian homologue, PIKfyve, it is classified as a type III PIPK (Shisheva *et al.*, 1999). Sequence data from other PIPK homologues have now been described in both the plant and animal kingdoms and these show wide distribution and conserved function in organisms. PIPKIγ is the most diverse PIPKI due to the variety of splice variants that the gene can give rise to (Balla, 2013). In humans, these splice versions are designated $PIPKI\gamma_{V1\text{-}6}$. The 87 kDa form, V1 is most prevalent while the 90 kDa V2 variant is predominantly expressed in the brain (Balla, 2013). Both localise to the plasma membrane (PM) and the V2 form localises to focal adhesions in association with talin (Thapa *et al.*, 2013). $PIPKI\gamma_{V2}$ associates with Src in focal adhesions and regulates its localisation in tandem with talin. This association stabilises Src in response to integrin engagement and growth factor stimulation: thereby regulating anchorage independent growth (Thapa *et al.*, 2013). The 93 KDa $PIPKI\gamma_{V3}$ localises to the PM and intracellular vesicles while $PIPKI\gamma_{V4}$ was identified in nuclear speckles (Balla, 2013). $PIPKI\gamma_{V5}$ associates with SNX5 which binds various PI lipids including $PI(4,5)P_2$. Both proteins localise to late endosomes and are required for

sorting of the epidermal growth factor receptor (EGFR) into intraluminal vesicles of MVBs (Sun *et al.*, 2013).

1.2.2.2 Type II PI(5)PKs (PIPKIIs)/PIP4Ks

As mentioned earlier, these were the first PIPKs to be cloned and they are structurally homologous to the type I enzymes (Boronenkov and Anderson, 1995; Divecha *et al.*, 1995). These enzymes utilise PI(5)P as substrate and are thus referred to as PI(5)P 4-kinases. Like the type I enzymes, mammalian type II PIPKs exist in three forms: PIPKIIα, PIPKIIβ and PIPKIIγ, with PIPKIIα being the most active isoform (Bultsma *et al.*, 2010; Clarke *et al.*, 2010). PIPKIIβ was the first PIPK with a defined crystal structure. The quaternary structure of PIPKIIβ comprises a dimer in which two identical subunits interact with one another at the *C*-terminus via a combination of α-helices and β-sheets (revieved by Anderson et al. 1999). It localises to both the cytosol and nuclear speckles where it can recruit PIPKIIα (Balla, 2013). PIPKIIγ is mostly associated with intracellular vesicles but also associates with the ER and endosomal membranes in neurones (Itoh *et al.*, 1998). Due to its low enzyme activity, it is thought to serve as a scaffold that recruits PIPKIIα to designated membranes (Clarke *et al.*, 2008). PIPKIIα synthesises PI(4,5)P_2 required for platelet secretion (Rozenvayn and Flaumenhaft, 2001, 2003) as well as platelet formation via fragmentation of megakaryocytes (Schulze *et al.*, 2006). PIPKIIβ on the other hand is suggested to be a regulator of insulin signalling in muscle cells as loss of function of this isoform elevates insulin sensitivity in mice via increased Akt activation (Lamia *et al.*, 2004).

1.2.2.3 Type III PIPKs (PIP5K3s)

These enzymes phosphorylate PI(3)P to make PI(3,5)P_2. The first type III PIPK activity to be described was Fab1, which was identified in a yeast screen for nuclear segregation. Fab1 was previously described as a type II PIPK based on the degree of sequence homology with the first cloned type II PIPK particularly in the catalytic domain (Yamamoto *et al.*, 1995). Fab1 PI(3)P 5-kinase activity was identified in yeast when osmotic stress led to an increase in PI(3,5)P_2 and this was determined to be reliant on Fab1 activity

(Dove *et al.*, 1997; Cooke *et al.*, 1998; Gary *et al.*, 1998). This was further strengthened by *in vitro* studies which showed that, Fab1 phosphorylates PI(3)P to PI(3,5)P_2. Fab1 is essential for vacuolar trafficking pathways in yeast and deletion of the Fab1 gene results in the development of enlarged vacuoles blocking transport of vacuolar hydrolases (Gary *et al.*, 1998). Vac14 serves as an upstream regulator of Fab1 and deletion the gene encoding Vac14 eliminates Fab1 PI(3)P 5-kinase activity resulting in vacuolar sorting defects (Gary *et al.*, 1998; Bonangelino *et al.*, 2002; Dove *et al.*, 2002). Vac14 serves as a scaffold that holds Fab1 and the 5-phosphatase, Fig4 in a complex. Removal of Vac14 destabilises this complex, impairing Fab1 activity (Botelho *et al.*, 2009).

PIKfyve is the mammalian orthologue of yeast Fab1 (Shisheva *et al.*, 1999). It shows structural and functional similarities with Fab1 in having a PI(3)P recognising FYVE domain and interacting with proteins that are homologues of yeast proteins that regulate Fab1 (Jin *et al.*, 2008; Sbrissa *et al.*, 2008). ArPIKfyve is the mammalian homologue of Vac14 which holds PIKfyve and Sac3 in a complex analogous to that in yeast cells. Sac3 is the homologue of yeast Fig4 which balances kinase activity and keeps PIKfyve in the active conformation (Ikonomov *et al.*, 2009, 2010).

The switch from PI(3)P to PI(3,5)P_2 is regarded as a critical step for membrane sorting from early endosomes to MVBs as the depletion of PIKfyve by RNA results in defective trafficking of lysosomal hydrolases (de Lartigue *et al.*, 2009). While depletion of PIKfyve alone is not sufficient to block EGFR degradation, combined loss of PIKfyve and Vac14 impedes EGFR degradation (de Lartigue *et al.*, 2009), indicating the functional relevance of the PIKfyve-Vac14 complex.

1.2.3 Phosphatidylinositol 4,5-bisphosphate (PI(4,5)P_2) kinases (Class I PI3Ks)

Discovery of a kinase with specificity for PI(4,5)P_2 as a substrate marked the identification of the lipid, PI(3,4,5)P_3 (Auger *et al.*, 1989). The first 3-kinase

activity to be reported was described as a class I PI3 kinase. A parallel study showed that this activity responds to oncogenic signalling and growth factor stimulation by producing $PI(3,4,5)P_3$ and was subsequently termed a $PI(4,5)P_2$ 3-kinase (Ghigo *et al.*, 2012; Toker, 2012; Balla, 2013). Class I PI3Ks are the most sensitive to wortmannin (IC_{50}= 1-5 nM; (Wymann, 2012)), are able to phosphorylate PI to PI(3)P and PI(4)P to $PI(3,4)P_2$ *in vitro* but have a strict specificity for $PI(4,5)P_2$ *in vivo* (Pirola *et al.*, 2001). They differ from other PI3K classes in that their activation loops bear specific arginine and lysine side chains that are positioned to interact with the dense negative charges on higher phosphorylated PIs. These facilitate tight interactions that are required for successful transfer of the γ-phosphoryl group from ATP to the D3-position of the PI substrate (Pirola *et al.*, 2001). Mutation or replacement of these residues to mimic the activation loops in other PI3K classes obliterates the ability of class I PI3Ks to use $PI(4,5)P_2$ as a substrate (Pirola *et al.*, 2001).

Class I PI3Ks serve as downstream mediators of signals generated by ligand stimulated plasma membrane receptors (Auger *et al.*, 1989; Guillermet-Guibert *et al.*, 2008; Zoncu *et al.*, 2011). They exist as heterodimers with a catalytic subunit of 110 kDa and are also known as p110 proteins. Mammalian class I PI3Ks are encoded by four distinct but related genes of the PIK3c family and the gene products are PI3Kα (encoded by PIK3ca), PI3Kβ (encoded by PIK3cb), PI3Kγ (encoded by PIK3cg) and PI3Kδ (encoded by PIK3cd) (Reviewed by Balla, 2013; Sasaki et al., 2009).

Class I PI3Ks are further classified based on their interactions with regulatory proteins as Class IA and Class IB PI3Ks. PI3Kα, PI3Kβ and PI3Kδ comprise are class IA. They form complexes with a regulatory protein p85 which bears two SH2 homology domains that permits docking to phosphorylated tyrosines in pY-x-x-M motifs on growth factor receptors or tyrosine kinase substrates (Backer *et al.*, 1992). Formation of these complexes induces membrane recruitment, thereby increasing lipid kinase activity. These adaptor proteins are encoded by three genes in mammalian cells; PIK3r1 (encodes p85 and its two splice variants), PIK3r2 (encodes p85β) and PIK3r3 (encodes p55γ)

(Sasaki *et al.*, 2009; Balla, 2013). PI3Kγ is the sole class IB PI3K. It forms a complex with a p101 or p84/p87 regulatory subunit which lack an SH2 domain and couple PI3Kγ to G-protein coupled receptors (Guillermet-Guibert *et al.*, 2008).

Class I PI3Ks are implicated in several cellular processes including nutrient metabolism, immune cell function and mitogenic signalling. In addition, these enzymes were initially reported as lipid kinases associated with viral oncogenes and links with cancer have been established over the last three decades with the identification of druggable targets (Reviewed by: Balla, 2013; Sasaki et al., 2009; Wymann, 2012).

1.2.4 Class II PI3Ks

This class comprises three members: PI3KC2α, PI3KC2β and PI3KC2γ that have molecular weights ranging from 170-200 kDa. All members of this class have a *C*-terminal extension which bears a phox homology (PX) domain and a calcium insensitive C2 homology domain. Unlike other PI3Ks, they have no regulatory subunits. There are conflicting findings regarding substrate specificities of the class II PI3Ks. *In vitro* studies reveal that they are able to convert PI, PI(4)P and PI(4,5)P_2 to PI(3)P, PI(3,4)P_2 and PI(3,4,5)P_3 respectively (Falasca *et al.*, 2007; Leibiger *et al.*, 2010). This seems not to be the case *in vivo* as PI3KC2α depletion significantly diminishes cellular levels of PI(3,4)P_2 but not PI(3)P, PI(4,5)P_2 or PI(3,4,5)P_3 (Posor *et al.*, 2013). In addition, the activation loop sequences of class II PI3Ks also predict that these enzymes are specified for PI(3,4)P_2 synthesis and utilise PI(4)P as the preferred substrate. The activation loop comprises two basic amino acid residues that stabilise the phosphate group on PI(4)P and facilitate phosphate transfer to the lipid substrate. Replacement of these residues with corresponding sequences from hVps34 abolishes PI(3,4)P_2 synthesis and converts PI3KC2α to a type III PI3K. Similarly, mutation of specific sequences in order to mimic the activation loop of p110 proteins confers an ability to synthesise PI(3,4,5)P_3 from PI(4,5)P_2 (Posor *et al.*, 2013).

PI3KC2β also phosphorylates PI(4)P to generate PI(3,4)P_2 but can, to a lesser extent generate PI(3)P and PI(3,4,5)P_3 from PI and PI(4,5)P_2 respectively, *in vitro* (Marat *et al.*, 2017). PI3KC2β suppresses mTORC1 signalling in serum starved mammalian cells, thereby increasing autophagy and lysosomal degradation of proteins. Localised synthesis of PI(3,4)P_2 from PI(4)P on LE/lysosomes is required for the recruitment of 14-3-3 which binds the Raptor subunit of mTORC1 thereby suppressing the activation of downstream targets, S6 kinase and phosphorylated 4E-binding protein 1 (4E-BP1) (Marat *et al.*, 2017). The links between mTORC1 signalling and diseases including diabetes, obesity and cancer suggest that pharmacological targeting of PI3KC2β may present new opportunities for the medical management of these diseases.

PI3KC2γ is mainly expressed in hepatocytes (Ono *et al.*, 1998; Braccini *et al.*, 2015) where it may play a role in liver regeneration (Ono *et al.*, 1998). It is recruited to early endosomes in a Rab5 dependent manner during insulin signalling. On early endosomes, PI3KC2γ generates PI(3,4)P_2 which sustains activation of Akt2. PI3KC2γ loss in mice diminishes Akt2 activation, thereby affecting glycogen metabolism in the liver, resulting in insulin resistance (Braccini *et al.*, 2015).

1.2.5 Phosphoinositide phosphatases

These enzymes along with phospholipases, mediate phosphoinositide hydrolysis. They are highly conserved in eukaryotes and unlike the kinases, are more promiscuous enzymes in terms of substrate specificity. PI lipid phosphatases comprise several large families, with over 35 in mammals and they regulate a myriad of processes which including growth factor signalling, nutrient metabolism, development and invasion in cancer, myopathies and neurodegenerative disorders (reviewed by Dyson et al., 2012; Liu and Bankaitis, 2010; Strahl and Thorner, 2007).

The best-studied lipid phosphatases are PM localised PTEN (phosphatase and tensin homologue deleted on chromosome 10) and SHIPs (SH2 domain containing inositol phosphatases) which are 3-phosphatases and 5-phosphatases respectively. Both enzymes are of remarkable physiological importance in that they are central to the regulation of signalling pathways emanating from receptor tyrosine kinases (RTKs) following growth factor stimulation (Maehama and Dixon, 1998; Myers *et al.*, 1998; Zhuang *et al.*, 2007). PTEN antagonises class I PI3Ks which catalyse the synthesis of PI(3,4,5)P_3 from PI(4,5)P_2 and is often mutated or deleted in a variety of human cancers including glioblastomas, endometrial and prostate carcinomas (Maehama and Dixon, 1998; Myers *et al.*, 1998; Robinson *et al.*, 2015). SHIPs hydrolyse the D5-phosphoester of the inositol rings in PI(3,4,5)P_3 and *Ins*(1,3,4,5)P_4 (Damen *et al.*, 1996; Pesesse *et al.*, 1998) and negatively regulate growth factor signalling (Lioubin *et al.*, 1996; Ishihara *et al.*, 1999; Liu *et al.*, 1999).

The 5-phosphatases, OCRL (oculocerobrorenal Lowe syndrome protein) and synaptojanins hydrolyse the 5-phosphate of PI(4,5)P_2 resulting in the production of PI(4)P. OCRL localises to the Golgi, PM and endosomes and associates with clathrin and AP-2 (Ungewickell *et al.*, 2004; Chowdhury *et al.*, 2005; Faucherre *et al.*, 2005). OCRL controls endosomal traffic and its depletion impairs recycling of cell surface receptors including megalin in kidney epithelial cells (Vicinanza *et al.*, 2011). Loss of function of OCRL

underlies the pathogenesis of Lowe's syndrome ─a congenital X-linked human disorder characterised by a variety of neurological, renal, ocular and muscular abnormalities (Bökenkamp and Ludwig, 2016; Song *et al.*, 2017).

Synaptojanins (SYNJs) are dual function phosphatases conserved from yeast to humans. They are modified by alternative splicing in different tissues resulting in two major isoforms: SYNJ1 and SYNJ2 (Ramjaun and McPherson, 1996). The phosphatase activity of SYNJ1 is required for disassembly of clathrin coats in nerve cells and genetic ablation of this isoform impairs nerve transmission in mice resulting in their death within two weeks of birth (Cremona *et al.*, 1999; Kim *et al.*, 2002). SYNJ2 regulates clathrin mediated endocytosis in non-neuronal cells (Hill *et al.*, 2001; Rusk *et al.*, 2003). siRNA-mediated depletion of SYNJ2 impedes the early steps of clathrin coated vesicle formation thereby preventing internalisation of the EGFR in lung carcinoma cells (Rusk *et al.*, 2003).

Sac1 (initially called suppressor of actin) which localises to the ER and Golgi shows *in vivo* specificity for PI(4)P and is involved in actin organisation and membrane trafficking (Guo *et al.*, 1999; Rivas *et al.*, 1999; Xie *et al.*, 2001). Sac2 is a 4-phosphatase that hydrolyses PI(4)P *in vivo* and has also been described in mammalian cells where it acts in tandem with OCRL/INPP5B. Along with these phosphatases, Sac2 regulates late stages of CME and sorting onto Rab5 positive membrane compartments (Nakatsu *et al.*, 2015).

The Myotubularins (MTMs) and MTMRs (myotubularin related) are 3-phosphatases that localise to endosomal membranes and dephosphorylate PI(3)P and PI(3,5)P_2 to form PI and PI(5)P respectively (Blondeau *et al.*, 2000; Ketel *et al.*, 2016). Mutations in genes encoding several members of MTM and MTMR enzyme families underlie the pathogenesis of myotubular myopathies and Charcot-Marie-Tooth neuropathies, which affect motor and sensory nerves and result in muscle weakness and atrophy (Laporte *et al.*, 1996; Blondeau *et al.*, 2000; Taylor *et al.*, 2000).

1.2.6 Intracellular distribution of phosphoinositides

PI lipids are not evenly distributed on membranes, rather the concerted action of different phosphoinositide modifying enzymes leads to a characteristic distribution of these lipids on intracellular membranes (Figure 1-4). The coincident detection of specific PI lipid species has led to a dogma in which certain these lipids are confined to certain organelle membranes. As a result, it is perceived that seven different PI lipids can be linked to certain organelle membranes, creating a cellular lipid distribution pattern referred to as the cell's phosphoinositide map (Cullen and Carlton, 2012).

Regarding membrane localisation, PI(4,5)P_2, PI(3,4)P_2 and PI(3,4,5)P_3, are predominantly found on the inner leaflet of the plasma membrane and on endocytic vesicles (Szentpetery *et al.*, 2010; Balla, 2013; Posor *et al.*, 2013). PI(4)P is mainly found on Golgi membranes but can also be found in lesser amounts on endosomal membranes as well as the plasma membrane (Hammond *et al.*, 2009, 2012, 2014; Dong *et al.*, 2016; Henmi *et al.*, 2016; Ketel *et al.*, 2016; Marquer *et al.*, 2016). The 3-phosphoinositides, PI(3)P and PI(3,5)P_2 are found on early and late endosomes respectively where they coordinate membrane traffic through the lysosomal degradative pathway or recycling complex (de Lartigue *et al.*, 2009; Cullen and Carlton, 2012; Balla, 2013). In addition to the use of lipid binding probes, expression of mutant PI lipid modifying enzymes (Posor et al., 2013; Vicinanza et al., 2011) and acute recruitment of modifying enzymes to specific membranes to which certain PI lipids are commonly localised (Varnai *et al.*, 2006; Zoncu *et al.*, 2009; Szentpetery *et al.*, 2010; Hammond *et al.*, 2012) have enabled mapping of individual lipid species to distinct intracellular organelles. The approaches used in studying membrane localisations of different PIs species have their own limitations in that: (1) some lipid probes have greater affinities for their cognate PIs on certain membrane compartments due to secondary interactions with some other proteins which may bias them to these compartments, leading to poor resolution of PIs on other organelles and (2) the physiological state of the cell may underscore the true membrane identity of some organelles. For example, nutrient starvation increases PI3KC2β

activity thereby raising $PI(3,4)P_2$ levels on late endosomes while nutrient supply does the opposite (Marat *et al.*, 2017). Thus, it is difficult to give a concise cellular PI map as cells constantly undergo metabolic changes in which membrane lipids are regularly turned over.

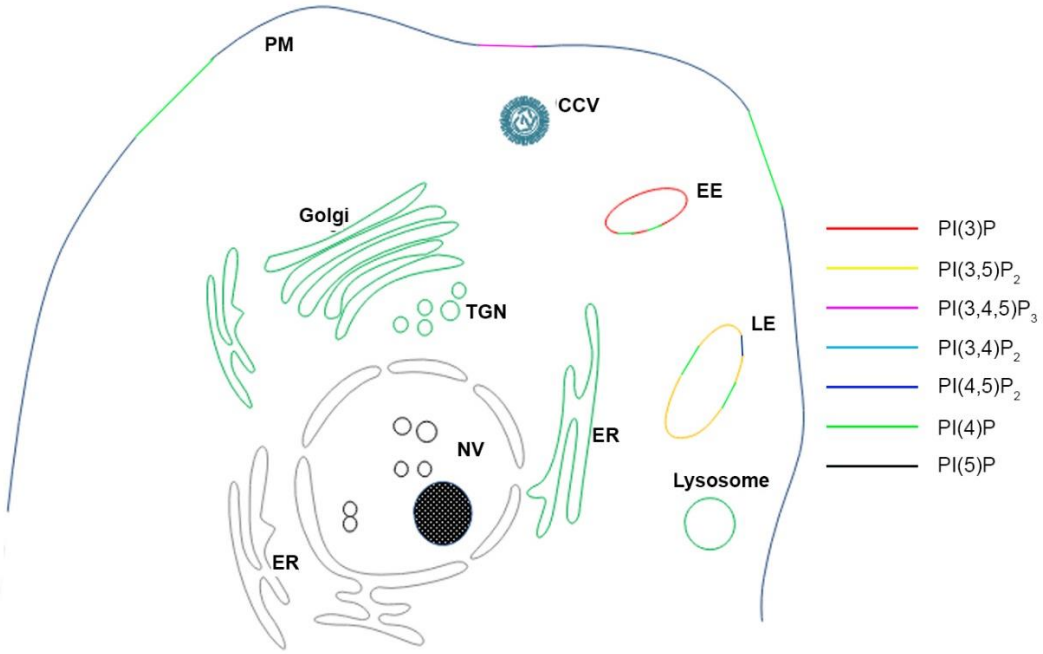

Figure 1-4. The phosphoinositide map of mammalian cells.

PI(4)P is predominantly concentrated on ER and Golgi membranes but can be found in varying amounts on endo- and lysosomal membranes. The 3-phosphoinositides: PI(3)P and $PI(3,5)P_2$, are concentrated on early (EE) and late endosomes (LE) while $PI(4,5)P_2$ localises to the plasma membrane (PM) but can also be found on LE. $PI(3,4)P_2$ is associated with the clathrin coated endocytic vesicles (CCVs) while PI(5)P has been described in nucleoplasmic vesicles (NV) but its metabolism is unclear.

1.2.7 Phosphoinositide mediated protein localisation

Phosphoinositides could be referred to as molecular signposts as they are concentrated at membrane/cytosol interfaces where they interact with signalling and trafficking molecules.

These membrane interactions involve the establishment of ionic contacts between negatively charged phosphate groups on the inositol head group and certain phosphoinositide binding motifs in the protein. Such lipid interaction motifs exist in two major forms: (1) as clusters of polybasic amino acid side chains within unstructured regions which can be found in myristoylated alanine-rich C-kinase substrate (MARCKS) effector domain (Wang *et al.*, 2002) as well as small GTPases, K-Ras, Rin and Rit (Heo *et al.*, 2006) and (2) the binding motif may exist as a folded domain such as the pleckstrin homology (PH) domain found in several proteins. PH domains exist in different forms with selectivity for different PI lipid species. Examples include the PI(4,5)P_2 binding PH domain of PLCδ (Stauffer *et al.*, 1998; Hammond *et al.*, 2009); the PI(4)P binding PH domain of 4-phosphate adaptor proteins (FAPPs; (Dowler *et al.*, 2000; Godi *et al.*, 2004) and the PI(3,4,5)P_3 PH domains of Grp1 (Klarlund *et al.*, 1998), Btk and Tiam-1 (Rameh *et al.*, 1997a).

Several other phosphoinositide binding domains occur in different proteins and those worthy of being mentioned here include the PI(3)P binding FYVE domain found in proteins such as early endosome autoantigen (EEA1; (Lawe *et al.*, 2000)), the signalling protein, Hrs (Miura *et al.*, 2000). Some other phosphoinositide binding domains include the ENTH, FERM, and GLUE domains (Table 1-1), which have been characterised in proteins involved in the regulation of cellular processes that include endocytosis, actin polymerisation and cell signalling. The number of lipid binding domains in this category is expanding and their potentials in regulating different cellular processes emphasise the importance of PI lipids.

In vitro data have previously shown that some phosphoinositide binding domains commonly associate with their cognate PI lipids with relatively low affinities (Baumeister *et al.*, 2003; Yu *et al.*, 2004). This possibly enables these proteins to continuously and dynamically associate with membranes following depletion or enrichment of PI lipids at their target sites; however, such interactions are not enough for these proteins to mediate their functions at their respective membrane targets (Cullen *et al.*, 2001). In such cases, lipid recognition is not reliant on headgroup binding alone but by additional membrane interaction mechanisms. For instance, PH domains also bind proteins and the simultaneous lipid and protein binding (called coincidence detection; (Carlton and Cullen, 2005)) induces membrane recruitment. The protein input for PH domains frequently comes from interactions with small GTPases. For example, the PH domain of FAPP1 binds PI(4)P at the Golgi via interactions with Arf1. Inhibition of Arf1 with the fungal toxin, Brefeldin A diminishes FAPP1 PI(4)P-binding at the Golgi, resulting in its cytoplasmic translocation (Godi *et al.*, 2004). Some other domains enhance their PI-lipid interactions by undergoing dimerization. Examples of these include the PH domain of dynamin (Klein *et al.*, 1998) and the FYVE finger domain of EEA1 (Stenmark *et al.*, 1996; Dumas *et al.*, 2001). The ability of PI binding domains to engage in multiple engagements increases the avidity of the protein-lipid complexes at target membranes despite the weak strength of interactions between individual units. Such interactions are perceived to enhance links between peripheral membrane proteins and their cognate membrane lipids.

Table 1-1. Common phosphoinositide binding domains

Domain name	Lipid species	Examples of proteins
FYVE	PI(3)P	Hrs (Miura *et al.*, 2000) EEA1 (Lawe *et al.*, 2000) Endofin (Chen *et al.*, 2007)
Phox homology (PX)	PI(3)P	SNX3 (Xu *et al.*, 2001)
Pleckstrin homology (PH)	$PI(4,5)P_2$	PLCδ (Várnai and Balla, 2008; Hammond *et al.*, 2009)
	$PI(3,4)P_2$	TAPP1 and TAPP2 (Marshall *et al.*, 2002)
	$PI(3,4,5)P_3$	Grp1 (Klarlund *et al.*, 1998), Btk, Tiam-1, Sos (Rameh *et al.*, 1997a)
	PI(4)P	FAPP1 (Dowler *et al.*, 2000; Godi *et al.*, 2004)
ENTH/ANTH	PI(4)P, $PI(4,5)P_2$	Epsins, AP180 (Reviewed by Guo et al., 2014; Saarikangas et al., 2010)
FERM	$PI(4,5)P_2$	Talin (Kwiatkowska, 2010; Thapa *et al.*, 2013)
GLUE	3-phosphoinositides (especially PI(3)P)	ESCRT II complex (Teo *et al.*, 2006)

1.3 Phosphatidylinositol 4-kinases (PI4Ks)

PI(4)P is synthesised by two families of enzymes, type II and III PI4Ks which exhibit starkly different biochemical characteristics. Molecular cloning of these enzymes led to the identification of two type II PI4Ks of approximately 55 kDa, PI4KIIα and PI4KIIβ (Barylko *et al.*, 2001; Minogue *et al.*, 2001; Balla *et al.*, 2002; Wei *et al.*, 2002) and two type III PI4Ks, 230 kDa PI4KIIIα and 92 kDa PI4KIIIβ (Balla *et al.*, 1997; Gehrmann *et al.*, 1999). Cloning of these PI4Ks in *Saccharomyces* revealed the presence of three different PI4Ks namely Stt4 (the mammalian PI4KIIIα orthologue), Pik1 the mammalian PI4KIIIβ orthologue) and Lsb6, which is the only type II gene in yeast. Lower eukaryotes such as *Drosophila* and *Caenorhabditis* also express two type III PI4K but only one type II PI4K activity.

The kinase domains of type III PI4Ks show homology with those of PI3Ks including a conserved lysine residue (corresponding to Lys549 and Lys1791 in PIKIIIβ and -α respectively) that covalently binds the PI3K inhibitor, wortmannin, hence the sensitivity of type III PI4Ks to wortmannin, albeit at higher concentrations (Balla *et al.*, 1997, 2008). On the other hand, the type II PI4Ks form a distinct lipid kinase family of two closely related enzymes which share little homology with PI3Ks and type III PI4Ks (discussed in 1.3.1). They are insensitive to wortmannin but are inhibited by micromolar (μM) concentrations of Adenosine and have a low K_M for ATP (Barylko *et al.*, 2001; Minogue *et al.*, 2001; Balla *et al.*, 2002). For several years, these biochemical characteristics (Table 1-2) were the only distinguishing features for studying the different isoforms (Balla and Balla, 2006). This resulted in difficulties in probing the function of individual activities, as in many cases, results were obscured by contamination with trace amounts of the highly active type II enzyme (Minogue and Waugh, 2012). Fortunately, advancements in genomics in the past two decades made unambiguous characterisation of the different isoforms possible.

Mammalian PI4K isoforms also differ in their membrane localisations and generate distinct membrane PI(4)P pools. Mammalian PI4KIIIα controls a

plasma membrane pool of PI(4)P possibly through transient ER-PM contact sites (Nakatsu *et al.*, 2012; Bojjireddy *et al.*, 2014; Hammond *et al.*, 2014) while PI4KIIIβ localises to the Golgi (Jović *et al.*, 2012; Tokuda *et al.*, 2014). The type II PI4Ks, on the other hand, are associated with the Golgi, PM and endosomal membranes and would be discussed further in subsequent sections.

Table 1-2. Distinctive biochemical features of mammalian PI4K isoforms

Features	PI4KIIα	PI4KIIβ	PI4KIIIα	PI4KIIIβ
Yeast Homologue	Lsb6(Pik2p)	Lsb6(Pik2p)	Stt4	Pik1p
Apparent Molecular weight	55-56 kDa	55-56 kDa	210 kDa	110 kDa
Calculated Molecular Weight	54 kDa	55 kDa	230 kDa	92 kDa
Wortmannin	Insensitive	Insensitive	IC_{50}= 50–300 nM	IC_{50}= 50–300 nM
LY-294002	Insensitive	Insensitive	IC_{50}= 50–100 mM	IC_{50}= 100 mM
Phenylarsine Oxide	IC_{50}>100 µM	IC_{50}>100 µM	IC_{50}~1-5 µM	IC_{50}~30 µM
Ca^{2+}	Inhibits	Inhibits	No direct effect	No direct effect
K_i(Adenosine)	10-70 µM	10-70 µM	Millimolar	Millimolar
Triton x-100	Activates	Activates	Activates	Activates
K_M (ATP)	10-50 µM	10-50 µM	700 µM	400 µM
K_M (PtdIns)	20-60 µM	20-60 µM	100 µM	100 µM

The mammalian genome encodes four PI4K isoforms which are classified into two families: type II (PI4KIIα and IIβ) and type III (PI4KIIIα and PI4KIIIβ). Both families have divergent biochemical features summarised in this table. Adapted from *Balla, 2006.*

1.3.1 Mammalian type II phosphatidylinositol 4-kinases

PI4KIIs are the most active PI kinases in isolated membranes and detergent extracts (Balla *et al.*, 2002; Waugh *et al.*, 2003). PI4KII activity is tightly membrane associated (predominantly PI4KIIα), requiring detergent extraction for its solubilisation (Minogue *et al.*, 2001; Jung *et al.*, 2008; Barylko *et al.*, 2009).The two closely related isoforms, PI4KIIα and PI4KIIβ are encoded by separate genes in vertebrates while type II PI4 kinase activity arises from a single gene in invertebrates. Type II PI4K activity is also expressed from a single gene in primitive eukaryotes such as the budding yeast (Minogue and Waugh, 2012). The mammalian PI4KIIs exhibit a great degree of similarity, particularly in the catalytic domain where they share ~68% sequence similarity. They possess divergent sequences in their *N*-termini (Figure 1-5) with the *N*-terminal region of PI4KIIα comprising a stretch of hydrophobic amino acids (V^{76}AAQAQALAAQAAVA^{90}) while that of PI4KIIβ comprises two stretches of acidic amino acids (E^{19}EEEDGERE^{28} and E^{55}EGEAGDEE^{63} (Balla *et al.*, 2002; Barylko *et al.*, 2009)). The entire *N*-termini of both proteins are dispensable for membrane interaction as deletion of the first 90 amino acid residues has no impact on membrane localisation of either proteins (Jung *et al.*, 2008; Zhou *et al.*, 2014) but may be important for protein-protein interactions. For example, the *N*-terminal region of PI4KIIα harbours a dileucine sorting signal (E^{57}RQPLL^{62}) that permits interaction with clathrin adaptor, AP-3 (Craige *et al.*, 2008) as well as a proline motif (PPxY) that interacts with the ubiquitin E3-ligase, Itch (Mössinger *et al.*, 2012). The *N*-terminus of PI4KIIβ also contains an acidic cluster dileucine motif (E^{26}REPLL^{30}) that interacts with adaptor protein, AP-1 and is required for post-Golgi cargo sorting (Wieffer *et al.*, 2013).

The kinase domain, which comprises ~360 amino acids is conserved between both proteins. It assumes a similar folding pattern in both proteins (see 1.3.1.1 and 1.3.1.2) and in both cases, bears a cysteine-rich CCPCC motif that is s-palmitoylated by palmitoyl acyl-transferases (PATs). Both PI4KII isoforms exhibit differences in palmitoylation as PI4KIIα is constitutively palmitoylated and approximately 90% of the cellular PI4KIIα is

tightly associated with membranes and is weakly extracted with 1M NaCl or 0.1M Na_2CO_3 (pH 11). It can only be eluted from membranes by non-ionic detergents such as Triton X-100, suggesting it is an integral membrane protein (Jung *et al.*, 2008; Barylko *et al.*, 2009). On the other hand, ~30% of PI4KIIβ is loosely associated with membranes and can be eluted with 0.1M Na_2CO_3 (pH 11; Barylko et al., 2009; Jung et al., 2008; Wei et al., 2002). This suggests that a fraction of PI4KIIβ is peripherally associated with membranes. PI4KIIβ is dynamically palmitoylated and unlike PI4KIIα which is constitutively palmitoylated, its membrane localisation is regulated (Jung *et al.*, 2008; Barylko *et al.*, 2009). Palmitoylation of the CCPCC motif is required for catalytic activity and membrane localisation of both PI4KIIs. Inhibition of palmitoyl transferase activity or mutation of the CCPCC motif of PI4KIIs eliminates their catalytic activity and alters subcellular localisation (Jung *et al.*, 2008; Barylko *et al.*, 2009).

Figure 1-5. Sequence alignment of mammalian PI4KIIα and PI4KIIβ.

Sequence alignment of human PI4KIIα and PI4KIIβ. Red indicates sequence identity. The *N*-terminal domains (~1-100 amino acid residues) are highly diverse. These comprise a stretch of acidic (E^{19}EEEDGERE^{28} and E^{55}EGEAGDEE^{63} in PI4KIIβ) and hydrophobic (V^{76}AAQAQALAAQAAVA^{90} in PI4KIIα) amino acid R groups. The kinase domains extend from ~100 amino acids and comprise conserved sequences (the most conserved among most kinases). The CCPCC palmitoylation motifs are boxed. Sequences were aligned using the Constraint-based multiple alignment tool (COBALT) from NCBI (Papadopoulos and Agarwala, 2007).

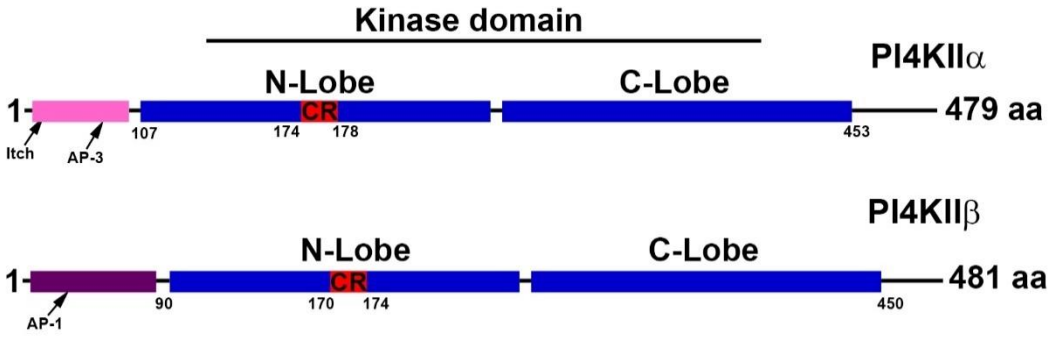

Figure 1-6. Schematic representation of type II PI4Ks structural domains.

The two isoforms share similarity in their kinase domains which comprise N- and C-lobes. The signatory feature of these enzymes is the presence of a cysteine rich palmitoylation motif (CR) that permits membrane association. Both isoforms exhibit divergence in their N-termini that harbour interaction sites for proteins such as ubiquitin ligase, Itch and clathrin adaptors, AP-1 and AP-3.

1.3.1.1 Molecular features of PI4KIIα

PI4KIIα is a 55 kDa protein that is conserved in mammals. Its primary structure comprises a *C*-terminal catalytic domain bearing a cysteine-rich CCPCC palmitoylation motif required for membrane insertion and catalytic activity (Figure 1-6). Over the years, lack of understanding of the molecular structure of the type II PI4Ks posed a major drawback in studying the mechanisms of regulating type II PI4 kinase activity. Recent works by two separate groups (Baumlova *et al.*, 2014; Zhou *et al.*, 2014) described the crystal structure of PI4KIIα catalytic domain by X-ray diffraction. These studies were carried out on PI4KIIα fragments lacking the highly disorganised *N*-terminal domain which decreases solubility, thereby affecting crystallisation (Baumlova *et al.*, 2014). In addition, the CCPCC palmitoylation motif also obscured crystallisation by inducing protein aggregation and was also altered by mutations (Zhou *et al.*, 2014) or insertion of a T4 lysozyme (Baumlova *et al.*, 2014). In addition, 12 residues at the *C*-terminus were deleted to improve crystallisation properties. Fragments lacking the CCPCC motif permitted the generation of high-quality crystals, albeit with low kinase activity, which could be ameliorated following reconstitution into liposomes. The crystal structure of PI4KIIα kinase domain reported by both groups

overlap in many aspects and provide numerous molecular information about this enzyme.

The kinase domain of PI4KIIα comprises two lobes; an N-lobe and a C-lobe separated by a nucleotide binding cleft. The N-lobe comprises a core of antiparallel β-sheets surrounded by four helices. The C-lobe comprises two β-sheets surrounded by three helices. Both lobes are covered by a roof-like arrangement of three helices, which represent the most distant part of the kinase domain from the membrane environment. The nucleotide (ATP) binding site lies between the N and C-lobes (Figure 1-7). ATP held in position by hydrogen bonds with side chains of residues K^{152}, S^{137} and D^{346} and with the protein backbone. In addition, two serine residues, Ser^{134} and Ser^{137} donate hydrogen bonds that stabilise the β-phosphate. The α-phosphate group is held in position through electrostatic interactions and hydrogen bonds through Lys^{152} and Asp^{346} respectively. Several amino acids with bulky side chains constitute a hydrophobic cavity that houses the adenosine moiety while the ribose sugar moiety engages in a water molecule mediated hydrogen bond with Asp^{269}. Four amino acids, Gln^{261}, Leu^{262}, Val^{264} and Tyr^{267} coordinate the adenine group via a network of hydrogen bonds (Figure 1-7b).

PI3Ks (p110s) and PI4KIIα share a common kinase domain arrangement in having an N- and a C-lobe but superimposition of the crystal structure of PI4KIIα kinase domain with those of different type III PI3K isoforms reveals root mean square variations, suggesting significant differences in overall folding patterns. Indeed, PI4KIIα has three insertions that are not found in the kinase domains of PI3Ks. These are I1 and I2 insertions in the N-lobe and I3 in the C-lobe. I1 is inserted between two α-helices in the N-lobe. It contains an amphipathic α-helix and is followed by the palmitoylation motif (Zhou *et al.*, 2014). I2 is also referred to as the RK-insertion due to its abundance of arginine and lysine side chains. It is inserted between two beta strands and comprises one α-helix and two small β-strands. I3 is located between two β-sheets in the C-lobe. In addition, the kinase domain of PI4KIIα also has three loops that are related to kinase activity. These are a glycine rich G-loop,

catalytic loop and the activation loop. The G-loop is reported to bind the phosphate group of nucleotides and shows no consensus between PI3K and PI4KIIα but is conserved among PI4Ks from different organisms.

Also, superimposition of the crystal structure of PI4KIIα catalytic domain with that of PI4KIIIβ revealed structural differences that suggest that the type II family of PI4Ks have a kinase architecture distinct from all other lipid kinase families (Baumlova *et al.*, 2014). Studies using protein databases suggest that PI4KIIα is not evolutionarily linked to lipid kinases but to Ser/Thr kinases including *Helicobacter pylori* pro-inflammatory kinase, Golgi casein Kinase and actin-fragmin kinase (Baumlova *et al.*, 2014; Zhou *et al.*, 2014). The three insertions, I1-I3 are unique to PI4KIIα and do not arise in the afore-mentioned structural analogues.

PI4KIIα behaves like an integral membrane protein (Barylko *et al.*, 2009) but lacks a transmembrane domain. Molecular simulations suggest that PI4KIIα tightly associates with the membrane and the ATP molecule is near the membrane environment. These simulation studies show that post-translational modifications and interactions between amino acid side-chains and the membrane lipid bilayer stabilise membrane insertion of PI4KIIα, a pre-requisite for kinase activity (Barylko *et al.*, 2009; Baumlova *et al.*, 2014).

The *C*-terminal region is also reported to engage in hydrophobic interactions that contribute to membrane binding as *C*-terminal deletion mutants had decreased membrane affinities. This was confirmed by elution from liposomes of these mutant proteins by increasing the pH of elution buffers or concentration of sodium chloride (Zhou *et al.*, 2014). Membrane binding is also dependent on the presence of bulky hydrophobic residues that are located at the membrane-protein interface. Mutation of three amino acid residues with bulky side-chains: Trp^{359}, Tyr^{365} and Trp^{368} was shown to lower kinase activity. PI4KIIα membrane association is further stabilised by electrostatic interactions involving three arginine residues: Arg^{129}, Arg^{275} and Arg^{276} and mutations of these residues to Ala or Gly decrease enzyme activity (Zhou *et al.*, 2014).

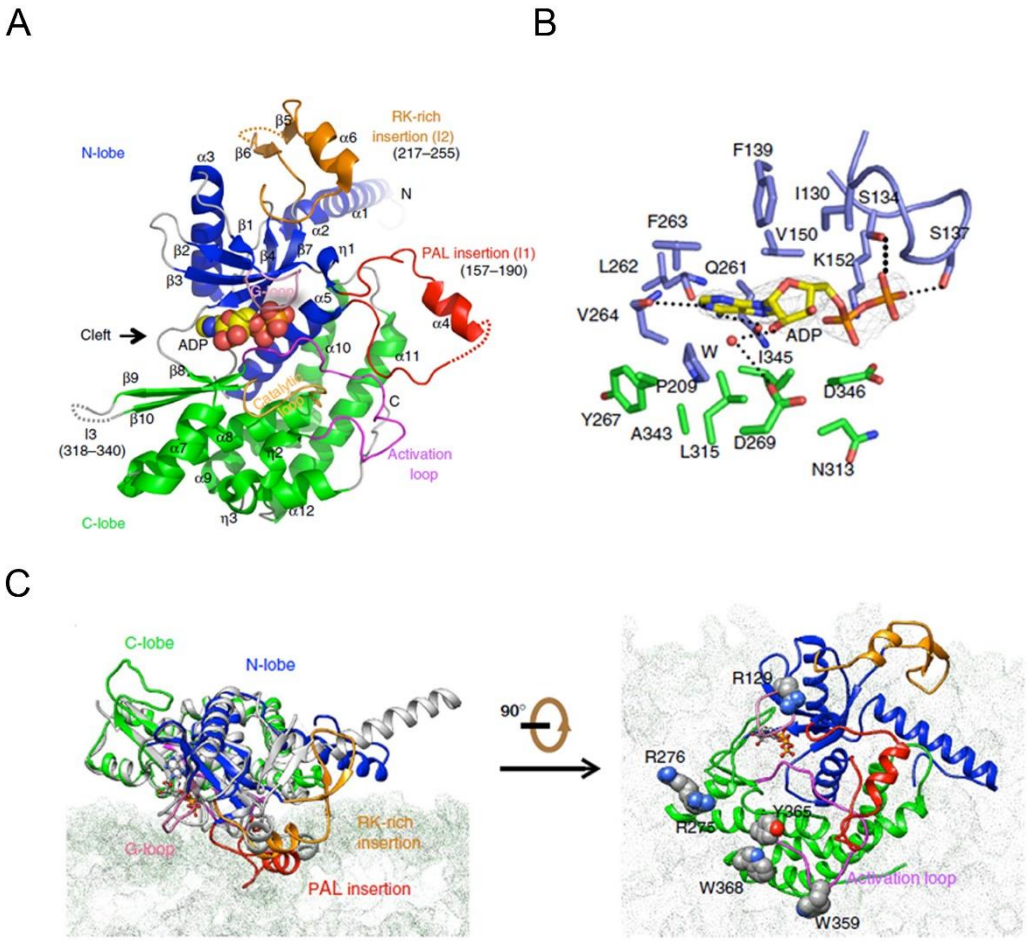

Figure 1-7. Structural and molecular features of PI4KIIα.

A. Cartoon model depicts the overall folding pattern of PI4KIIα kinase domain. **B.** Cartoon model showing the nucleotide binding pocket, interactions between amino acid side chains and ADP. **C.** Molecular simulation experiments reveal putative amino acid side-chains required for membrane association and the folding pattern in a membrane environment. Adapted (with permission) from: *Zhou et al. (2014). Molecular insights into the membrane-associated phosphatidylinositol 4-kinase IIα*.

1.3.1.2 Molecular features of PI4KIIβ

PI4KIIβ is a 55 kDa protein that possesses an overall fold like that of PI4KIIα due to sequence similarity. Both PI4KII isoforms exhibit differences in their N-termini that extend over approximately 1-100 amino acid residues (Figure 1-5). Like PI4KIIα, PI4KIIβ is insensitive to wortmannin, inhibited by micromolar (μM) concentrations of adenosine and has a low K_M for ATP

(Barylko *et al.*, 2001; Minogue *et al.*, 2001). Like PI4KIIα, characterisation of protein structure at the atomic level remained elusive for many years after its initial report. The crystal structure for PI4KIIβ was recently solved using x-ray diffraction (Klima *et al.*, 2015). The authors reported similar difficulties in obtaining pure crystals for the whole protein because of decreased solubility conferred by the disorganised *N*-terminus, leading to truncation of the *N*-terminal amino acid residues (1-89) which are not essential for catalytic activity (Jung *et al.*, 2011). These truncated constructs (90-481 amino acids) also had poor yields in bacteria, leading the authors to generate a construct with a truncated *C*-terminal (amino acid residues 90-450). As was the case with PI4KIIα, these features limited structural studies to the kinase domain. In addition, the CCPCC palmitoylation, which plays a role in membrane insertion, was replaced with a T4 lysozyme. This permitted high purity crystal production, and crystals were resolved at 1.9 Å, the highest resolution reported for a PI4-kinase, in complex with ATP.

Superimposition of the kinase domains of both PI4KIIα and PI4KIIβ reveal a conserved molecular architecture comprising an N-lobe and C-lobe that flank the ATP-binding groove (Figure 1-8, A-C). Like PI4KIIα, the N-lobe comprises two α-helices that surround four anti-parallel β-sheets while the C-lobe comprises two α-helices that surround two anti-parallel β-sheets. The C-lobe also comprises two other distal α-helices that form a scaffold for the catalytically active part of the kinase and may be involved in allosteric regulation of enzyme activity. Within the N-Lobe is a cysteine rich motif (replaced with a T4 lysozyme insertion), which is palmitoylated and required for membrane tethering (Barylko *et al.*, 2009).

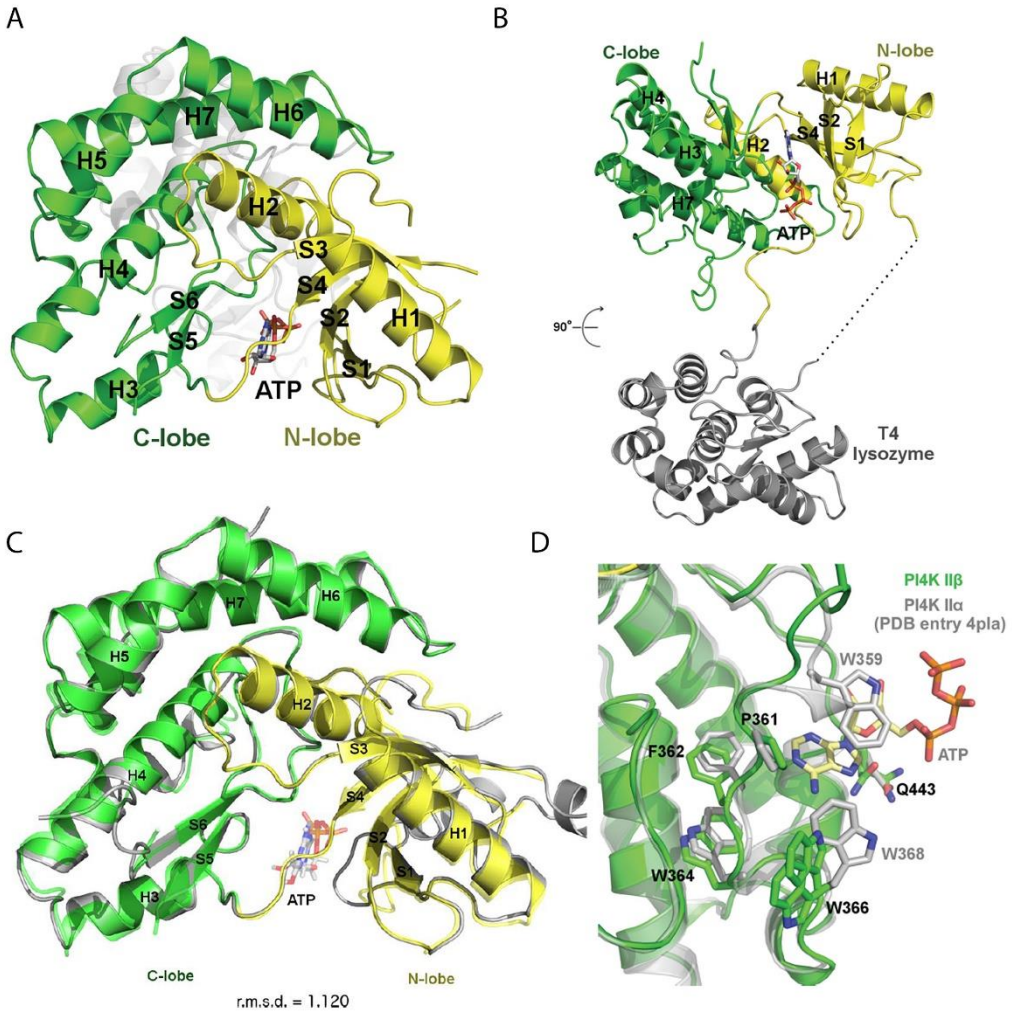

Figure 1-8. Structural and molecular features of PI4KIIβ.

A. Cartoon model representing the catalytic domain of PI4KIIβ, resolved by X-ray diffraction. **B.** Rotation of the kinase domain to illustrate the localisation of the T4 lysozyme insertion required to obtain crystals. **C.** Structural superimposition of the kinase domains of PI4KIIα and PI4KIIβ reveal conserved kinase domain architecture. N- and C-lobes of PI4KIIβ are depicted in yellow and green respectively, whilst PI4KIIα is shown in grey. **D.** Structural superposition of PI4KIIα and PI4KIIβ in the ATP binding site shows a conserved ATP (represented with a stick model) binding mode for both isoforms. *Reproduced with permission of the International union of crystallography.*

Modelling of the catalytic site reveal that ATP is held by a network of hydrogen bonds involving amino acid side chains in both the N- and C-lobes and are organised in a manner like the ATP binding site of PI4KIIα (Figure 1-8D).

The authors also studied the effects of inhibitors by obtaining crystals bound to a nucleoside analogue, MD59, but only succeeded in obtaining crystals with PI4KIIα. This crystal revealed the presence of three pockets proximal to the inhibitor and could be exploited for drug design (Klima *et al.*, 2015). Resolution of the crystal structures of these proteins has opened a new vista in enzymology and drug development. However, subtle differences between the catalytic domains of PI4KIIs, as well as the inability to crystallise the divergent N-termini of the two isoforms imply that the design of an inhibitor with the ability to discriminate between the two isoforms remains a big challenge.

1.3.1.3 Subcellular localisation of mammalian PI4KIIs

Both PI4KII isoforms exhibit some differences in their subcellular localisation. In addition to palmitoylation, PI4KIIα membrane localisation is also controlled by cholesterol content as alteration of membrane cholesterol affects its membrane localisation and lowers its kinase activity (Waugh *et al.*, 2006; Minogue *et al.*, 2010). PI4KIIα is the predominant PI4K activity in mammalian cells and mainly localises to the Golgi. PI4KIIα also localises to endosomal membranes where it regulates processes such as endo-lysosomal traffic of growth factor receptors (Minogue *et al.*, 2006; Henmi *et al.*, 2016), autophagy (Wang *et al.*, 2015) and phagocytosis (Jeschke *et al.*, 2015; Levin *et al.*, 2017). In lymphoid cells, it is trafficked under control of Rab27a from late endosomes to the plasma membrane where it provides PI(4)P for $PI(4,5)P_2$ synthesis: a key step in HIV viral coat packaging (Gerber *et al.*, 2015). PI4KIIα has also been identified on presynaptic vesicles (Salazar *et al.*, 2005), and in nuclear speckles where it may play a part in nuclear calcium signalling (Yoo *et al.*, 2014).

PI4KIIβ associates with membranes via dynamic palmitoylation of multiple cysteine residues within it catalytic domain (Barylko *et al.*, 2001, 2009). Molecular studies reveal that palmitoylation is required for catalytic activity of the type II PI4Ks (Barylko *et al.*, 2001, 2009). In unstimulated cells, approximately 30% of total cellular PI4KIIβ is palmitoylated and distributed

between membrane and cytosolic pools. Heat shock protein, Hsp90 stabilises the cytosolic pool of PI4KIIβ and renders it inactive. Short exposure to Hsp90 inhibitor, geldanamycin, relieves PI4KIIβ of this interaction and leads to palmitoylation, membrane recruitment of PI4KIIβ and synthesis of PI(4)P (Jung *et al.*, 2011). Growth factor stimulation of mammalian cells also induces membrane recruitment of PI4KIIβ. Platelet derived growth factor (PDGF) receptor activation results in the localisation of PI4KIIβ to membrane ruffles in a Rac GTPase dependent manner (Wei *et al.*, 2002). PI4KIIβ also localises to the TGN, where it interacts with AP-1 (Wieffer *et al.*, 2013) and was also reported to associate with tetraspanin, CD81 on non-endosomal vesicles (Mazzocca *et al.*, 2008). The different membrane distributions of PI4KIIs indicate that PI4KIIα is constitutively active in cells while PI4KIIβ is subject to regulation.

1.3.2 Cellular roles of PI4KIIs

PI4KIIs are instrumental in the control of membrane trafficking pathways that mediate cellular events such as the delivery of lysosomal enzymes, autophagy, phagocytosis and surface receptor trafficking. Because of their roles in these cellular processes, perturbation of PI4KII function is associated with pathologies such as rare hereditary disorders, neuropathies and certain human cancers.

1.3.2.1 Membrane recruitment of clathrin adaptors

PI4KIIα is a major contributor to *trans*-Golgi pools of PI(4)P and its depletion by siRNA delocalises the clathrin adaptor and PI(4)P effector, AP-1 from the TGN; however, the PI4KIIα/AP-1 interaction has not been identified in other studies (Craige *et al.*, 2008; Mössinger *et al.*, 2012; Wieffer *et al.*, 2013). PI4KIIα forms a direct complex with AP-3 via a dileucine motif ($E^{57}RQPLL^{62}$) and co-purifies with AP-3 containing vesicles along with AP-3 cargoes (Salazar *et al.*, 2005; Craige *et al.*, 2008). PI4KIIα and AP-3 exhibit a reciprocal interaction as the normal steady-state localisation of PI4KIIα is AP-3 dependent while the catalytic activity of PI4KIIα is required for AP-3 trafficking (Salazar *et al.*, 2005). PI4KIIβ also localises to the TGN, where it

significantly colocalises with AP-1. Like PI4KIIα, PI4KIIβ possesses an *N*-terminal dileucine motif ($E^{26}REPLL^{30}$) that binds AP-1, forming a complex that localises PI4KIIβ to the TGN. Conversely, PI4KIIβ depletion by siRNA delocalises AP-1 from the TGN (Wieffer *et al.*, 2013), indicating a reciprocal relationship reminiscent of that between PI4KIIα and AP-3. This indicates that PI4KII isoforms operate in separate TGN trafficking pathways by recruiting separate PI(4)P binding clathrin adaptors.

The GGAs are a family of clathrin adaptors that mediate TGN-endosome traffic. These proteins require PI(4)P (and Arf1) for TGN localisation and PI4KIIα depletion results in their delocalisation (Wang *et al.*, 2007). Thus, the kinase activity of PI4KIIα is a major determinant for TGN recruitment of different clathrin adaptors.

1.3.2.2 Regulation of endosomal trafficking

PI4KIIα controls early endosomal sorting and degradative trafficking of the EGFR (Minogue *et al.*, 2006). A recent study also showed that PI4KIIα is recruited onto early endosomes following depletion of PI3P by MTM, permitting the recruitment of components of the exocyst complex that regulates retrograde traffic from early endosomes (Ketel *et al.*, 2016). Both PI4KII isoforms control lysosomal traffic of the cation-independent mannose 6-phosphate receptor (CI-M6PR), which delivers soluble hydrolases and membrane proteins to endosomes. CI-M6PR is an AP-1 cargo (Chi *et al.*, 2008; Anitei *et al.*, 2014) that is trafficked to late endosomes via an AP-3 dependent pathway (Jović *et al.*, 2012). Consequently, PI4KIIβ generates a pool of PI(4)P that regulates AP-1 mediated TGN sorting of the mannose 6-phosphate receptor (Wieffer *et al.*, 2013) while PI4KIIα generates a PI(4)P pool that regulates AP-3 dependent late endosomal traffic (Salazar *et al.*, 2005). PI4KIIα is required for the TGN to endosome traffic of β-glucoceribrosidase (GBA) and its receptor, an AP-3 cargo, LIMP-2 (Jović *et al.*, 2012). Depletion of PI4KIIα results in lysosomal accumulation of glucoceribrosides and secretion of GBA (Jović *et al.*, 2012).

Phagocytic cells utilise late endosomes for the lysosomal delivery of cell debris and internalised pathogens. In these events, PI4KIIα is recruited onto phagocytic membranes where its PI(4)P product has been proposed to mediate heterotypic fusion with lysosomes possibly via the recruitment of the Rab7 effector, RILP (Jeschke *et al.*, 2015; Levin *et al.*, 2017). The interaction between PI4KIIα and the Atg8 family member, γ-amino butyric acid receptor associated protein (GABARAP) has also been described in the control of heterotypic phagosome-lysosome fusion (Wang *et al.*, 2015). PI4KIIα depletion or overexpression of a kinase dead PI4KIIα mutant alters autophagosome morphology, phenocopying GABARAP depletion and can be rescued with re-expression of PI4KIIα or restoration of PI(4)P (Wang *et al.*, 2015). PI4KIIα is also trafficked from late endosomes to the plasma membrane, in a Rab27a mediated pathway in $CD4^+$ T-lymphocytes for the rate limiting production of PI(4)P in the synthesis of $PI(4,5)P_2$: a requirement for HIV-1 viral assembly at the plasma membrane (Gerber *et al.*, 2015).

1.3.2.3 Roles in intracellular signalling

PI4KIIα is required for sorting of the EGF receptor (EGFR) to late endosomes and subsequent degradation in lysosomes (Minogue *et al.*, 2006; Henmi *et al.*, 2016), having multiple consequences in EGFR signalling (Taub *et al.*, 2007; Murphy *et al.*, 2009; Platta and Stenmark, 2011). PI4KIIα has also been implicated in the early events of canonical Wnt signalling by promoting local synthesis of PI(4)P at the plasma membrane and regulating the formation of Wnt induced LRP6 aggregates in mammalian cells (Pan *et al.*, 2008; Qin *et al.*, 2009). PI4KIIα also regulates Wnt signalling via an early endosomal complex with the E3-ubiquitin ligase, Itch. This complex facilitates degradative sorting of internalised frizzled 4 (Fz4) receptors thereby downregulating canonical Wnt signalling (Mössinger *et al.*, 2012).

PI4KIIβ also regulates canonical Wnt signalling in zebrafish embryos in an AP-1 dependent manner (Wieffer *et al.*, 2013). PI4KIIβ regulates the endosomal recycling of Fz in the canonical Wnt signalling pathway which is linked to certain human cancers (Moon, 2005). Growth factor mediated

recruitment of PI4KIIβ to the plasma membrane is suggestive of a role in mitogenic signalling where PI4KIIβ possibly provides PI(4)P for second messenger synthesis (Wei *et al.*, 2002). Another study described PI4KIIβ as a negative regulator of chemotactic induced migration in HepG2 cells, a feature underlying metastasis. Through its interaction with the tetraspanin, CD81, PI4KIIβ orchestrates the formation of non-endosomal vesicles that sequester the actin binding protein, actinin-4, thereby altering cytoskeletal assembly, consequently preventing the migration of tumour cells (Mazzocca *et al.*, 2008). PI4KIIβ has also been described in tyrosine kinase pathways in response to T-cell activation (Sinha *et al.*, 2013) while its association with nucleoplasmic storage vesicles suggests it (along with PI4KIIα) plays a role in nuclear calcium signalling (Yoo *et al.*, 2014).

1.3.3 PI4KIIs in health and disease

The roles of these isoforms in membrane trafficking and cell signalling may underlie the mechanisms of some human diseases especially when dysregulated. For instance, increased expression of PI4KIIα has been described in some cancer types such breast carcinoma, fibrosarcomas and malignant melanomas (Li *et al.*, 2010). Down-regulation of PI4KIIα activity reduces xenograft induced tumour growth in mice, in a series of events that involve repression of hypoxia inducible factor 1α (HIF-1α) –a feature that regulates angiogenesis in tumours (Li *et al.*, 2010). PI4KIIβ is implicated in certain human cancers and its strong expression in the liver (Balla *et al.*, 2002; Guo *et al.*, 2003) suggests an anti-metastatic role in hepatocellular carcinoma (HCC; (Mazzocca *et al.*, 2008)). Although PI4KIIβ was described as a negative regulator of HCC cell motility (Mazzocca *et al.*, 2008), its anti-metastatic role remains unclear.

Beyond their purported roles in the pathology of certain cancers, PI4KIIs are also described in other human disorders. For instance, PI4KIIα along (with another Golgi PI4K, PI4KIIIβ) regulates trafficking of the Gaucher's disease enzyme, GBA from the Golgi to lysosomes. This results in the secretion of GBA into the medium, a characteristic phenotype of Gaucher's disease

characterised by symptoms such as hepatomegaly, splenomegaly, erosion of long bones and mental retardation in infants (Jović *et al.*, 2012). Some studies describe either PI4KII isoform in neurological disorders including bipolar disorder, age-related neurodegeneration and Alzheimer's disease (Houlihan *et al.*, 2009; Simons *et al.*, 2009; Kang *et al.*, 2013). Studies in mouse models show that loss of PI4KIIα results in a late-onset neurodegenerative disorder characterised by loss of cerebellar Purkinje cells and deterioration of spinal axons (Simons *et al.*, 2009). Although this feature has not been described in humans, the symptoms resemble those observed in hereditary spastic paraplegia (Simons *et al.*, 2009). Other studies also showed that PI4KIIα (Guo *et al.*, 2003) is enriched in the brain and its expression inversely correlates with amyloid β-protein secretion (Kang *et al.*, 2013). Perturbation of membrane cholesterol alters PI4KIIα membrane localisation and activity (Waugh *et al.*, 2006; Minogue *et al.*, 2010; Kang *et al.*, 2013) thereby permitting secretase mediated cleavage of β-amyloid precursor protein (APP), an underlying feature of Alzheimer's disease (Kang *et al.*, 2013). The PI4KIIβ gene lies within chromosome 4p15-p16, which is linked with bipolar disease and recurrent depression within a Scottish family. However, genomic analysis using SNPs and expression studies (mRNA and protein) revealed no significant differences in PI4KIIβ levels between bipolar and normal patients. Despite the lack of statistical significance, data from the study reveal that the PI4K2B gene may, nonetheless play a significant role in schizophrenia (Houlihan *et al.*, 2009).

PI(4)P serves as an anchor that facilitates pathogenic invasion of mammalian cells (Hilbi *et al.*, 2011; Hammond *et al.*, 2014; Luo *et al.*, 2015). Despite the higher kinase activities of PI4KIIs, most studies attribute PI(4)P-mediated pathogen entry to PI4KIIIs (Berger *et al.*, 2011; Reiss *et al.*, 2013; Bojjireddy *et al.*, 2014). The use of TGN and endosomal membrane PI(4)P pools as points of anchorage for the pathogen's accessory proteins is suggestive of roles for this family of lipid kinases in the development of microbial infections in mammalian cells. In addition, PI4KIIs have also been implicated in immune responses and diseases which sabotage the immune system. PI4KIIα is recruited to the PM where it catalyses the rate limiting synthesis of PI(4)P for

$PI(4,5)P_2$ dependent HIV coat particle packaging in infected $CD4^+$ T-lymphocytes and macrophages (Gerber *et al.*, 2015) and may thus serve as a druggable target in HIV infections. Recent studies also implicate PI4KIIα dependent PI(4)P production in various steps of phagocytosis (Levin *et al.*, 2017) and in the regulation of phagosome-lysosome fusion (Jeschke *et al.*, 2015; Wang *et al.*, 2015), indicating a role for this enzyme in the innate immune response. PI4KIIβ may also be involved innate immune responses as it has been described in the early phases of phagosome maturation in macrophages (Jeschke *et al.*, 2015). It has also been implicated in other immune responses involving T-lymphocytes and may contribute to the anti-tumour response by $CD4^+$ T lymphocytes (Griffioen *et al.*, 2008; Sinha *et al.*, 2013). A previous study also showed that both PI4KIIs promote AP-1 dependent internalisation of *Listeria monocytogenes* in LoVo and HeLa cells (Pizarro-Cerdá *et al.*, 2007), thereby implicating both enzymes in phagocytosis.

1.4 Research Background/Aims and Objectives

1.4.1 Background

This project is concerned with the PI4KIIs, specifically the less well-characterised beta isoform that was identified based on homology with the alpha isoform (Minogue *et al.*, 2001). Both proteins have been linked to the TGN and endosomal membranes and coordinate trafficking pathways emanating from or terminating at these subcellular compartments. It is well known that interfering with functions of these enzymes leads to trafficking defects that affect important functions such as downregulation of EGFR signalling. However, most of these trafficking defects are attributable to PI4KIIα while the roles of PI4KIIβ are often overlooked or sometimes conflated with those of PI4KIIα. As described previously, only a few cellular roles are attributable to this isoform and this may be, partly because ~50% of the cellular pools of PI4KIIβ is non-membrane associated and thus catalytically inactive.

Previous data from our lab implicated PI4KIIα in a pathway that controls lysosomal traffic of the EGFR (Minogue *et al.*, 2006). Subsequent work demonstrated that PI4KIIα depletion by RNAi impedes EGFR degradation via the lysosomal pathway, thereby sustaining receptor activation and downstream phosphorylation of signalling targets (Minogue, unpublished). Interestingly, knockdown of the beta isoform more potently sustained signalling through the MAPK pathways (unpublished). EGFR signalling is regulated by clathrin-mediated endocytosis and trafficking via the endo-lysosomal route for degradation of activated receptor (Vieira *et al.*, 1996; Ceresa and Bahr, 2006; Sun *et al.*, 2013). The consequence of dysregulation of this pathway is increased proliferation, motility and invasiveness, features that underlie the mechanisms of angiogenesis and metastatic dissemination of tumour cells (Prenzel *et al.*, 2001; Herbst and Bunn, 2003). The involvement of both enzymes in regulating EGFR trafficking to the lysosomal compartment and its signalling pathway suggests that one or both may serve as tumour suppressors. The outstanding questions are:

1. Do both isoforms localise to similar membranes?

2. If they do, are they on similar or distinct membrane domains?

3. How do PI4KIIα and PI4KIIβ regulate trafficking pathways from their associated membrane compartments. Do they operate differently or have a similar point of convergence?

4. What are the phenotypic outcomes of impaired membrane trafficking following loss of function of either isoform?

1.4.2 Aims and Objectives

The overall aim of this thesis was to delineate the non-redundant (and redundant) cellular roles of PI4KII isoforms PI4KIIα and PI4KIIβ in mammalian cells. This was particularly important in identifying unique roles for PI4KIIβ to which only a few cellular roles have been ascribed. As such, the following chapters in this thesis will outline approaches to address the following aims:

1. To define membrane localisation of both isoforms in a mammalian cell line using fluorescent imaging.
2. To determine optimum conditions for specific depletion of either isoform using RNA interference.
3. To identify specific membrane pools of PI(4)P attributable to either isoform.
4. To explore major membrane trafficking pathways coordinated by these isoforms.
5. To observe effects of depletion of either isoform on overall cellular behaviour such as regulation of cell shape and migratory potential.
6. To explore the association of these two enzymes with human cancers.

Chapter 2 Materials and Methods

2.1 Reagents and chemicals

2.1.1 Buffers and solutions

Buffer solutions for specific experiments are mentioned in relevant sections. Unless otherwise stated, solutions were prepared with ultrapure water (18.2 mΩ).

2.1.2 Molecular weight markers

- 0.1-10 kb Ladder (Invitrogen)
- 1 kb Ladder (Invitrogen)
- ProtoMarkers, pre-stained protein standards (National Diagnostics)
- Biotinylated ladder (Cell Signalling Technology, Inc.)
- Precision plus protein™ All Blue standards (Bio-Rad Laboratories)

2.1.3 Antibodies

All primary antibodies were used at dilutions for specific applications as demonstrated by the manufacturers (Table 2-1). For immunoblotting, antibodies were diluted in 1% BSA+TBST or non-fat milk (for non-phosphorylated proteins). Horseradish peroxidase (HRP)-linked antibodies and Alexa-Fluor® conjugates were used as secondary antibodies in immunoblotting and immunofluorescent labelling respectively (Table 2-2).

Table 2-1. Primary antibodies

Antibody	Host	Clonality	Supplier	Dilutions		
				IF[2]	**WB**[3]	**FC**[4]
CD63	Mouse	Monoclonal	BD Pharmingen (BD, Oxford, England)	1:400		
Cortactin (H222)	Rabbit	Polyclonal	Cell Signalling (New England Biolabs, UK)	1:100	1:1000	
EEA1 (C45B10)	Rabbit	Monoclonal	Cell Signalling	1:100		
EGF Receptor(D38B1)	Rabbit	Monoclonal	Cell Signalling		1:1000	
GAPDH (14C10)	Rabbit	Monoclonal	Cell Signalling		1:1000	
GFP (D5.1)	Rabbit	Monoclonal	Cell Signalling		1:1000	
GGA1	Rabbit	Polyclonal	ThermoFisher (Fischer Scientific, UK)	1:50		
GGA2	Rabbit	Polyclonal	ThermoFisher	1:200		
GST (26H1)	Mouse	Monoclonal	Cell Signalling	1:800		
HA-Tag (6E2)	Mouse	Monoclonal	Cell Signalling	1:100	1:1000	
MT1-MMP [LEM-2/63.1] (ab78738)	Mouse	Monoclonal	Abcam (Cambridge, UK)	1:400		
MT1-MMP (ab3644)	Rabbit	Polyclonal	Abcam	1:100	1:500	1:50
MT1-MMP [LEM-2/15.8]	Mouse	Monoclonal	Merck (Darmstadt, GmBH)	1:50	1:500	
p44/42 MAPK (Erk1/2) #9102	Rabbit	Polyclonal	Cell Signalling		1:1000	
Phospho p44/42 MAPK (Thr202/Tyr204)	Rabbit	Polyclonal	Cell Signalling		1:1000	

[2] IF-Immunofluorescence microscopy
[3] WB-Western blotting
[4] FC-Flow cytometry

Phospho-EGF Receptor (Tyr1068) (D7A5)	Rabbit	Monoclonal	Cell Signalling		1:1000	
Phosphotyrosine (P-Tyr-100)	Mouse	Monoclonal	Cell Signalling	1:1600	1:2000	
PI4KIIα	Mouse	Monoclonal	Shane Minogue (UCL)	1:6	1:2	
PI4KIIβ	Rabbit	Polyclonal	Sigma-Aldrich	1:32	1:250	
Rab11 (D4F5)	Rabbit	Monoclonal	Cell Signalling	1:100		
Rab5 (C8B1)	Rabbit	Monoclonal	Cell Signalling	1:200		
Rab7 (D95F2)	Rabbit	Monoclonal	Cell Signalling	1:100		
Rab8 (D22D8)	Rabbit	Monoclonal	Cell Signalling	1:200		
Rab9 (D52G8)	Rabbit	Monoclonal	Cell Signalling	1:100		
Rac1 (ARCO3)	Mouse	Monoclonal	Cytoskeleton Inc	1:20		
Syntaxin 6 (C34B2)	Rabbit	Monoclonal	Cell Signalling	1:100		
TGN46	Sheep	Polyclonal	AbD Serotec (Now BioRad)	1:250		
α-Tubulin	Mouse	Monoclonal	Molecular Probes (Fischer Scientific, UK)		1:2000	
β1-Integrin (CD29)	Mouse	Monoclonal	BD Biosciences (BD, Oxford, England)	1:100	1:1500	
γ-Adaptin (AP-1)	Mouse	Monoclonal	Sigma-Aldrich	1:200		

Table 2-2. Secondary antibodies

Secondary Antibody	Host	Clonality	Supplier	Dilutions		
				IF	WB	FC
Alexa Fluor®conjugated anti-mouse IgG	Goat	Polyclonal	Molecular Probes	1:500		
Alexa Fluor®conjugated anti-rabbit IgG	Goat	Polyclonal	Molecular Probes	1:500		1:500
Alexa Fluor®conjugated anti-Sheep IgG	Donkey	Polyclonal	Molecular Probes	1:500		
HRP-linked anti-Biotin	Horse	Polyclonal	Cell Signalling		1:1500	
HRP-Linked anti-mouse IgG	Horse	Polyclonal	Cell Signalling		1:1500	
HRP-Linked anti-Rabbit IgG	Goat	Polyclonal	Cell Signalling		1:1500	

2.1.4 siRNA

ON-TARGET*plus* SMARTpool™ siRNA oligonucleotides from Dharmacon™ (GE Healthcare) were used to deplete PI4KIIα and PI4KIIβ in mammalian cells. These were sold as sets of four siRNA duplexes targeting different sequences within the primary transcripts of named genes (Table 2-3). In addition, a non-targeting siRNA oligo was procured and used for control experiments. The following siRNA oligonucleotides were used for rescue experiments: PI4KIIα, GGAUCAUUGCUGUCUUCAAUU (Mössinger *et al.*, 2012), PI4KIIβ, GGUUCAAGUGGAAGUUACUUU (Wieffer *et al.*, 2013). Stocks (20 µM) were prepared by resuspending the siRNA oligos in 1x RNA resuspension buffer and 50 µl aliquots were stored at -20^{o}C.

Table 2-3. siRNA oligonucleotide information

Target gene	siRNA sequence (5'-3')	Target Region in primary transcript
PI4K2A	GGUUGGUGGUGCUGGAUUA	944-962
	CAACACUGAUCGAGGCAAU	972-990
	GAGACGAGCCCACUAGUGU	64-82
	GCAUCGGGCUACCACCAAA	806-824
	GGAUCAUUGCUGUCUUCAA[5]	594-512
PI4K2B	GGUAGUAAAUGUCAGAGUA	1575-1593
	GUUACAAGGAGGCUGAAUA	918-936
	UGGUUUGGCUUGUCAGUGA	759-777
	UCUCAAGGUUCAAGUGGAA	512-530
	GGUUCAAGUGGAAGUUACUU[6]	518-537

2.1.5 Plasmids

pCIpreEGFP-CIMPR$_{tail}$ was the generous gift of Dr Mihaela Anitei, (Technische Universität Dresden, Germany). This construct encodes a chimeric protein composed of a signal peptide and 21 residues from the *N*-terminal of preproglucagon, the complete EGFP, a linker sequence (6 residues), and the transmembrane and cytoplasmic domains of CI-M6PR. The mCherry tagged version of this chimeric protein was also provided by Dr Mihaela Anitei. This was generated by cutting the EGFP ORF from pCIpreEGFP-CIMPR$_{tail}$ as well as cutting the mCherry ORF from the pmcherry-C1 (Clonetech) via Age1 and XhoI restriction sites and ligating the two fragments (Waguri *et al.*, 2003).

GFP-tagged-human-PI4KIIα was generated by ligating human PI4K2A cDNA into a pEGFP-CI vector (Minogue *et al.*, 2006). A mouse PI4K2A gene fused into a pcEGFP-Ml vector and wild-type rat PI4K2B fused into a pcEGFP-Ml

[5] Single oligo used for rescue experiments.
[6] Single oligo used for rescue experiments.

vector were kindly provided by Prof Volker Haucke (Leibniz Institut für Molekulare Pharmakologie, Berlin, Germany). The resulting constructs encode chimeric proteins that are resistant to single siRNA oligonucleotides targeting human PI4KIIα (Mössinger *et al.*, 2012) or PI4KIIβ (Wieffer *et al.*, 2013) and were thus used for rescue experiments.

Table 2-4. Plasmids

Plasmid construct	Vector Backbone	Antibiotic resistance
EGFP-CI-M6PR	pCIneo	Kanamycin
mCherry-CI-M6PR	pCIneo	Kanamycin
GFP-PI4KIIα (WT)	pEGFP-CI	Kanamycin
GFP-PI4KIIα (siRNA resistant)	pcEGFP-MI	Ampicillin
HA-PI4KIIβ (siRNA resistant)	pc-HA-MK	Ampicillin

2.1.6 Antibiotics, inhibitors and other reagents

All reagents were solubilised in specified solvents and stored at 4^{o}C or -20^{o}C as specified.

Table 2-5. Dilutions of inhibitors used

Reagent	Supplier	Solvent	Stock Solution	Final concentration	Type
Cycloheximide	Sigma Aldrich	DMSO	1 mg/ml	200 µg/ml	Inhibitor of protein synthesis
Complete Mini (EDTA Free)	Roche	ddH_20	1 mM	1 µM	Protease inhibitor cocktail
PhoSTOP	Roche	ddH_20	I mM	1 µM	Phosphatase inhibitor
Sodium OrthoVanadate	Sigma Aldrich	ddH_20	200 mM	0.2 mM	Phosphatase inhibitor

Wortmannin	Merck (Darmstadt, GmBH)	DMSO	5 mM	10 µM	PI3K and Type III PI4K inhibitor

Table 2-6. Reagents used

Reagent	Supplier	Solvent	Stock Solution	Final concentration	Type
Albumin from Bovine serum	Sigma Aldrich	PBS or TBST	-	Assay dependent	Blocking agent
BCA protein reagent	Bio-Rad	-	-	Assay dependent	Protein stain
Digitonin	Merck (Darmstadt, GmBH)	DMSO	20 mM	20 µM	Detergent
DMSO	Sigma Aldrich	-	-	Variable	Solvent /Cryoprotectant
EGF (murine)	Sigma Aldrich		100 µg/ml	100 ng/ml	Growth Factor
Fluorescein Isothiocynate (FITC)	Sigma Aldrich	Sodium Borate	-	0.03 mg/ml	Fluorescent dye
Foetal Bovine Serum	Sigma Aldrich	DMEM	Variable	Variable	Cell culture supplement
Form-aldehyde	Polysciences (Eppelheim, GmBH)	ddH_20	16% (w/v)	2-4% (v/v)	Fixative
Gelatin from porcine skin	Sigma Aldrich	PBS	2% (w/v)	0.2% (w/v)	Extracellular matrix protein
Glutar-aldehyde	Sigma Aldrich	ddH_20	25% (w/v)	0.02% (v/v)	Fixative
Hoechst 33342	Molecular Probes	-	-	1:5000	Fluorescent dye
LB-Agar	Sigma Aldrich	ddH_20	-	35 g/L	Bacterial growth medium
LB-Broth	Sigma Aldrich	ddH_20	-	20 g/L	Bacterial growth medium
Phalloidin, Alexa-Fluor conjugates	Molecular Probes	Methanol	200 units/ml (6.6 µM)	1 unit	Fluorescent dye

Phorbol 12-myrsitate 13-acetate (PMA)	Sigma Aldrich	DMSO	0.5 mg/ml (w/v)	50 ng/ml	Protein kinase C agonist
PI(4)P Grip (GST-SidC-3C)	Echelon Biosciences	ddH_20	2.5 µg/ml	0.5 µg/ml	PI(4)P probe
ProLong® Gold Antifade Mountant	Molecular Probes	-	-	-	Liquid mountant
Saponin	Sigma Aldrich	ddH_20	5% (v/v)	0.1% (v/v)	Detergent
SDS	Sigma Aldrich	ddH_20	20% (v/v)	Variable	Detergent
Sodium Borohydride	Sigma Aldrich	PBS	-	0.1% (w/v)	Quenching agent
Triton X-100	Sigma Aldrich	ddH_20	1% (v/v)	0.05% (v/v)	Detergent
Tween-20	Sigma Aldrich	-	Assay dependent	Assay dependent	Detergent
Type I Collagen, from Rat tail	Molecular Probes	Acetic acid	-	Assay dependent	Extracellular matrix protein

2.2 Experimental procedures

2.2.1 Cell culture manipulations

2.2.1.1 Cell culture

HeLa, MCF-7 and MDA-MB-231 cell-lines were all purchased from the European collection of authenticated cell cultures (ECACC). 1C4 monoclonal antibody-secreting hybridomas were obtained from Shane Minogue (UCL)[7]. Frozen vials of cells were thawed in a 37^{O}C water bath for one minute and immediately transferred to a 15 ml centrifuge tube containing 9.5 ml complete medium. This was followed by centrifugation at 300$\times$g for three minutes. Cryoprotectant (DMSO) was removed by gentle aspiration and the cell pellet was re-suspended in 12 ml, complete medium. This was then transferred to a culture flask and maintained under standard conditions of temperature, humidity and CO_2 concentration. HeLa and MCF-7 cells were cultured in Dulbecco's modified Eagle's medium (DMEM) supplemented with 10% foetal bovine serum (FBS) and antibiotics (1000 U/ml penicillin and 0.1 mg/ml streptomycin; Sigma) and were maintained at 37ºC, 5% CO_2.

MDA-MB-231 cells, on the other hand, were cultured in Leibowitz's L-15 medium (Gibco®) supplemented with 15% FBS and maintained at 37ºC and 0.1% CO_2 as the medium is modified for culture in a low CO_2 environment. L-15 media were also supplemented with 2 mM L-Glutamine and antibiotics (1000 U/ml penicillin and 0.1 mg/ml streptomycin).

Cell growth was routinely monitored by phase-contrast microscopy and cells were sub-cultured (passaged) after three to four days in culture. To minimise overcrowding, cells were routinely passaged. This involved removal of growth media followed by two rinses with 1X-PBS and then incubation with 2 ml dissociation reagent (Gibco®). Cells were detached after five minutes at 37ºC

[7] 1C4 hybridoma cell lines were generated by Dr Claudia Weildermann.

and re-suspended in 8 ml complete medium. All cell cultures were kept at low passages (max p25) to minimise unwanted changes to the cells.

Cell stocks were prepared following a full passage by re-suspending cells in freezing medium, culture medium plus 20% FBS and 10% DMSO (cryoprotectant) and making 1.5 ml aliquots in freezing vials. Vials were slow-frozen at -80^{o}C in isopropanol-containing freezing boxes for 24-48 hours followed by storage in liquid nitrogen.

Table 2-7. Media composition for HeLa and MCF-7 cells

Media Components	Amount
Dulbecco's Modified Eagle's medium (Gibco)	500 ml
Penicillin/Streptomycin (Sigma-Aldrich)	1% (v/v)
Foetal Bovine Serum (Sigma-Aldrich)	5% (v/v)

Table 2-8. Media composition for MDA-MB-231 cells

Media Components	Amount
Leibowitz L-15 medium (Gibco)	500 ml
Penicillin/Streptomycin (Sigma-Aldrich)	1% (v/v)
L-Glutamine (Gibco)	2 mM
Foetal Bovine Serum (Sigma-Aldrich)	15% (v/v)

2.2.1.2 Mycoplasma screening

The LookOut® Mycoplasma PCR detection kit (Sigma) was routinely used to ensure cell cultures were free of contamination from Mycoplasma and related species. Briefly, approximately 200 µl of cell culture was collected from each culture flask, heated at 95-100^{o}C to remove inactivating substances. Aliquots (2 µl) of the supernatant were then added to PCR tubes containing the master –mix of primers, Mg^{2+}, dNTPs and JumpStart™ Taq polymerase (Sigma). The reaction was setup for 40 cycles after which amplicons were analysed

by agarose Gel electrophoresis. The presence of a band at approximately 250 bp indicates the presence of contamination while the intensity determines the degree of mycoplasma contamination. Potential contamination was also monitored by fluorescence microscopy. Cells were routinely labelled with the nuclear stain, Hoechst 33342 hydrochloride which labels both the host and pathogenic DNAs.

2.2.1.3 Production of monoclonal antibodies

Frozen vials of 1C4 producing mouse hybridoma cells retrieved from liquid nitrogen and immediately thawed at 37^{o}C. These were then reconstituted in 9.5 ml complete medium and spun down at 800$\times$g for five minutes. Supernatants were removed and cells were re-suspended in fresh medium. This was followed by plating onto T-75 culture dishes and maintenance at 37^{o}C, 5% CO_2 with passages at every three to five days. Culture supernatants (which contain the secreted antibodies) were retained after each passage.

Table 2-9. Media composition for hybridoma cell culture

Media Components	Amount
RPMI (Gibco)	500 ml
Penicillin/Streptomycin (Sigma-Aldrich)	1% (v/v)
DomaDrive (Immune Systems, UK)	10% (v/v)

2.2.1.4 Culture on gelatin matrices

To coat each well of a 6-well plate with gelatin (Sigma-Aldrich), 2 ml 0.2% gelatin (w/v in PBS) was applied to each well and incubated for 10 minutes at 4^{o}C on a rocking platform to allow solidification. Excess gelatin was aspirated and then 2 ml 0.5% glutaraldehyde (v/v, in PBS) was pipetted into each well of a 6-well plate followed by incubation for 30 minutes at 4^{o}C with gentle rocking. Each well was subsequently washed three times with PBS followed by equilibration with culture medium at 37^{o}C for 30 minutes prior to cell seeding.

2.2.1.5 RNA interference and siRNA-resistant plasmid rescue experiments

Procedure

The day before transfection (day 0), cells were detached, seeded into wells of culture plates and cultured at 37^{o}C for 12 to 16 hours. On the transfection day (day 1), transfection reagent from two tubes, one containing siRNA oligos in serum free medium (tube 1) and the other containing transfection reagent (DharmaFECT4) in serum free medium (tube 2). Following five-minute incubation at room temperature, contents of both tubes were combined and incubated for 20 minutes to obtain the transfection mix (Table 2-10).

Culture medium was removed from culture plates, and cells rinsed twice with 1X PBS. Cells were then treated with the transfection mix along with complete medium (10% FBS+DMEM) in the absence of antibiotics. Cells were cultured for 4-6 hours at 37^{o}C after which transfection medium was removed and replaced with complete medium without antibiotics (Penicillin/Streptomycin). Gene silencing was confirmed by western blotting of cell lysates, 72-hours post-transfection.

Gene expression was rescued by transfecting 30% confluent monolayers with ~ 25 nM single siRNA oligos (see 2.1.4 above) using DharmaFECT4 as described previously. Transfection was repeated after 48 hours in culture along with or without the siRNA resistant plasmids to the transfection mix using the Lipofectamine2000 protocol (Invitrogen; Table 2-11). Four hours post transfection, medium was replaced with fresh complete medium and cells were cultured for 24 hours prior to analysis.

Controls

Gene silencing validation experiments comprised the following samples in triplicate:

1. Desired test siRNA (PI4KIIα and PI4KIIβ)
2. Negative control (GAPDH siRNA)
3. Non-targeting control (Scrambled siRNA)

We routinely used the scrambled siRNA as control for all experiments.

Table 2-10. Volumes per well for transfecting siRNA (at 25 nm final concentration) in different plate formats

	Tube 1: siRNA (µl/well)		Tube 2: DharmaFECT (µl/well)			
Culture Vessel	**Volume of 5µM siRNA (µl)**	**Serum-free Medium (µl)**	**Volume of DharmaFECT reagent (µl)***	**Serum-free Medium (µl)**	**Complete Medium (µl/well)**	**Total Transfection volume (µl/well)**
24-well plate	2.5	47.5	0.25-2.5	47.5-49.75	400	500
6-well plate	10	190	1.0-10.0	190-199	1600	2000
35 mm dish	10	190	1.0-10.0	190-199	1600	2000
60 mm dish	20	380	2.0-20.0	380-398	3200	4000

*Volumes for DharmaFECT™ were optimised for different cell-lines and plate formats. We arrived at optimal volumes of, 1.2, 6.0 and 10.0 µl for 24-, 6-well plates (as well as 35 mm dish) and 60 mm dishes respectively. Adapted from Dharmacon™ (GE healthcare).

2.2.1.6 Determination of cell proliferation using the thiazolyl blue tetrazolium bromide (MTT) assay.

This is a colorimetric assay for estimating metabolic activity and therefore proliferation. It is based on the ability of mitochondrial dehydrogenases to convert MTT, a yellowish solution, into dark-blue, water insoluble MTT-

formazan crystals. These blue crystals are solubilised into acidified isopropanol and intensity is measured spectrophotometrically at 570 nm (Mosmann, 1983). In details, 5 mg/ml (w/v in PBS) MTT solution was applied 1:10 in culture medium (without phenol red) to cells seeded at 5×10^5/ml and incubated at 37^{O}C for two hours. Culture medium was removed from cells and then converted MTT dye was dissolved in acidic isopropanol (0.04 M HCl in absolute isopropanol). This was followed by a 30-minute incubation at 37^{O}C. The dissolved dye was subsequently transferred into a 1.5 ml centrifuge tube and spun at 13,000 rpm for two minutes. Supernatants were transferred into 1 ml disposable cuvettes (1 cm path-length) and the absorbance of converted dye was measured at 570 nm with background subtraction at 650 nm.

2.2.1.7 Transient ectopic expression of recombinant proteins

Lipofectamine™ 2000 (Invitrogen) transfection protocol was used for transient over-expression of recombinant proteins in HeLa and MCF-7 cells. In details, on the day prior to transfection, monolayers were trypsinised and seeded at a density that enables ~60-70% confluency (~$3.5\text{-}4\times10^4$ cells/ml) on the transfection day. Transfection medium was prepared by combining contents of two tubes, one containing Lipofectamine™ 2000 transfection reagent in serum-free medium and the other containing purified plasmid DNA in serum-free medium (Table 2-11). Contents of both tubes were combined after incubating at room temperature for five minutes. The transfection mix was incubated for a further 20 minutes prior to cell treatment. Cell monolayers were washed twice with PBS and then treated with appropriate volumes (Table 2-11) of the transfection mix supplemented with complete medium, without antibiotics.

Table 2-11. Seeding densities and transfection volumes for different culture vessels

Culture Vessel	Seeding density on day 0	Volume of plating medium	DNA (µg) and Dilution volume (µl)	Lipofectamine™ 2000 (µl)* and Dilution volume (µl)	Complete Medium
24-well	4×10^4 cells/ml	500 µl	0.5 µg in 50 µl	1.0 µl in 50 µl	400 µl
6-well	1.5×10^5 cells/ml	2 ml	3 µg in 250 µl	5 µl in 250 µl	1.5 ml
35-mm dish	1.5×10^5 cells/ml	2 ml	3 µg in 250 µl	5 µl in 250 µl	1.5 ml
60-mm dish	3.0×10^5 cells/ml	5 ml	5 µg in 500 µl	10 µl in 500 µl	4 ml

*Volumes for Lipofectamine™ were optimised for different plate formats to minimise cell death and achieve optimal expression.

2.2.2 Bacterial cell culture and DNA preparation

2.2.2.1 Preparation of selection plates and liquid media

To prepare colony selection plates, 35g LB agar powder was added to 1L ddH_20 in a flask and heated to boiling while stirring, to dissolve the powder. The flask was autoclaved at 121^{O}C for 15 minutes and then cooled to 55^{O}C in a clean oven (Table 2-12). The LB agar solution was supplemented with antibodies and 20 ml of this solution was poured onto 10 cm polystyrene petri dishes. These were allowed to cool (with lids on) for 30-60 minutes (or until solidified). Plates were inverted and stored at 4^{O}C.

To prepare liquid culture media, powdered LB broth was suspended in ddH_20 with gentle stirring and then autoclavied at 121^{O}C for 15 minutes. Antibiotics were added at recommended concentrations (Table 2-12) after cooling to 55^{O}C. Liquid medium was stored at 4^{O}C after cooling to room temperature.

Table 2-12. Antibiotic dilutions

Reagent	Supplier	Solvent	Stock solution	Final concentration	Type
Ampicillin	Sigma Aldrich	ddH_20	100 mg/ml	100 µg/ml	Cell membrane synthesis inhibitor
Kanamycin	Sigma Aldrich	ddH_20	50 mg/ml	50 µg/ml	Inhibitor of protein synthesis

2.2.2.2 Bacterial transformation using the heat-shock method

All steps were done in a sterilised environment and next to a Bunsen flame. In detail, 50 µl high-efficiency NEB® 5-alpha competent *E. coli* (New England Bio-labs, UK) and 1-5 µl of 5 ng/ml plasmid DNA were mixed by flicking and then incubated on ice for 30 minutes. The heat-shock step was performed by transferring the bacteria/DNA mix to a heating block at 42ºC for exactly 30 seconds. The mix was immediately placed back on ice and incubated for five minutes. SOC medium (950 µl) was added to the bacteria/DNA mix and then cells were transferred to a shaking incubator. Mixing was done at 250 rpm at 37ºC for 60 minutes. Several 10-fold dilutions were performed in SOC medium and then 50 µl of transformed bacteria was spread onto pre-warmed selection plates using a plastic cell spreader. Plates were incubated upside down at 37^{O}C for ~12 hours.

2.2.2.3 Plasmid DNA preparation

Plasmid DNA was prepared from transformed highly competent cells by scrapping single colonies from selection plates using sterile pipette tips and inoculating 3 ml of LB broth supplemented with antibiotics in round-bottomed polypropylene flasks. For larger DNA preparations, isolated colonies were used to inoculate 250 ml LB broth supplemented with antibiotics in a conical flask. Inoculated media were incubated overnight at 37^{O}C in a shaking incubator (with mixing at 250 rpm). Plasmid DNA isolation was performed using the Qiagen® mini/midi prep kit per the manufacturer's instructions.

Plasmid DNA concentration was estimated using the NanoDrop™ spectrophotometer (Thermo Fischer Scientific). Briefly, 1.5 µl of purified DNA was used for each measurement. Plasmid DNA was routinely eluted in Tris-EDTA (TE) buffer (pH 8.0) and TE buffer was used as blank.

2.2.2.4 Preparation of bacterial glycerol stocks

This was done to facilitate long term storage of bacterial plasmids and have an abundant supply of plasmid DNA without the need to re-transform competent cells. An overnight culture was inoculated and following cell growth, 500 µl of cell culture was added to 500 µl 50% (v/v in ddH_20) glycerol, with gentle pipetting up and down in a cryovial which was frozen at -80^{O}C. Bacteria were recovered from glycerol stocks by gently scraping some frozen cells with a sterile pipette and streaking onto an LB agar plate (see 2.2.2.3).

2.2.2.5 Agarose gel electrophoresis

This was used to analyse plasmid DNA yields and quality. Plasmid DNA was resolved and analysed on 1.2% agarose gels (prepared in Tris-Acetate-EDTA (TAE) buffer; pH 8.0). Ethidium bromide was included at a final concentration of 0.5 µg/ml to permit visualization of DNA bands when exposed to UV-light. DNA samples were diluted in DNA loading buffer to facilitate loading into wells of the agarose gel while molecular weights were estimated by loading a 1 kb pre-stained DNA ladder on the same gel. DNA sample (10 µl) was loaded into wells and samples were separated by running at 120V for one hour in TAE buffer.

2.2.3 Protein manipulations

2.2.3.1 Preparation of cell lysates for western immunoblotting

Growth medium was aspirated from cell monolayers, followed by two washes with 1X PBS. Cell lysis was achieved by scraping monolayer cells in 1X RIPA buffer (200 µl per well of 6-well plates and 500 µl to 60 mm dishes; Table 2-13) with a cell scraper into pre-cooled centrifuge tubes. Cell extracts were subsequently sonicated 3 times for 5 seconds each using a probe sonicator

(Sonics and Materials Vibra-Cell™ VC 130 PB) to shear genomic DNA and reduce sample viscosity followed by centrifugation at 14000×g for 10 minutes. Supernatants were transferred into clean, pre-chilled micro-centrifuge tubes. supernatants were reserved for total protein determination while remnants were solubilised in 2x-Laemlii sample buffer. Aliquots were stored -80^{o}C. Prior to gel loading, supernatants were solubilised in 2x-Laemlii sample buffer and boiled for three minutes at 95-100^{o}C.

Table 2-13. RIPA buffer recipe

Components	**Concentrations**
EDTA	2 mM
EGTA	0.5 mM
Glycerol	10% (v/v)
NP-40	1% (v/v)
Protease inhibitor cocktail	250 µl stock/10 ml lysis buffer
Sodium Chloride	150 mM
Sodium deoxycholate	0.5% (w/v)
Sodium OrthoVanadate	0.2 mM
Tris-HCl (pH 7.6)	20 mM

Table 2-14. 2x-Laemmli sample buffer recipe

Components	Concentrations
SDS	2% (w/v)
Tris-HCl (pH 6.8)	62.5 mM
Glycerol	25% (v/v)
β-mercaptoethanol	710 mM
Bromophenol Blue	0.01% (w/v)

2.2.3.2 Total protein quantification

To achieve equal protein loading on electrophoretic gels, total protein contents of cell lysates were estimated using the DC protein assay protocol (Bio-Rad). The standard assay protocol described by the manufacturer was followed and BSA was used to generate a standard curve. The absorbance of each sample was read at 750 nm after 15 minutes' incubation at room temperature.

Table 2-15. Dilutions for BSA standard curve

µg/µl BSA	µl BSA (1.5 µg/µl)	ddH_2O (ml)	Working reagent (µl)	Reagent B (ml)
0	0	100	500	4.0
0.2	13.33	86.67	500	4.0
0.4	26.67	73.33	500	4.0
0.8	53.33	46.67	500	4.0
1.0	66.67	33.33	500	4.0
1.2	80	20	500	4.0

2.2.3.3 Sodium dodecyl sulphate-polyacrylamide gel electrophoresis (SDS-PAGE)

This is a routinely used method for analysing proteins as it allows separation of proteins based on their molecular weights. The detergent, SDS facilitates protein denaturation as well as the introduction of a uniform negative charge onto the protein samples. Thus, proteins will separate based on their mass to charge ratios.

Approximately equal amounts (20-30 µg) of protein samples were loaded into the wells of a 10% Criterion™ TGX™ precast gel (Bio-Rad) while 10 µl pre-stained molecular weight markers were loaded to verify electro-transfer. The Tris-Glycine-SDS running buffer was purchased from National Diagnostics. Pre-stained protein markers (National Diagnostics) were used as molecular size standers to determine approximate protein size as well as the success of an electro-transfer onto a membrane. Biotinylated markers (CST) were also loaded to verify molecular weights in immunoblots. Protein lysates loaded onto wells were resolved at 150V for 60-90 minutes.

2.2.3.4 Electro-transfer onto membranes

This technique is commonly used to transfer proteins separated by Gel electrophoresis onto a membrane such as nitrocellulose or PVDF. We used the iBlot® system (Thermo Fischer Scientific) to transfer separated proteins onto PVDF membranes s described by the manufacturer. Briefly, the pre-run gel was placed on the PVDF membrane of the anode stack, this was followed by the placement of a pre-wetted filter paper onto the gel. The cathode stack was unsealed and placed onto the filter paper with the electrode side facing up. Air bubbles were eliminated by applying a roller across the stack and a disposable sponge was placed on top in contact with the lid. Electro-transfer was routinely achieved at 23V for four to seven minutes.

2.2.3.5 Membrane blocking and antibody probing

To prevent non-specific antibody binding, membranes were incubated with 5% (w/v) BSA or 5% (w/v) non-fat milk (NFM) in 1X-Tris buffered saline with 0.1% (v/v) plus Tween-20 (TBST) for one hour at room temperature with mild agitation (it is inappropriate to use NFM as a blocking agent when using antibodies against phosphorylated proteins, due to the milk protein, casein, a phosphoprotein that may significantly increase background noise). Membranes were subsequently washed three times for five minutes each with TBST and then incubated with primary antibodies in 1% BSA or NFM in TBST (antibody diluent) overnight at $4^{O}C$ (this can be done by incubation for 1hr at room temperature, but overnight incubation increases signal intensity for antibodies with lower affinity) with gentle rocking. Membranes were washed three times for five minutes each with TBST and subsequently incubated with species specific HRP-linked secondary antibodies at dilutions of 1:1500-1:3000 in antibody diluent for one hour at room temperature with gentle rocking. This was followed by three five-minute washes with TBST.

2.2.3.6 Membrane development and image acquisition

Protein bands were visualised using the SuperSignal™ West Pico Chemiluminescent substrate, an enhanced chemiluminescent (ECL) horseradish peroxidase (HRP) substrate for low-level detection by western blotting (Thermo Fisher Scientific). Working reagent was prepared by mixing equal amounts of the stable peroxide solution and the Luminol enhancer solution. This was used at 0.1 ml per cm^2 of membrane. After three washes with TBST, membranes were incubated with the working solution reagent for five minutes. Membranes were removed from the solution and drained of excess reagent. They were subsequently wrapped in clean plastic film and rid of air bubbles. Blots were then imaged on a FluorChem M Multifluor imaging system (ProteinSimple, CA) and analysed by densitometry using its AlphaView® software.

2.2.3.7 Cell fractionation

Invadopodia fractions were prepared as previously described (Bowden *et al.*, 1999, 2001). In detail, 1×10^6 HeLa cells/ml were seeded onto gelatin coated 60 mm dishes and subsequently transfected with siRNA as described (2.2.1.5). Following siRNA transfection and subsequent culture for 36 hours at $37^{O}C$, cells were re-seeded onto collagen coated coverslips and then cultured in complete medium for 24 hours. This was followed by one wash with ice-cold PBS and another with MOPS/phosphotyrosine buffer (YPP) (10 mM MOPS, pH 6.8, 100 mM KCl, 2.5 mM $MgCl_2$, 1 mM $CaCl_2$, 0.3 M sucrose, 1 mM Na_3VO_4, 1x protease inhibitor cocktail and 0.02 % (w/v) sodium azide). The cell body fraction was prepared by shearing the cell bodies with gentle rolling of a cell spreader across the monolayer of cells in a small volume (250 µl) of YPP buffer. Detached cell bodies were centrifuged at $9000\times g$ for 20 minutes at $4^{0}C$. Supernatants were transferred to pre-chilled tubes and labelled the cytosolic fractions while the pellets were solubilised in RIPA buffer and labelled the cell body fraction (CBF). Meanwhile, the remnants on culture plates (extracellular matrix plus invadopodia) were rinsed once with YPP buffer, lysed with RIPA buffer using a cell scraper, transferred to pre-chilled tubes and labelled the invadopodia fraction (INV). Protein content was determined using the Lowry method and appropriate amounts were solubilised in 2x-laemmli sample buffer prior to loading onto electrophoretic gels. Fractions and whole cell lysates (to control for total protein) were separated using SDS-PAGE followed by electro-transfer onto PVDF membranes and subsequent probing with primary and secondary antibodies.

2.2.3.8 EGFR degradation assay

siRNA treated cells were serum starved, 54 hours post-transfection, in 0.5 % FBS (in DMEM) for 18 hours. This was followed by two rinses in PBS and treatment with 10 µg/ml cycloheximide for one hour to inhibit synthesis of new receptors. Following two rinses with PBS, cells were treated with 100 ng/ml EGF ligand for indicated times and then lysed in RIPA buffer. Protein content was determined using the DC protein assay reagent (Bio-Rad) while lysates resolved by SDS-PAGE and analysed by western blotting.

2.2.4 Microscopy

2.2.4.1 Confocal laser scanning microscopy

Images were acquired using a Zeiss LSM 510 confocal laser scanning microscope. Excitation and emission settings for various fluorophores are shown in Table 2-16. Each fluorophore was scanned sequentially (using the multi-track function) to avoid spectral bleed-through. The pinhole was set at a diameter corresponding to 1 airy unit to obtain true confocal images. Z-stacks were acquired by scanning at ~100 nm intervals (unless otherwise stated) throughout the depth of cells being imaged. Randomly chosen representative fields were selected and images were acquired using identical detector gain and offset settings across all treatments.

Table 2-16. Excitation and emission settings for various fluorophores.

Fluorophore	Laser-line	Excitation (nm)	Emission (nm)
Hoecsht	Diode	405	415-485
Alexa-Fluor® 488, GFP, FITC	Argon-Ion	488	500-550
Alexa-Fluor® 546, mCherry, Rhodamine	Helium-Neon (HeNe)	543	555-620
Alexa-Fluor® 633	HeNe	633	650-700

2.2.4.2 Sample preparation

Monolayers were seeded onto 13 mm glass coverslips for fluorescence microscopy. Although these coverslips appear clean when opened, they usually contain traces of grease which may alter cell adhesion (Fischer *et al.*, 2008) and also affect the quality of fluorescence images. This necessitates washing for optimal cell adhesion. Coverslips were washed with 1 N HCl for two hours with gentle rocking and then neutralised with dilute NaOH (concentration <1 M) followed by several washes in dd$H_2$0. pH was determined using a universal indicator, with pH values between 6.8 and 7.4 considered suitable for cell culture. Washed coverslips were stored in 70%

ethanol at 4ºC. Prior to use, each coverslip was briefly flamed using a Bunsen-burner and washed twice with 1x PBS to remove residual ethanol prior to cell seeding.

To prepare thin layers of collagen matrices on glass coverslips, 50 µg/ml of collagen (Gibco®) was prepared in 20 mM acetic acid as described by the manufacturer and then added at 5 µg/cm^2 to each washed and flamed cover slip (100 µl required to coat a 13-mm coverslip). Coated coverslips were incubated at room temperature for one hour. Excess solution was carefully aspirated from each well followed by three rinses with sterile PBS to remove the acid, prior to cell seeding.

To prepare gelatin coated glass coverslips, 100 µl 0.2% gelatin (w/v in PBS) was applied to 13 mm glass coverslips in each well of a 24-well culture plate and incubated for 10 minutes at 4ºC on a rocking platform to allow solidification. Excess gelatin was aspirated and then 0.5 ml 0.5% glutaraldehyde (v/v, in PBS) was pipetted into each well, followed by incubation for 30 minutes at 4ºC with gentle rocking. Each well was subsequently washed three times with PBS followed by equilibration with culture medium at 37ºC for 30 minutes prior to cell seeding.

2.2.4.3 General indirect immunofluorescence staining

This was performed using a method described by Minogue et al. (2006). In details, growth media were aspirated from coverslips and cells were washed once with PBS to remove residual growth media. Then, cells were fixed for five minutes in 4% formaldehyde (FA) in PBS containing 20 mM HEPES. Excess FA was removed from cells by washing three times with PBS followed by permeabilization with 0.05% Triton X-100 (v/v in PBS) for five minutes at 4^{O}C. After three washes with PBS, fixed cells were incubated in blocking solution (30 mg/ml bovine serum albumin (BSA) in PBS) for 30 minutes at room temperature to minimise non-specific antibody binding. Following two washes with PBS, cells were probed with primary antibodies targeting specific proteins of interest (using concentrations described by the

manufacturers) in 3 mg/ml BSA for one hour at room temperature. After two washes with PBS, cells were incubated with species specific Alexa-Fluor conjugated antibodies, nuclear counter stain: Hoechst 33342 trihydrochloride and other fluorescent probes of interest (e.g. phalloidin conjugates) in antibody diluent for 45 minutes at room temperature. After extensive washing with PBS, and once in ultrapure water to remove excess salts, coverslips were mounted onto clean microscopic slides using ProLong® Gold antifade reagent (Thermo Fischer Scientific) and stored in the dark to minimise photobleaching, prior to image acquisition. Images were acquired using (unless otherwise stated) the Zeiss LSM 510 confocal laser scanning microscope as previously specified.

2.2.4.4 Visualisation of membrane PI(3)P and PI(4)P pools

This was performed using the procedures described by Hammond et al. (2009). All steps were carried out at room temperature. Cells were fixed – after removal of growth medium and one wash with PBS– by incubating with pre-warmed 2% FA in PBS for 15 minutes. Excess FA was removed by rinsing the coverslips three times with PBS containing 50 mM ammonium chloride (NH_4Cl). Cells were subsequently permeabilised by incubating in 20 µM digitonin in buffer A (20 mM PIPES (pH, 6.8), 137 mM NaCl, 2.7 mM KCl in ultrapure water) for five minutes. Then, coverslips were incubated with buffer A supplemented with 1% BSA and 50 mM NH_4Cl (blocking buffer) for 45 minutes. 1 µg/ml GST-PH-FAPP1 or 5µg/ml GST-P4C domain of Sid C protein from *Legionella pneumophilla* was also included in the blocking buffer for detection of PI(4)P.

For detection endosomal pools of PI(3)P, 0.5 µg/ml GST-2X-FYVE-Hrs was used in place of GST-PH-FAPP1[8] or GST-P4C in the blocking step. Residual proteins were removed by washing coverslips three times with buffer A. Cells were then probed with mouse monoclonal anti-GST antibodies and other primary antibodies of interest in antibody diluent (Buffer A supplemented with

[8] Recombinant GST-2X-FYVE-Hrs, GST-PH-FAPP and GST-PLCδ-PH were prepared by Ruth Jacobs of UCL.

1% BSA). Unbound antibodies were removed by washing three times with buffer A and the coverslips were incubated with Alexa-Fluor® conjugated secondary antibodies for 45 minutes. Unbound antibodies were removed by three washes with buffer A and cells were post-fixed in 2% FA in PBS for five minutes. Then, coverslips were rinsed three times with PBS containing 50mM NH_4Cl and once in ultrapure water. Coverslips were mounted onto clean microscopic slides using ProLong® Gold Antifade and stored as previously described. Images were acquired using a Zeiss LSM 510 confocal laser scanning microscope.

2.2.4.5 Visualisation of plasma membrane pools of $PI(4,5)P_2$

Culture medium was removed from cells and after one wash with ice-cold 1X PBS, cells were fixed by incubating coverslips with 4% FA and 0.02% glutaraldehyde (GA) in PBS at room temperature for 15 minutes. Coverslips were subsequently rinsed three times with PBS containing 50 mM NH_4Cl, while GA auto-fluorescence was quenched by rinsing coverslips with freshly prepared 0.1% Sodium borohydride ($NaBH_4$) followed by three rinses in PBS containing 50 mM NH_4Cl. Subsequent steps were carried out at 4^oC. For blocking and permeabilisation of fixed cells, cell monolayers on coverslips were incubated with buffer A supplemented with 50 mM NH_4Cl, 1% BSA and 0.5% (w/v) Saponin (blocking buffer). GST-PLCδ-PH (0.5 µg/ml) was included in the blocking buffer for detection of plasma membrane pools of PIP_2. Unbound proteins were removed by three washes with buffer A and the cells were incubated with mouse monoclonal anti-GST antibody in antibody diluent (buffer A supplemented with 1% BSA and 0.1% saponin) for one hour. Unbound antibodies were removed by three washes with buffer A and the cells were incubated with Alexa-Fluor® conjugated goat anti-mouse IgG for 45 minutes. Unbound Alexa-Fluor conjugated antibodies were removed by three washes with buffer A and the cells were post-fixed in 2% FA in PBS for ten minutes and then for five minutes at room temperature. Coverslips were rinsed three times with PBS containing 50 mM NH_4Cl and once in ultrapure water and subsequently mounted on clean microscopic slides as previously

described. Images were collected using the Zeiss LSM 510 confocal laser scanning microscope as previously specified.

2.2.4.6 Transferrin uptake and surface labelling

A method described by Ketel et al (2016) with slight modifications was used. In detail, HeLa Cells were seeded onto collagen coated glass coverslips at 2.5×10^4 cells/ml, transfected with siRNA as previously described and serum starved for two hours, 70-hours post-transfection. For quantitation of transferrin uptake, cells were treated with 25 µg/ml Alexa-Fluor-555-labelled transferrin for 10 minutes at 37^{O}C. After two washes with ice-cold PBS, cells were acid washed (0.2 M Sodium acetate, 0.2 M NaCl) for one minute to strip off surface bound transferrin. Cells were washed twice with PBS, fixed and permeabilised with formaldehyde and Triton X-100 respectively, as previously described.

For uptake and co-immunostaining, cells were treated with 25 µg/ml Alexa-Fluor-555-labelled transferrin for 30 minutes at 37^{O}C to allow transferrin reach saturation. After acid and PBS washes, cells were fixed and permeabilised as previously stated and probed with anti-EEA1 antibodies.

For surface labelling, cells were incubated with 25 µg/ml Alexa-Fluor-555-labelled transferrin for 45 minutes at 4^{O}C to block endocytosis and washed three times with PBS. Cells were fixed and permeabilised at room temperature.

2.2.4.7 Transferrin and epidermal growth factor binding and internalisation

HeLa Cells were seeded onto 13 mm glass coverslips at 2.5×10^4 cells/ml, transfected with siRNA as previously described and serum starved for as described in 2.2.4.6. After two washes with PBS, cells were incubated in serum free medium containing 40 µg/ml Alexa-Fluor 488-labelled EGF and 25 µg/ml Alexa-Fluor 633-labelled transferrin. Cells were incubated at 4^{O}C for one hour (PULSE), washed twice with ice-cold PBS and then incubated

with complete medium for indicated times. Cells were subsequently fixed and processed for microscopy as previously described.

2.2.4.8 Transferrin uptake and recycling assay

HeLa cells were plated at 2.5×10^4 cells/ml on 13 mm glass coverslips in 24-well plates and treated with siRNA as previously described. Cells were serum starved for one hour at 37^{o}C, 71-hours post transfection and subsequently rinsed twice with 1X PBS. Cells were then loaded with 100 µg/ml Alexa-Fluor 555-labelled transferrin for one hour at 37^{o}C (LOAD). Cells were subsequently acid washed once and then washed three times with PBS. This was either followed by fixation and preparation for fluorescence microscopy or further incubation for 30 or 60 minutes (CHASE) at 37^{o}C with subsequent processing for microscopy.

2.2.4.9 Fluorescent recovery after photo-bleaching (FRAP)

FRAP experiments were carried out on the heated stage (37^{o}C) of the Zeiss LSM 510 inverted confocal microscope as previously described (Nola *et al.*, 2011). The pinhole was set at greater than 7 µm for image acquisition. One or two regions of interest (ROIs) were selected within the Golgi regions of HeLa cells moderately expressing EGFP-CI-M6PR. A time-lapse series was acquired with 5 frames and 200 frames (one second/frame) before and after photo-bleaching respectively. For signal quantitation, the sum GFP-CI-M6PR fluorescence was quantified over time and then normalised to the mean fluorescence intensity in the period before photo-bleaching (Appendix 1).

2.2.4.10 EGFP-CI-M6PR trafficking assay

M6PR trafficking was assayed as previously described (Chi *et al.*, 2008), with some modifications. EGFP-M6PR expressing cells were incubated for two hours at 20^{o}C, in the presence of 10 µg/ml cycloheximide, to block Golgi exit and prevent synthesis of new M6PR. This was followed by a one-hour incubation at 37^{o}C to permit M6PR transport. Cells were subsequently processed for fluorescence microscopy and imaging as described above (see

2.2.4.3). EGFP-M6PR fluorescence intensity within the Juxtanuclear region of EGFP-M6PR expressing cells was measured in ImageJ (see 2.3.3).

2.2.4.11 Immunofluorescent staining of active Rac1 pools

MCF-7 cells were seeded onto collagen coated coverslips and cultured for 12 hours prior to siRNA transfection. RNAi was carried out for 60 hours followed by serum starvation for another 12 hours. Cells were stimulated with 100 ng/ml EGF for 10 minutes at 37^{o}C. We used the glutaraldehyde fixation and saponin permeabilisation method described previously (see 2.2.4.5) to preserve plasma membranes and included 30 µg/ml of the GST-PAK-CRIB fusion protein in the blocking buffer for detection of active pools of Rac1 (as well as Cdc42). Unbound proteins were removed by three washes in buffer A followed by indirect immunofluorescent staining for the GST tagged protein.

2.2.4.12 Preparation of fluorescently labelled gelatin

The method described by Bowden et al (2001) was used to prepare fluorescent labelled gelatin from porcine skin (Sigma). Briefly, 2% gelatin (w/v in high salt conjugation buffer) was dialysed against 10 mg FITC in 333 ml low salt conjugation buffer for approximately 90 minutes in the dark at 37^{O}C with constant stirring (Table 2-17). Subsequently, the FITC/low-salt conjugation was replaced with PBS and dialysis was continued for three days at 37^{O}C with PBS change twice daily. FITC-gelatin was removed from the dialysis tubing and sucrose added at a final concentration of 2% (w/v). The resulting solution was divided into 0.5 ml aliquots and stored in the dark at 4^{O}C.

Table 2-17. Materials required for preparing FITC-gelatin

Materials	Description
Low Salt conjugation buffer	50 mM Sodium Borate, pH 9.3
High Salt conjugation buffer	50 mM Sodium Borate, 40 mM NaCl, pH 9.3
Dialysis tubing	MWCO= 3000
Gelatin	2% (w/v)
Sucrose	2% (w/v)

2.2.4.13 2D-gelatin degradation assay

To prepare fluorescent labelled glass coverslips, FITC-gelatin was melted by incubating at 37^{O}C for 15 minutes in the dark. Then ~200 µl FITC-gelatin was pipetted onto flame-sterilised 13 mm glass coverslips and then incubated in the dark, at 4^{O}C for 30 minutes. Excess FITC-gelatin was gently aspirated and coated coverslips were treated with 0.5% glutaraldehyde (v/v in PBS) for 15 minutes at 4^{o}C followed by three washes with PBS (five minutes per wash). Coverslips were then treated with 0.5% sodium borohydride (v/v in PBS) for three minutes at room temperature to quench glutaraldehyde auto-fluorescence. After three washes in PBS, labelled coverslips were sterilised with 70% ethanol at (five minutes, room temperature), washed three times with PBS and then incubated with serum free medium for 30 minutes at 37^{O}C, prior to cell seeding.

Cells were seeded at a density of 2.5×10^4 cells/ml, fixed and permeabilised 12 hours post seeding and then stained with Alexa-Fluor-546-conjugated phalloidin and Hoechst 33342. Matrix degradation was observed as the focal loss of fluorescence intensity (black) relative to the non-degraded matrix (green) and quantified using ImageJ software.

2.2.4.14 Transwell® migration assay

Polyester Transwell™ insets (upper chamber) with pore sizes of 8 µm (Corning®), were coated with 50 µg/ml type I collagen to form a thin layer of extracellular matrix. These were allowed to set for one hour at room temperature and washed three times with PBS. Subsequently, 5×10^4 cells/ml (in serum free medium) of serum starved siRNA treated or control cells were added to the upper chamber. Complete medium (10% FCS+DMEM) was added to the lower chambers and cells were cultured for 12 hours. Cells were removed from the upper chamber by gentle aspiration and cleaning with a sterile cotton swab. After three washes with PBS, cells on the other side of insets were fixed by treating with 3.7% formaldehyde for 10 minutes (by placing the inset in the lower chamber containing formaldehyde) and permeabilised with 0.05% Triton X-100 (v/v, PBS) at 4^OC for five minutes. Cells were visualised by staining with Alexa-Fluor-546-conjugated phalloidin and five random fields were counted for cells that migrated to the underside of the inset membrane using the 20x objective using ImageJ (NIH, Bethesda). In addition, Z-series of 10 sections at 2.5 µm also acquired to analyse cell migration. Relative invasion of the Transwell® migration chamber was calculated by dividing the number of cells that migrated to the lower chamber in response to chemoattractant by the number of cells seeded (5×10^4) onto the serum-free upper chamber.

$$Relative\ invasion = \left(\frac{Number\ of\ cells\ invaded}{5 \times 10^4}\right)$$

2.2.5 Flow cytometry

2.2.5.1 Analysis of MT1-MMP trafficking

We used a method described by Kean et al. (2009). In detail, MCF-7 cells were seeded at 1.0×10^5 cells/ml into wells of a 6-well plate and siRNA transfected as previously described. After subsequent culture for 36 hours at 37^{O}C, cells were re-seeded onto collagen coated coverslips and then incubated for another 24 hours in complete medium at 37^{O}C and then serum starved for four hours to facilitate internalisation of MT1-MMP. For trafficking of endogenous MT1-MMP, cells were pulsed with an anti-MT1-MMP antibody (Abcam) for one hour at 4^{o}C. Cells were subsequently fixed, permeabilised and immunostained as described in 2.2.4.3.

For analysis of MT1-MMP trafficking by flow cytometry, MCF-7 cells were seeded at 1.0×10^5 cells/ml onto wells of a 6-well plate, siRNA transfected and cultured for 58 hours. siRNA treated cells were subsequently serum-starved overnight to induce internalisation of MT1-MMP. To quantify surface labelled MT1-MMP, cells were treated with 100 ng/ml EGF for 10 minutes. This was followed by detachment with FACS buffer (5mM EDTA in PBS, pH 7.4). Subsequent steps were carried out at 4^{O}C to limit internalisation of MT1-MMP. Cells were labelled with rabbit anti MT1-MMP (Abcam) for one hour, washed three times with PBS and then labelled with anti-Rabbit Alexa-Fluor-488 antibody. Cells were analysed using a FACS LSRII cell sorter (BD Biosciences) and about 10,000 cells were counted per treatment.

2.2.6 FACS-based EGFR recycling assay

FACS analysis was performed according to a previously described method (Tan *et al.*, 2015). To quantify total internalised EGFR, PI4KII and control siRNA treated HeLa cells were serum starved for 14 hours, 58-hours post-transfection and subsequently treated with 10 µg/ml cycloheximide for one hour to inhibit new receptor synthesis. Cells were washed three times with PBS and then stimulated with 10 nM Alexa-488-labelled EGF for 15 minutes. These were subsequently rinsed three times with PBS, detached in ice-cold

FACS buffer (5mM EDTA in PBS, pH 7.4) and then fixed in 3.7% formaldehyde for five minutes at room temperature.

To quantify recycled EGFR, cycloheximide treated cells were stimulated with 10 nM unlabelled EGF for 15 minutes (PULSE). After three washes with PBS, cells were chased for 0, 30 or 60 minutes to facilitate EGFR recycling. After subsequent washes with PBS, these cells were labelled with 10 nM Alexa-488-labelled EGF for 15 minutes, washed, detached and fixed as described above. Alexa-488-labelled EGF taken up by cells treated this way represents EGFR after stimulation with unlabelled EGF. Geometric means of EGF for each treatment were analysed by FACS and amount of EGFR recycled was computed using the equation below.

$$Recycled\ EGFR = \frac{[\mathrm{I}_t - \mathrm{I}_0]}{[\mathrm{I}_{total} - \mathrm{I}_0]}$$

Where I_t represents EGFR recycled at a given time and I_0 represents EGFR recycled prior at time 0 of chase and I_{total} is the total amount of internalised EGFR.

2.3 Data Analysis

2.3.1 Oncogenomic data mining[9]

The cBIO cancer Genomics Portal (http://cbioportal.org/) (Cerami *et al.*, 2012; Gao *et al.*, 2013) and Oncomine (Rhodes *et al.*, 2004) are open access resources for cancer genomics data sets containing data from 69 cancer genomics studies with a total number of 17,177 samples (cBioPortal), and 715 datasets with 86,733 samples (Oncomine). Heterozygous loss of the PI4K2B allele was analysed in all cancers as were copy number alterations in pancreatic cancers and hepatocellular carcinoma. Additionally, correlations of PI4KIIβ mRNA expression, recurrence, metastatic events or overall survival in breast cancer cases were investigated.

2.3.2 Statistical analysis

This was performed using Prism software (GraphPad, CA). Statistical comparisons were performed using one-way analysis of variance (ANOVA) followed by a Tukey's (equal variances) or Dunnett's (Kruskal-Wallis non-parametric test for unequal variances) post-test at a 95% confidence level.

2.3.3 Computational image analyses

Computational analyses of confocal micrographs permit processing of huge data sets, generation of quantitative and less biased results (unlike visual judgement) as well as detection of minute phenotypic changes through statistical analysis. In this thesis, all confocal micrographs were subjected to computational analysis using the software, ImageJ version 1.48 (http://imagej.nih.gov/ij/). Images were imported in the LSM or ND2 formats using the LSM importer and NDi6d plugins respectively.

[9] The author acknowledges the help of Dr Christina A. Gewinner

2.3.3.1 Quantitation of PI(4)P pools

Golgi PI(4)P pools were quantified according to a previously described method (Hammond *et al.*, 2009), with slight modifications. In addition to stains for GST-tagged proteins for detecting PI(4)P, we also used TGN46 or syntaxin 6 to mark different domains of the TGN. Image stacks were reduced to 8-bit single images and subjected to a rolling ball algorithm to subtract background fluorescence.

Images of interest (TGN46 or syntaxin 6) were auto-thresholded using 'make binary' command. Binary images were dilated by a single pixel using the 'dilate' command and resulting images were used as masks for the PI(4)P (GST-P4C) staining image. Regions of interest corresponding to the Golgi were selected using the ROI command and integrated pixel intensities were measured using the analyse particles function. Parameters for particle analysis in the Golgi/TGN region are shown in Table 2-18.

Table 2-18. Parameters for analysing TGN localised particles

Parameters	Value
Size	600 μm^2-Infinity (To exclude cytoplasmic vesicles)[10]
Circularity	0.00-1.0[11]
Show	Overlay outlines[12]

To quantify PI(4)P-positive puncta, binary images of the GST-P4C channel were dilated using the dilate function and the resulting image was analysed using the analyse particle command to count the total number of PI(4)P-positive vesicles and measure their fluorescent intensities (Table 2-19).

[10] These values may vary and require some calibration prior to image analysis.
[11] This should be left this way as increasing the value may result in the selection of cytoplasmic vesicles.
[12] Any other option could be used.

Table 2-19. Parameters for analysing PI(4)P-positive puncta

Parameters	Value
Size	1-300 μm^2 (To exclude cytoplasmic vesicles)[13]
Circularity	0.6-1.0[14]
Show	Overlay outlines[15]

The integrated pixel intensity, *I* was normalized to pool results across three independent experiments using the following expression:

$$Normalised\ integrated\ fluorescence = \frac{(I - Ibg)}{Ictrl - Ibg}$$

Where I_{ctrl} represents the mean intensity for the control sample and I_{bg} represents the intensity of the background specimen in which antibodies or binding probes were omitted (Hammond *et al.*, 2009). Pooled, normalised fluorescence intensities were subjected to a Kruskal-Wallis test with Dunn's multiple comparisons using Prism 5 software (GraphPad™).

2.3.3.2 Quantitation of plasma membrane PI(4,5)P_2 levels

This was done according to a previously described method (Hammond *et al.*, 2009), albeit with a few alterations. In details, image stacks were converted to single 8-bit images. The GST-PLCδ image was thresholded and subjected to background fluorescence subtraction as previously described (2.3.3.1). The gray-level watershed plugin (http://bigwww.epfl.ch/sage/soft/watershed/) was run on binary images and the resulting watershed patterns were subtracted from the binary GST-PLCδ image using the image calculator function to define boundaries between touching cells. The analyse particles

[13] These values may vary and require some calibration prior to image analysis.
[14] This should be left this way as increasing the value may result in the selection of cytoplasmic vesicles.
[15] Any other option could be used.

function was then used to measure area and intensity of cells that were not touching edges of the image field.

2.3.3.3 Quantitation of total cellular fluorescence intensities

Images were converted to grayscale, subjected to background fluorescence subtraction and thresholded using identical parameters across all fields. Regions of interest were then selected using the ROI command and integrated pixel intensities were measured at randomly selected fields. The integrated pixel intensity *I*, was normalized to pool results across independent experiments. This was done using the following equation described in 2.3.3.1.

2.3.3.4 Quantitative analysis of actin based structures[16]

For analysis of actin based structures: cortical actin and stress fibres, multi-channel, 8-bit, fluorescent images were segmented using global intensity thresholds (Thr) for red and green pixels such that ThrG=25 on the actin channel and ThrR=73 on the phosphotyrosine (pY) channel. The total area of actin and pY (phosphotyrosine) foreground pixels on each image was then computed using the 'Measure' command. The ratio of the segmented pY/actin area was calculated using LibreOffice Calc (version 5.0.4.2).

2.3.3.5 Quantitative analysis of matrix degradation

Confocal images of F-actin and degraded matrix were captured using a Nikon C2+ confocal microscope equipped with an NIS-nd2 software. Experiments were carried out in triplicates with at least 20 cells captured per experiment. Area of degradation for the FITC-gelatin field was computed using the 'measure' command while total cell counts from the DAPI (nuclear) channel corresponding to the degraded areas in a $4x10^4$ μm^2 field using the 'analyse particles' command. Parameters for particle analysis were set such that only cell nuclei could be counted (Table 2-18). Adjacent nuclei were separated

[16] This was performed in collaboration with Dr Kriston-Vizi of the MRC Laboratory for Molecular Cell Biology (MRC-LMCB), University College London.

using the ‘watershed’ command to prevent the program from counting touching cells as one. The total degraded area was expressed as a percentage of the total cell area.

2.3.3.6 Colocalisation analysis

Multi-channel image stacks were converted into 8-bit single channel image, subjected to thresholds and background fluorescence subtraction using ImageJ. These were then subjected to correlation analysis using the JACoP ImageJ plugin which bridges statistical approaches and novel object based analyses (Bolte and Cordelières, 2006). The Pearson’s correlation coefficients (r) between pixel intensities in two channels were calculated and set as r=1 for perfect colocalisation, and r=0 for the minimum overlap between two pixels.

Chapter 3 PI4KIIα and PI4KIIβ produce distinct pools of phosphatidylinositol 4-phosphate[17]

3.1 Introduction

Phosphatidylinositol 4-phosphate, PI(4)P is synthesised by four PI4K isoforms that are categorised into two distinct structured families, type IIs (PI4KIIα and PI4KIIβ) and type IIIs (PI4KIIIα and PI4KIIIβ). The biochemical and functional features of these enzyme families are discussed in detail in Chapter 1. This chapter focuses on the membrane localisation of the type II PI4Ks and their isoform specific PI(4)P pools.

Although both type II PI4Ks localise to the Golgi and endosomal membrane compartments, the broad subcellular distribution of the PI4KIIs has, in some cases led to differing interpretations of PI4KII function. Differences in cell type may be partially responsible for this, for example, PI4KIIα has been localised to the TGN, EE and LE membranes in epithelial and fibroblast-like cells (Balla *et al.*, 2002; Wang *et al.*, 2003; Waugh *et al.*, 2003) but to synaptic vesicles in neurones (Guo *et al.*, 2003; Salazar *et al.*, 2005; Robinson *et al.*, 2014). In addition, most studies focus on PI4KIIα because its regulation and membrane localisation are better understood. PI4KIIα localises to the Golgi and its kinase activity is required for the recruitment of clathrin adaptor, AP-1. AP-1 directly binds PI(4)P at the Golgi and RNA interference (RNAi) of PI4KIIα blocks Golgi recruitment of AP-1 and disrupts AP-1 dependent functions (Wang *et al.*, 2003). PI4KIIα also localises to endosomal membrane compartments (Balla *et al.*, 2002; Minogue *et al.*, 2006; Craige *et al.*, 2008; Gerber *et al.*, 2015; Dong *et al.*, 2016; Henmi *et al.*, 2016) and specialised trafficking organelles such as secretory, autophagic and exocytic vesicles (Wang *et al.*, 2015; Ketel *et al.*, 2016). In comparison with PI4KIIα, relatively little is known about the cellular roles of PI4KIIβ although it is recruited to membranes in response to stimuli such as PDGF-receptor activation (Wei *et*

[17] Some data from this chapter and Chapter 5 were published in Molecular Biology of the cell (Alli-Balogun *et al.*, 2016). See Appendix 4

al., 2002). PI4KIIβ also localises to the TGN and endo-lysosomal system (Balla *et al.*, 2002; Jung *et al.*, 2008; Wieffer *et al.*, 2013), leading to the assumption that it has overlapping functions with PI4KIIα.

In addition, both enzymes are regulated by different means. PI4KIIα is stably palmitoylated and constitutively associates with membranes while PI4KIIβ is dynamically palmitoylated such that ~30% of total cellular PI4KIIβ is palmitoylated (Balla *et al.*, 2002; Wei *et al.*, 2002; Barylko *et al.*, 2009). Immunocytochemical approaches reveal that PI4KIIs localise to the juxtanuclear region corresponding the Golgi and on vesicles marked by the presence of early and late endosomal proteins (Balla *et al.*, 2002; Wang *et al.*, 2003; Waugh *et al.*, 2003; Barylko *et al.*, 2009). Unlike PI4kIIα, regulation of PI4KIIβ is quite complex, but its membrane recruitment is partly controlled by its interaction with the molecular chaperone, Hsp90 (Jung *et al.*, 2011). Hsp90 binds PI4KIIβ tightly and sequesters it in the cytoplasm, thereby diminishing its catalytic activity by as much as 70% by denying it access to its membrane bound substrate. This interaction is relieved by brief treatment with an Hsp90 inhibitor or by growth factor stimulation (Jung *et al.*, 2011), resulting in an almost equal distribution of PI4KIIβ between the cytoplasm and intracellular membranes (Barylko *et al.*, 2009; Li *et al.*, 2012).

PI4KIIα is responsible for the synthesis of PI(4)P pools on the Golgi (Wang *et al.*, 2007; Waugh *et al.*, 2011) and endosomal membranes (Waugh *et al.*, 2011; Dong *et al.*, 2016; Henmi *et al.*, 2016; Ketel *et al.*, 2016); however, little is known about the pools of PI(4)P synthesised by PI4KIIβ or whether they are distinct from the PI4KIIα pool as this isoform is often overlooked due to its low kinase activity (Balla *et al.*, 2002) and sometimes considered to possess overlapping functions with PI4KIIα (Dong *et al.*, 2016; Lopes da Silva *et al.*, 2016). This may equally be due to interactions of either isoform with, clathrin adaptor, AP-1. PI4KIIα recruits AP-1 to the Golgi in a kinase dependent manner while PI4KIIβ interacts directly with AP-1 at the TGN via an acidic cluster dileucine sorting motif in its *N*-terminal region (Wang *et al.*, 2003; Wieffer *et al.*, 2013).

It is well known that the TGN, is organised into sorting microdomains that permit segregation of cargo proteins enabling efficient membrane transport (Guerriero *et al.*, 2008; Treyer *et al.*, 2016; Zurzolo and Simons, 2016), but the domain localisation of both PI4KIIS remains unclear. In addition, the reported association of both isoforms with clathrin adaptor, AP-1 makes it difficult to assign the isoforms to specific TGN domains. Fluorescent imaging techniques for identifying TGN pools of PI(4)P include the use of PH domain containing lipid transfer proteins such as: Four-phosphate adaptor proteins (e.g. FAPP1), the oxysterol binding protein, OSBP, as well as PI(4)P binding vesicle tethering factors from *Legionella pneumophila*. However, many of these proteins engage in coincident interactions with other membrane proteins which may bias PI(4)P staining to one cellular compartment at the expense of other intracellular membranes containing PI(4)P. For instance, FAPP proteins interact with the GTPase Arf1 and may thus bias PI(4)P labelling to Arf1-containing regions of the Golgi, and not report PI(4)P pools outside the Golgi. The P4M domain of *SidM* protein from *L.pneumophila* is a more versatile PI(4)P reporter as it is able to label PI(4)P pools in regions other than the Golgi such as endosomes and PM (Hammond *et al.*, 2014) but is also limited by its interaction with Rab1 which biases its PI(4)P recognition to the Golgi (Luo *et al.*, 2015).

This chapter describes distinct membrane localisations of the type II PI4Ks. In this case, endogenous proteins rather than fluorescent or epitope tagged were co-immunostained with various membrane markers. This was done to avoid the production of artefactual phenotypes that may occur due to over-expression of recombinant proteins (Tan and Brill, 2014). For instance, overexpression of PI4KIIs may saturate Golgi membranes resulting in a spill over to a variety of intracellular vesicles, thereby overemphasising the membrane localisations of these proteins (Wang *et al.*, 2003). With the use of immunofluorescent staining techniques coupled with isoform-specific RNA interference (RNAi), we demonstrated that PI4KIIα and PI4KIIβ localise to distinct subcellular membrane compartments and synthesise distinct pools of PI(4)P. In addition, the use of a recombinant protein containing the P4C domain of the SidC protein from *Legionella pneumophila* as a reporter for

PI(4)P revealed the presence PI(4)P on membrane compartments other than the Golgi as previously described (Luo *et al.*, 2015; Lopes da Silva *et al.*, 2016). Another advantage of using this recombinant protein domain as a PI(4)P reporter is that it possesses a greater PI(4)P sensitivity than the P4M domain of SidM (as well as FAPP1 and OSBP) at the plasma membrane and perinuclear region which corresponds to the Golgi and cytoplasmic vesicles (Luo *et al.*, 2015). In addition, it directly binds PI(4)P and engages with membranes without interacting with accessory proteins. These features permitted visualisation of PI(4)P pools synthesised by the type II PI4Ks on different intracellular membranes and enabled distinctions between these pools through co-immunostaining with organelle/membrane markers.

3.2 Results

3.2.1 PI4KIIα and PI4KIIβ localise to distinct cellular compartments

To visualise the cellular localisation of PI4KIIs, HeLa cells were immunostained with antibodies specific for PI4KIIα and PI4KIIβ and imaged using confocal microscopy. Endogenous PI4KIIα exhibited a predominant juxtanuclear vesicular staining pattern while PI4KIIβ displayed a diffuse, largely perinuclear staining pattern. Both proteins were also seen in scattered cytoplasmic punctae as previously described (Balla *et al.*, 2002; Minogue *et al.*, 2006; Barylko *et al.*, 2009; Jung *et al.*, 2011) but displayed minimal colocalization (r=0.3), suggesting that they localise to distinct membrane domains (Figure 3-1). In addition, PI4KIIβ was also observed on plasma membrane ruffles as previously reported (Wei *et al.*, 2002; Jung *et al.*, 2008; Barylko *et al.*, 2009).

The identities of these membrane locations were characterised by co-immunostaining PI4KIIα or PI4KIIβ together with organelle membrane markers, TGN46, syntaxin 6, EEA1 and CD63 which are reporters for the TGN, early and late endosomes. Again, endogenous PI4KIIα localised to the juxtanuclear region and on scattered cytoplasmic punctae where it colocalised with syntaxin 6 (Figure 3-2) confirming results from a previous study where PI4KIIα was reported to localise to cholesterol enriched microdomains characterised by the presence of SNARE protein, syntaxin 6 (Waugh *et al.*, 2011). PI4KIIα also localised to TGN46 positive membranes, thereby mapping it to the TGN substantiating its role in TGN trafficking pathways (Figure 3-2). PI4KIIα also partly localised to cytoplasmic punctae containing EEA1 and CD63 (Figure 3-3), reinforcing its previously reported role in endosomal trafficking pathways (Balla *et al.*, 2002; Minogue *et al.*, 2006; Henmi *et al.*, 2016).

PI4KIIβ in comparison with PI4KIIα showed significantly greater colocalisation with TGN46 while it colocalised less with syntaxin 6 (Figure 3-2). These results suggest that both isoforms are found on different sub-

membrane domains within the TGN. PI4KIIβ also colocalised with CD63-positive vesicles but showed little, yet statistically non-significant colocalisation with EEA1 in comparison with PI4KIIα (Figure 3-3). These findings are consistent with earlier studies linking PI4KIIα to the TGN, LE and EE (Balla *et al.*, 2002; Minogue *et al.*, 2006; Wang *et al.*, 2007; Henmi *et al.*, 2016). Although relatively little is known about the membrane localisation of PI4KIIβ, data from the present study support the evidence of localisation to endosomal membranes, consistent with previous reports (Balla *et al.*, 2002; Wieffer *et al.*, 2013).

A

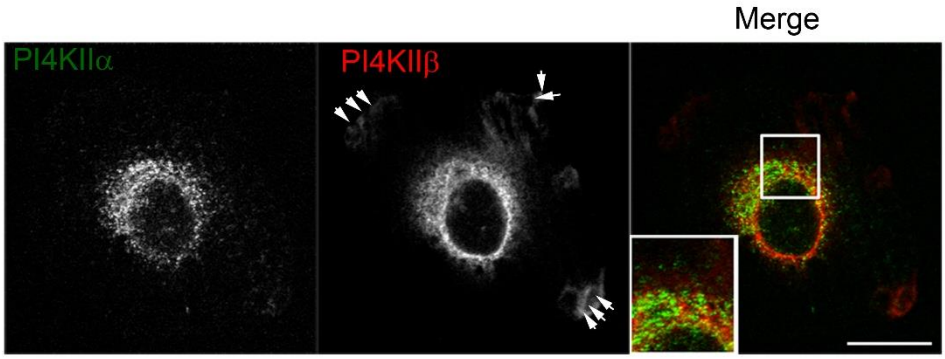

B

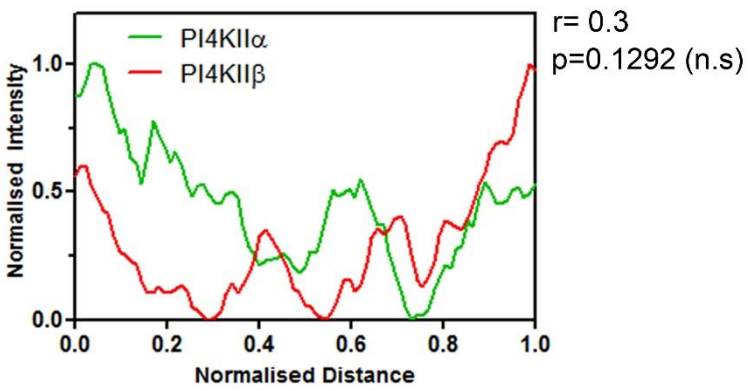

Figure 3-1. Immunofluorescent staining of PI4KIIα and PI4KIIβ.

A. HeLa cells were fixed and stained with anti-PI4KIIα (green) and anti-PI4KIIβ (red). Arrows indicate the presence of PI4KIIβ in plasma membrane ruffles. Zoom boxes represent emphasise areas co-immunostaining. Images are single confocal sections. Scale bars, 10 µm. **B.** The box-profile plot shows limited colocalisation between PI4KIIα and PI4KIIβ in the zoom-box corresponding to the perinuclear and juxtanuclear cell regions. Pearson's correlation coefficient (r) was computed for normalised PI4KIIα and PI4KIIβ fluorescent intensities in the selected region, n.s (not significant).

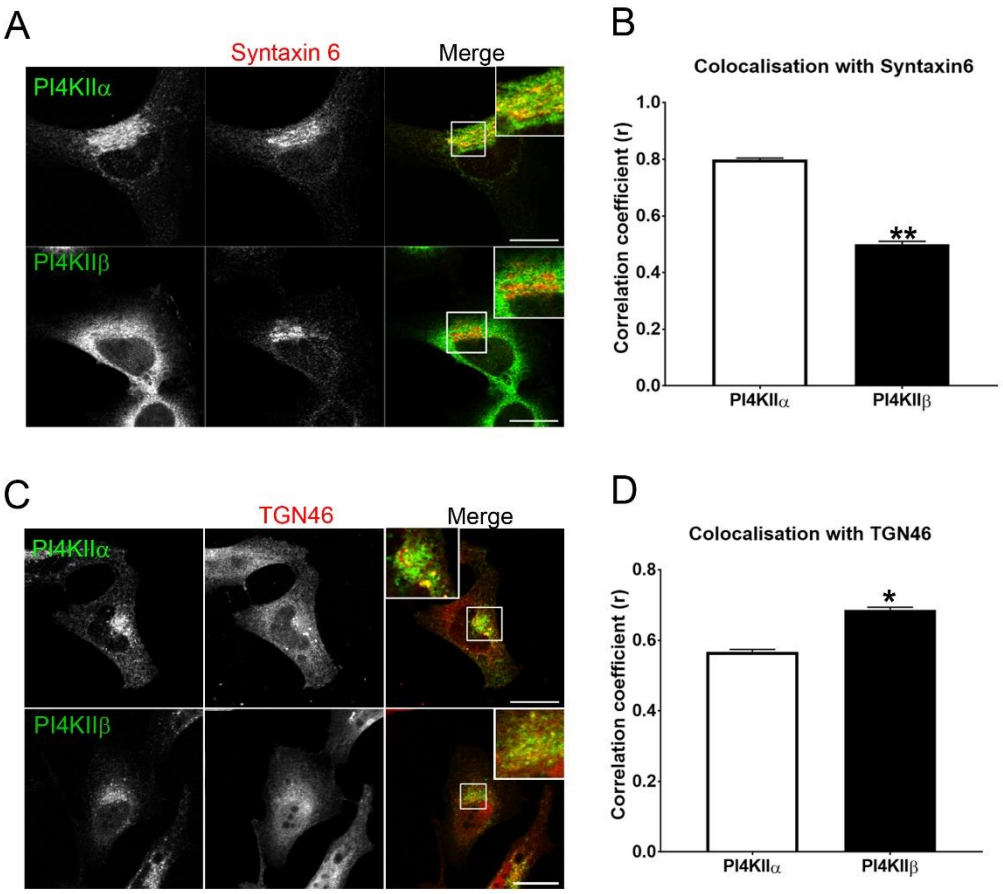

Figure 3-2. Differential staining of PI4KIIα and PI4KIIα with TGN markers.

A and **C**. HeLa cells were fixed and stained with anti-PI4KIIα or anti-PI4KIIβ (green) along with anti-syntaxin 6 (red). Zoom boxes represent magnified areas of colocalisation between green and red channels. Images are single confocal sections, acquired with identical experimental settings. Scale bars, 10 µm. **B** and **D**. Histogram shows Pearson's correlation coefficients computed for colocalization between PI4KIIα or PI4KIIβ and (B) syntaxin6 or (D) TGN46. *, $p<0.05$, **, $p<0.001$, n.s (not significant). Histogram bars represent as means ± SEM (n=30 cells, three independent experiments).

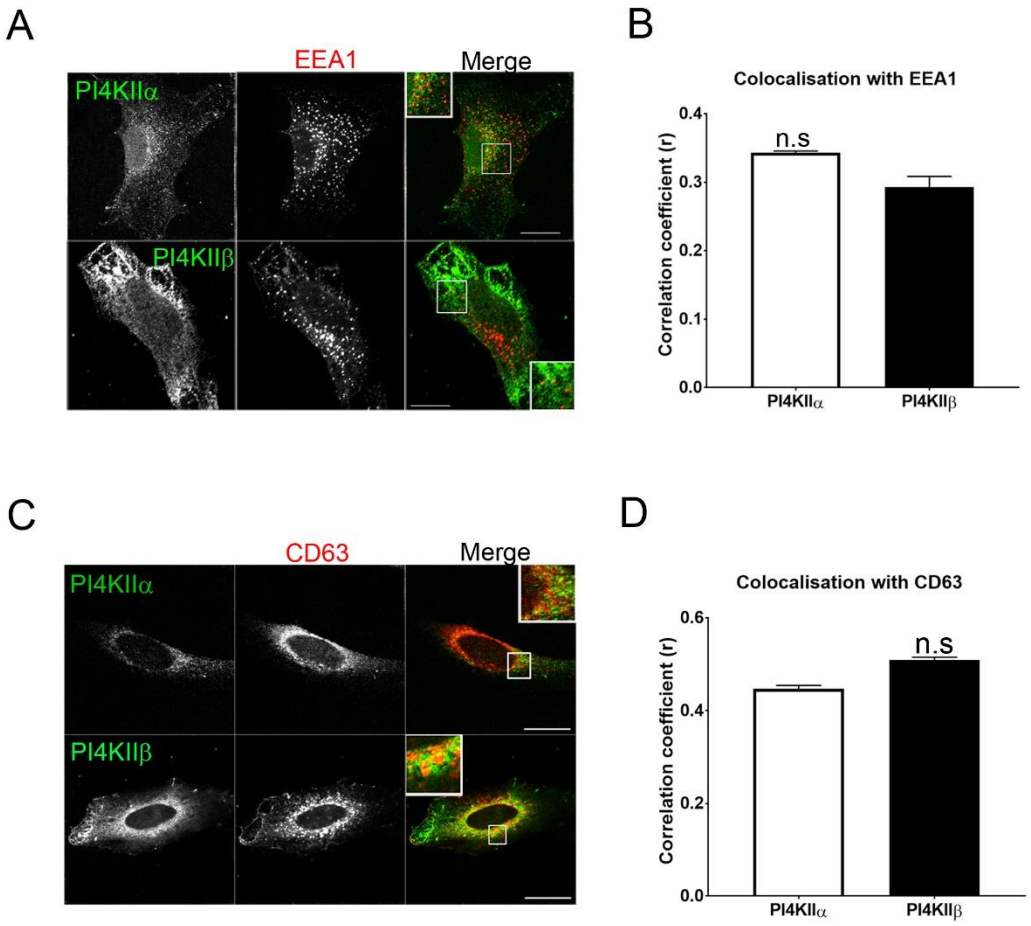

Figure 3-3. Co-immunostaining of PI4KIIα and PI4KIIβ with endosomal markers.

A and **C**. Co-immunostaining of PI4KIIα or anti-PI4KIIβ (green) and (A) EEA1 or (C) CD63 (both red). Zoom boxes represent magnified areas of co-staining. Images are single confocal sections, acquired with identical experimental settings. Scale bars,10 µm. **B** and **D**. Pearson's correlation coefficients for colocalization between PI4KIIα or PI4KIIβ and (B) EEA1 or (D) CD63. *, $p<0.05$, **, $p<0.001$, n.s (not significant). Bars are means ± SEM (n=20 cells, three independent experiments).

3.2.2 Optimising conditions for RNA interference

RNA interference (RNAi) was used to induce loss of function of PI4KIIα or PI4KIIβ. A single scrambled siRNA oligo and SMARTpool targeting GAPDH served as non-targeting and negative control respectively. Optimal concentrations of siRNA stocks and transfection reagents were determined using dose dependent and time-course assays (not shown). We tested the toxic effects of siRNAs and transfection reagents using the MTT (3-(4,5)-dimethylthiazo-2-yl)-2,5-diphenyl tetrazolium) assay. Results showed that siRNA transfection had negligible effects on cell viabilities in PI4KII and control siRNA transfected cells within 72 hours (Figure 3-4). The efficiency of gene silencing was evaluated by immunoblotting and time course assays revealed significant gene silencing 72 hours post-transfection with minimal cell death (not shown).

Expression levels of target proteins were compared with those of non-targeted controls, as measured by western immunoblotting of total cell extracts while protein loading was normalised using α-Tubulin as a loading control. In comparison with Non-targeting siRNA transfected HeLa cells, ~80% gene silencing was achieved for the PI4K2A gene (relative protein expression= 0.18±0.001) while ~85% was recorded for PI4K2B (relative protein expression= 0.08±0.25). Similar effects were observed with siRNA targeting the GAPDH gene without having any impact on PI4K2A or PI4K2B expression (Figure 3-5). These effects confirm effective depletion of the PI4KII isoforms by the siRNAs.

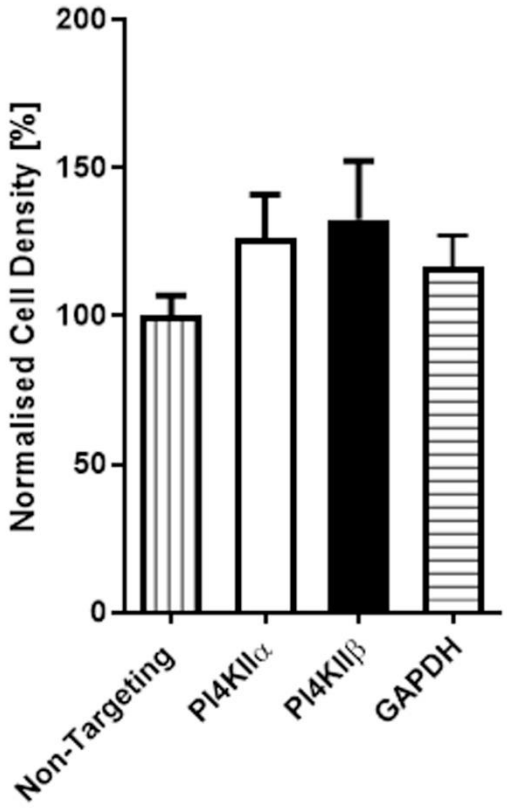

Figure 3-4. The MTT assay as an index of cellular tolerance to siRNA and transfection reagent.

HeLa cells were subjected to the MTT assay to evaluate patterns of cell growth (and cell survival) following treatment with siRNA and transfection reagents. All values were normalised to control. Histogram bars indicate means ± SEM (three independent experiments).

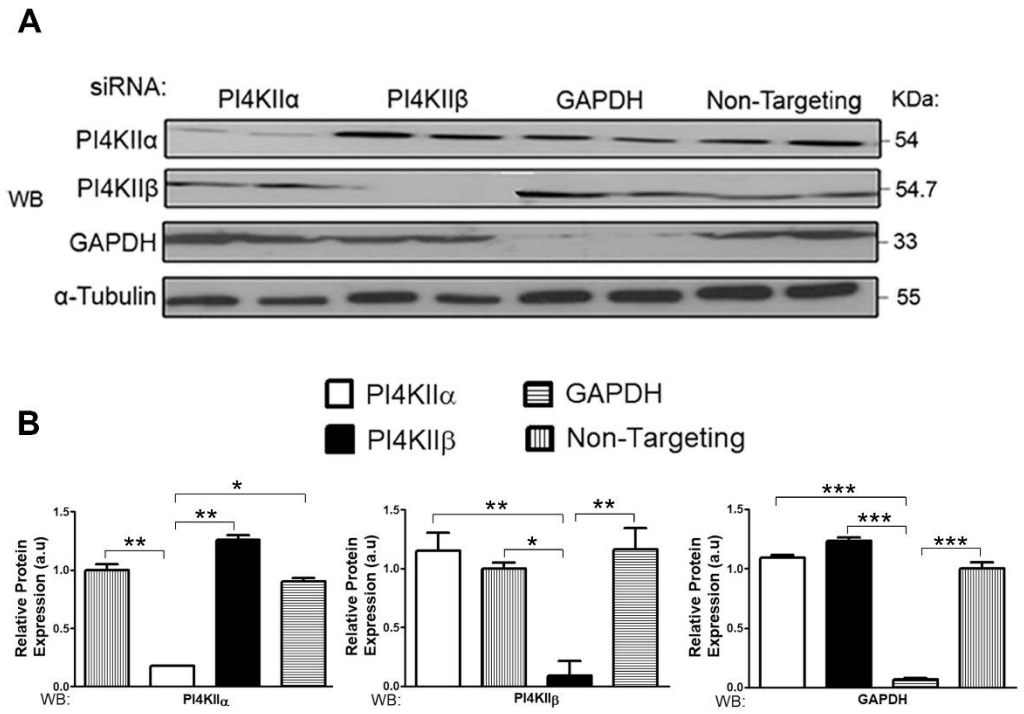

Figure 3-5. PI4K2A and PI4K2B gene expression are specifically and efficiently suppressed by siRNA.

A. Total cell lysates of PI4KIIα, PI4KIIβ, GAPDH and Non-targeting siRNA transfected HeLa cells were analysed for protein expression by western blot. Antibodies to α-tubulin were also used to probe the membranes to control for protein levels. **B.** Densitometric analysis of western blot signals derived from three independent experiments. Protein expression of PI4KIIα (left panel), PI4KIIβ (middle panel) and GAPDH (right panel) was measured relative to that of non-targeting siRNA transfected cells which served as control. Histograms are presented as mean ± SEM (three independent experiments). *, $p<0.05$, **, $p<0.01$, ***, $p<0.001$, ns (not significant).

3.2.3 Fluorescent detection of membrane PI(4)P pools

3.2.3.1 FAPP1 does not distinguish separate pools of PI4P synthesised by PI4KIIα and PI4KIIβ

Recombinant GST-tagged lipid binding probes were used as reporters for studying the effects of PI4KII gene silencing on localisation and membrane lipid content. We anticipated that knockdown of either PI4KII isoform would alter the distribution of PI(4)P on Golgi and endosomal membranes, the predominant location of this species. To determine the extent to which these lipid kinases contribute to Golgi pools of PI(4)P, we probed fixed cells with a recombinant version of the PH domain from GST-FAPP1 as a reporter for PI(4)P. Depletion of either isoform, had minimal impacts on GST-PH-FAPP1 signal intensities while colocalisation between PI(4)P (GST-PH-FAPP1) and syntaxin 6 (Figure 3-6, a and b) or TGN46 (Figure 3-6, c and d) remained unaffected. This, nevertheless, does not prove that Golgi pools of PI(4)P are unaffected by depletion of either type II PI4K isoform. Rather, the PI(4)P reporter used in this case may not specifically report the PI(4)P synthesised by either isoform as PH-FAPP1 co-incidentally localises to the Golgi via its interaction with Arf1 and may bias PI4P detection to the Golgi (Godi *et al.*, 2004; Shin and Nakayama, 2004), rendering it unsuitable for the detection of pools such as those localised to the TGN, endosomes and other vesicular structures which do not harbour this GTPase. We also hypothesised that this may occur due to upregulation of type III PI4Ks as a cellular response to compensate for the loss of one PI4K isoform. These together represent major impediments to the fluorescent identification of individual PI(4)P pools generated by the PI4KIIs using this lipid binding probe.

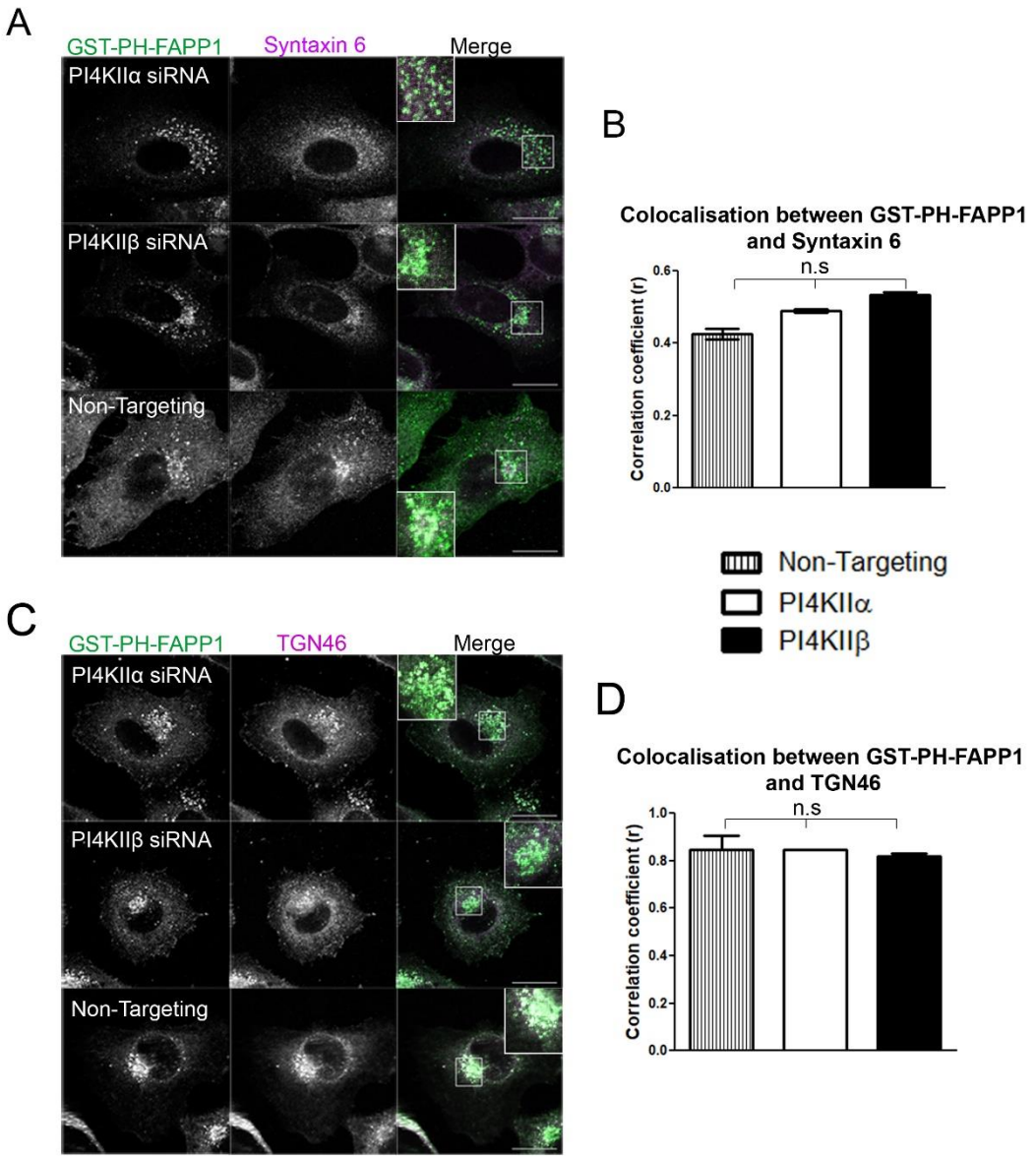

Figure 3-6. Identifying PI(4)P pools generated by the PI4KIIs in HeLa cells.

A and **C.** A recombinant GST-fusion of the PH domain of FAPP1 (GST-PH-FAPP1) was used to indirectly stain membrane pools of PI(4)P. PI(4)P was detected by probing fixed cells with anti-GST antibodies, followed by Alexa-Fluor® conjugated secondary antibodies. These cells were co-stained with (A) syntaxin 6 using an anti-syntaxin 6 antibody or (C) TGN46 using an anti-TGN46 antibody to identify membrane pools of PI(4)P localised to cellular membranes containing these proteins. Images are single confocal sections. Scale bars, 10 µm. Zoom boxes represent magnified areas of colocalization. **B** and **D**. Histograms represent Pearson's correlation coefficients for colocalization between PH-FAPP (PI(4)P) and (B) syntaxin 6 or (D) TGN46. n.s (not significant). (n=20 cells, three independent experiments).

3.2.3.2 GST-tagged P4C domain of SidC protein can be used to report membrane PI(4)P generated by PI4KII isoforms

We used the GST-tagged P4C domain of the SidC protein from *L.pneumophila* in place of PH-FAPP1 or SidM to report membrane PI(4)P pools. Since this protein serves as an unbiased PI(4)P reporter, we hypothesised that it would report PI(4)P pools attributable to either PI4KII isoform. A similar issue of the inability to completely distinguish the pools contributed by either type II PI4K isoform was observed and this led us to conclude that this confounding effect was due to the type III PI4K activity (Figure 3-7 a (upper panel)). To eliminate confounding signals due to PI4KIII activities, cells were treated with 10 µM of PI3K inhibitor, wortmannin for 10 minutes, 72 hours post-transfection to inhibit these enzymes as previously demonstrated (Balla *et al.*, 2002). The residual GST-P4C signal was primarily in the Golgi region and on cytoplasmic punctae and this permitted visualisation of PI(4)P pools derived from the activities of PI4KIIα (PI(4)$P^{PI4KII\alpha}$) and PI4KIIβ (PI(4)$P^{PI4KII\beta}$), (Figure 3-7a (lower panel)). Wortmannin treatment decreased total cellular PI(4)P by ~60% in PI4KIIα depleted cells, indicating PI4KIIα's high kinase activity (Figure 3-7). In comparison with PI4KIIα-depleted cells, depletion of PI4KIIβ had a significantly lower impact on total cellular PI(4)P (Figure 3-7b). This is consistent with previous studies reporting that this isoform has a lower *in vitro* kinase activity compared with PI4KIIα (Balla *et al.*, 2002). Nonetheless, depletion of this isoform lowered wortmannin resistant PI(4)P levels by ~30% suggesting a significant role for PI4KIIβ in the maintenance of PI(4)P levels.

Wortmannin treated PI4KIIα-depleted cells showed residual PI(4)$P^{PI4KII\beta}$ staining which significantly colocalised with TGN46 but showed minimal colocalisation with syntaxin 6 (Figure 3-8, a-d). Conversely, PI4KIIβ depletion revealed cellular PI(4)$P^{PI4KII\alpha}$ that mostly colocalised with syntaxin 6, a protein that labels both the TGN and endosomes but weakly colocalised with TGN46 (Figure 3-8, a-d). Over-expression of an siRNA resistant GFP-tagged mouse PI4KIIα plasmid construct ((Mössinger *et al.*, 2012); Figure 3-9a) partly rescued PI4KIIα depletion by significantly increasing PI(4)P colocalisation

with syntaxin 6 in comparison with non-transfected PI4KIIα depleted cells (Figure 3-9b and 3-10a) while over-expression of an siRNA resistant HA-tagged human PI4KIIβ plasmid construct ((Wieffer *et al.*, 2013); Figure 3-9a) in PI4KIIβ depleted HeLa cells had negligible effects on PI(4)P colocalisation with syntaxin 6 but restored the PI(4)P pool that colocalises with TGN46 (Figure 3-9 and 3-10). This demonstrates that the wortmannin-resistant $PI(4)P^{PI4KII\alpha}$ and $PI(4)P^{PI4KII\beta}$ pools generated by PI4KIIs exist in distinct subdomains of TGN/endosomal membranes and that knockdown of each isoform affects a metabolically distinct PI(4)P compartment.

PI(4)P recruits the clathrin adaptor, AP-1 to the TGN and is required for the control of TGN to endosome traffic (Wang *et al.*, 2003; Wieffer *et al.*, 2013). Wortmannin treatment permitted imaging of PI(4)P pools that associate with other membrane domains described by clathrin adaptor proteins, AP-1, GGA 1 & 2. Wortmannin-resistant PI(4)P colocalised with clathrin adaptor, AP-1 and depletion of either PI4KII isoform significantly diminished AP-1 positive PI(4)P pools but had negligible effects on colocalisation between the GGAs and PI(4)P (Figure 3-11). It was hypothesised that depletion of TGN PI(4)P as a result of PI4KII siRNA and wortmannin treatment would have a significant impact on AP-1-positive PI(4)P and post-TGN membrane trafficking pathways (discussed further in Chapter 4). Over-expression of an mCherry tagged cation-independent mannose-6-phosphate receptor (CI-M6PR) permitted imaging of wortmannin-resistant PI(4)P pools that associate with this AP-1 cargo. PI(4)P colocalised with mCherry-CI-M6PR in the juxtanuclear region of fixed cells and depletion of either PI4KII isoform significantly decreased colocalisation between PI(4)P and this AP-1 cargo (Figure 3-12 a and c). In addition, PI4KIIβ depletion diminished the vesicular staining pattern of mCherry-CI-M6PR and is suggestive of disrupted AP-1 cargo transport (Figure 3-12b and addressed further in Chapter 4).

PI4KIIα depletion affected EEA1-positive PI(4)P pools in wortmannin treated cells indicating the presence of $PI(4)P^{PI4KII\alpha}$ on early endosomes (Figure 3-13). Wortmannin-resistant PI(4)P puncta colocalised with the LE/lysosomal tetraspanin, CD63 and depletion of either PI4KIIs reduced the amount of

PI(4)P colocalising with this marker: a feature that was more prominent in PI4KIIα depleted cells (Figure 3-14). These results are consistent with previous reports which showed that PI4KIIs synthesise PI(4)P on endosomal membranes (Wang *et al.*, 2003; Minogue *et al.*, 2010; Jović *et al.*, 2012, 2014; Mössinger *et al.*, 2012; Wieffer *et al.*, 2013; Dong *et al.*, 2016; Henmi *et al.*, 2016; Ketel *et al.*, 2016).

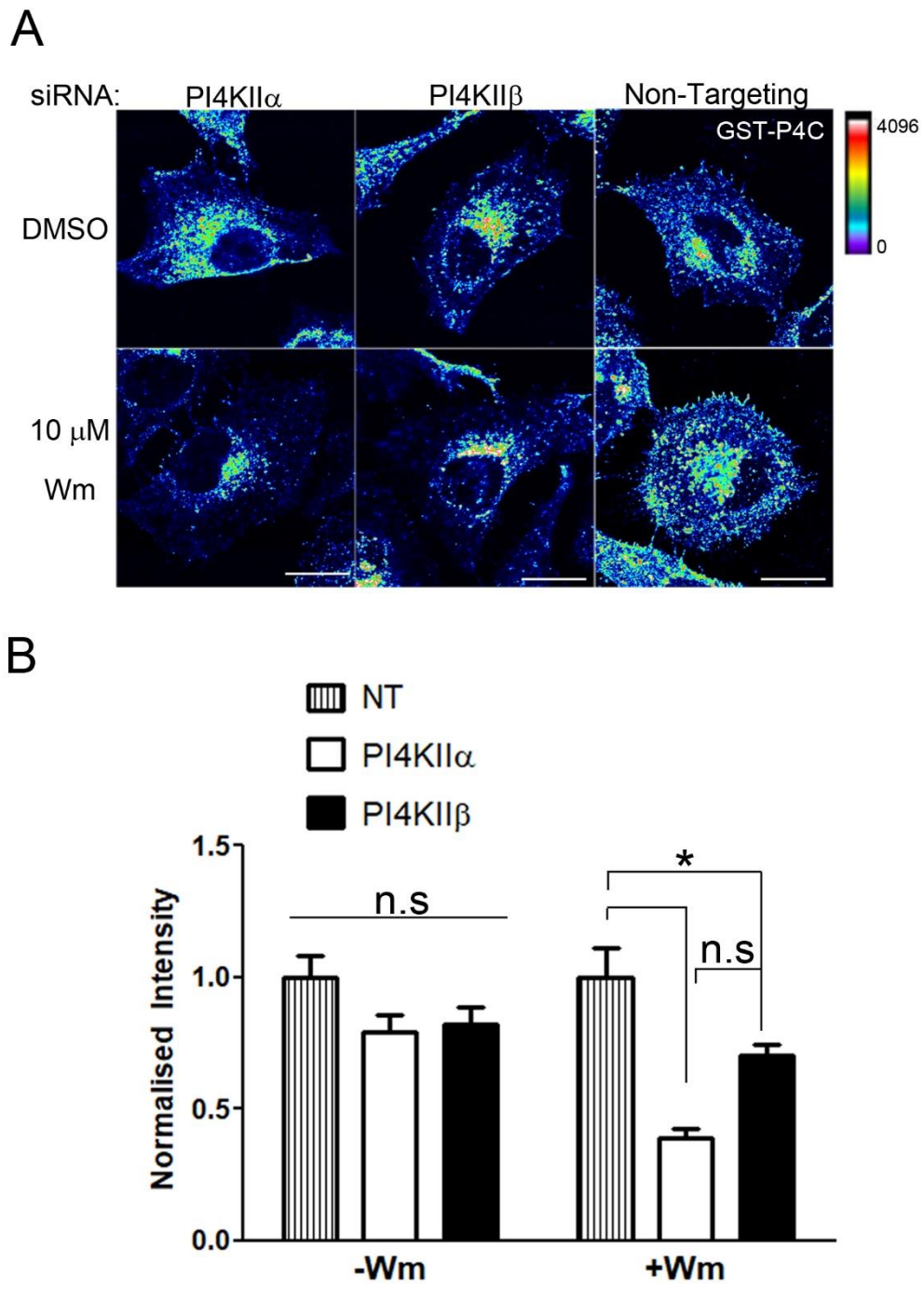

Figure 3-7. Visualising wortmannin resistant PI(4)P pools with GST-P4C.

A. Recombinant GST-tagged protein containing the P4C domain from the *Legionella pneumophila* SidC protein (GST-P4C) was used to indirectly stain membrane pools of PI(4)P (green) in HeLa cells. Images are single confocal sections. Scale bars, 10 μm. Heat map shows fluorescence intensities **B.** Cellular PI(4)P levels were measured by quantifying signal intensities from the GST-P4C (green) channels and normalising to control levels. Bars represent sample means ± SEM (6 images were acquired for each siRNA treatment per independent experiment (n=3)). *, $p<0.05$, ***, $p<0.001$, n.s (not significant).

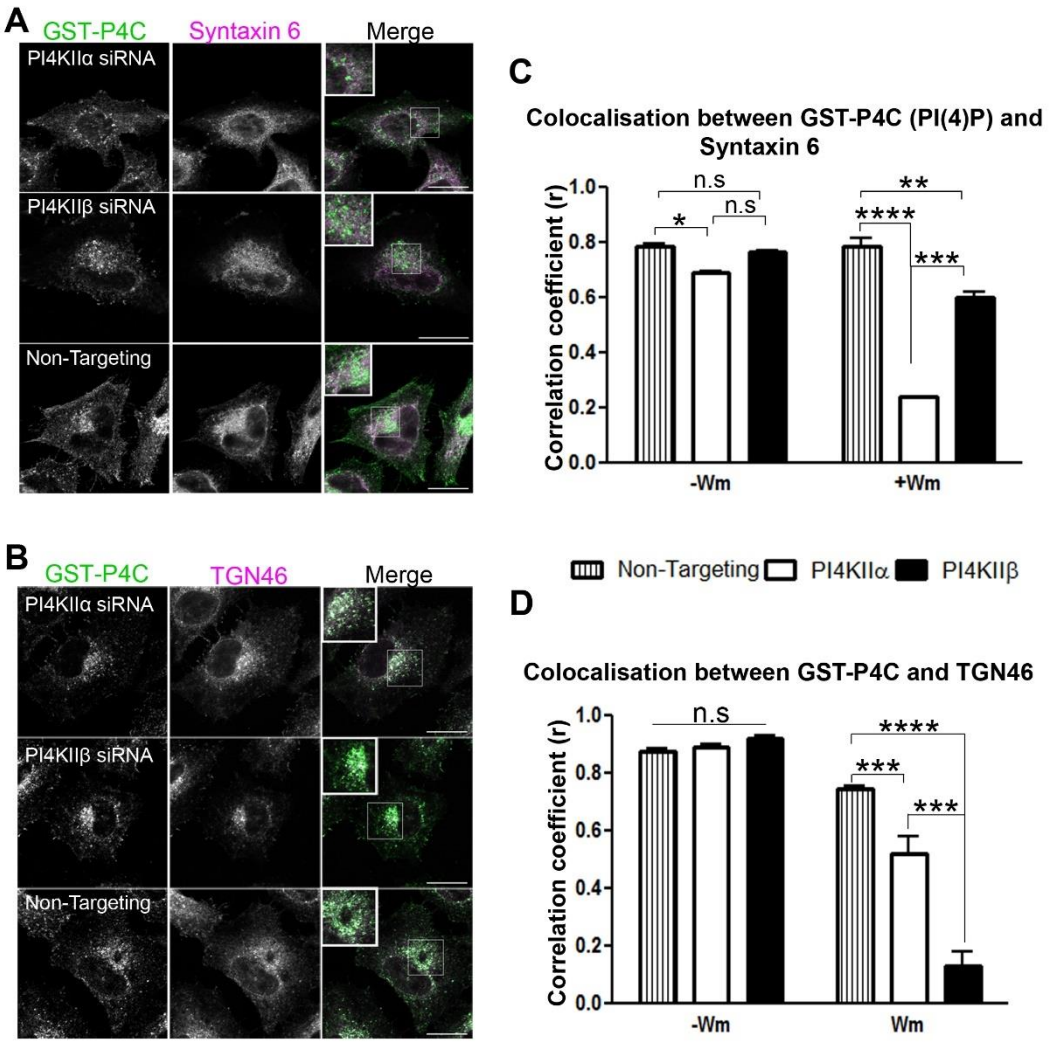

Figure 3-8. PI4KII siRNA and wortmannin treatment unmask distinct membrane pools of PI(4)P.

A, B. HeLa cells were treated with 10 µM wortmannin, 72-hours post-siRNA transfection, for 10 minutes prior to fixation. Images are single confocal sections which, depict co-immunostaining between GST-P4C (green) and (A) syntaxin 6 or (B) TGN46 (magenta). Scale bars,10 µm. **C, D**. Histograms depict Pearson's correlation coefficients calculated for co-localising pixels between the green channel (PI(4)P) and magenta channel (syntaxin 6 or TGN46 channel), n=25 cells, three independent experiments. *, $p<0.05$, **, $p<0.01$, ***, $p<0.001$, ****, $p<0.0001$, n.s (not significant).

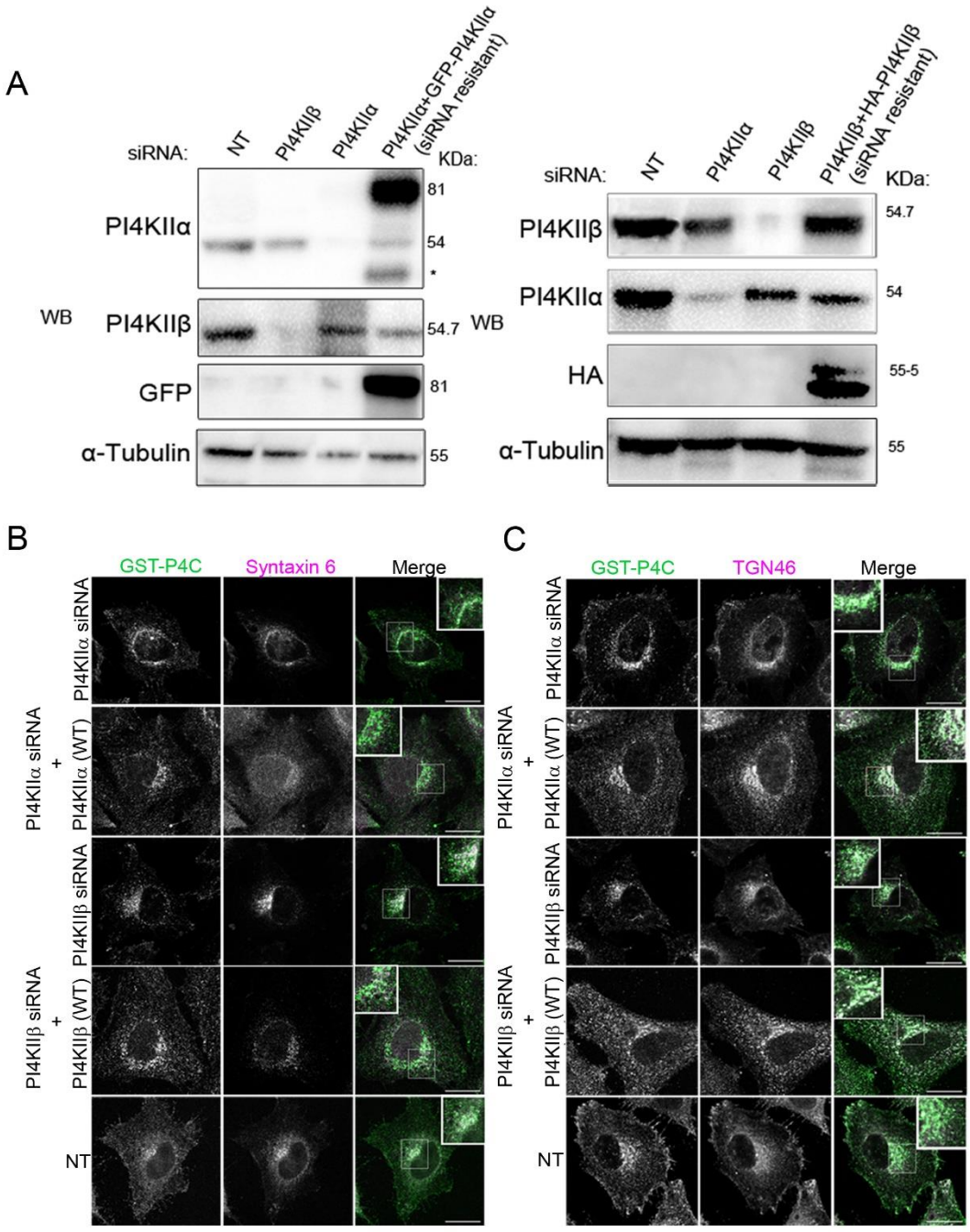

Figure 3-9. Expression of siRNA resistant PI4KIIα and PI4KIIβ restore their respective membrane PI(4)P pools.

A. Rescue of siRNA in HeLa cells. Western blots show the loss and re-expression of siRNA-resistant recombinant PI4KIIα and PI4KIIβ following siRNA-mediated depletion. Asterisk indicates proteolytic fragments resulting from the overexpression of resistant GFP-PI4KIIα. **B** and **C.** Representative confocal images showing immunostaining for GST-P4C (green) and (B) syntaxin 6 or (C) TGN46 (magenta) following siRNA mediated silencing with or without rescue with siRNA-resistant constructs. Scale bars, 10 µm.

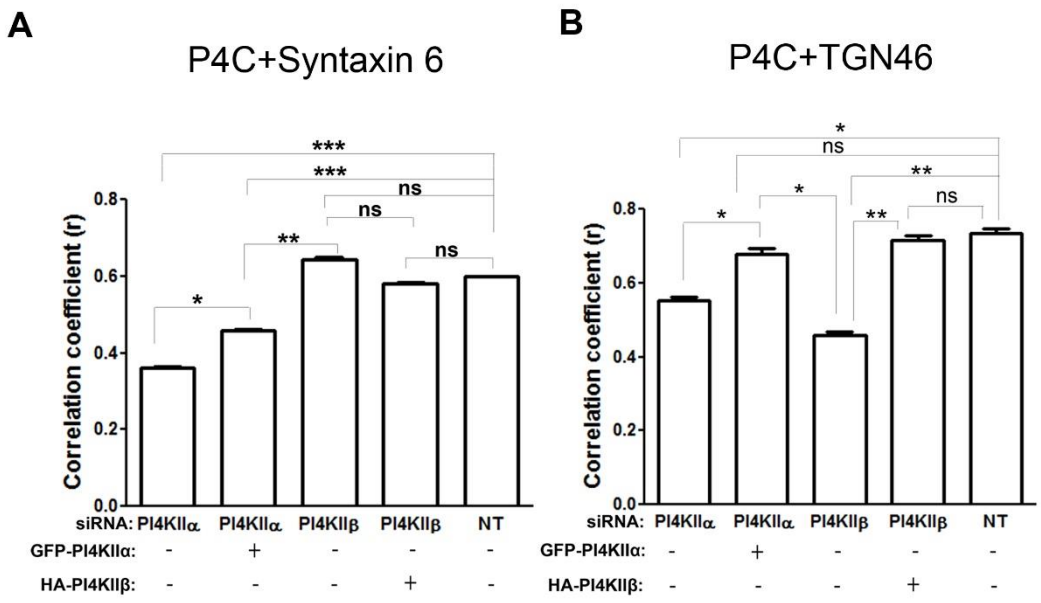

Figure 3-10. Restoration of wortmannin insensitive TGN PI(4)P pools with siRNA-resistant type II PI4K plasmid constructs.

Histograms show Pearson's correlation coefficients computed for co-localisation between PI(4)P and (A) syntaxin 6 or (B) TGN46 following siRNA mediated silencing with or without subsequent transfection with siRNA resistant constructs and wortmannin treatment (n=20 cells, three independent experiments). *, $p<0.05$, **, $p<0.01$, ***, $p<0.001$, ns (not significant).

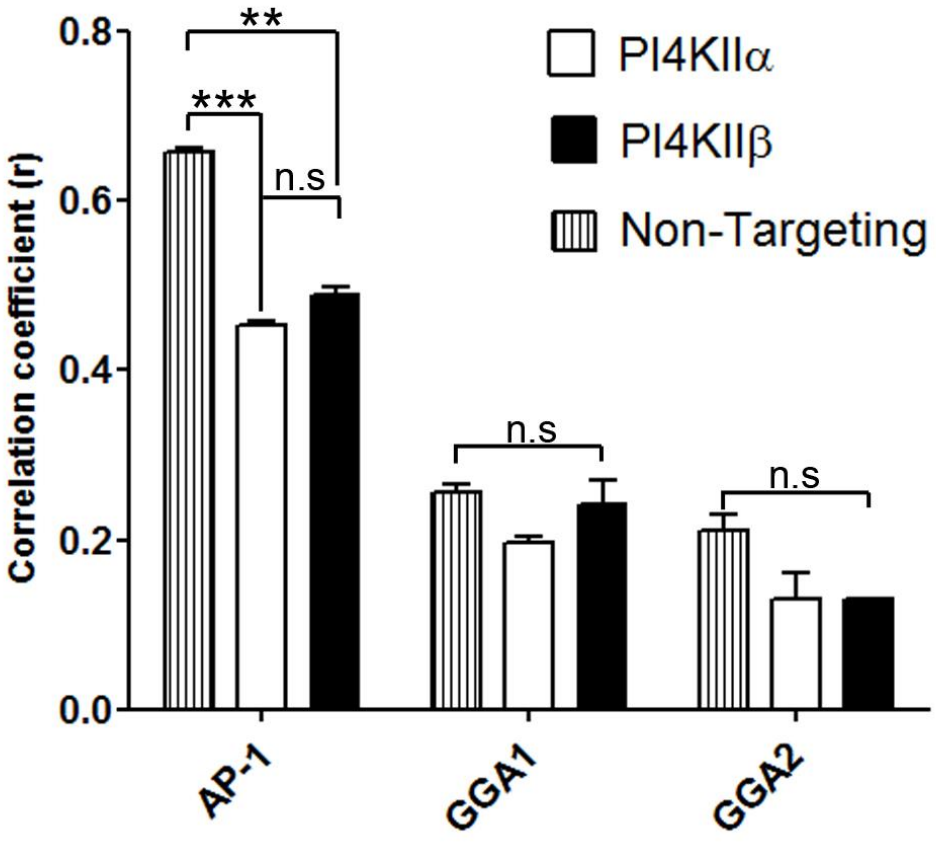

Figure 3-11. Colocalisations between wortmannin insensitive PI(4)P and clathrin adaptor proteins.

siRNA transfected HeLa cells were treated with wortmannin 72-hours post-transfection for 10 minutes and then co-stained for PI(4)P and various membrane/organelle markers. The histogram shows colocalisation between PI(4)P (imaged by labelling cells with GST-P4C) and clathrin adaptor proteins; AP-1, GGA1&2. The histogram represents Pearson's correlation coefficients for colocalisation between PI(4)P and the named proteins. Data are presented as means ± SEM *, $p<0.05$, **, $p<0.01$, ***, $p<0.001$, n.s (not significant).

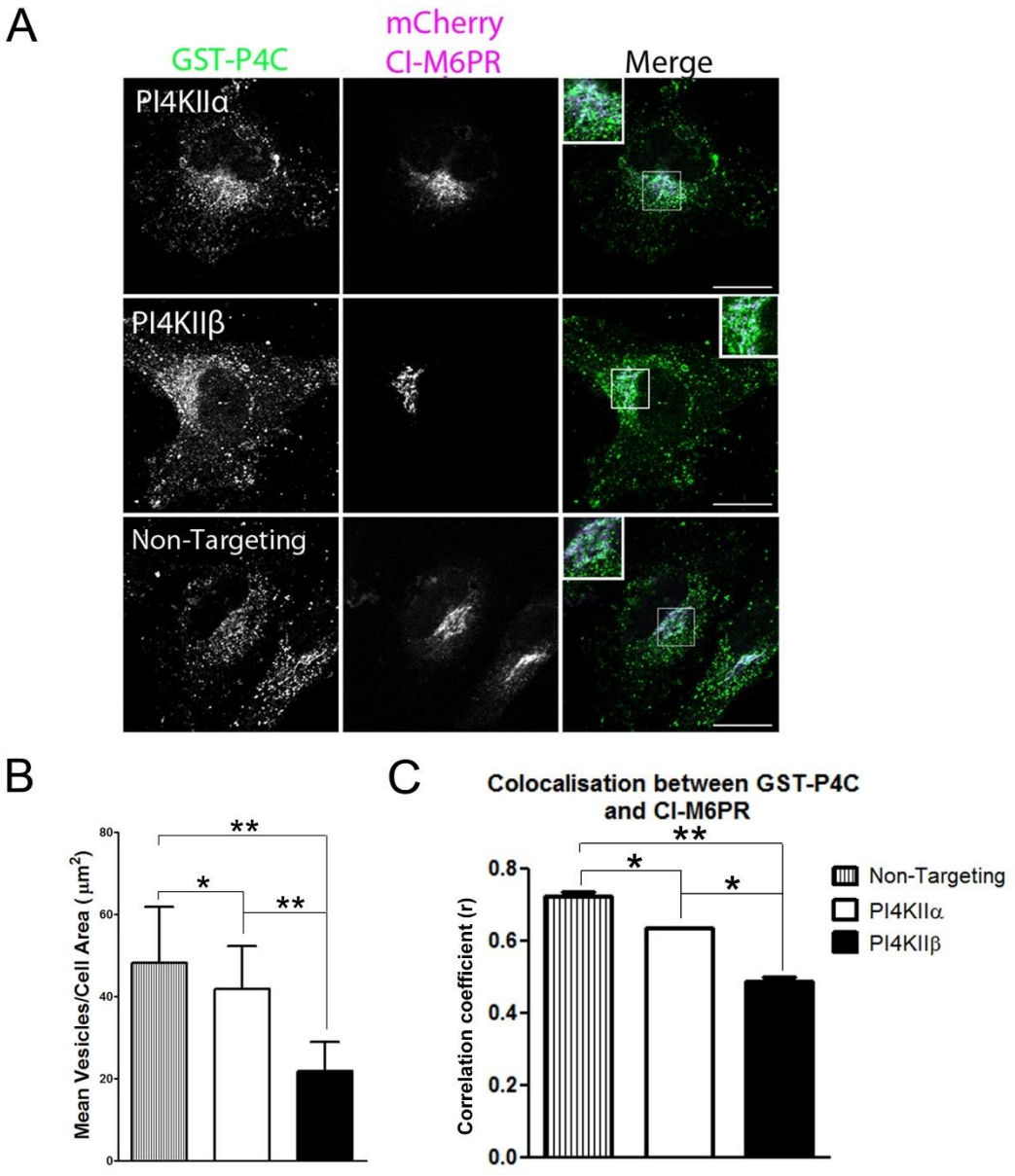

Figure 3-12. Type II PI4Ks synthesise pools of PI(4)P that interact with AP-1 cargo, CI-M6PR.

A. Recombinant GST-tagged P4C was used to indirectly stain membrane pools of PI(4)P in fixed HeLa cells. HeLa cells were transfected with an mCherry-tagged cation-independent mannose-6-phosphate receptor (mCherry-CI-M6PR) 48 hours post-transfection with respective siRNA. Images are single representative confocal sections. Scale bars, 10 μm. Zoom boxes represent magnified areas of colocalization. **B.** The histogram shows changes in vesicular staining pattern of CI-M6PR in target and control siRNA transfected cells. To quantify vesicular CI-M6PR, 8-bit images were subjected to a rolling ball algorithm in ImageJ to subtract background fluorescence and then thresholded to eliminate other CI-M6PR-positive structures except those on cytoplasmic puncta. This generated binary images that were subsequently dilated by a single pixel using the 'dilate' function. The resulting image was then analysed using the 'analyse particles' command to count the total number of CI-M6PR-positive vesicles and measure total cell area covered.

C. The histogram shows Pearson's correlation coefficients calculated for co-localising pixels between the green channel (PI(4)P) and magenta channel (CD63), n=25 cells, three independent experiments. *, p<0.05, **, p<0.01.

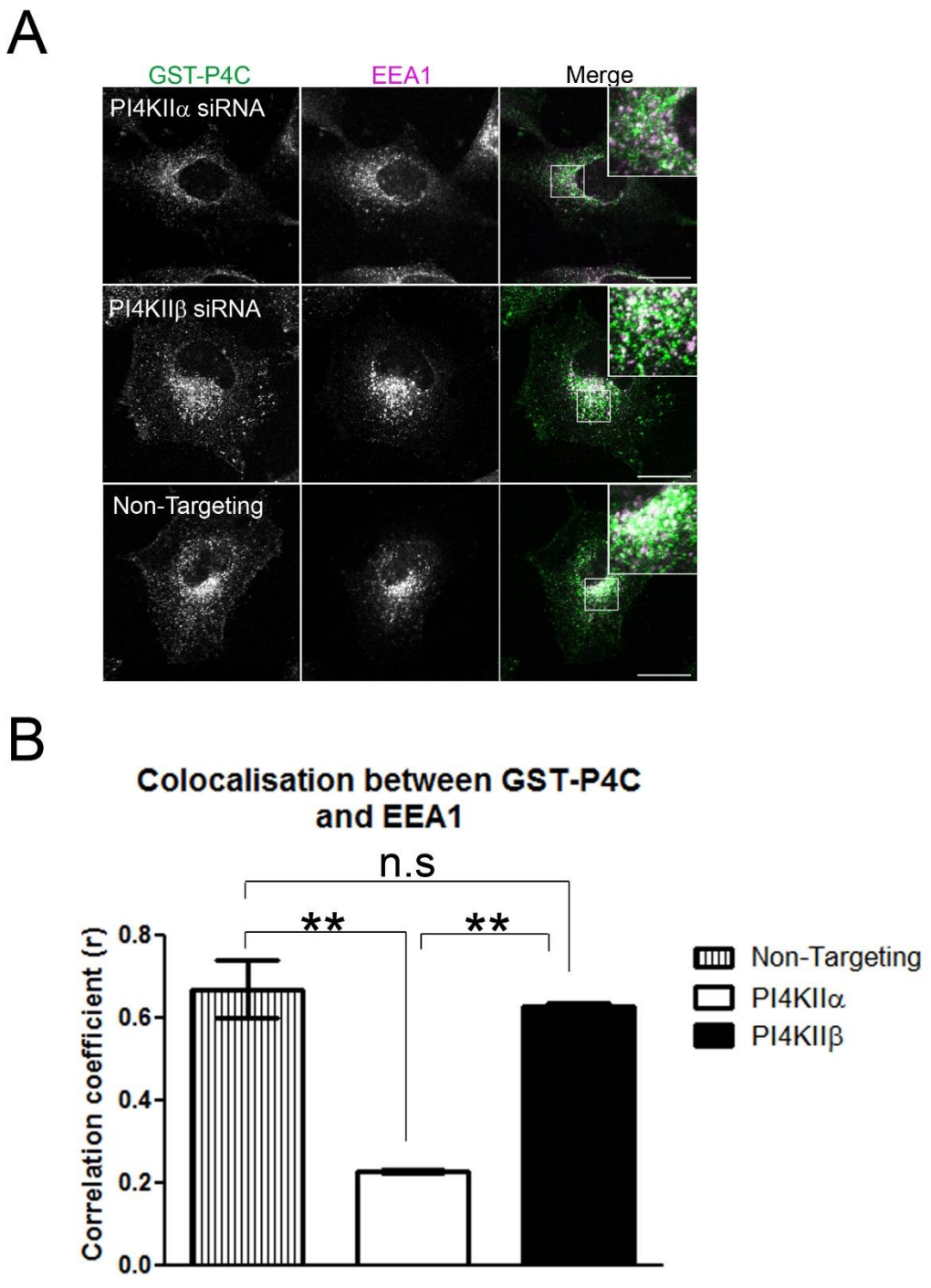

Figure 3-13. PI4KIIα controls a PI(4)P pool on early endosomes.

A. Fixed HeLa cells were co-stained for PI(4)P and EEA1. Images are single confocal sections. Scale bars, 10 µm. Zoom boxes are magnified areas of colocalising pixels. **B.** Histograms depict Pearson's correlation coefficients calculated for co-localising pixels between the green channel (PI(4)P) and magenta channel (EEA1), n=25 cells, three independent experiments. *, p<0.05, **, p<0.01.

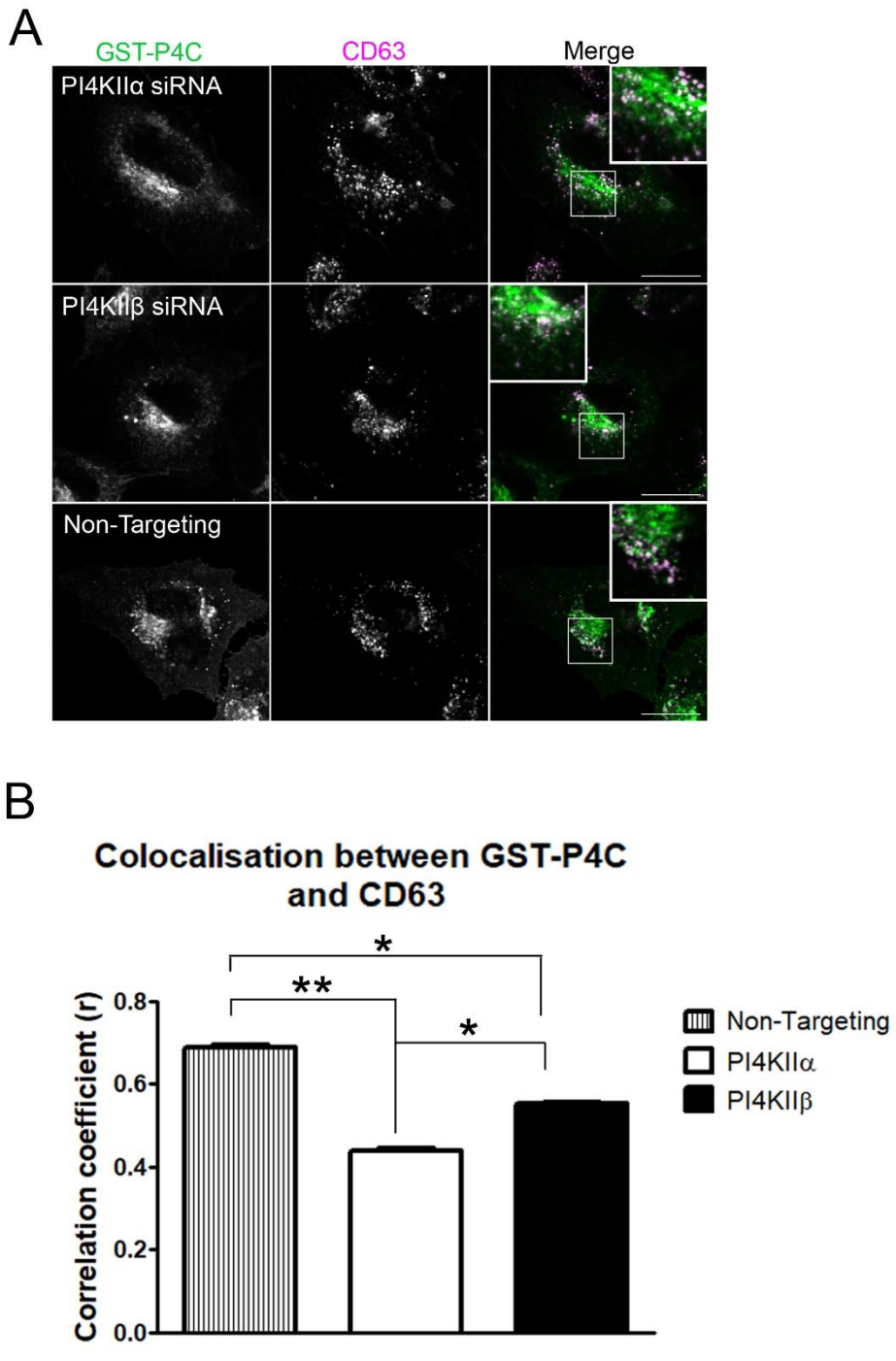

Figure 3-14. Wortmannin resistant PI(4)P pools colocalise with CD63.

A. Fixed HeLa cells were co-stained for PI(4)P and LE/lysosomal marker, CD63. Images are single confocal sections. Scale bars, 10 µm. Zoom boxes are magnified areas of colocalising pixels. **B.** Histograms depict Pearson's correlation coefficients calculated for co-localising pixels between the green channel (PI(4)P) and magenta channel (CD63), n=25 cells, three independent experiments. *, $p<0.05$, **, $p<0.01$.

3.2.4 The type II PI4Ks have different effects on PIP_2 synthesis

$PI(4,5)P_2$ is mainly found at the PM where it mediates a variety of cellular processes including cell signalling, membrane traffic and actin polymerisation. $PI(4,5)P_2$ can also be found on endosomal membranes where it regulates membrane trafficking (Vicinanza *et al.*, 2011; Thapa *et al.*, 2013; Tan *et al.*, 2015). Although PI(4)P is the immediate precursor of $PI(4,5)P_2$, there are conflicting reports regarding the role of PI(4)P in maintaining $PI(4,5)P_2$ levels at the plasma membrane (Hammond *et al.*, 2012; Bojjireddy *et al.*, 2014; Dickson *et al.*, 2014, 2016). It is widely believed that the contribution of PM PI(4)P to $PI(4,5)P_2$ synthesis is minimal and $PI(4,5)P_2$ is derived from other PI(4)P sources such as endosomes and PM-Golgi contact sites. PI4KIIα has been indirectly linked to $PI(4,5)P_2$ synthesis and this led us to evaluate the effects of PI4KII depletion on PM $PI(4,5)P_2$ levels. To achieve this, we treated HeLa cells with siRNA to either PI4KII isoform and then briefly treated these cells with wortmannin to diminish type III PI4K activity as previously described (section 3.2.3.2). We used a staining procedure that preserves PM membrane lipids and a bacterial recombinant version of the PH domain of the δ1 isoform of Phospholipase C (GST-PH-PLCδ1) was used to label plasma membrane $PI(4,5)P_2$ in fixed cells (Hammond *et al.*, 2009).

A previous study reported that overexpression of PI4KIIα leads to a minimal increase in ^{32}P incorporation into $PI(4,5)P_2$ synthesis in comparison with control (Balla *et al.*, 2002; Wang *et al.*, 2003) while PI4KIIβ had negligible effects (Balla *et al.*, 2002). In the present study, depletion of PI4KIIα had minimal impacts on plasma membrane levels of $PI(4,5)P_2$ and neither did depletion of PI4KIIβ (Figure 3-15) but wortmannin treatment significantly decreased $PI(4,5)P_2$ staining at the PM in PI4KIIα depleted cells by ~70% (0.279±0.018 vs 1.0±0.116 in control (Figure 3-15). In addition, loss of PI4KIIα induced $PI(4,5)P_2$ distribution onto membrane ruffles and blebs (Figure 3-15a); a feature reminiscent of the recruitment of PI4KIIβ to membrane ruffles and blebs following growth factor stimulation. Although wortmannin treatment caused no statistically significant difference in $PI(4,5)P_2$ staining between PI4KIIα and PI4KIIβ depleted cells (Figure 3-14b),

the residual pool of PI(4,5)P_2 (0.491±0.022 vs 0.279±0.018 in PI4KIIα depleted cells) which corresponds to PI4KIIα activity present after PI4KIIβ depletion suggests that PI4KIIα has a greater contribution towards PI(4,5)P_2 synthesis than PI4KIIβ. This also agrees with previous reports which demonstrated that PI4KIIα has a greater kinase activity than its isozyme (Balla *et al.*, 2002; Waugh *et al.*, 2003).

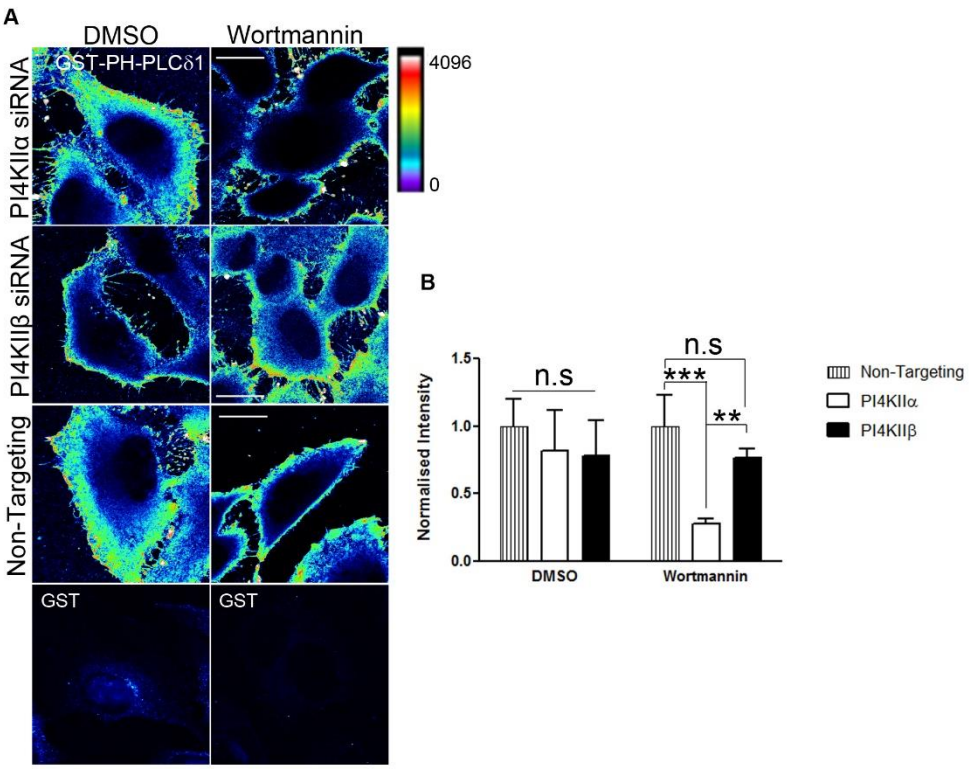

Figure 3-15. Effects of PI4KII siRNA on PM PI(4,5)P_2.

A. siRNA transfected HeLa cells treated with vehicle (DMSO) or wortmannin were fixed and labelled with a recombinant GST-tagged construct of the PH domain of PLCδ1 (GST-PH-PLCδ1) as described. Images are single confocal sections. Scale bars, 10 µm. **B**. Quantitation of PI(4,5)P_2 staining (n=15 cells, 3 experiments). Histogram bars represent means ± SEM, *, p<0.05, **, p<0.01, ***, p<0.01, n.s (not significant).

3.3 Discussion

Data presented here demonstrate major differences and similarities in membrane localisations of PI4KIIs. Using immunofluorescent microscopy, we demonstrated that both PI4KII isoforms localise to distinct TGN domains. In addition, the data suggest that the isozymes possess non-redundant PI4KII activities, based on the generation of metabolically separate pools of PI(4)P at the TGN. Both PI4KIIs localised to regions proximal to the cell centre, with PI4KIIα exhibiting a juxtanuclear and puncta staining pattern while PI4KIIβ showed a largely diffuse perinuclear staining pattern but could also be found at the cell periphery. These distinct staining patterns gave the first indication that the PI4KII isoforms localise to distinct membranes. Most PI4KII function has been assigned to PI4KIIα and this is partly due to the lack of information regarding PI4KIIβ. Although both proteins exhibit similarities within their *C*-terminal kinase domains, the proteins have a limited degree of sequence homology in their *N*-terminal regions (Balla *et al.*, 2002; Balla, 2013; Klima *et al.*, 2015). In addition, both isoforms interact with membranes differently (Wei *et al.*, 2002; Jung *et al.*, 2008). Membrane binding and catalytic activity of PI4KIIα is largely controlled by palmitoylation of specific cysteine residues in a CCPCC motif present in its catalytic domain (Barylko *et al.*, 2001). This post-translational modification ensures that PI4KIIα associates closely with membranes and is also required for localisation to lipid rafts (Barylko *et al.*, 2009). Disruption of palmitoyl acyltransferase (PAT) activity alters PI4KIIα membrane localisation and diminishes its catalytic activity (Barylko *et al.*, 2001, 2009). PI4KIIβ, on the other hand, is partly regulated by palmitoylation as it is equally distributed between membranes and the cytoplasm (Jung *et al.*, 2008). Compared with PI4KIIα, only a fraction of PI4KIIβ is palmitoylated and catalytically active (Jung *et al.*, 2008). Although disruption of PAT activity slightly alters the balance between membrane and cytoplasmic pools of PI4KIIβ, palmitoylation of the CCPCC motif is a requirement for 4-kinase activity (Wei *et al.*, 2002; Jung *et al.*, 2008). In the early years of PI4KII biology, it was reported that the divergent *N*-terminal of PI4KIIβ is required, in addition to palmitoylation, for membrane localisation. Deletion of 96 *N*-terminal amino acid residues of PI4KIIβ results in a predominantly

cytoplasmic distribution and these deletion mutants (PI4KIIβ$^{\Delta 1\text{-}96}$) were extractable with 1 M NaCl (Balla *et al.*, 2002) indicating that PI4KIIβ behaves like a peripheral membrane protein.

Immunocytochemical approaches presented in this chapter show that both isoforms localise to the TGN and both proteins colocalise differently with TGN markers, TGN46 and syntaxin 6. Syntaxin 6 distributes between the TGN and endosomes (Reverter *et al.*, 2014). At the TGN, syntaxin 6 colocalises with TGN46 and VAMP4, a SNARE which also localises to the TGN. Cells also contain a distinct population of syntaxin 6 which does not colocalise with TGN46 on vesicles and may represent early endosomes and/or TGN derived secretory vesicles (Reverter *et al.*, 2014). PI4KIIα significantly colocalised with syntaxin 6 (more than it did with TGN46 (Figure 3-2)), suggesting that it controls membrane trafficking between the TGN and endosomes. PI4KIIβ on the other hand significantly colocalised with TGN46 while it weakly colocalised with syntaxin 6. In a recent study, it was proposed that both proteins act in synergy but in a non-redundant manner in coordinating cargo sorting at the TGN. In that study, depletion of PI4KIIβ but not PI4KIIα perturbed sorting of the von Willebrand factor (VWF) into Weibel-Palade bodies, in primary human endothelial cells. Simultaneous depletion of both PI4KIIs had a greater effect on sorting of this clotting factor into its respective secretory vesicle (Lopes da Silva *et al.*, 2016); suggestive of additive roles for both isoforms in TGN trafficking but the mechanism by which this occurs was not fully described. It is possible that PI4KIIβ controls an early step in cargo sorting while PI4KIIα controls the secretory phase which involves syntaxin 6 that also localises to TGN-derived secretory vesicles which stain negatively for TGN46 (Reverter *et al.*, 2014). Subcellular fractionation studies by Waugh et al. (2011) revealed that PI4KIIα localises to cholesterol rich fractions corresponding to the ERC (endocytic recycling compartment) and TGN, which are positive for syntaxin 6. Membrane cholesterol content controls activity and membrane distribution of PI4KIIα (Minogue *et al.*, 2010). Imbalances in cellular cholesterol levels deplete TGN cholesterol causing the membrane redistribution of syntaxin 6 from the TGN and secretory vesicles (Reverter *et al.*, 2014). Since cholesterol regulates localisation of both

PI4KIIα and syntaxin 6, it would be interesting to investigate the roles of both proteins in TGN mediated secretion. PI4KIIα is also enriched in buoyant fractions positive for LE markers, syntaxin 8, LAMP-1 and Rab9 but only moderately associated with fractions positive for EEA1 (Waugh *et al.*, 2011). In agreement with this study, albeit through immunocytochemical staining, it was observed that PI4KIIS localise to cytoplasmic vesicles positive for endosomal markers; EEA1 and CD63. Although both PI4KIIs isoforms colocalised with CD63, only PI4KIIα colocalised with EEA1 (albeit with moderate colocalisation; r=0.35 for PI4KIIα vs r=0.28 for PI4KIIβ). Colocalisation of PI4KIIα and EEA1 is consistent with a previous report (Balla *et al.*, 2002) and others (Minogue *et al.*, 2006; Burgess *et al.*, 2012; Henmi *et al.*, 2016; Ketel *et al.*, 2016) which demonstrate that this isoform localises to early endosomal compartments where it regulates cargo sorting and trafficking.

Lack of coimmunostaining between PI4KIIβ and EEA1 contrasts with a previous report demonstrating that both type II PI4Ks co-localise with EEA1 on cytoplasmic vesicles (Balla *et al.*, 2002) but transiently over-expressed fluorescent/epitope tagged proteins were used in that study. Over-expression of recombinant proteins may overwhelm the membrane space available to accommodate them and may spill onto neighbouring vesicles (Wang *et al.*, 2003). In another study, it was described that PI4KIIβ is involved in the early stages of phagosome formation and colocalises with EEA1 positive early endocytic compartments in phagocytes (Jeschke *et al.*, 2015). This feature may be cell type dependent as phagocytic cells act in response to external stimuli (such as cytokines) and this phenomenon is consistent with an earlier study which demonstrated that PI4KIIβ is recruited to membranes in a PDGF dependent manner (Wei *et al.*, 2002; Jung *et al.*, 2011). In this present study, we maintained cells in complete medium (DMEM supplemented with 10% FCS) prior to fixation and antibody labelling. It is possible that a higher concentration of growth factors is required to obtain a quantifiable PI4KIIβ signal on early endosomes. A possible explanation for this finding is the gradual loss of PI4KIIβ from the endocytic compartment following endocytosis. Molecular brightness analysis showed that PI4KIIβ strongly

associates with clathrin light chain as demonstrated by increased signal intensities of both proteins at the early stage of endocytosis (Li *et al.*, 2012), but signal intensities of both proteins decrease over time suggesting a dynamic association between PI4KIIβ and early endocytic compartments (including early endosomes).

Both isoforms colocalised with the late endosomal marker, CD63 on cytoplasmic vesicles. This is consistent with previous reports that showed that both proteins can be found on late endosomes (Minogue *et al.*, 2006; Wieffer *et al.*, 2013; Gerber *et al.*, 2015; Wang *et al.*, 2015). While PI4KIIα seems to control cargo transport through late endosomes (Minogue *et al.*, 2006; Gerber *et al.*, 2015), it appears that PI4KIIβ controls a step in the delivery of lysosomal hydrolases to late endosomes possibly via a TGN/EE trafficking route (Wieffer *et al.*, 2013).

PI4KIIα is the predominant PI4K activity in mammalian cells (Balla *et al.*, 2002; Waugh *et al.*, 2003). Although both proteins have structurally similar catalytic domains (Klima *et al.*, 2015), PI4KIIβ has a lower kinase activity and overexpression of this isoform raises cellular PI(4)P levels by just ~20% of that achieved with PI4KIIα (Balla *et al.*, 2002). Previous studies used radioisotope labelling methods to assay PI4K activities in cell extracts. Experimental approaches highlighted in this thesis describe an immunocytochemical technique for visualising unbiased cellular PI(4)P pools. Using isoform specific RNAi and inhibition of type III PI4Ks with 10 μM wortmannin, it was possible to visualise cellular PI(4)P attributable to either isoform: PI(4)$P^{PI4KIIα}$ and PI(4)$P^{PI4KIIβ}$. Depletion of PI4KIIα revealed a pool of PI(4)P, PI(4)$P^{PI4KIIβ}$ of which ~20% colocalised with syntaxin 6, but over 50% of that pool significantly colocalised with TGN46. Conversely, PI4KIIβ depletion unmasked PI(4)$P^{PI4KIIα}$ and this significantly colocalised with syntaxin 6 (~60% PI(4)P colocalised with syntaxin 6) but weakly colocalised with TGN46 (~20% PI(4)P colocalised with TGN46). Colocalisation between PI(4)$P^{PI4KIIα}$ and syntaxin 6 is consistent with previous studies demonstrating that PI4KIIα activity is confined to cholesterol rich and buoyant fractions positive for TGN markers (syntaxin 6 and AP-1) and also controlled by

membrane cholesterol levels (Minogue *et al.*, 2010; Waugh *et al.*, 2011). PI(4)P$^{PI4KII\beta}$ in comparison with PI(4)P$^{PI4KII\alpha}$ had a significantly greater colocalisation with TGN46 thereby suggesting a role for PI4KIIβ in TGN membrane sorting/trafficking. Depletion of either PI4KII isoform had similar effects on PI(4)P colocalisation with adaptor proteins, AP-1 and GGAs 1 and 2 (Figure 3-11). Both proteins are implicated in the recruitment of clathrin adaptor proteins, but it is not well known if either isoform is dispensable for the recruitment of adaptor proteins, or has overlapping functions. One possibility is that each isoform recruits these proteins in a PI(4)P dependent manner to different membrane domains as observed with differential staining with syntaxin 6 and TGN46 but this warrants further investigation.

Disrupting the recruitment of clathrin adaptors such as AP-1 is linked with TGN membrane trafficking defects such as misdirection of M6PR and secretion of lysosomal hydrolases (Chi *et al.*, 2008). In comparison with PI4KIIα, the loss of PI4KIIβ had a greater impact on PI(4)P pools positive for M6PR (Figure 3-12). Depletion of PI(4)P pools positive for M6PR following loss of PI4KIIβ is consistent with disrupted AP-1 recruitment at the TGN (Chi *et al.*, 2008; Anitei *et al.*, 2014) and is suggestive of defective TGN-to-endosome traffic as previously demonstrated (Wieffer *et al.*, 2013). Previous studies emphasise the role of PI4KIIα in the delivery of lysosomal hydrolases from the TGN to late endosomes in a PI(4)P and M6PR dependent manner (Jović *et al.*, 2012). This pathway also involves Golgi localised, PI4KIIIβ, indicating the presence of three metabolically independent PI(4)P pools. This also raises the possibility of both proteins possessing synergistic or overlapping functions in regulating TGN-to endosome traffic, which is partly addressed in Chapter 4.

PI4KIIα depletion significantly lowered EEA1-positive PI(4)P pools confirming a previous report describing the kinase activity of PI4KIIα on early endosomes (Henmi *et al.*, 2016). Although PI4KIIα depletion had a greater effect on CD63-positive PI(4)P pools, PI4KIIβ loss significantly affected these PI(4)P pools, indicating the presence of both isoforms on late endosomes. A recent study identified both type II PI4Ks on vesicles positive for EE marker,

Rab5 and LE marker, Rab7. PI4KIIs on these vesicles synthesise PI(4)P, which recruits actin nucleators, such as the WASH complex to endosomal compartments (Dong *et al.*, 2016). Depletion of PI(4)P pools positive for CD63 (like Rab7, it localises to late endosomes/MVBs) is consistent with this study albeit without considering molecular differences between both isoforms. Nonetheless, loss of PI(4)P colocalisation with CD63 is suggestive of the roles of PI4KIIs in regulating transport and membrane recruitment on endo-lysosomal membranes.

Data from the plasma membrane $PI(4,5)P_2$ staining experiment are consistent with a previous report which showed that PI4KIIα only contributes moderately towards $PI(4,5)P_2$ synthesis while PI4KIIβ's contribution is negligible (Balla *et al.*, 2002). Wortmannin treatment enhances $PI(4,5)P_2$ levels following PI4KIIα expression (Balla *et al.*, 2002). Recent studies have shown that PM $PI(4,5)P_2$ is derived from other non PM sources such as endosomes (Hammond *et al.*, 2012; Gerber *et al.*, 2015) and that PI(4)P has its own role at the PM beyond $PI(4,5)P_2$ synthesis (Levin *et al.*, 2017). Since we used wortmannin at a dose which inhibits endosomal PI3K, hVps34, it is possible that this causes increased synthesis of $PI(4,5)P_2$ via endosomal trafficking to the plasma membrane. Wortmannin treatment mimics an EE membrane in which myotubularins hydrolyse PI(3)P allowing PI4KIIα recruitment on EEs (Ketel *et al.*, 2016). Because PI4KIIα is required for endosomal $PI(4,5)P_2$ synthesis (Henmi *et al.*, 2016), elevated $PI(4,5)P_2$ levels following wortmannin treatment can thus be linked to increased PI4KIIα localisation to EEs, $PI(4,5)P_2$ synthesis by endosomal PIPK1s and subsequent delivery to the PM by vesicular traffic. In the present study, depletion of PI4KIIβ and wortmannin treatment unmasked a pool of $PI(4,5)P_2$ that can be linked to PI4KIIα activity. This makes a case for a PI4KIIα derived PI(4)P pool that is furnished into $PI(4,5)P_2$ synthesis at the PM. In addition, a recent study showed that showed that PI4KIIα controls an LE pool of PI(4)P that is channelled into $PI(4,5)P_2$ at the plasma membrane in HIV infected lymphocytes and macrophages (Gerber *et al.*, 2015). These together, suggest that PI4KIIs control some minor PI(4)P pools that are directed into $PI(4,5)P_2$ synthesis under certain cellular conditions.

Chapter 4 PI4KIIs coordinate TGN-endosomal trafficking and intracellular signalling.

4.1 Introduction

Endosomes are heterogenous membranous organelles that represent platforms for protein sorting and bi-directional transport to and from various cellular destinations including the plasma membrane (Ivaska *et al.*, 2005; Kim *et al.*, 2006), Golgi complex (Arighi *et al.*, 2004; Silhankova *et al.*, 2010) and lysosomes (Minogue *et al.*, 2006; Mössinger *et al.*, 2012; Wang *et al.*, 2015). Endosomes can be classified as early endosomes (also called sorting endosomes), recycling endosomes and late endosomes. These organelles can exist in other morphologically different forms, especially in specialised cells such as those of epithelial or haematopoietic origin but would not be discussed here. In this chapter, the term, sorting endosomes (SE) is used interchangeably with early endosomes and is regarded the more appropriate term for this membrane compartment (Maxfield and McGraw, 2004; Hsu *et al.*, 2012). Endosomes control a variety of physiologically relevant cellular processes that include phagocytosis (Jeschke *et al.*, 2015; Levin *et al.*, 2017), cell adhesion (Ivaska *et al.*, 2005; Thapa *et al.*, 2012) and intracellular signalling (Joffre *et al.*, 2011; Zhou *et al.*, 2012; Tan *et al.*, 2015).

Uptake of substances such as nutrients from the external milieu occurs via endocytosis, resulting in sorting and packaging onto endocytic vesicles. There are several means of internalising surface derived cargos but the best-studied pathway is that mediated by clathrin (Conner and Schmid, 2003; Elde *et al.*, 2005; Posor *et al.*, 2013) and termed clathrin-mediated endocytosis (CME). This pathway involves multiple interactions between the internalised cargo, clathrin adaptors (Conner and Schmid, 2003; Elde *et al.*, 2005), PI lipids (Posor *et al.*, 2013) and accessory proteins such as Rab GTPases (Wiesner *et al.*, 2013), dynamin (Elde *et al.*, 2005; Joffre *et al.*, 2011) and BAR domain proteins (van Weering *et al.*, 2010). These regulate cargo recognition, membrane deformation, budding to form endocytic vesicles

(EVs) and coupling to molecular motors. Coat complexes dissociate from EVs following endocytosis and EVs fuse with existing SEs (reviewed by Cullen and Carlton, 2012; Hsu et al., 2012; Maxfield and McGraw, 2004; van Weering et al., 2010). SEs have tubular extensions with high surface area to volume ratio that permits geometric sorting of internalised cargoes onto distinct membrane microdomains. In addition, internalised proteins may possess sorting signals required for interactions with accessory proteins that facilitate vesicular/membrane transport.

Membrane sorting is accompanied by a series of membrane changes characterised by recruitment of proteins such as small GTPases and PI lipid modifying enzymes onto specific microdomains. A well-known event that occurs during endosomal sorting of cargoes is the interconversion of different PI lipid species (Zoncu *et al.*, 2009; Silhankova *et al.*, 2010; Posor *et al.*, 2013; Henmi *et al.*, 2016; Ketel *et al.*, 2016; Levin *et al.*, 2017). PI modifying enzymes control the availability of their lipid substrates which regulate membrane localisation of some components of the endosomal transport machinery such as SNAREs and motor proteins (Niu *et al.*, 2013; Jović *et al.*, 2014). This is achieved through a balance in the activities of kinases and phosphatases that control PI homeostasis at the respective membranes. Disruption of this balance perturbs the dynamics of intracellular transport and underlies the pathogenesis of some genetic disorders (Vicinanza *et al.*, 2011; Jović *et al.*, 2012; Ketel *et al.*, 2016). As mentioned in previous chapters, PI4Ks regulate trafficking pathways on endosomal and Golgi membranes and while PI4KIIα has been extensively described in many of these events, the role played by its closely related isozyme is not fully clear.

Following endocytic uptake, endocytic vesicles fuse with SEs, which acquire Rab 4 and 5 (Nielsen *et al.*, 2000; Murray *et al.*, 2002; Schenck *et al.*, 2008; Zoncu *et al.*, 2009) and begin to tubulate. As SEs move towards the juxtanuclear region, tubules bud off into smaller vesicles that are directly retrieved at the PM or to the Rab11 positive endocytic recycling compartment (ERC). A paradigmatic example is provided by endocytosis of the transferrin receptor (TfR). Transferrin (Tf) binds its ligand, ferric iron (Fe^{3+}) from

circulation at neutral pH which prevents dissociation of Fe^{3+}. Transferrin (along with Fe^{3+}) then binds its cognate receptor at the cell surface forming a tripartite complex. This complex is endocytosed and the TfR-Tf-Fe^{3+} complex is then delivered to SEs. The acidic pH of SEs causes dissociation of Fe^{3+} which is transported to the cytoplasm by transporters such as DMT1 (divalent mineral transporter 1) and SFT (stimulator of Iron (Fe) transport) for cell use and storage. The iron-free transferrin (apo-transferrin) remains bound to its receptor and is retrieved at the PM via the ERC (reviewed by Hsu et al., 2012; Maxfield and McGraw, 2004). Perturbation of trafficking events on SEs often results in defective TfR trafficking and depletion of PI4KIIα in mammalian cells leads to a cellular phenotype characterised by perturbed TfR uptake or recycling (Jović *et al.*, 2014; Henmi *et al.*, 2016; Ketel *et al.*, 2016). Other proteins of physiologic relevance that utilise a similar trafficking route include the integrin family of cell surface proteins which are retrieved to the plasma membrane in a Rab11 dependent manner (Ivaska *et al.*, 2005; Williams and Coppolino, 2011). The presence of PI4KIIα in $\alpha_3\beta_1$ integrin positive complexes at focal sites is suggestive of a role for PI4KIIα in endocytic recycling of these receptors to the cell surface and a potential function for this PI4KII isoform in cell migration (Berditchevski *et al.*, 1997).

As SEs migrate closer to the juxtanuclear region of the cell, they lose Rab5 and acquire Rab7. At the interphase of this Rab switch, they also become more acidic and acquire lysosomal membrane proteins and hydrolases from the Golgi (Jović *et al.*, 2012; Wieffer *et al.*, 2013; Kucera *et al.*, 2016) thus maturing into late endosomes (LEs). LEs are larger than SEs and are characterised by the presence of small intraluminal vesicles (ILVs; for this reason, they are also called multi-vesicular bodies (MVBs)). Sequestration of receptor complexes into the acidic environment of ILVs enhances receptor-ligand dissociation and fusion with lysosomes facilitates degradation of internalised cargoes by acid hydrolases. Defective internalisation of surface receptors or trafficking through the endo-lysosomal route impedes receptor degradation and can lead to sustained downstream signalling (Teis *et al.*, 2002; Taub *et al.*, 2007; Joffre *et al.*, 2011) — a phenotype characteristic of certain human cancers. Depletion of PI4KIIα also disrupts EGFR trafficking

through the endo-lysosomal route (Minogue *et al.*, 2006; Henmi *et al.*, 2016) and may serve an important role in tumorigenesis.

CI-M6PR, which facilitates delivery of lysosomal hydrolases to endosomal compartments, is retrieved from these compartments and delivered back to the TGN via retrograde transport. This trafficking step is coordinated by the interplay of protein complexes including retromer (Arighi *et al.*, 2004), SNAREs (Jović *et al.*, 2014) and PI lipids PI(3)P and PI(4)P (van Weering *et al.*, 2010; Niu *et al.*, 2013). Both PI4KII isoforms have been described in anterograde transport of CI-M6PR where depletion of either isoform results in mistrafficking and exocytic secretion of lysosomal hydrolases (Jović *et al.*, 2012, 2014; Wieffer *et al.*, 2013).

The previous chapter described the subcellular localisations of the PI4KIIs and revealed some major differences between the enzymes. In addition, unmasking of wortmannin resistant PI(4)P pools strengthened the hypothesis that the enzymes have both overlapping and non-redundant cellular roles. While PI4KIIα has been described in the regulation of endosomal membrane trafficking, the role played by PI4KIIβ remains unclear. This chapter covers the roles played by this enzyme in the regulation of intracellular membrane trafficking pathways. In addition, it also demonstrates the impacts of PI4KII depletion on intracellular signalling using trafficking of the EGFR as an experimental system.

4.2 Results

4.2.1 PI4KIIs control transport of CI-M6PR from the Golgi to the endosomal system

In the previous chapter, depletion of PI4KII isoforms altered PI(4)P pools colocalising with AP-1 as well as one of its cargoes, CI-M6PR (Figure 3-12). This led us to investigate the roles of the PI4KII isoforms in TGN trafficking of CI-M6PR. Trafficking of CI-M6PR from the TGN to endosomes is AP-1 dependent (Chi *et al.*, 2008). We initially immunostained EGFP-tagged CI-M6PR expressing HeLa cells with anti-γ-adaptin (AP-1) antibodies to examine the effects of PI4KII siRNA on AP-1 mediated M6PR trafficking. It was observed that depletion of PI4KIIβ had a greater impact on colocalisation between AP-1 and CI-M6PR (at steady-state) than that of PI4KIIα or control siRNA treated cells (Figure 4-1). In addition, depletion of PI4KIIβ significantly diminished the amount of EGFP-CI-M6PR positive cytoplasmic vesicles which is indicative of disrupted TGN/endosomal trafficking (Figure 4-1a).

To substantiate this observation, we employed a previously described M6PR trafficking assay (Chi *et al.*, 2008) albeit with slight modifications to study the effects of PI4KII depletion on TGN exit of CI-M6PR. EGFP-CI-M6PR expressing cells were incubated at 20^{o}C for two hours to block Golgi exit of CI-M6PR in the presence of cycloheximide, to inhibit nascent protein synthesis. Cells were then either fixed and processed for immunofluorescence microscopy or shifted to 37^{o}C for one hour to permit EGFP-CI-M6PR Golgi exit (Figure 4-2a). We also immunolabelled temperature-shifted cells with antibodies to AP-1 or Rab9 to study the effects of PI4KII depletion on M6PR TGN exit and subsequent entry into endosomal compartments. Rab9 also plays a role in endosomal membrane delivery of CI-M6PR by regulating traffic of CI-M6PR to an early-late endosomal compartment characterised by the loss of Rab5 and acquisition of Rab7 (Rab conversion) following delivery of CI-M6PR (Kucera *et al.*, 2016).

Cells expressing EGFP-CI-M6PR at moderate levels were selected and fluorescent intensities of EGFP-CI-M6PR signals within the Golgi and cytoplasm measured for each siRNA treatment (Figure 4-2). At 20^{o}C, CI-M6PR was retained in the Golgi region in control and PI4KII siRNA treated cells as expected (Figure 4-2, b and c). The shift to 37^{o}C caused dispersal of CI-M6PR from the TGN to peripheral cytoplasmic vesicles in control cells while a greater proportion of EGFP-CI-M6PR fluorescence intensity was retained within the juxtanuclear Golgi region in cells deprived of either PI4KII isoform (Figure 4-2, b-c). In addition, colocalisation between EGFP-CI-M6PR and AP-1 or Rab9 was markedly reduced in PI4KII depleted cells, in comparison with control (Figure 4-3). These data are indicative of dysfunctional trafficking of CI-M6PR from the TGN to endosomes.

Following the delivery of lysosomal membrane proteins and hydrolases to late endosomes, CI-M6PR is retrieved at the Golgi via anterograde traffic from endosomal compartments. PI(4)P has been described in the retrograde delivery of cargoes by binding to SNX6 (Niu *et al.*, 2013), a component of the retromer complex. We previously showed that these PI4KII isoforms generate separate PI(4)P pools but seem to have overlapping PI4K activity on LEs. To investigate the roles played by these isoforms in the control of cargo transport to the Golgi, we analysed retrograde trafficking of EGFP-CI-M6PR by fluorescent recovery after photobleaching (FRAP). Regions of interest were selected within the perinuclear regions of cells moderately expressing EGFP-CI-M6PR and then photobleached with 100% laser power at 488 nm with fluorescence recovery monitored over 200 seconds. Fluorescent recovery of EGFP-CI-M6PR was faster in selected regions of control siRNA-treated cells in comparison with cells depleted of either PI4KII isoform, suggesting retarded retrograde delivery of CI-M6PR from endosomes to the Golgi (Figure 4-4; Appendix 2, Movies 1-3).

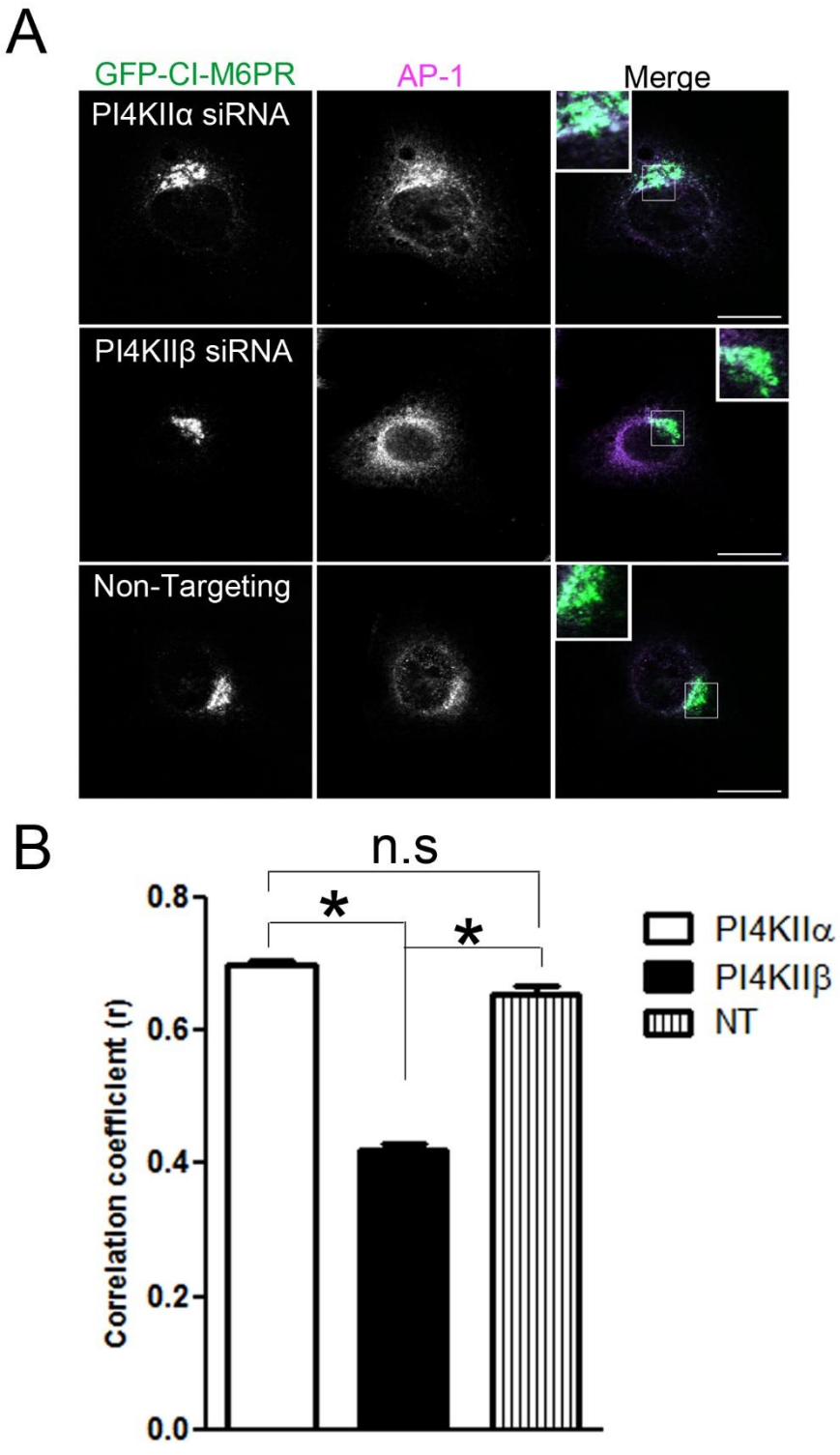

Figure 4-1. Depletion of PI4KIIβ alters steady state distribution of CI-M 6PR.

A, B. PI4KIIβ depletion alters vesicular staining pattern of CI-M6PR and diminishes its colocalisation with AP-1. Images shown in (A) are single confocal sections. Scale bars, 10 µm. **B**. The histogram shows Pearson's correlation coefficients for colocalisation between CI-M6PR and AP-1. *, $p<0.05$, n.s (not significant).

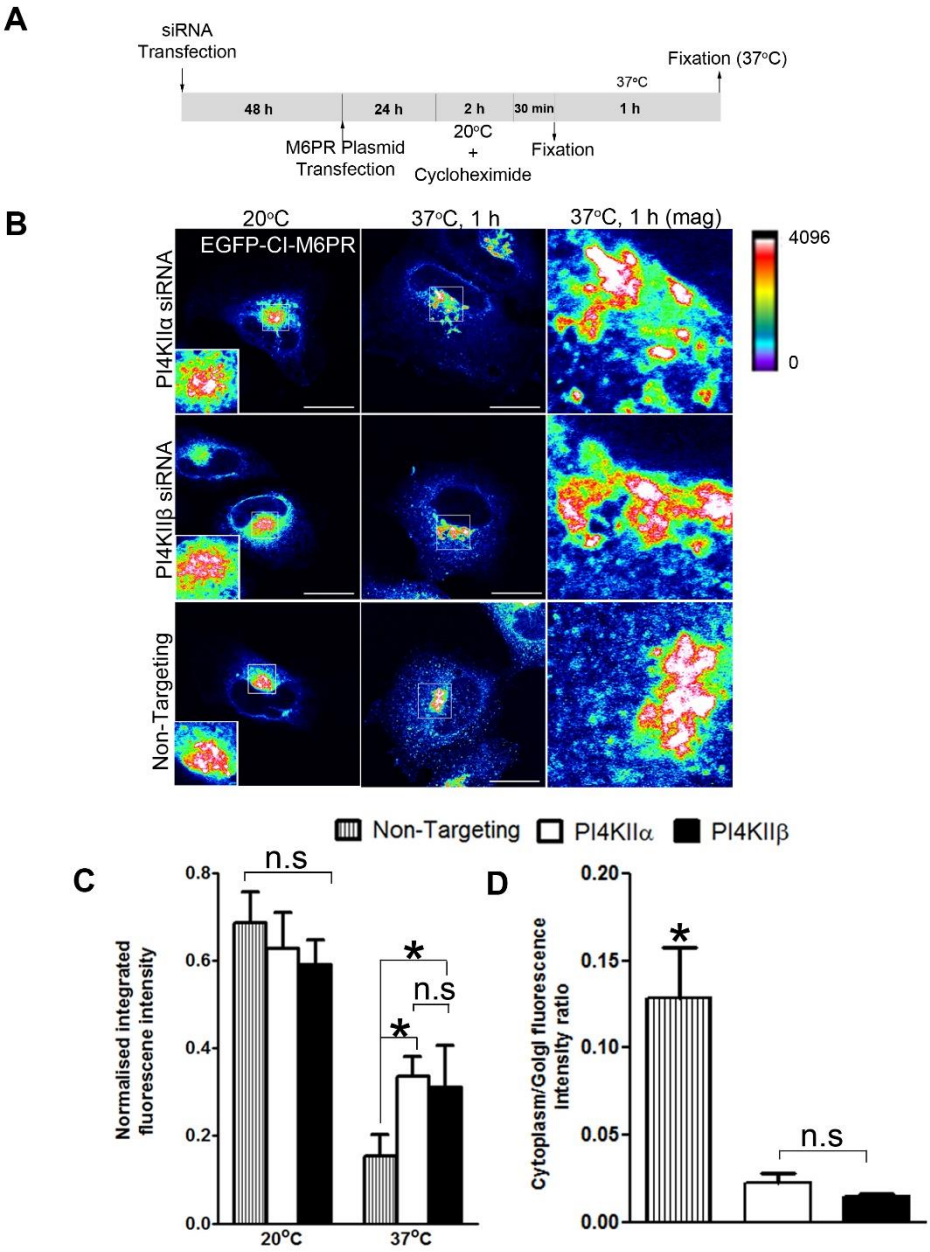

Figure 4-2. PI4KIIs are required for anterograde transport of CI-M6PR.

A. Schematic depicts the experimental procedure used to study M6PR trafficking from the Golgi. **B** and **C**. EGFP-CI-M6PR expressing cells were incubated at 20ºC to block Golgi exit of M6PR, followed by fixation or a shift to 37ºC for one hour to allow transport to endosomal compartments. **C**. Quantitation of fluorescent signal intensities within the Golgi area after the temperature block or after one hour at 37ºC in PI4KII or control siRNA treated cells. **D**. Ratio of cytoplasmic vesicle and Golgi EGFP-CI-M6PR fluorescence intensities. Data are presented as Means ± SEM. (n= 15 cells per condition). *, $p<0.05$, n.s (not significant).

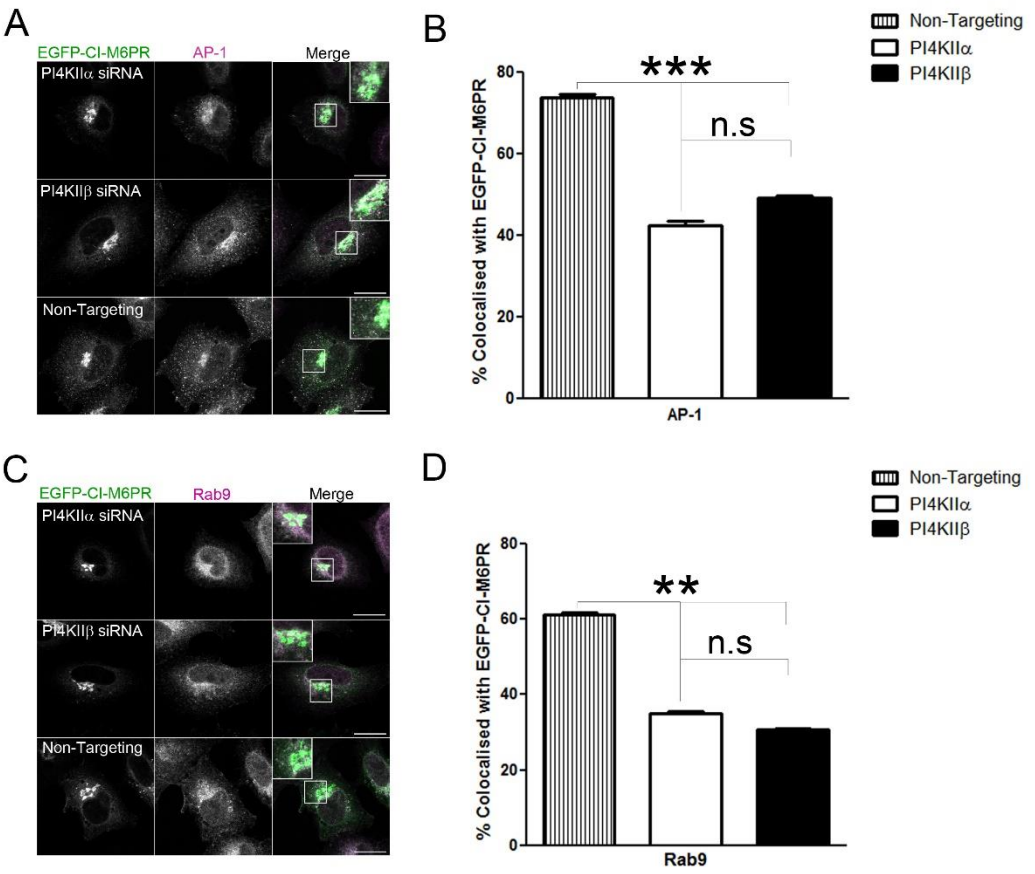

Figure 4-3. PI4KII depletion affects endosomal delivery of CI-M6PR.

A-D. EGFP-CI-M6PR expressing HeLa cells were stained for (A) AP-1 or (C) Rab9 following temperature block and release at 20^{o}C and 37^{o}C respectively. Images are single confocal sections. Scale bars, 10 µm **B, D**. Quantitation of colocalisation between (B) AP-1 or (D) Rab9 and EGFP-CI-M6PR. Data are presented as means ± SD (n=15 cells/each of three independent experiments). *, $p<0.05$, **, $p<0.01$, ***, $p<0.001$, n.s (not significant).

A

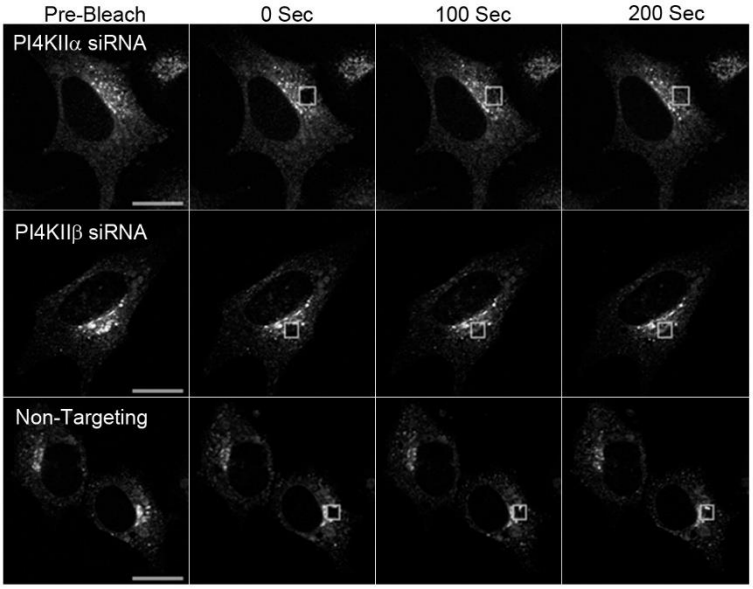

B

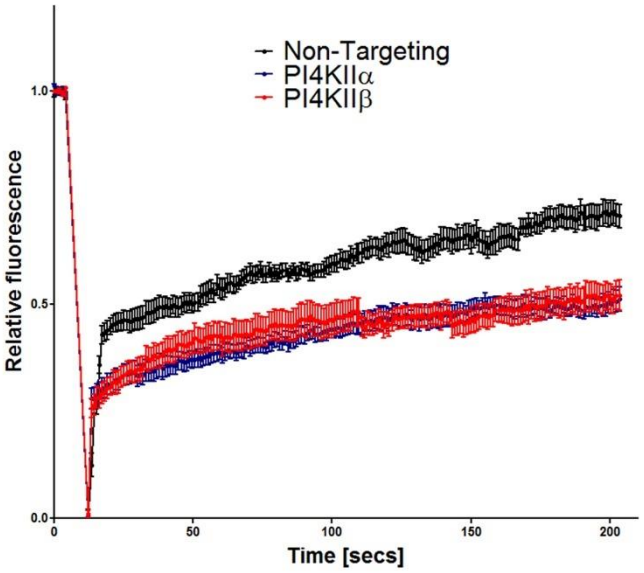

Figure 4-4. PI4KIIs also control retrograde transport of CI-M6PR.

A. HeLa cells were treated with control or PI4KII siRNA for 48 hours, transfected with EGFP-CI-M6PR and then incubated for 24 hours. Cells were treated with 100 µg/ml cycloheximide for one hour, and then FRAP analysis was performed. Time lapse image shows selected images before, during and post photo-bleaching. For FRAP analysis, the pinhole set at greater than 7 µm for imaging and photo-bleaching. Boxes indicate bleached regions and their fluorescence recovery over time. Scale bars, 10µm. **B.** Graph indicates fluorescence recovery of GFP-CI-M6PR at the Golgi.

4.2.2 PI4KIIs regulate endosomal trafficking pathways

Previous studies showed that PI4KIIα depletion impairs endosomal traffic of cargoes such as the EGFR (Minogue *et al.*, 2006) and the Wnt receptor frizzled (Fz) (Mössinger *et al.*, 2012). This led us to inquire whether this feature was unique to PI4KIIα or was shared with PI4KIIβ. To test the contribution of either PI4KII isoform to receptor endocytosis, we initially analysed the uptake of transferrin, which is internalised along with its receptor and subsequently recycled to the plasma membrane after cellular delivery of Fe^{3+}.

PI4KII siRNA and control siRNA-treated cells exhibited similar total to surface transferrin ratios, indicating that loss of either PI4KII isoform neither alters cellular uptake of this cargo nor of its cognate receptor (Figure 4-5, a and b). Following internalisation at 37ºC for 30 minutes, transferrin displayed increased colocalisation with EEA1 on juxtanuclear puncta in cells depleted of either PI4KII isoform. This was not the case in control siRNA transfected cells, suggesting impaired endosomal trafficking. We also examined the distribution of transferrin along with the ligand, EGF, which is internalised via a similar CME pathway but sorted into the endo-lysosomal pathway in complex with EGFR for degradation. Transferrin and EGF were loaded simultaneously and chased for 40 and 60 minutes in HeLa cells. Transferrin and EGF were internalised and after 10 minutes, there were no differences in colocalisation between both ligands in PI4KII or control siRNA treated cells (Figure 4-6). A significant proportion of EGF colocalised with transferrin in PI4KII depleted cells in comparison with control (40.63±4.04% for PI4KIIα siRNA-, 48.69±4.06% for PI4KIIβ siRNA- vs 25.04±1.29% in control siRNA-treated cells, colocalised with transferrin) after 40 minutes (Figure 4-6). A similar but less significant pattern was observed after 60 minutes' chase, an indication of perturbed endosomal sorting of both ligands.

We also studied the effects of PI4KII depletion on recycling of transferrin. Control siRNA-treated cells and those depleted of either PI4KII isoform were loaded with Alexa-555-labelled Tf for one hour at 37ºC and then chased in

complete medium for 40 or 60 minutes to permit transferrin recycling. We expressed transferrin recycling as a ratio of transferrin intensity before and after chase in complete medium and recorded slower recycling rates of internalised transferrin in PI4KII depleted cells compared with control siRNA treated cells (Figure 4-7b). These data indicate that depletion of either PI4KII isoform perturbs endosomal sorting of the TfR thereby delaying its recycling to the cell surface.

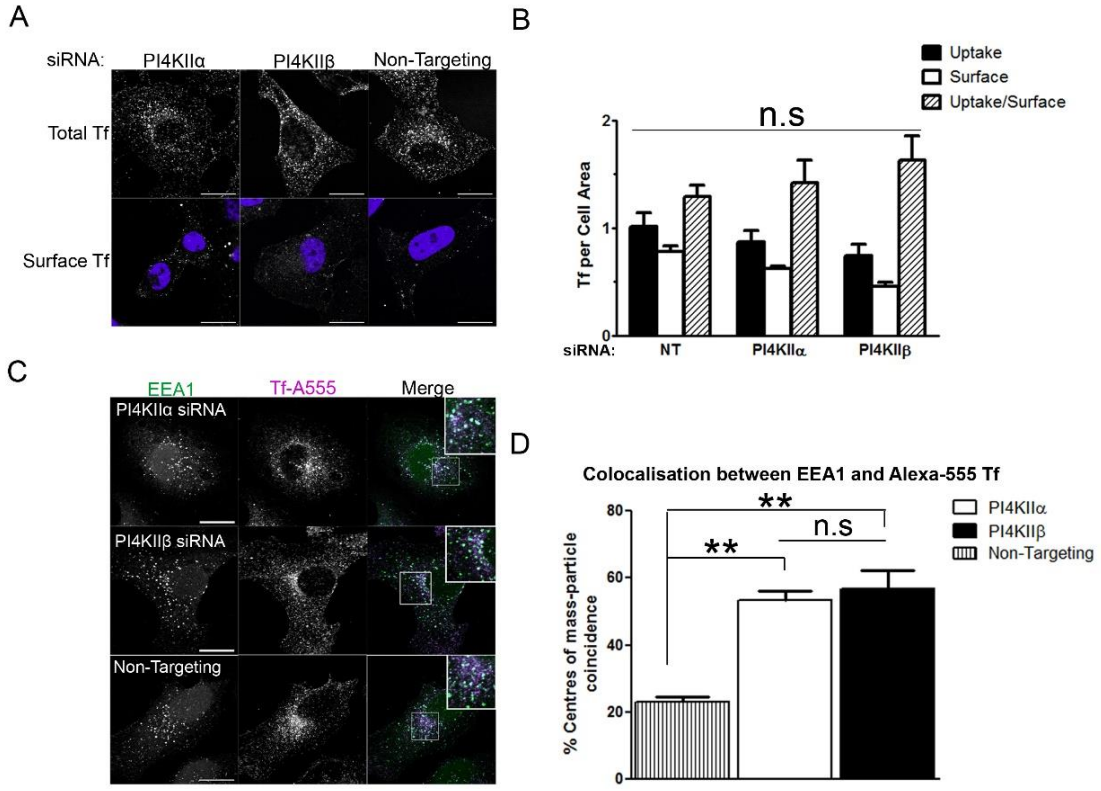

Figure 4-5. Transferrin is retained in sorting endosomes in of PI4KII-depleted cells.

A, B. Transferrin (Tf) uptake, surface levels and the ratio of uptake to surface bound Tf in HeLa cells treated with PI4KII or control (non-targeting, NT) siRNA. **C**. Cells treated with PI4KII or control siRNA were labelled with Alexa-Fluor 555-Tf at 37ºC for 30 minutes and co-stained with EEA1.Images are single confocal sections. Scale bars, 10 µm. **D**. Histogram depicts colocalisation between transferrin and EEA1 was measured in using an object based method that analyses the spatial interaction between pixels (Bolte and Cordelières, 2006). Data are means ± SEM (n=20 cells, three independent experiments). **, $p<0.01$, n.s (not significant).

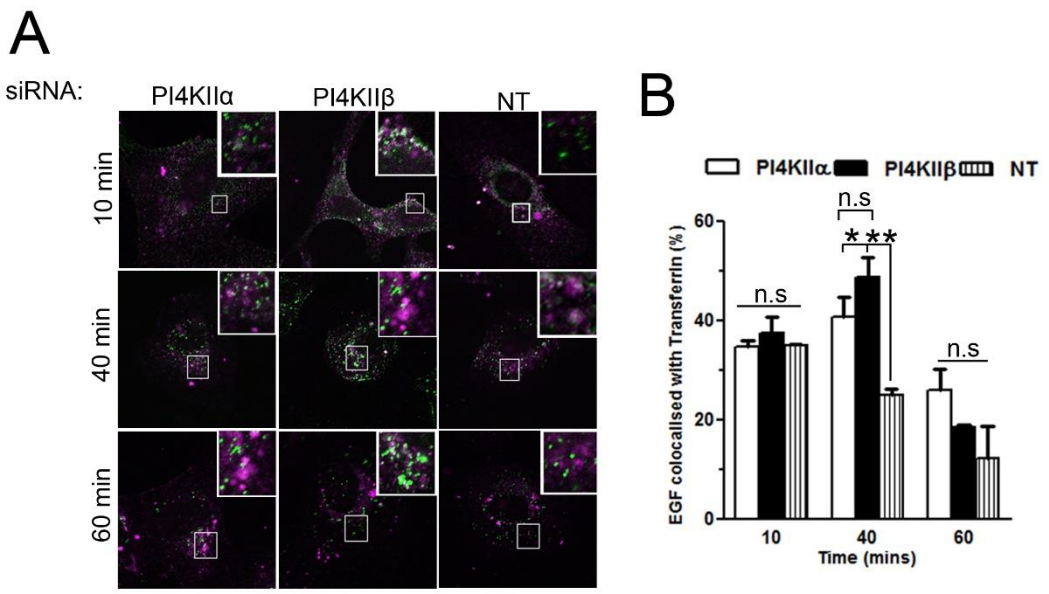

Figure 4-6. PI4KIIs control endosomal sorting of transferrin and EGF.

A. PI4KII or siRNA treated HeLa cells were labelled with Alexa-Fluor-488 EGF (green) and Alexa-Fluor-633-transferrin (magenta) on ice for one hour (PULSE), acid washed and incubated for 10-60 minutes (CHASE). **B.** Colocalisation of EGF and transferrin was measured and computed for 18 cells from three independent experiments. *, $p<0.05$, **, $p<0.01$, n.s (not significant).

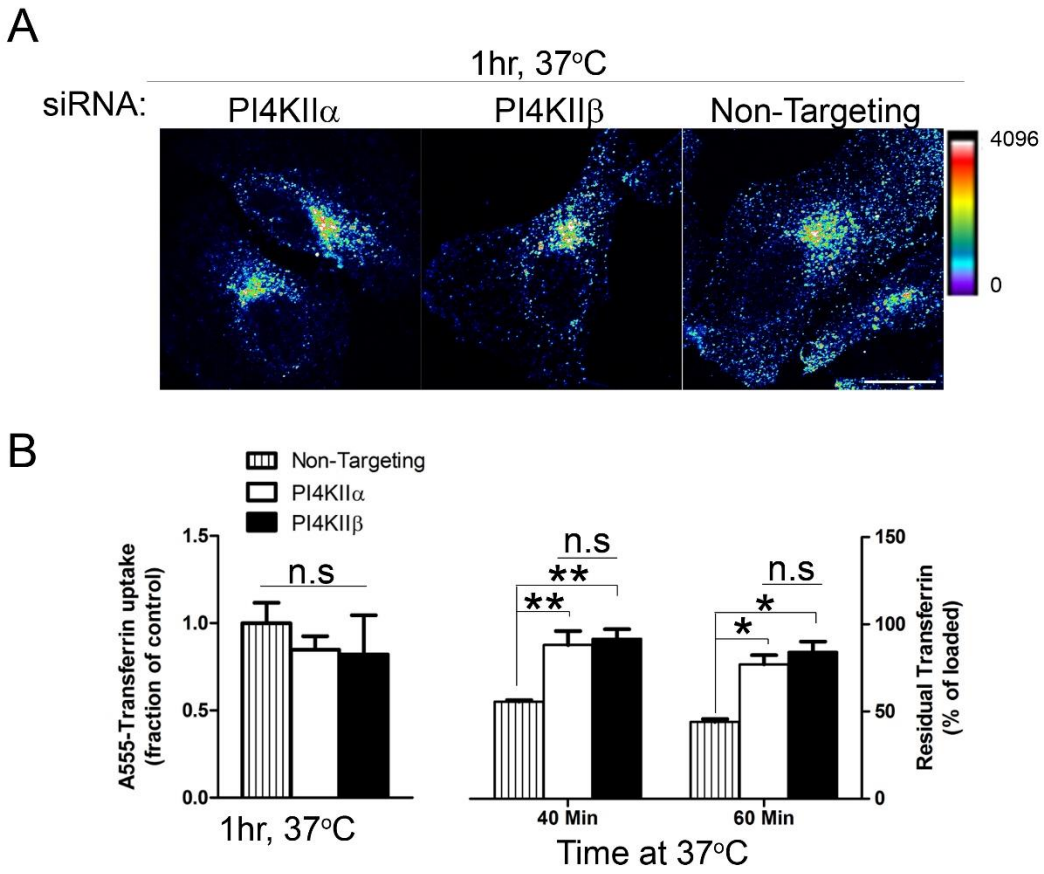

Figure 4-7. PI4KII knockdown impairs transferrin recycling.

A, B. HeLa cells treated with PI4KII or control siRNA were loaded with Alexa-Fluor 555-conjugated transferrin for one hour at 37°C (LOAD) and then chased in complete medium for 40 and 60 minutes (CHASE). **B**. Fluorescent intensities of cells after 40 and 60 minutes of chase were quantified as percentages of loaded transferrin.

4.2.3 Both PI4KII isoforms are required for lysosomal trafficking and degradation of EGFR

A previous study in our lab showed that depletion of PI4KIIα impairs endosomal trafficking and degradation of EGFR (Minogue *et al.*, 2006). Structural similarities between PI4KII isoforms (Klima *et al.*, 2015) and their localisation to endosomal compartments (Balla *et al.*, 2002; Dong *et al.*, 2016) led us to investigate the role of PI4KIIβ in endosomal trafficking of EGFR. In addition, data from the previous section (Figure 4-6) demonstrated that loss of either isoform alters endosomal sorting of the EGF ligand suggesting impaired EGFR trafficking to lysosomes. To confirm this, we studied the effects of PI4KII siRNA on EGF-induced endosomal EGFR trafficking by immunofluorescence microscopy. HeLa cells were stimulated with 100 ng/ml EGF for indicated times. After 15 minutes of EGF stimulation, ~45% of EGFR colocalised with CD63 in control siRNA treated cells, while ~28 and 33% of EGFR colocalised with CD63 in PI4KIIα and PI4KIIβ depleted cells respectively (Figure 4-8). After 60 and 120 minutes of EGF stimulation, a sizeable proportion of EGFR (up to 73% after 120 mins) colocalised with CD63 in control siRNA-treated cells, suggesting efficient sorting onto late endosomes while ~50% of internalised EGFR colocalised with CD63 upon depletion of either PI4KII isoform (~56% and 50% of EGFR colocalised with CD63 in cells depleted of PI4KIIα and PI4KIIβ respectively (Figure 4-8)).

We also performed a time-course experiment to evaluate the kinetics of EGFR degradation, following depletion of either PI4KII isoform. PI4KII and control siRNA treated cells were stimulated for indicated times and cell lysates analysed by western immunoblotting. In comparison with control, depletion of either PI4KII impaired EGF-induced lysosomal EGFR degradation, with PI4KIIβ depletion having a greater impact (Figure 4-9, a and b). Impaired EGFR degradation is indicative of defective endo-lysosomal sorting and this leads to sustained activation of downstream signalling pathways. To confirm this, we tested the kinetics of EGFR activation by western blotting with antibodies to pTyr^{1068} , which serves as a docking signal for Grb2— a scaffold protein that orchestrates signalling cascades such as

the Erk1/2 phosphorylation pathway (Rojas *et al.*, 1996; Fortian and Sorkin, 2014). Impaired EGFR degradation upon depletion of either PI4KII isoform was accompanied by increased phosphorylation of $pTyr^{1068}$ and once again, PI4KIIβ depletion had a greater impact on the kinetics of EGFR phosphorylation (Figure 4-9, a and c). Impaired receptor degradation was accompanied by sustained phosphorylation of Erk1/2 mitogen activated protein kinases (MAPK) in cells depleted of either PI4KII isoform in comparison with control (Figure 4-9, d and e). These data suggest that both PI4KII isoforms are required for the control of mitogenic signalling pathways.

As PI4KII depletion inhibits endo-lysosomal traffic of EGFR, the receptors accumulated on endosomes could be recycled to the PM, thereby sustaining signalling (Chi *et al.*, 2011). To rule this out, we analysed EGFR recycling in PI4KII and control siRNA treated cells by flow cytometry (Tan *et al.*, 2015) but depletion of neither PI4KII increased EGFR recycling in comparison with control (Figure 4-10). These results indicate that loss of either PI4KII isoform promotes EGFR signalling on endosomes due to impaired sorting into the lysosomal pathway without affecting EGFR recycling.

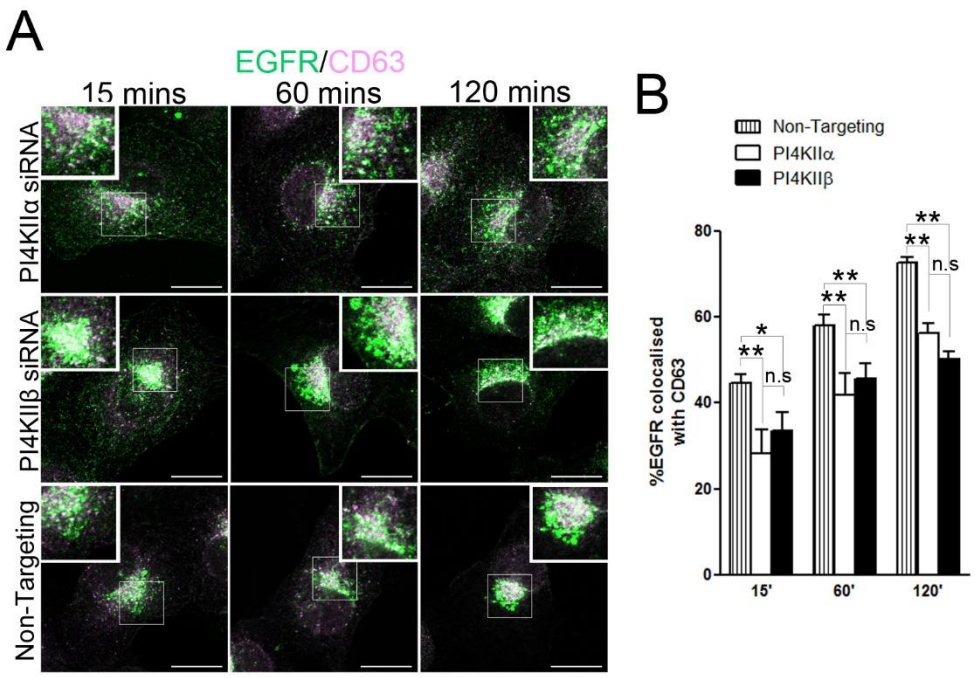

Figure 4-8. PI4KII depletion impairs endosomal trafficking of EGFR.

Control and PI4KII siRNA treated cells were serum starved for 18 hours and stimulated with 100 ng/ml EGF for indicated times. **A.** EGFR localisation was evaluated by immunofluorescence where cells were labelled with antibodies against EGFR and anti-CD63. Images are single confocal sections. Scale bars, 10 µm. **B.** Colocalisation of EGFR and CD63 along different time points was quantified as the percentage of EGFR pixels that coincided with CD63. *, $p<0.05$, **, $p<0.01$, n.s (not significant).

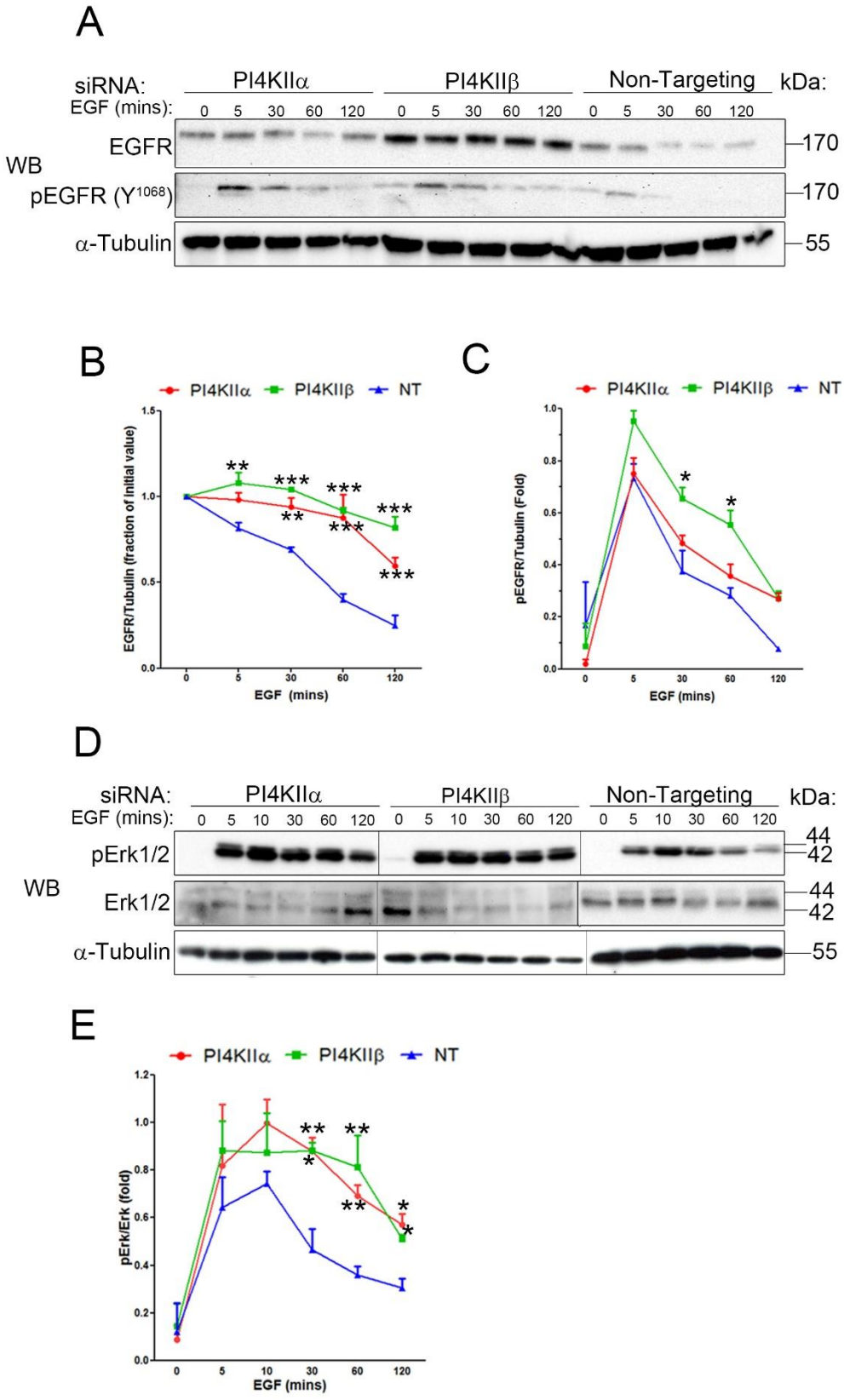

Legend on next page.

Figure 4-9. Depletion of either PI4KII isoform impairs EGFR degradation and sustains signalling.

A, D. HeLa cells were transfected with the siRNA indicated, cultured in complete medium for 58 hours and then serum starved for 14 hours. Cells were subsequently stimulated with 100 ng/ml EGF for the indicated times. Whole cell lysates separated by SDS-PAGE and immunoblotted for the indicated proteins. **B, C** and **E**. Signal intensities were quantified by densitometry. Data are mean ± SEM (three independent experiments). *, $p<0.05$, **, $p<0.01$, ***, $p<0.001$.

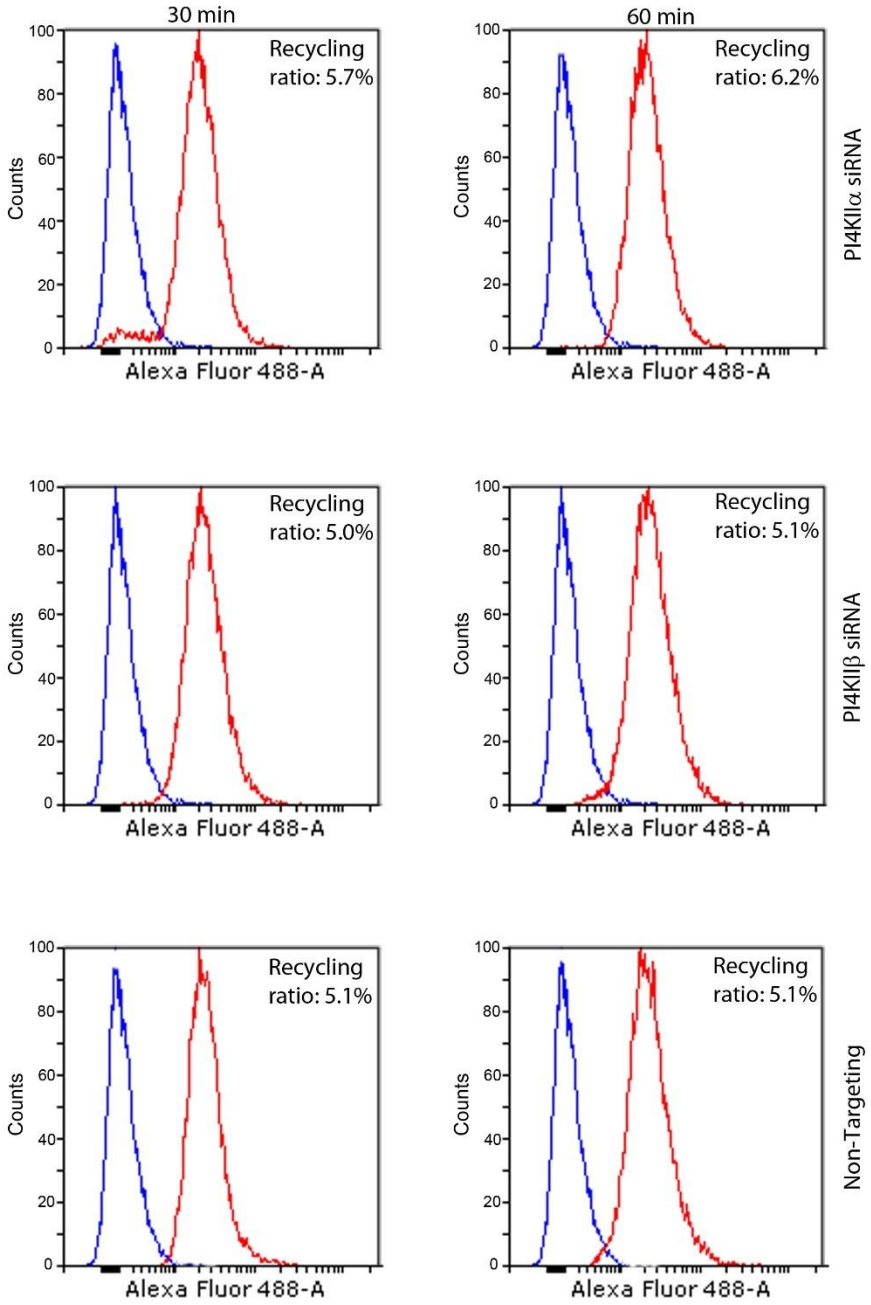

Figure 4-10. PI4KII depletion does not affect EGF induced EGFR recycling.

Isoform specific PI4KII or control siRNA transfected cells were serum starved and processed for the EGFR flow cytometry recycling assay. Panels show the amounts of Alexa-488-EGF binding to cells after 30 or 60 min of chase following a pulse with 100 ng/ml EGF. Histograms show Alexa-488 EGF binding to cells before (blue) and 30 or 60 minutes after (red) a 15-minute pulse with 100 ng/ml unlabelled EGF.

4.3 Discussion

The PI4KIIs have been described in the regulation of cargo transport on *trans*-Golgi and endosomal membranes. Most of the events controlled by this family of enzymes have been attributed to PI4KIIα but less is known about the roles of PI4KIIβ in membrane trafficking pathways at these membrane compartments. Here we describe the functions of both PI4KII isoforms in membrane cargo trafficking and partially address the issue of functional overlap.

Several studies have described the roles of PI4KIIs in post-TGN traffic and we observed that PI4KIIβ loss had a greater impact on the distribution of CI-M6PR. Depletion of PI4KIIβ but not PI4KIIα significantly lowered colocalisation between AP-1 and CI-M6PR. AP-1 is required the Golgi exit of CI-M6PR (Chi *et al.*, 2008) and diminished colocalization between both proteins upon PI4KIIβ depletion is indicative of altered post-TGN trafficking. When we performed a temperature dependent CI-M6PR transport assay, depletion of either PI4KII isoform delayed Golgi exit of CI-M6PR and its delivery to Rab9 positive endosomal compartments which mark the interphase between early and late endosomes. In addition, colocalization of CI-M6PR and AP-1 was significantly diminished in cells depleted of either isoform. In a previous study, it was reported that PI4KIIα loss blocks TGN recruitment of AP-1 thereby altering TGN to PM transport of HA (Influenza virus haemagglutinin) and delaying VSVG Golgi exit (Wang *et al.*, 2003).

PI4KIIα also controls the delivery of β-glucoceribrosidase to late endosomes (Jović *et al.*, 2012) and this conforms with our findings as PI4KIIα loss delays TGN exit of CI-M6PR, a protein involved in the delivery of lysosomal hydrolases. We observed similar results with PI4KIIβ loss and this is supported by data from Haucke's lab (Wieffer *et al.*, 2013). It was demonstrated that PI4KIIβ directly interacts with the σ1γ1 sub-complex of AP-1 via its acidic-cluster dileucine motif and that this interaction is a prerequisite for PI4KIIβ localisation to the TGN (Wieffer *et al.*, 2013). Similarly, the authors showed that PI4KIIβ but not PI4KIIα directly interacts

with AP-1 (Wieffer *et al.*, 2013). PI(4)P is predominantly found on Golgi membranes and PI4KIIα has the highest PI4K activity in mammalian cells (Balla *et al.*, 2002; Waugh *et al.*, 2003). Since AP-1 recruitment is PI(4)P dependent, a possible explanation is the formation of a complex which involves PI(4)P (as a result of PI4KIIα activity) binding and a direct physical interaction with PI4KIIβ, supporting the idea of overlapping roles for both isoforms in the regulation of post-TGN trafficking events. Our data demonstrate that both isoforms mediate TGN-endosome transport and this is supported by published work showing that depletion of either isoform results in mistrafficking and secretion of lysosomal hydrolases (Jović *et al.*, 2012; Wieffer *et al.*, 2013). A recent study demonstrated that depletion of PI4KIIβ alters packaging of von Willebrand factor (VWF) into Weibel-Palade bodies (WPBs) in endothelial cells (Lopes da Silva *et al.*, 2016). While depletion of PI4KIIα alone had negligible effects on the secretion of this clotting factor, simultaneous loss of both isoforms had a greater impact on packaging, transport and secretion of VWF (Lopes da Silva *et al.*, 2016). Although the mechanisms of clotting factor sorting, and secretion was not fully described, data from that study supports the idea of a functional overlap between both PI4KII isoforms.

The partitioning of PI(4)P pools generated by either isoform into separate domains marked by two different TGN markers, TGN46 and syntaxin 6 is supported by a previous study which showed that PI4KIIβ but not PI4KIIα colocalises with AP-1 and TGN38 (Wieffer *et al.*, 2013). PI4KIIα localises to cholesterol enriched membrane domains marked by the presence of syntaxin 6 (Minogue *et al.*, 2010; Waugh *et al.*, 2011). Since syntaxin 6 controls secretion from the TGN and localises to membranes devoid of TGN46 (Reverter *et al.*, 2014), it is possible that PI4KIIβ and PI4KIIα control the early and late stages of TGN traffic respectively. This may explain why PI4KIIβ depletion has a greater impact on AP-1 dependent TGN trafficking pathways, and this is supported by the fact that PI4KIIβ is a direct binding partner of AP-1 (Wieffer *et al.*, 2013).

Cells depleted of either PI4KII isoform displayed reduced colocalisation of CI-M6PR with Rab9 following the temperature shift. Rab9 mediates delivery of CI-M6PR from the TGN to endosomes at the early-to-late but is dispensable for retrograde trafficking of CI-M6PR (Kucera *et al.*, 2016). Thus, diminished colocalisation of CI-M6PR and Rab9 following the temperature shift demonstrates perturbed delivery of lysosomal hydrolases to late endosomes (Figure 4-3).

Depletion of either PI4KII isoform perturbed CI-M6PR retrieval at the Golgi, indicative of perturbed retrograde trafficking of cargoes from endosomal compartments to the Golgi. PI4KIIα regulates retrograde transport of CI-M6PR by controlling the cargo release step (Niu *et al.*, 2013). This requires the catalytic activity of PI4KIIα as PI(4)P competes with the $p150^{Glued}$ subunit of the dynein-dynactin complex for binding to SNX6 (a component of the retromer) at the TGN (Niu *et al.*, 2013; Marquer *et al.*, 2016). PI(4)P binding to the PX domain of SNX6 facilitates motor-cargo dissociation when retrograde cargoes reach the Golgi and depletion of PI4KIIα results in accumulation of SNX1/6 retromer vesicles (Niu *et al.*, 2013). In the previous chapter, we demonstrated that depletion of either PI4KII isoform alters Golgi PI(4)P pools, with PI4KIIα having a greater contribution to PI4K activity than its isozyme. Thus, diminished local production of PI(4)P at the TGN due to PI4KII depletion may be responsible for defective retrograde delivery of CI-M6PR as observed in our FRAP experiments. The precise role of PI4KIIβ in anterograde cargo transport is yet to be deciphered but published work identified this isozyme as a regulator of CI-M6PR trafficking (Anitei *et al.*, 2014). Since PI4KIIβ depletion results in Golgi fragmentation and phenocopies nocodazole treatment (Anitei *et al.*, 2014), it is possible that this isoform controls tethering of retromer associated vesicles to the dynein-dynactin motor complex.

PI4KIIs control various endosomal membrane trafficking event which range from phagocytosis (Jeschke *et al.*, 2015; Levin *et al.*, 2017), autophagy (Wang *et al.*, 2015), to receptor recycling (Ketel *et al.*, 2016) and lysosomal degradation (Minogue *et al.*, 2006; Mössinger *et al.*, 2012; Robinson *et al.*,

2014). As stated in previous sections of this thesis, many of these studies indicate the function of PI4KIIα in regulating these processes while only a few link PI4KIIβ to the regulation of endosomal membrane trafficking. An early study showed that overexpression of kinase dead PI4KII mutants altered transferrin uptake in COS cells (Balla *et al.*, 2002). That was not the case in the current study as depletion of either PI4KII isoform neither affected the uptake of Alexa-633-labelled transferrin nor Alexa-555-labelled EGF. This indicates that neither isoform contributes to $PI(4,5)P_2$ required for endocytic uptake of these cargoes as PI4KIIIα maintains PM PI(4)P pools (Nakatsu *et al.*, 2012; Bojjireddy *et al.*, 2014; Hammond *et al.*, 2014).

Previous studies showed that transferrin traffics through PI(4)P and PI4KII positive compartments (Balla *et al.*, 2002; Niu *et al.*, 2013) on its route to perinuclear endosomal recycling compartment (ERC). Depletion of either isoform increased colocalisation of transferrin and EEA1 following 30 minutes of transferrin loading, implying increased retention of the TfR-Tf complex in this compartment. This was manifested by decreased recycling of transferrin in cells depleted of either PI4KII isoform. A previous study showed that PI4KIIα controls endosomal trafficking of transferrin via its interaction with VAMP3 and depletion of PI4KIIα perturbs transferrin recycling to the PM (Jović *et al.*, 2014). Another study showed that PI(4)P regulates trafficking of TfR-Tf to the ERC by regulating the interaction between SNX4 and KIBRA, a dynein light-chain-binding protein (Niu *et al.*, 2013). Because SNX4 binds PI(4)P (as well as PI(3)P), PI(4)P promotes dissociation of dynein-dynactin from SNX4 associated vesicles. General inhibition of PI4K activity with chemical agents such as PAO impedes TfR-Tf trafficking to the ERC thereby reducing transferrin recycling (Niu *et al.*, 2013). Although the study did not identify the PI4K isoform involved in this pathway, the requirement for PI4KIIα in the phosphoinositide switch for exit from early endosomes (Ketel *et al.*, 2016; Levin *et al.*, 2017) suggests a pivotal role for PI4KIIα.

The involvement of PI4KIIβ in transferrin recycling was somewhat surprising as we couldn't detect PI4KIIβ on EEA1 positive vesicles (Figure 3-3). Published work from Balla and colleagues demonstrated that PI4KIIβ positive

compartments also participate in the processing of the TfR and AT_{1A} angiotensin receptor (Balla *et al.*, 2002). In addition, we observed that PI4KIIβ depletion frequently altered the distribution of EEA1 positive vesicles (data not shown) and is indicative of perturbed endosomal membrane trafficking. Hoflack and colleagues showed that depletion of PI4KIIβ distorts Golgi morphology (Anitei *et al.*, 2014), while data from Haucke's lab revealed that PI4KIIβ regulates TGN-endosomal sorting (Wieffer *et al.*, 2013). The distortion of post-TGN trafficking events due to PI4KIIβ knockdown may impinge on endosomal dynamics.

Depletion of either PI4KII isoform resulted in an accumulation of EGF and transferrin in the juxtanuclear region (Figure 4-6). Thus, EGF accumulation with transferrin in this cellular location is indicative of disrupted cargo sorting on early endosomes. This finding was corroborated by diminished colocalisation between EGFR and CD63 (Figure 4-8): indicating perturbed lysosomal trafficking of activated receptor. Agonist stimulated cell surface receptors continue signalling on endosomal compartments until the ligand dissociates from the receptor or the receptor complex is sorted into intraluminal vesicles of MVBs (Sorkin and von Zastrow, 2009; Sun *et al.*, 2013; Tan *et al.*, 2015). EGFR signalling is controlled by sorting and lysosomal degradation of activated receptor (Sorkin and von Zastrow, 2009). In this study, we demonstrated that both PI4KIIs are essential for this regulatory pathway as depletion of either isoform retards EGFR degradation resulting in sustained Erk1/2 MAPK phosphorylation (Figure 4-9). Several studies have described the functions of PI4KIIs in pathways that contribute to endo-lysosomal traffic. PI4KIIα directs lysosomal traffic of surface receptors such as the EGFR and Wnt receptor, frizzled-4 (Fz4) (Mössinger *et al.*, 2012). This is achieved via interactions with (among others) AP-3 clathrin adaptor protein complex (Salazar *et al.*, 2005; Craige *et al.*, 2008) and ubiquitin ligases such as Itch and NEDD4 (Mössinger *et al.*, 2012) which facilitate endo-lysosomal traffic and delivery of lysosomal hydrolases. Furthermore, PI4KIIα generates endosomal PI(4)P (Henmi *et al.*, 2016), which serves as a potential substrate for endosomal type 1γ PIP5-K that controls lysosomal sorting of the EGFR (Sun *et al.*, 2013). PI4KIIβ, on the

other hand, mediates TGN-endosome traffic of lysosomal membrane proteins and hydrolases (Wieffer *et al.*, 2013). Depletion of this isoform results in failure to acidify LE/lysosomal compartments thereby impeding degradation of internalised surface receptors (Wieffer *et al.*, 2013). Thus, data from this study and published work indicate that each isoform contributes to TGN-endosomal traffic by acting at different points in a pathway that culminates in lysosomal degradation.

Chapter 5 PI4KIIs control cell migration and invasion[18]

5.1 Introduction

PI4KIIs have been linked with the development of human cancers including breast and hepatic carcinomas (Mazzocca *et al.*, 2008; Li *et al.*, 2010, 2014). Previously published data demonstrate that PI4KIIs control intracellular membrane trafficking pathways which when disrupted, affect cellular events known to underlie the pathogenesis of cancer (Minogue *et al.*, 2006; Mössinger *et al.*, 2012). As shown in published work and the previous chapter, PI4KIIs control endosomal traffic of the EGFR (Minogue *et al.*, 2006) thereby regulating downstream signalling. The EGFR is a recognised human oncogene and dysregulated EGFR signalling is a common feature of numerous human cancers (Rusch *et al.*, 1997; Zhu *et al.*, 2001; Herbst and Bunn, 2003; Hanawa *et al.*, 2006; López *et al.*, 2012). The regulation of EGFR trafficking and signalling implies that PI4KIIs are potential tumour suppressors. While dysregulated signalling is a key phenotypic change in oncogenesis, other factors control the invasiveness of tumour cells.

An important factor determining cancer mortality is the acquisition of invasive and migratory capabilities by tumour cells, leading to metastasis, the process by which tumour cells are disseminated from their original site and colonise distant tissues. A crucial requirement for metastatic dissemination of tumour cells is the ability of these cells to breach the extracellular matrix (ECM). This involves changes in cellular migratory patterns as well as proteolytic remodelling of ECM components. This also involves cytoskeletal changes that enable the cell to generate forces required for breaching the ECM (Palamidessi *et al.*, 2008; Hogan *et al.*, 2009; Sanz-Moreno *et al.*, 2011). Proteolytic remodelling of the ECM is mediated by several extracellular proteases including matrix metalloproteinases (MMPs) (Poincloux *et al.*, 2009; Ren and Guo, 2012; Loskutov *et al.*, 2014; Ewald, 2015). About 25

[18] Some data from this chapter and Chapter 3 were published in Molecular Biology of the cell (Alli-Balogun *et al.*, 2016). See Appendix 4

different MMPs are expressed in mammals and these exist as multifunctional zinc-dependent endopeptidases that can degrade a variety of ECM components including collagen, fibronectin, laminin and elastin (Sato *et al.*, 2005; Snoek-van Beurden and Von den Hoff, 2005; Itoh and Seiki, 2006). Almost all MMPs are secreted, except for six which are membrane anchored and are called membrane type-matrix metalloproteinases. MMPs are synthesised as zymogens which are activated by proteolytic cleavage. MMP14 (otherwise called MT1-MMP) for example, is produced as a 64 kDa zymogen which is activated by furin cleavage at the TGN (Sato *et al.*, 2005; Itoh and Seiki, 2006) prior to its transport to the PM. MT1-MMP degrades ECM components including collagen and laminins but also processes cell surface membrane proteins including CD44, syndecan-1 and metalloproteinases, MMP2 and MMP9 (Sato *et al.*, 2005). It localises to specialised membrane protrusions such as lamellipodia and invadopodia where it facilitates proteolytic degradation of ECM proteins (Williams and Coppolino, 2011; Hoshino *et al.*, 2013c; Monteiro *et al.*, 2013; Rossé *et al.*, 2014). Overexpression of MT1-MMP is associated with poor prognosis in a wide range of human cancers including breast, colorectal, melanoma, lung, and squamous cell carcinomas (Egeblad and Werb, 2002). Metastatic dissemination of tumour cells is partly controlled by actin-rich structures called invadopodia. These appear in fluorescence microscopy as rosettes or a cluster of individual cytoplasmic puncta. When viewed in 3-dimensions, they appear as extensions of the PM that protrude into the ECM. These structures are stabilised by F-actin networks and are capable of focal degradation of ECM components through directional vesicular traffic of MMPs including MT1-MMP (Hoshino *et al.*, 2012, 2013b; Monteiro *et al.*, 2013; Williams *et al.*, 2014). The term, invadopodia is sometimes used interchangeably with podosomes. Although these structures have several morphological similarities, they possess distinct roles. Podosomes are typically found in cells of monocytic origin particularly in osteoclasts and endothelial tissues. Invadopodia, on the other hand, are found in transformed cells and mediate invasion and metastasis (Flynn *et al.*, 2008; Murphy and Courtneidge, 2011).

Invadopodium formation is initiated by the establishment of focal adhesions with the ECM through engagement of integrins, assembly of focal adhesion complexes, and tyrosine kinases including EGFR, Met, Src and TKS5 (Murphy and Courtneidge, 2011; Hoshino *et al.*, 2013a). RTKs activate a subset of the Rho family GTPases; Rac1 and Cdc42. These proteins act upstream of WASP, SCAR/WAVE and Arp 2/3 complexes that promote actin nucleation (Marchesin *et al.*, 2015). Tyrosine kinase activation also leads to cortactin phosphorylation, relieving it of inhibition by cofilin. Cortactin reinforces the N-WASP-WIP complex (Gimona *et al.*, 2008) and these interactions produce a stable invasive protrusion that pushes against the ventral cell membrane, promoting ECM penetration. MT1-MMP is a major regulator of invadopodium formation as its recruitment facilitates activation of soluble MMPs, MMP2 and MMP9 (Sato *et al.*, 2005). The Invasive potential of many tumour cells is positively correlated with their ability to form invadopodia. Over-expression of invadopodia components such as cortactin in some human cancers is associated with aggressive phenotypes and a poor prognosis in primary glioma, breast and bladder carcinomas (Paz *et al.*, 2014).

Invadopodia are considered as plasma membrane domains with unbalanced endocytic and exocytic rates for MT1-MMP (Remacle *et al.*, 2003; Gálvez *et al.*, 2004; Bravo-Cordero *et al.*, 2007). Vesicular transport regulates surface levels of MT1-MMP and it is expected that regulators of membrane trafficking, vesicle biogenesis, transport and fusion determine trafficking fates of MT1-MMP and ultimately regulate proteolytic cell invasion. Since PI4KIIs are implicated in some of these membrane events, we hypothesise that these enzymes control traffic of MT1-MMP to invasive structures by directing it into the endo-lysosomal route and that PI4KIIs negatively regulate metastatic cell migration. Little is known about the roles of PI4KIIs in actin regulation, the formation of invasive structures and ECM remodelling. This chapter describes the impacts of PI4KII loss on actin cytoskeleton, and the development of invasive cellular phenotypes. It also establishes links between PI4KIIβ expression and certain human cancers suggesting that it is, in fact, a suppressor of metastasis.

5.2 Results

5.2.1 Depletion of either PI4KII affects the actin cytoskeleton.

When we specifically depleted PI4KIIs by siRNA treatment, we noted that monolayers of cells treated PI4KIIβ siRNA were more dispersed than with PI4KIIα and controls (not shown) as described previously (Mazzocca et al., 2008). To investigate this, we stained the actin cytoskeleton in PI4KIIα and PI4KIIβ depleted cells with fluorescent phalloidin. In comparison with controls, loss of PI4KIIα led to increased actin stress fibre formation at the leading edges of cells, showing some clear focal colocalisation with phosphotyrosine (Figure 5-1c). In comparison, PI4KIIβ loss diminished actin stress fibres and resulted in the appearance of scattered phosphotyrosine positive, actin-rich puncta which were absent in PI4KIIα or control siRNA transfected cells (Figure 5-1c). Actin remodelling was confirmed by computational analysis of cortical actin and actin stress fibre ratios which revealed opposite effects of the two PI4Ks on cortical actin/stress fibre ratios (Figure 5-1d). This was supported by re-expression of siRNA resistant PI4KII plasmids which restored the actin phenotypes generated upon loss of either isoform (Figure 5-2). These data indicate that loss of PI4KIIα and PI4KIIβ has markedly different effects on the actin cytoskeleton.

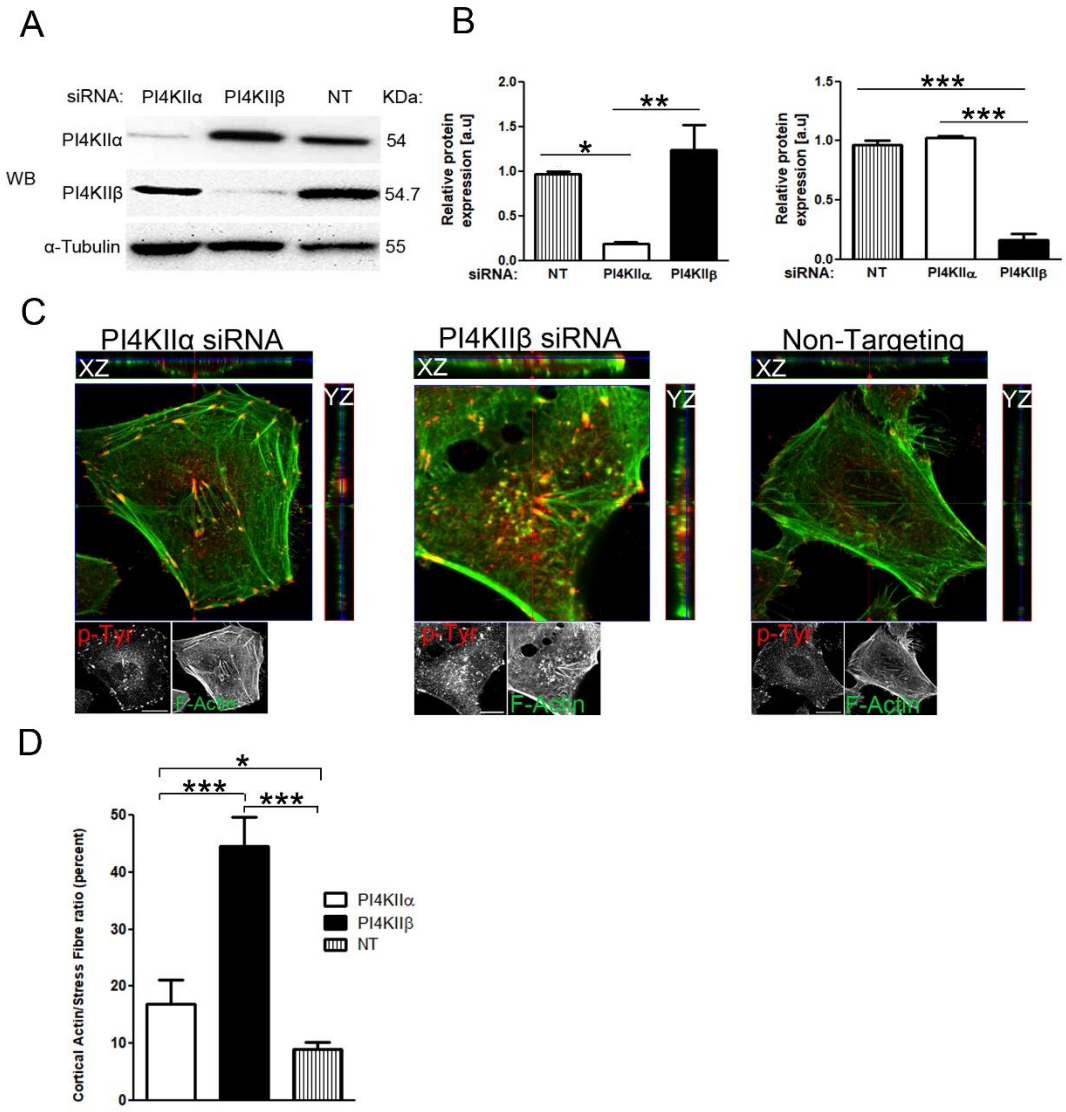

Figure 5-1. PI4KIIα and PI4KIIβ exert different effects on the actin cytoskeleton.

A, B. Total cell lysates of PI4KIIα, PI4KIIβ and control siRNA-transfected HeLa cells were analysed for protein expression by western blot using. **B.** HeLa cells were analysed for protein expression by western blotting with α-tubulin serving as a control for protein levels. **C**. HeLa cells transfected with the indicated siRNAs for 36 hours were re-seeded onto collagen matrix then co-stained for tyrosine phosphorylated proteins and the actin cytoskeleton. Images are single confocal sections and Insets represent magnified regions of rectangles shown in merged planes in which the green (F-actin) and red (phosphotyrosine (p-Tyr)) pixels co-localise. Scale bars,10 µm. **D.** Ratio of cortical actin to stress fibre ratio across three independent experiments (n= 20 cells). Data are presented as mean ± SEM, *, $p<0.05$, **, $p<0.01$, ***, $p<0.001$, ns (not significant).

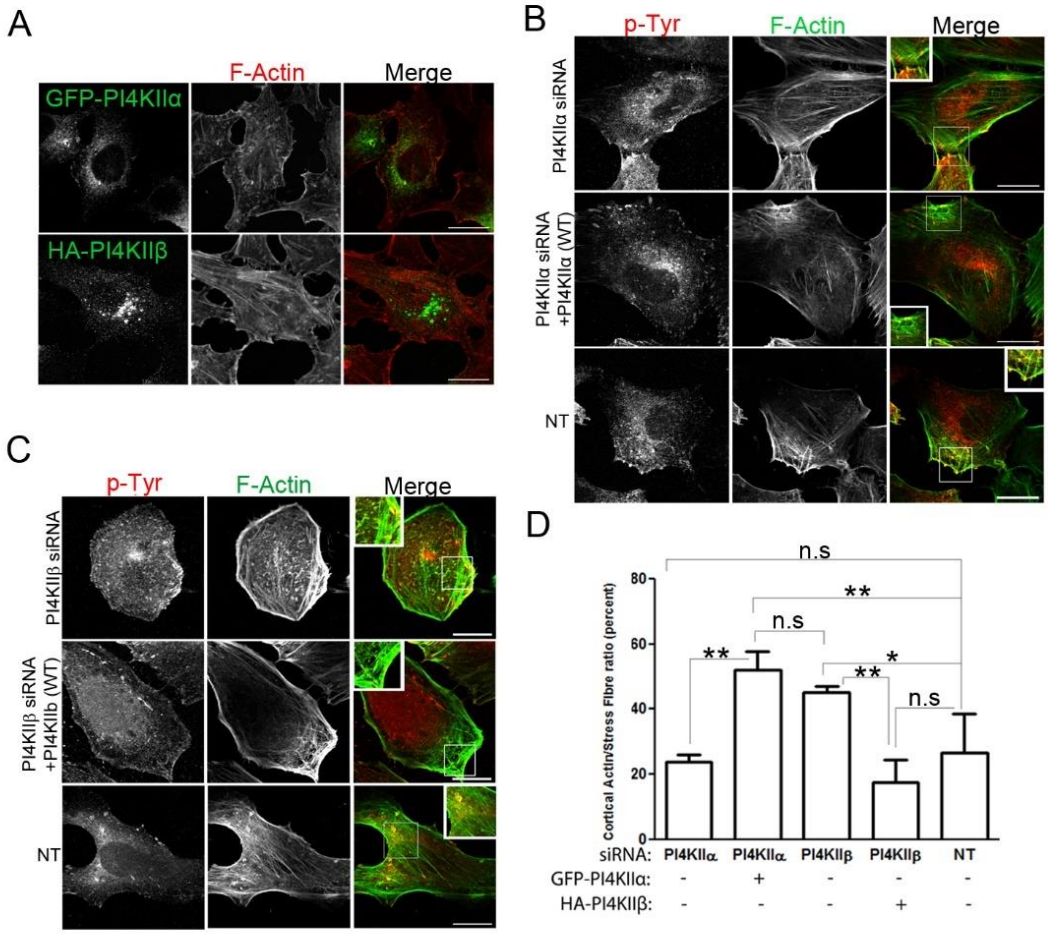

Figure 5-2. siRNA resistant PI4KII plasmids rescue actin cytoskeletal phenotypes induced by loss of either PI4KII isoform.

A. Confocal images showing expression of siRNA resistant GFP-tagged PI4KIIα and HA-tagged PI4KIIβ. Scale bars, 10 µm. **B, C**. Confocal images showing immunostaining for phosphotyrosines (green) and F-actin (red) following siRNA mediated silencing with or without transfection with siRNA resistant constructs. **D**. Histogram shows effects of expression of siRNA resistant plasmids on cortical actin to actin stress fibre ratios.

5.2.2 Loss of Type II PI4KS enhances activation of Rac1 and Cdc42

Ligand stimulation of growth factor receptors or integrins results in the activation of the Rho family of GTPases which include, Rac1 and Cdc42 (Tatin *et al.*, 2006; Palamidessi *et al.*, 2008; Huveneers and Danen, 2009). Activation of these proteins culminates in changes in actin polymerisation and cell migration. To identify these effects, we initially immunostained HeLa cells for total cellular Rac1 observing only subtle changes in the distribution of Rac1 (not shown). Because immunostaining total protein made it impossible to distinguish between active (GTP bound) and inactive (GDP bound) pools of Rac1, we probed cells with the GST-PAK-CRIB fusion protein to identify active pools Rac1 (as well as Cdc42). This enabled identification of active pools of Rac1, which are usually localised to the plasma membrane (Palamidessi *et al.*, 2008). MCF-7 cells were seeded onto collagen coated glass coverslips and transfected with target or control siRNAs. 54 hours post-transfection, cells were serum starved for 18 hours and then stimulated with 100ng/ml EGF for five minutes. In comparison with PI4KIIα and control siRNA treated cells, PI4KIIβ showed increased GST-PAK-CRIB staining following EGF stimulation. In addition, Z-series of 20 confocal sections of each siRNA treatment revealed increased localisation of active pools of Rac1/Cdc42 to membrane ruffles and the ventral surface of PI4KIIβ-depleted cells (Figure 5-3 a, arrowheads).

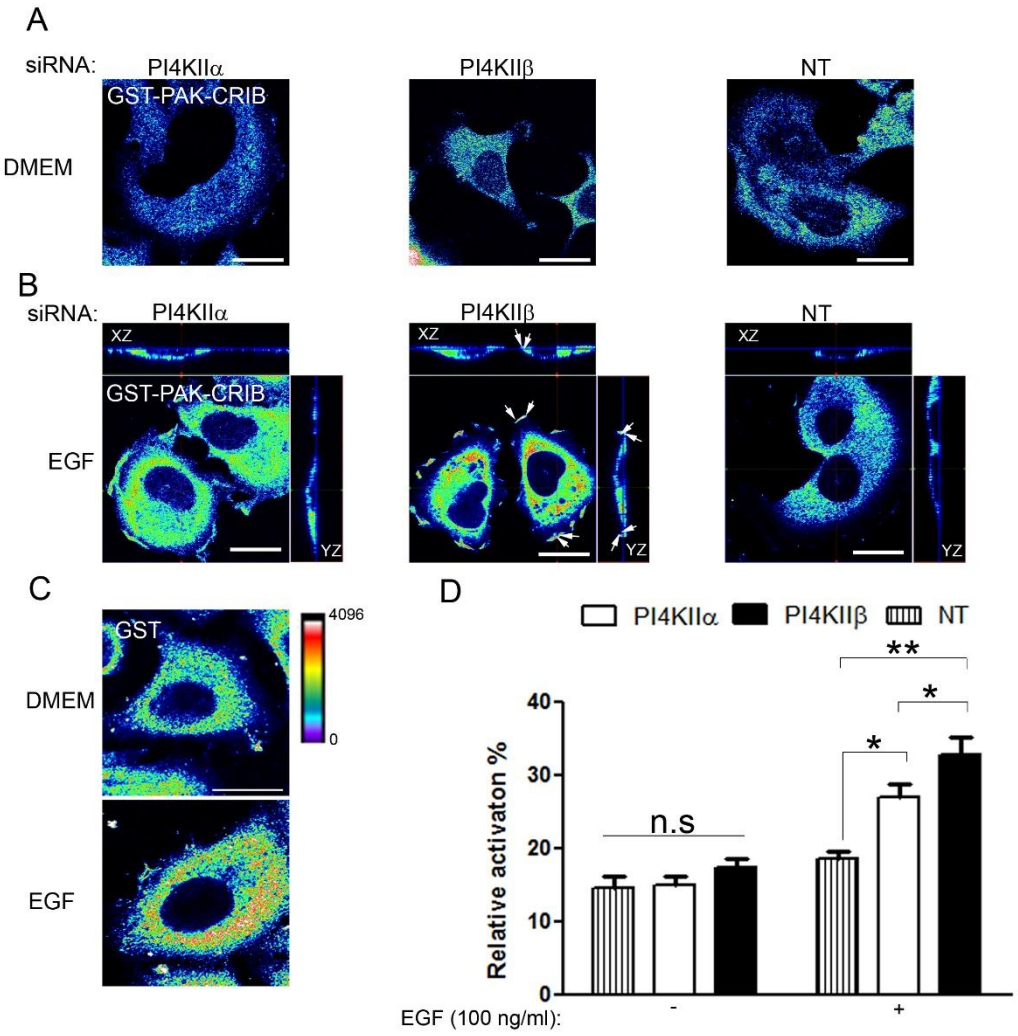

Figure 5-3. Loss of PI4KIIβ potentiates Rac1/Cdc42 activation in response to EGF stimulation.

A. siRNA transfected cells were grown on collagen-coated coverslips, serum starved (DMEM) or **(B)** stimulated with 100 ng/ml EGF for 10 mins, then fixed and stained with GST-PAK-CRIB fusion protein to report GTP-bound Rac1 and Cdc42. Orthogonal views of 20 optical sections acquired at 0.25µm intervals showing the relative intensity of GST-PAK-CRIB staining. Arrows indicate regions of membrane ruffling and localisation to the ventral surface of PI4KIIβ-depleted cells. Scale bars, 10 µm. **C.** Single confocal sections show that MCF-7 cells labelled with GST only (GST-control) lack PM GST staining with or without EGF stimulation. **D**. Relative activation of Rac1/CDC42 at the cell periphery (PM) in siRNA treated cells. Data are mean ± SEM (n=30 cells) *, $p<0.05$, **, $p<0.001$, ***, $p<0.0001$.

5.2.3 PI4KIIβ loss induces invadopodia formation

PI4KIIβ depletion resulted in the formation of actin-rich puncta which were visible as belts or rosettes in peripheral regions of the cell (Figure 5-1c). We then sought to confirm the identity of these actin-rich puncta formed as a result of PI4KIIβ depletion. Initial staining with endosomal markers, EEA1 (Figure 5-4a) and CD63 (not shown) indicated that these were distinct from actin comets that localise to endosomal compartments. Furthermore, these structures had average diameters ≤0.25 μm and were clustered around the nuclear regions of cells and were thus suggestive of invadopodia. Invadopodia are branched actin -rich structures that can be identified by co-immunostaining between actin puncta and regulators of actin polymerisation such as the Arp2/3 complex, cortical actin binding protein (cortactin), N-WASP, and the Src family kinases (Blangy *et al.*, 2012). To observe this feature, we treated HeLa cells with 50 ng/ml Phorbol 12-myristate 13-acetate (PMA) (Tatin *et al.*, 2006) for different times. A 30-minute treatment induced the formation of scattered individual punctae and rosettes that co-stained with cortactin in peripheral and cytoplasmic regions of the cell (Appendix 3; Figure A 2).

We then immunostained siRNA transfected HeLa cells for F-actin and cortactin. In comparison with PI4KIIα and control siRNA transfected cells, loss of PI4KIIβ resulted in the formation of scattered actin rich punctae that co-stained with cortactin (Figure 5-4b). In addition, we took orthogonal projections which showed that these punctae were localised proximal to the basal surface of the cell as observed in PMA-stimulated cells (Figure 5-4c).

We also seeded MCF-7 cells onto collagen coated coverslips and captured 20 confocal sections for each treatment. Maximum intensity projections were used to visualise the localisation of MT1-MMP and marker proteins, cortactin and β1-integrin. The Z-series data revealed the colocalisation between MT1-MMP and cortactin or β1-integrin at the basal membrane in PI4KIIβ-depleted cells in comparison with PI4KIIα and control siRNA treated cells (Figure 5-5).

To further analyse the protein composition of these structures, we used the cell fractionation method described by Bowden et al. (1999) to evaluate the enrichment of proteins in invadopodia fractions. In comparison with control and PI4KIIα transfected cells, we observed increased enrichment of β1-integrin, cortactin, and MT1-MMP in invadopodia (INV) fractions of PI4KIIβ depleted cells (Figure 5-5). All named proteins are associated with invasive structures and these findings suggest that loss of PI4KIIβ may lead to the development of an invasive phenotype.

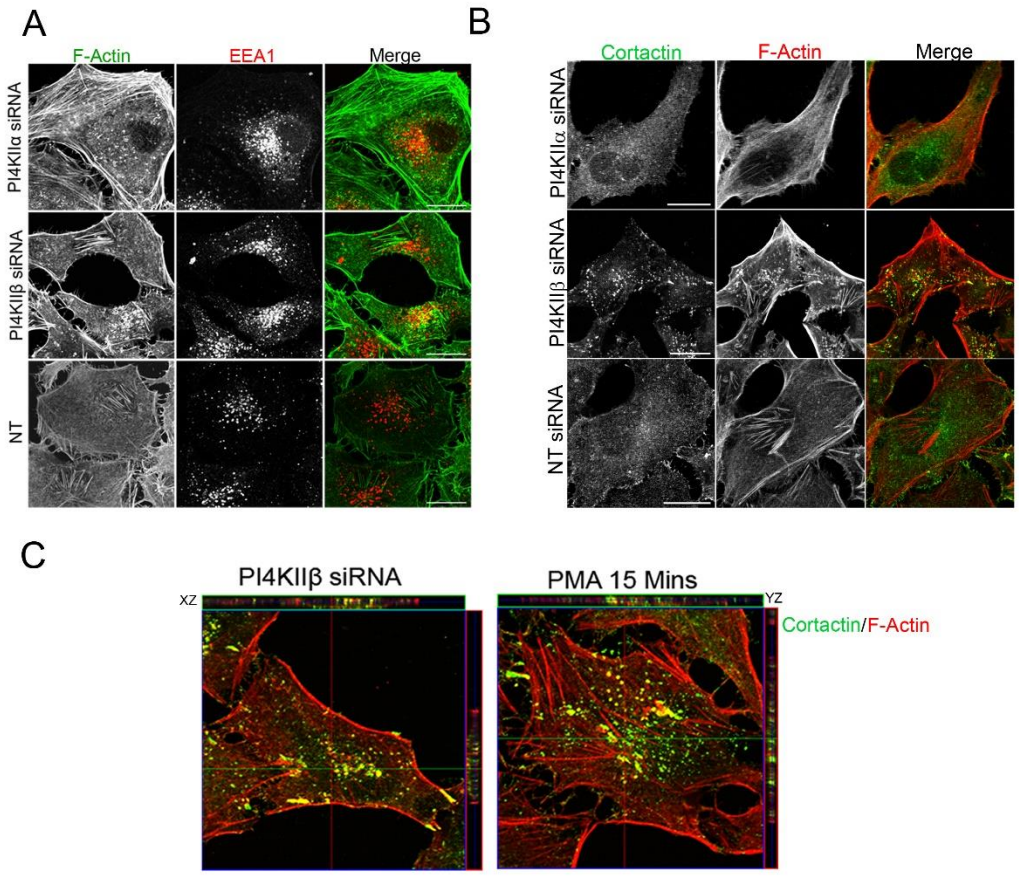

Figure 5-4. Loss of PI4KIIβ specifically induces invadopodia formation.

A. Confocal images showing that scattered actin punctae induced upon PI4KIIβ depletion do not contain the endosomal marker EEA1. **B.** siRNA treated HeLa cells were fixed and co-stained for F-actin and cortactin using Alexa-546-phalloidin and rabbit anti-cortactin antibodies respectively. Co-immunostaining of actin puncta with cortactin is indicative of invadopodia in these cells. F-actin and cortactin co-immunostaining reveals invadopodia in PI4KIIβ depleted cells. Images are single confocal sections. Scale bars, 10 µm. **C.** Comparison of PI4KIIβ-depleted cells with those treated with 50 nM PMA for 15 minutes. Z-series data demonstrates the localisation of actin and cortactin-rich punctae on the ventral surface of the cells, thereby confirming invadopodia formation in both cells.

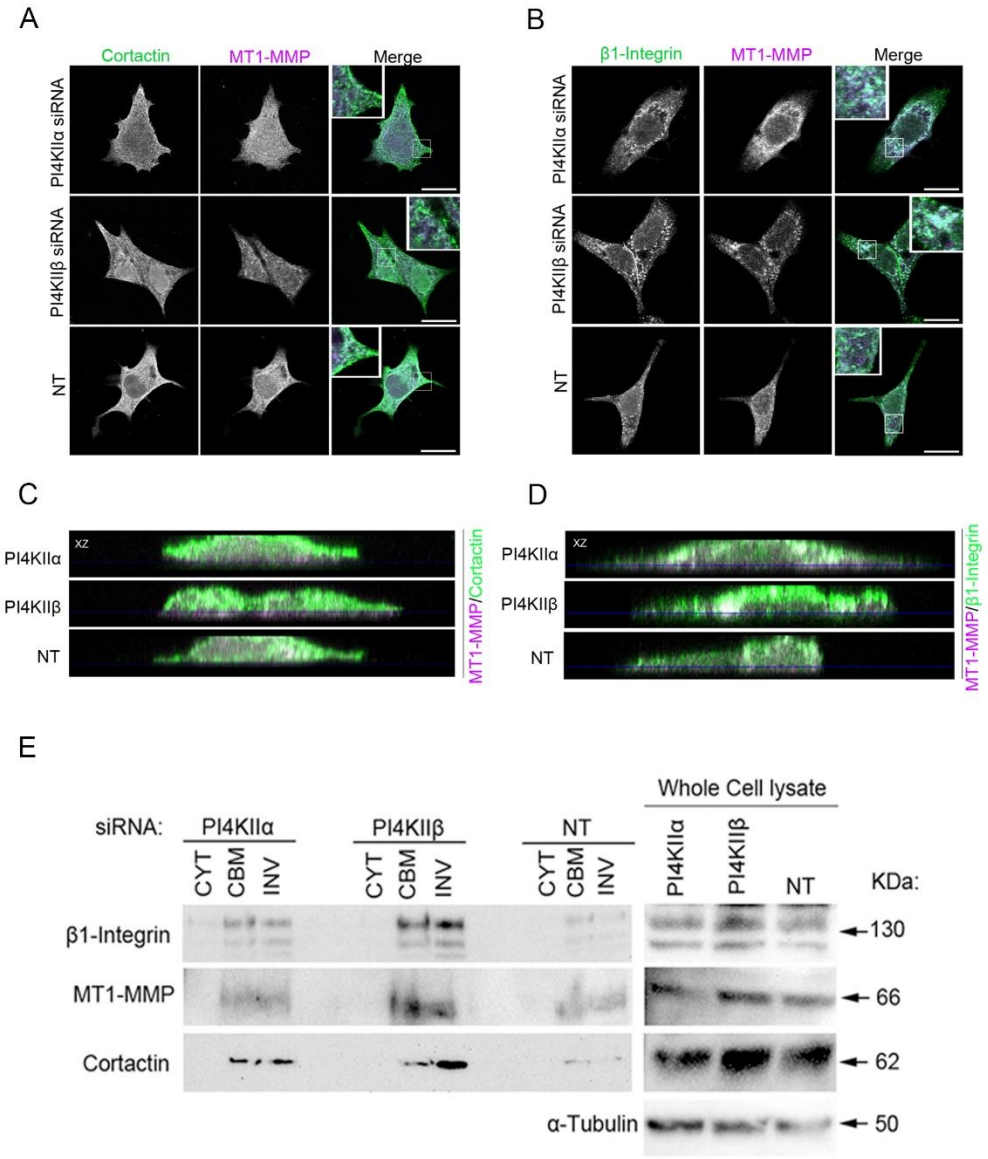

Figure 5-5. Further characterisation of invadopodia in PI4KIIβ depleted cells.

A-D. Confocal images showing cells grown on thick layers of collagen, and co-immunostained for MT1-MMP (magenta) and (A) cortactin or (B) β1-integrin (green). **C, D**. XZ rendering of 20 confocal sections acquired at 0.25-µm intervals, showing localization of MT1-MMP to ventral structures containing cortactin (C) or β1-integrin (D). Horizontal lines indicate the position of the ECM surface. Scale bars, 10 µm. **E.** Identification of invadopodia components by cell fractionation. Immunoblots of fractions show the distribution of protein markers of invadopodia. CYT- Cytoplasmic fraction, CBM- Cell body membranes, INV- invadopodia and matrix fractions.

5.2.4 PI4KIIβ loss increases proteolytic ECM degradation and migration through Transwell chambers

To determine the function of these structures formed upon PI4KIIβ depletion, we plated target and control siRNA transfected HeLa, MCF-7 cells as well as MDA-MB-231 cells (a strongly invasive breast adenocarcinoma cell line) on 0.2% cross-linked FITC conjugated gelatin. In comparison with PI4KIIα and control siRNA transfected cells, loss of PI4KIIβ resulted in ~4-fold increase in fluorescent matrix degradation. Furthermore, areas of degradation also corresponded to clusters of actin-rich punctae (Figure 5-6) suggesting that they were the source of the gelatinolytic activity.

We also performed a Transwell invasion assay to measure the relative potential of PI4KII-depleted cells to transverse a collagen-coated Transwell membrane in response to a chemoattractant (10% FCS (v/v DMEM); Figure 5-7a)). We inverted collagen coated polyethene Transwell membranes on microscopic slides and captured 20 Z-sections over 20 µm at intervals of 2 µm (Figure 5-7, b-d). This enabled us to visualise cells invaded the matrix and Transwell membrane in response to the chemoattractant. After 12 hours of incubation, more PI4KIIβ-depleted cells migrated through the collagen coated insets than PI4KIIα and control siRNA transfected cells (~ 2- and 2.5-fold greater than PI4KIIα and NT siRNA transfected cells respectively; Figure 5-7d). These findings suggest that PI4KIIβ may be essential for the control of cell invasion.

5.2.4.1 Loss of PI4KIIβ confers invasiveness on MCF-7 cells.

We enquired whether PI4KIIβ loss was sufficient to confer a migratory phenotype onto a minimally invasive MCF-7 cell line derived from a minimally invasive ductal breast carcinoma. To test this, we evaluated the ability of PI4KIIβ-depleted MCF-7 to degrade FITC-gelatin matrix and migrate through a collagen coated Transwell membrane in response to a chemoattractant. PI4KIIβ-depleted MCF-7 cells degraded FITC-gelatin to an extent comparable to the invasive MDA-MDB-231 line (Figure 5-8, a and b). Furthermore, they displayed increased ability to migrate through collagen

coated Transwell membranes in response to a chemoattractant (Figure 5-8c). These data suggest that PI4KIIβ suppresses an invasive phenotype *in vitro*.

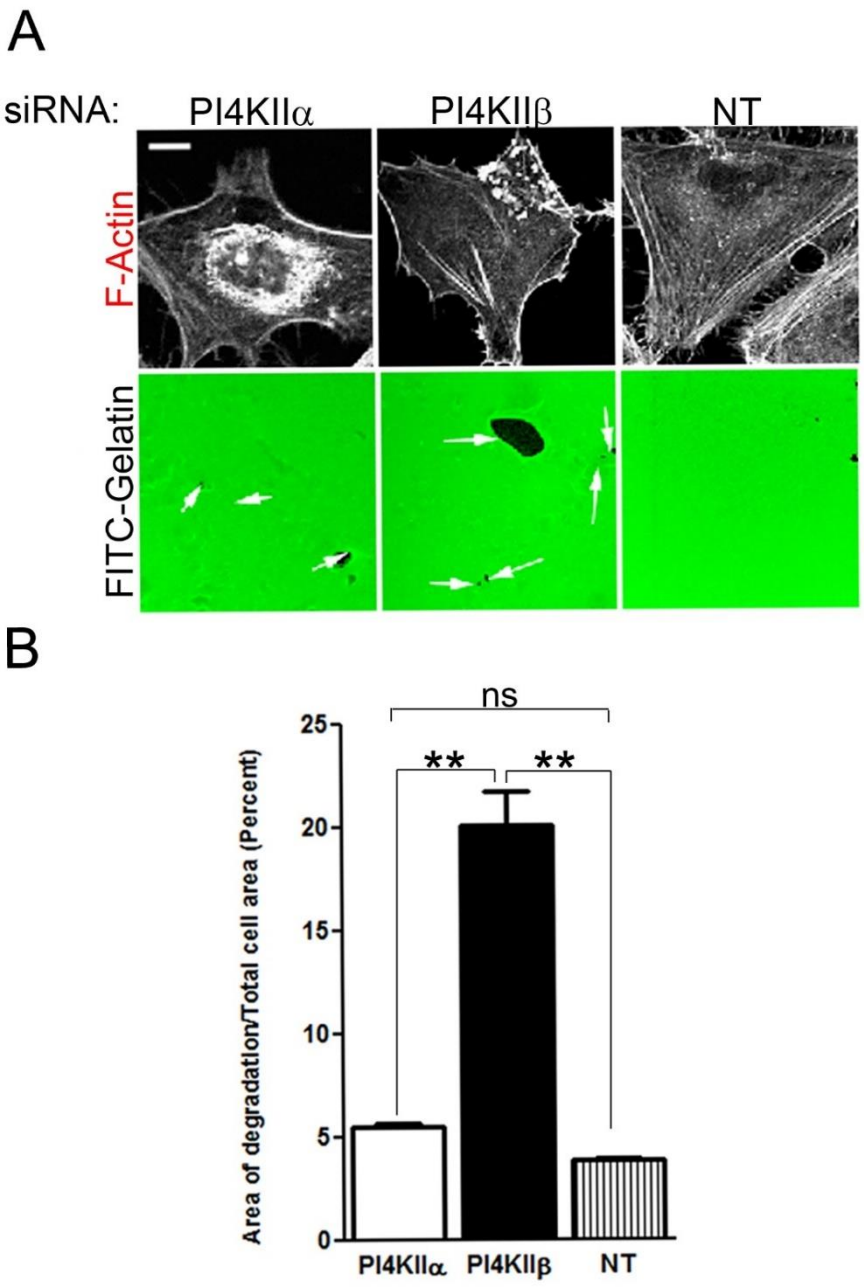

Figure 5-6. Loss of PI4KIIβ promotes matrix degradation

A. Cells were treated with siRNA for 56 hours and then seeded on FITC labelled gelatin (green) and incubated for a further 12 hours in complete medium. Cells were then fixed and stained with fluorescent phalloidin to label F-actin. Areas of matrix degradation are indicated with arrows. **B.** Percentage of proteolytic degradation per total cell area. Data are mean ± SEM (n=30 cells, three independent experiments) *, $p<0.05$, **, $p<0.01$, ns (not significant).

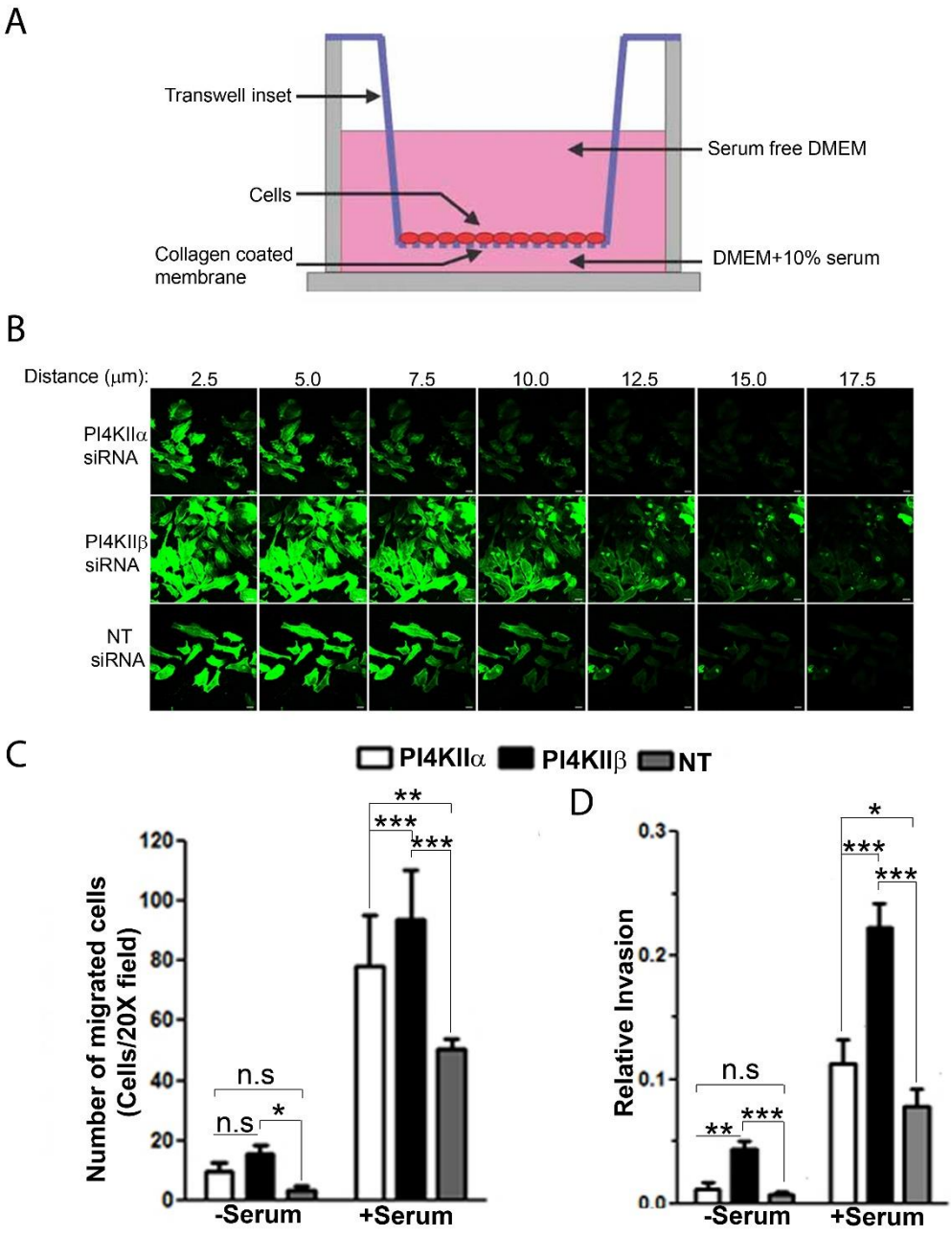

Figure 5-7. PI4KIIβ depletion promotes cell migration through a Transwell membrane.

A. Complete assembly of a Transwell migration experiment. **B.** Migration of siRNA treated cells via collagen-coated Transwell inserts towards a chemoattractant. After staining with Alexa-488-labelled phalloidin, fixed cells were visualised by confocal microscopy. Optical sections were acquired at 2.5 µm apart and are shown side by side with increasing depth. **C**. Average number of cells that invaded the collagen-coated Transwell membrane after two hours of stimulation with foetal calf serum. **D.** Relative invasion of Transwell membrane in response to chemo-attractant. Data are mean ± SEM, *, $p<0.05$, **, $p<0.001$, ***, $p<0.0001$.

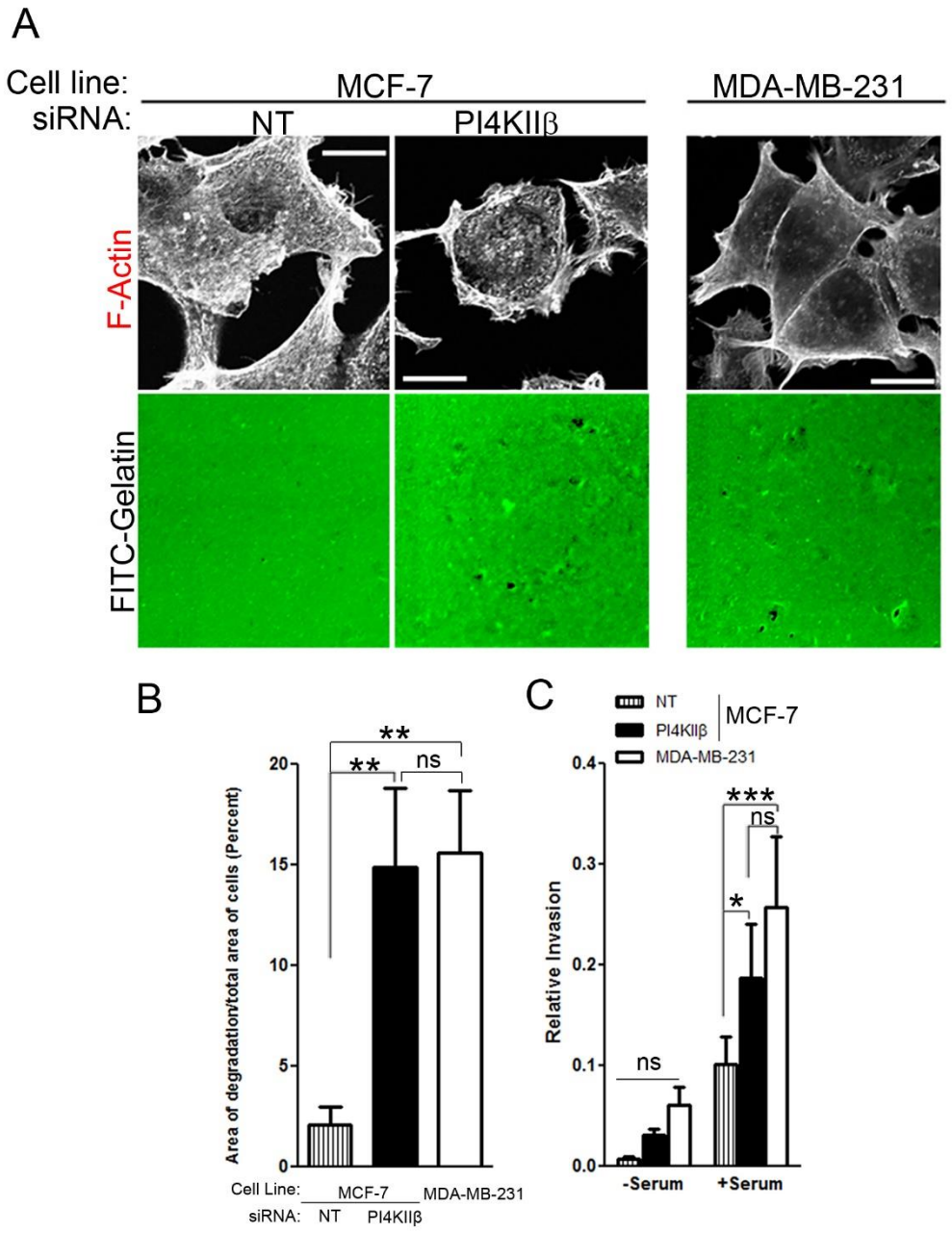

Figure 5-8. PI4KIIβ depletion is sufficient to confer a migratory and invasive phenotype.

A. siRNA treated MCF-7 and untreated MDA-MB-231 cells were re-seeded onto FITC-gelatin coated coverslips 58 hours post-transfection (except MDA-MB-231) and then labelled for F-actin (red). **B.** Percentage areas of proteolytic degradation per total cell in a $4\times10^4\,\mu m^2$ area. Data are mean ± SEM (n=30, three independent experiments). **C.** MCF-7 or MDA-MB-231 cells were re-seeded onto collagen-coated Transwell inserts 58 hours post transfection and placed in a chemoattractant (10% FCS) for 12 hours. Index of cell migration through an artificial barrier in response to a chemoattractant. Data are mean ± SEM, *, $p<0.05$, **, $p<0.01$, ***, $p<0.001$, ns (not significant).

5.2.5 PI4KIIβ depletion alters MT1-MMP trafficking

As previously mentioned, invadopodia can be considered as plasma membrane domains with unbalanced endocytic and exocytic rates for MT1-MMP. MT1-MMP is rapidly internalised by endocytosis and trafficked towards lysosomes for degradation while recycling via early or late endosomal compartments is a proposed means of regenerating the active enzyme (Remacle *et al.*, 2003; Poincloux *et al.*, 2009; Wiesner *et al.*, 2013). Basal surface expression of MT1-MMP is low in most cell types due to efficient removal from the cell surface by endocytosis. Transformed cells use several mechanisms to counteract clearance of active protease from the cell surface. One such mechanism involves increased endosomal recycling of internalised MT1-MMP to cell-matrix contacts (Remacle *et al.*, 2003; Itoh and Seiki, 2006; Loskutov *et al.*, 2014), reminiscent of the front-to-back model of endosomal recycling of integrins (Poincloux *et al.*, 2009). Transformed cells also mobilise MT1-MMP from the secretory pathway, such as the Rab8 dependent trafficking of MT1-MMP from the Golgi to collagen contact sites (Bravo-Cordero *et al.*, 2007, 2016). These features indicate the importance of endosomal trafficking in the delivery of MT1-MMP to cell-ECM contact sites and thus prompted us to evaluate the impacts of PI4KII depletion on MT1-MMP trafficking. We initially assessed surface and total MT1-MMP levels in antibody chased MCF-7 cells using flow cytometry and this revealed that loss of PI4KIIβ, in comparison with PI4KIIα and control siRNA treated cells, increases surface levels of MT1-MMP (Figure 5-9, a and b). These findings suggest that loss of this isoform impairs MT1-MMP homeostasis, thereby increasing its cell surface levels.

Previous studies have shown that some Rab GTPases involved in vesicular trafficking pathways control surface levels of MT1-MMP (Bravo-Cordero *et al.*, 2007; Wiesner *et al.*, 2013). This prompted a co-immunostaining of MT1-MMP and a selected panel of Rab GTPases (Rab 5, 7, 8, 9 and 11) in target and control siRNA transfected cells. In comparison with control, depletion of both PI4KII isoforms decreased colocalisation of MT1-MMP with Rab5 and Rab7. However, PI4KIIβ loss increased MT1-MMP colocalisation with Rab8

(Figure 5-9, c and d). Loss of either PI4KII resulted in undetectable changes in colocalisation of MT1-MMP with Rab9 or Rab11. Impaired endo-lysosomal traffic of MT1-MMP was confirmed by co-immunostaining with CD63 where MT1-MMP showed significantly less colocalisation with CD63 in PI4KII depleted cells in comparison with control (Figure 5-9, e and f). The Rab8 data suggests that PI4KIIβ depletion redirects MT1-MMP from a degradative Rab5/7 endo-lysosomal route to a Rab8 positive exocytic route.

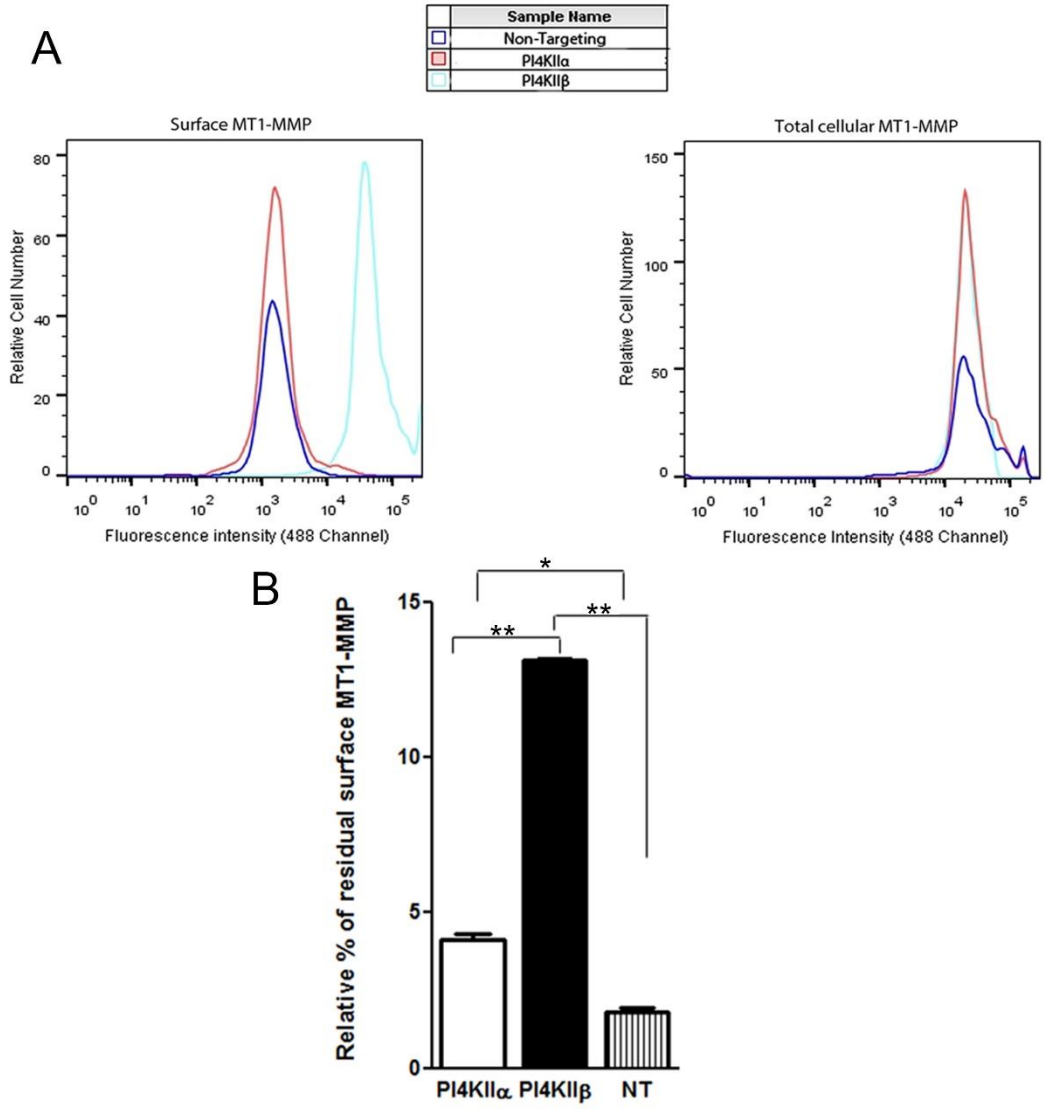

Figure 5-9. Continued on next page

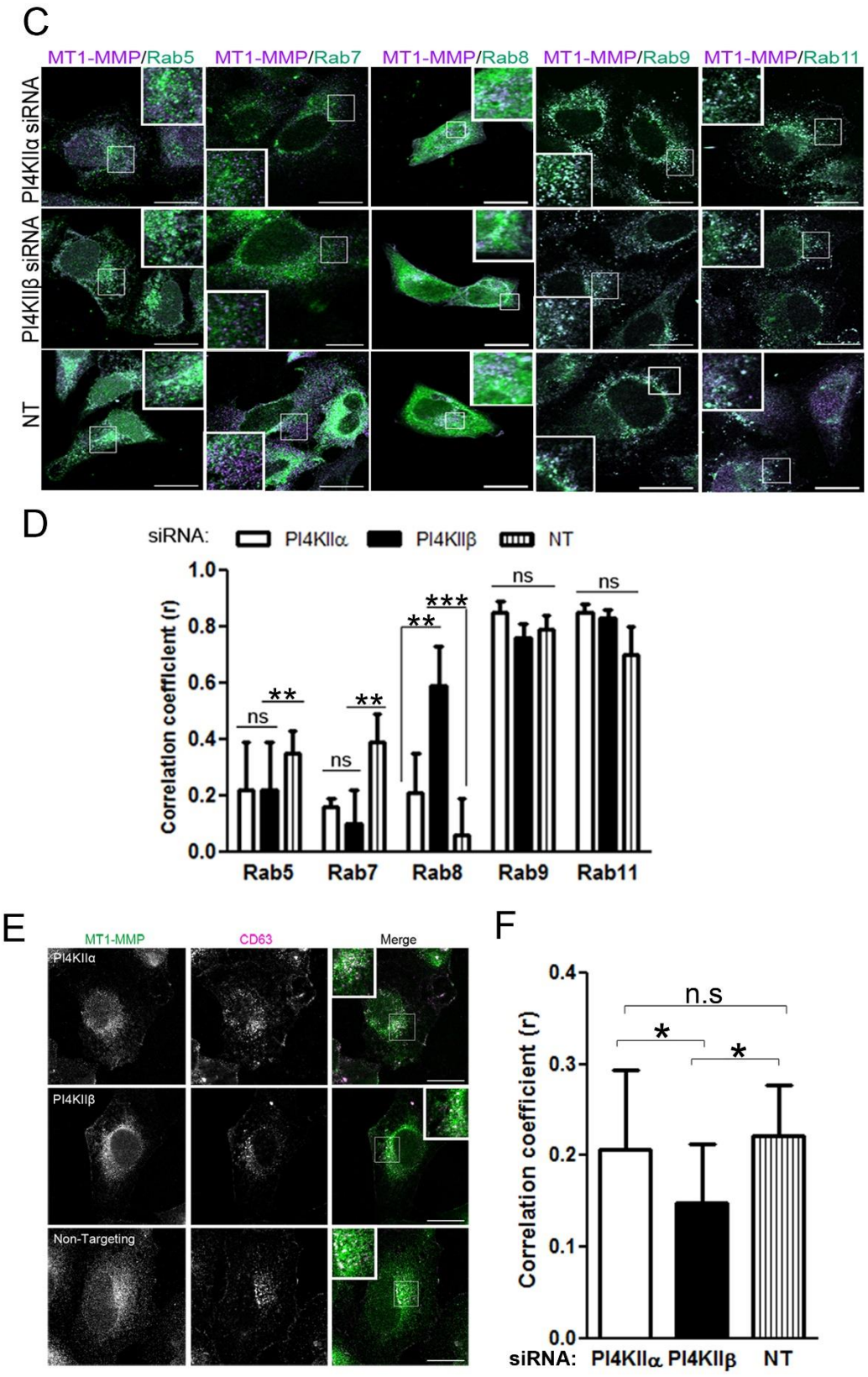

Legend on next page

Figure 5-9. PI4KIIβ regulates surface levels of MT1-MMP

A, B. Surface labelled (non-permeabilised cells) and total MT1-MMP (permeablised with 0.05% Triton X-100) were analysed by flow cytometry and (B) the relative percentage (%) MT1-MMP present on the cell surface versus total cellular MT1-MMP. Data are mean ± SEM (n=3, experiment in triplicate). *, $p<0.05$, **, $p<0.001$, ***, $p<0.001$. **C**. Confocal images showing immunostaining for MT1-MMP (magenta) and the indicated Rab GTPases (green). Insets represent magnified regions of rectangles shown in merged planes in which pixels co-localise. Scale bars,10 μm. **D**. Pearson's correlation coefficients for colocalised intensities between pixels for MT1-MMP and the indicated Rab GTPases. Data are presented as means ± SEM (n=30 cells, three independent experiments). *, $p<0.05$, **, $p<0.01$, ***, $p<0.001$, ns (not significant). **E, F**. Immunofluorescent staining of MT1-MMP and the lysosomal marker, CD63. *, $p<0.05$, (n=20 cells, three independent experiments).

5.2.6 Loss of PI4KIIβ is associated with human cancers

Data from previous sections demonstrate that PI4KIIβ suppresses cell migration and invasion of ECM *in vitro*, a key feature of tumour dissemination in clinical metastasis. This led to the question of PI4KIIβ being a tumour suppressor, or more specifically a suppressor of metastasis in mammalian cells. To answer this, we interrogated oncogenomic and transcriptomic data from cBioPortal and Oncomine databases (Rhodes *et al.*, 2004; Cerami *et al.*, 2012).

cBioPortal analysis revealed that heterozygous loss of PI4K2B is associated with lung (squamous cell and adenocarcinoma), oesophageal, pancreatic, prostate, breast, liver and various epithelial carcinomas (Figure 5-10a). 2.75% of pancreatic tumour samples displayed homozygous loss of PI4K2B while 43.1% and 12.8% of these samples displayed heterozygous loss of and unaffected copy number for PI4K2B respectively (n=109 samples; Figure 5-10b). Both PI4K2B alleles were deleted in 0.52% of hepatocellular carcinoma samples. 23.68% of these samples exhibited heterozygous deletion while 64.73% and 10.52% had unaffected or gain of PI4K2B expression respectively (n=190 samples; Figure 5-10c). Oncomine data revealed significant reductions in PI4K2B mRNA expression in invasive breast carcinoma (n=59; Figure 5-10d). Survival data were analysed in a small number of available breast carcinoma cases (Ciriello *et al.*, 2015) and it was observed that loss of PI4K2B expression correlated with poor patient survival, albeit with a low probability value (Figure 5-10e). These data together support the hypothesis that PI4K2B loss is a risk factor in human cancers.

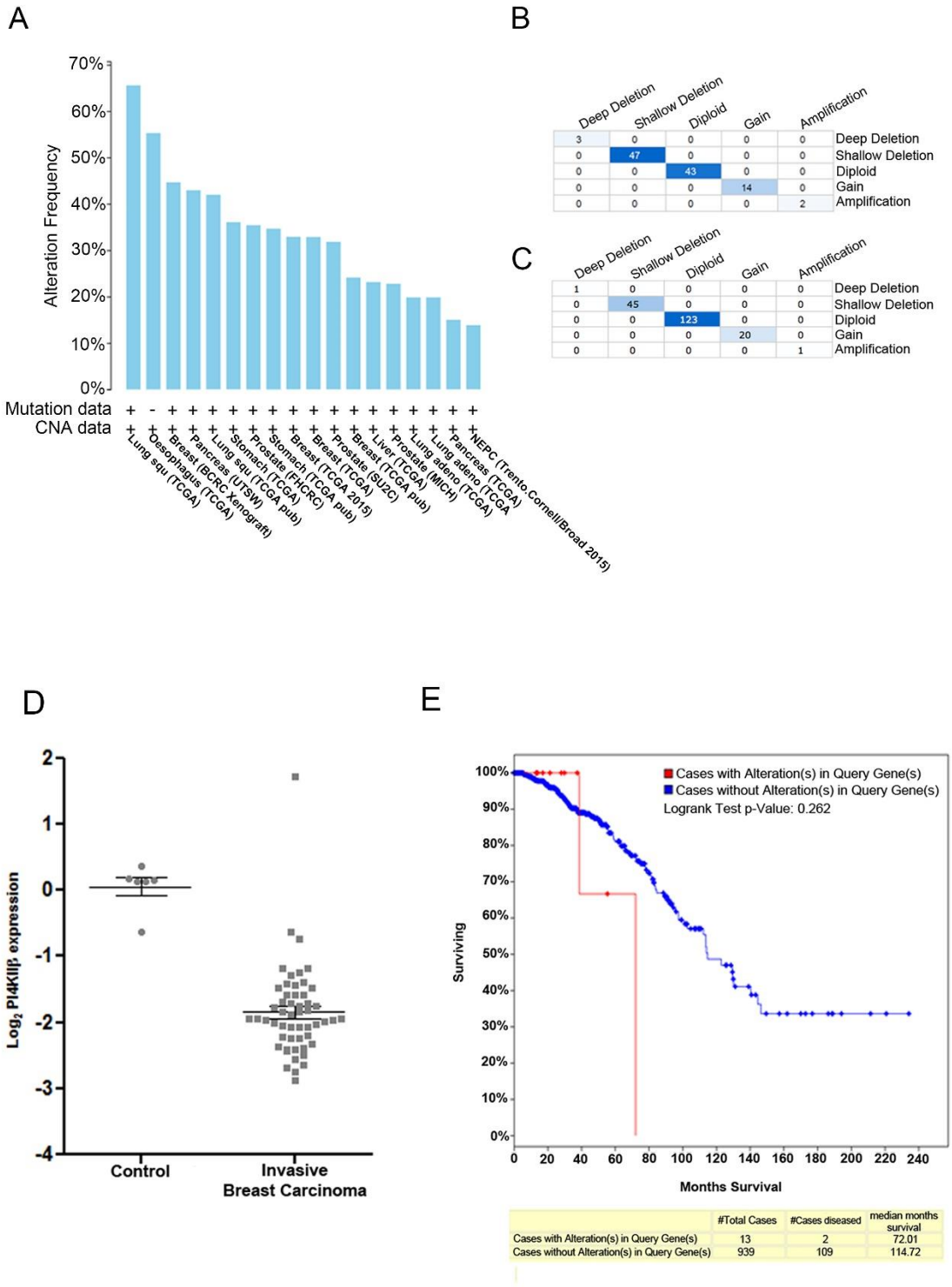

Legend on next page

Figure 5-10. Database analysis shows that loss of PI4KIIβ expression is associated with cancer.

A. Cross-cancer alteration summary of 18 selected cancer studies (squamous lung, oesophageal, breast, prostate and pancreatic) for heterozygous loss of the PI4K2B allele. Threshold= minimum 5% altered samples, cBioPortal analysis (Cerami *et al.*, 2012; Gao *et al.*, 2013). adeno, adenocarcinoma; NEPC, Neuroendocrine Prostate cancer; Squ, squamous cell carcinoma. Data sources are given in parenthesis: TCGA, The Cancer Genome Atlas; BCRC, British Columbia cancer research centre; UTSW, University of Texas Southwestern; FHCRC, Fred Hutchinson cancer research centre; SU2C, Stand up to cancer/Prostate cancer foundation (PCF); MICH, University of Michigan. **B.** PI4K2B putative copy number alterations from GISTICS for pancreatic cancers. Overall change in PI4K2B expression (deletion or amplification) in pancreatic cancers was analysed using cBioPortal. **C.** PI4K2B putative copy number alterations from GISTICS for hepatocellular carcinomas. Overall change in PI4K2B expression (deletion or amplification) in hepatocellular cancers was analysed using cBioPortal. **D**. Analysis of PI4K2B expression (Oncomine) in recurrent breast carcinoma (Finak breast, reporter: A_23_P18598). **E**. Overall survival Kaplan-Meier graph of breast carcinoma cases (CBioPortal) analysis with PI4K2B expression alteration (TCGA 2015).

5.3 Discussion

Data from this chapter highlight the ability of PI4KIIβ to suppress cell migration as silencing of this gene increased pericellular proteolysis of ECM components and invasion of a Transwell membrane in response to serum growth factors. Although there is limited evidence for the direct involvement of PI4KIIs in actin regulation, PI4KIIβ plays a role in the suppression of cell migration in HCC (Mazzocca *et al.*, 2008). The striking feature of PI4KIIβ-depleted cells was the appearance of actin-rich puncta on the ventral surface that were enriched with the actin regulatory protein cortactin which is a marker of invadopodia. In contrast, PI4KIIα loss increased stress-fibre formation at the expense of cortical actin. While these differences could not be directly linked to their enzymic activities, these phenotypes could be rescued with siRNA resistant PI4KII plasmids. Coupled with increased stress fibre formation, PI4KIIα depleted cells were more rounded in comparison with an elongated cell phenotype observed in PI4KIIβ depleted cells.

Changes in actin such as this are a feature of small GTPase activation and imply that PI4KII isoforms control different aspects of the cytoskeleton (Watanabe *et al.*, 2004; Palamidessi *et al.*, 2008; Joffre *et al.*, 2011; Lane *et al.*, 2014). This prompted us to evaluate GTPase activation in siRNA treated cells using a recombinant GST-PAK-CRIB fusion construct that binds active Rac1/Cdc42. However, our GST-PAK-CRIB pull-down assays were obscured by low signal intensities and increased background noise (data not shown). Pulldown assays provide a means of quantitating relative Rac1 activation; however, such assays only measure bulk GTPase activity within a cell population without the ability to reveal the coordinated regulation of these proteins in individual cells (Malliri *et al.*, 2002). Complex processes such as cell migration involve continuous turnover of cell adhesions and concurrent actin polymerisation/depolymerisation. It is also highly likely that the activities of Rac1/Cdc42 (and other Rho-like GTPases) differs spatiotemporally, necessitating the use of a technique that visualises these active GTPases in individual cells. Indirect fluorescent staining of active Rac1/Cdc42 with GST-PAK-CRIB revealed that loss of either isoform

increased activation of Rac1/Cdc42, while PI4KIIβ-depleted cells showed increased localisation of active GTPases to the ventral surface. The Rho family of small GTPases in their active forms recruit a variety of target proteins that regulate the cytoskeleton and do so in different ways. Rho-ROCK signalling, for example, promotes a rounded mode of cell motility that is characterised by increased actin stress fibre formation generating contractile forces that facilitate cell motility (Sahai and Marshall, 2003; Sanz-Moreno *et al.*, 2011). However, Rho-ROCK independent signalling involving Rac1 or Cdc42 decreases actin stress fibres (Joffre *et al.*, 2011) and promote the formation of cell protrusions which facilitate proteolytic remodelling of the ECM (Sahai and Marshall, 2003). Although the GST-PAK-CRIB construct clearly binds active Rac1 or Cdc42 GTPases (Pellegrin and Mellor, 2008), we, unfortunately were unable to investigate Rho-ROCK signalling in PI4KII depleted cells. Irrespective of that, the Rac1/Cdc42 data suggests that PI4KIIβ loss results in increased localisation of active GTPase to the ventral surface. Previously published work by Moreau and colleagues showed that Cdc42 activation drives the assembly of podosomes (structures morphologically identical to invadopodia) in endothelial cells (Tatin *et al.*, 2006). The localisation of active GTPase to the ventral surface of PI4KIIβ-depleted cells is indicative of a signal that orchestrates invadopodia assembly. This was confirmed by increased enrichment of invadopodia components such as cortactin, β1-integrin and MT1-MMP in ventral surface and matrix interacting fractions of PI4KIIβ-depleted cells.

We further confirmed that these were functional invadopodia by demonstrating their ability to degrade FITC-gelatin (fluorescent ECM). PI4KIIβ-depleted HeLa cells acquired an increased ability to degrade ECM and migrate through collagen coated Transwell membranes in response to serum growth factors. On the other hand, PI4KIIα and non-targeting siRNA treated cells showed limited abilities to degrade ECM nor migrate through these Transwell membranes in response to chemoattractant. These differences can be attributed to the increased localisation of active Rac1/Cdc42 GTPases at the ventral surfaces of PI4KIIβ depleted cells. Rac1 and Cdc42 GTPases control the cortical actin network while RhoA and

downstream effector, ROCK regulate stress-fibre assembly (Sahai and Marshall, 2003). Since PI4KIIα loss increases actin-stress fibre formation, it is possible in this scenario that PI4KIIα suppresses Rho-ROCK dependent assembly of stress fibres while PI4KIIβ functions as a negative regulator of cortical actin assembly. While Rho-ROCK signalling favours rounded cell motility, Rac1/Cdc42 signalling promotes elongated cell motility involving pericellular degradation of ECM components (Sahai and Marshall, 2003; Sanz-Moreno *et al.*, 2011). This raises the question of differential regulation of cell migration by the two closely related PI4KII isoforms thereby warranting further investigations.

Cells such as HeLa and MCF-7 are minimally invasive and express low surface levels of MT1-MMP (Poincloux *et al.*, 2009). This effect reflects the vital role of controlling surface metalloproteinase activity. Data from this chapter revealed that loss of either PI4KII isoform increase cellular levels of MT1-MMP due to disrupted endo-lysosomal traffic. The Rab GTPases play important roles in vesicular transport of MT1-MMP. For example, Rab5 controls endosomal sorting of MT1-MMP while Rab7 controls its traffic to late endosomal compartments (Remacle *et al.*, 2003; Williams and Coppolino, 2011; Wiesner *et al.*, 2013). Depletion of either PI4KII isoform decreased colocalization of MT1-MMP with Rab5 and Rab7 which are localised on sorting and late endosomes respectively. MT1-MMP showed less colocalization with CD63 in PI4KII depleted cells, consistent with a previous study showing that CD63 promotes lysosomal degradation of MT1-MMP (Takino *et al.*, 2003). These indicate that loss of either isoform impairs degradative traffic of MT1-MMP via the endo-lysosomal route.

However, only PI4KIIβ depletion increased surface levels of MT1-MMP, implying that surface traffic of this metalloproteinase is controlled in an isoform specific manner. This was made evident by increased colocalization of MT1-MMP with Rab8 positive membranes in PI4KIIβ-depleted cells. Rab8 operates in an exocytic pathway that directs traffic to the plasma membrane and mediates trafficking of MT1-MMP to invasive structures (Hattula *et al.*, 2006; Bravo-Cordero *et al.*, 2007). Although a mechanistic investigation of

Rab8 mediated trafficking was not done in this thesis, recent data showed that this GTPase activates Rac1 activity, thereby regulating actin cytoskeleton and cell motility (Bravo-Cordero *et al.*, 2016).

These data support a model in which MT1-MMP is redirected from the endo-lysosomal pathway into a Rab8 positive exocytic pathway. A possibility for this is increased recycling. We attempted to investigate this by live cell imaging but our experiments were fraught with technical difficulties arising from the presence of MT1-MMP signals in multiple subcellular compartments that obscured invadopodia dynamics. Nonetheless, increased MT1-MMP recycling remains a likelihood as we also detected invadopodial localisation of β1-integrin, a protein that is recycled along with MT1-MMP in a Rab8 dependent pathway (Macpherson *et al.*, 2014). PI4KIIα directs exocytic traffic of β1-integrin from endosomes to the PM following hydrolysis of PI(3)P (Ketel *et al.*, 2016), suggesting that endosomal PI(4)P generated by PI4KIIα plays a role in β1-integrin traffic. Whether PI4KIIβ loss results in increased PI4KIIα activity leading to increased β1-integrin recycling remains a question for further investigation.

The conferment of an invasive phenotype onto the weakly invasive MCF-7 cell line following PI4KIIβ depletion led to an inquiry on the anti-metastatic role of the PI4K2B gene. In addition, unidentified tumour suppressors map closely to the chromosomal location of PI4K2B (4p15.2) and undergo allelic losses in sporadic colorectal carcinomas (Zheng *et al.*, 2008). These features led us to carry out oncogenomic data mining which revealed that PI4K2B is a potential tumour suppressor gene. Loss of the PI4K2B allele and under-expression of this gene is associated with a variety of human cancers of epithelial origin. Furthermore, these data suggest that PI4K2B under-expression is associated with poorer patient survival in breast carcinomas; however, the low statistical power of this associated studies led to a lower probability value ($p=0.262$). While we thread cautiously in drawing conclusions, this finding may be of clinical significance and it is speculated that PI4KIIβ acts as a suppressor of metastasis by controlling an endo-lysosomal trafficking pathway that negatively regulates invadopodia

formation. It is also important to note that PI4KIIβ is implicated in embryonic development in Zebrafish (Wieffer *et al.*, 2013). The process of tumour dissemination and metastasis is related to the cellular events that occur during embryogenesis, angiogenesis and neurite outgrowth. Since PI4KIIβ membrane localisation is subject to cellular regulation, it is hypothesised that a PI(4)P dependent switch regulates lysosomal degradation and PM recycling of key molecules such as integrins and MMPs that are critical to the tissue remodelling process.

Chapter 6 Conclusions and future directions

PI4Ks initiate biosynthetic pathways leading to the generation of polyphosphoinositides. This thesis focused on the cellular roles of the closely related PI4KIIs which exhibit a great degree of similarities in their C-terminal catalytic domains but display variabilities in their *N*-termini. Strong evidence exists for the roles of PI4KIIα in Golgi and endosomal trafficking. However, only a few cellular functions have been ascribed to PI4KIIβ. This is partly due to the difference in regulation and membrane recruitment of both isoforms. PI4KIIα is constitutively membrane anchored and its activity is controlled by its membrane environment, particularly by substrate availability and cholesterol content. As a result, PI4KIIα acts like a sensor that responds to changes in its membrane environment with increased PI(4)P synthesis. This permits PI4KIIα to alter membrane identity and direct trafficking pathways on Golgi and endosomal membranes. Unlike its isozyme, PI4KIIβ is distributed between membrane and cytoplasmic pools. This enzyme can be regulated by extrinsic factors such as growth factors which facilitate plasma membrane recruitment. The plasma membrane recruitment of PI4KIIβ is intriguing as it demonstrates a role for PI(4)P at the PM, a role previously ascribed to PI4KIIIs. PI4KIIβ activity is also modulated by its interaction with Hsp90, a molecular chaperone which inhibits its activity by sequestering it in the cytoplasm. The divergence in regulation of both PI4KII isoforms implies differences in their membrane localisation and cellular functions.

6.1 Subcellular localisation of PI4KIIs

Previous studies have raised issues of redundancy and overlapping functions for both isoforms and this thesis partially addressed these features. Chapter 3 described how both isoforms localise to distinct TGN domains defined by immunostaining with the non-overlapping markers syntaxin 6 or TGN46. While PI4KIIα showed greater colocalization with syntaxin 6 than it did with TGN46, PI4KIIβ displayed the reverse. This localisation pattern is consistent with previously published data showing that both syntaxin 6 and PI4KIIα localise to cholesterol enriched domains of the TGN. PI4KIIβ colocalisation

is consistent with previous reports showing that PI4KIIβ localises to TGN46-positive domains of the TGN while PI4KIIα weakly colocalises with this marker (Minogue *et al.*, 2010; Wieffer *et al.*, 2013).

Contrary to a previous report (Balla *et al.*, 2002), only PI4KIIα localises to EEA1-positive early endosomes, consistently with recently published data (Henmi *et al.*, 2016); however, both isoforms could be found on CD63 positive vesicles, indicating their presence on LE/MVBs. Chapter 3 also highlighted the *in vivo* catalytic activities of the endogenous proteins using an immunofluorescent staining method to quantify cellular PI(4)P. Data from this thesis indicate that PI4KIIα has a significantly higher kinase activity than PI4KIIβ and both enzymes synthesise metabolically separate pools of PI(4)P at the TGN. These pools were identified by co-immunostaining with syntaxin 6 ($PI(4)P^{PI4KII\alpha}$) or TGN46 ($PI(4)P^{PI4KII\beta}$), proteins with which either isoform show differential colocalization. With these data and previously published work, it remains possible that the Golgi harbours three PI4K activities (PI4KIIα, PI4KIIβ and PI4KIIIβ) that localise to distinct domains of this cellular compartment and regulate different aspects of Golgi trafficking. Consistent with immunofluorescent labelling of PI4KIIs, PI4KIIα but not PI4KIIβ controls a pool of PI(4)P on EEA1 positive early endosomes while PI4K activity could be ascribed to both isoforms on CD63-positive vesicles, indicating some degree of functional redundancy at this subcellular compartment. It was also observed that PI4KIIα has a significant contribution to $PI(4,5)P_2$ at the plasma membrane, but it was not determined whether this isoform is resident at the PM or delivered to the PM by vesicular transport. The latter possibility is supported by previous data showing that PI4KIIα is trafficked from Rab27 positive late endosomes to the PM in $CD4^+$ T-lymphocytes (Gerber *et al.*, 2015).

6.2 Overlapping roles of PI4KIIs in Golgi and endosomal trafficking

Some trafficking pathways occurring on Golgi and endosomal membranes were explored in Chapter 4. Data from that chapter demonstrate that both isoforms possess overlapping roles in regulating vesicular trafficking

pathways occurring on Golgi and endosomal subcellular compartments. Both isoforms are required for post-Golgi traffic of CI-M6PR. FRAP data also revealed the possibility of PI4KIIα controlling retrograde traffic of this cargo from endosomal compartments. Similarly, both PI4KII isoforms were implicated in endosomal sorting and trafficking of transferrin and EGF-receptor, with the loss of either isoform impairing recycling of apo-transferrin and endo-lysosomal traffic of the EGFR. Impaired endo-lysosomal traffic of the EGFR sustained RTK activity and activation of downstream signalling targets Erk1/2. Although silencing of either isoform impaired EGFR degradation, PI4KIIβ had a greater impact on this pathway. While this was not explored, it is possible that this isoform — as demonstrated in published work— controls the delivery of lysosomal hydrolases that degrade internalised receptors in LE/MVBs. Published data also demonstrate that PI4KIIα controls endo-lysosomal traffic of internalised surface receptors, indicating that both PI4KIIs operate in tandem in regulating endo-lysosomal trafficking pathways. Data from Chapter 4, most of which are preliminary, demonstrate the roles of both PI4KIIs in Golgi and endosomal traffic. How PI4KIIs in the presence of other PI4K enzymes on the Golgi regulate Golgi-endosomal trafficking pathways is not fully understood and these remain questions for future research endeavours.

6.3 Anti-metastatic role of PI4KIIβ

Chapter 5 highlights the anti-metastatic potential of PI4KIIβ. Knockdown of either PI4KII isoform led to changes in the actin cytoskeleton, suggesting they exert different effects on the cytoskeleton. PI4KIIβ alone suppressed the formation of actin-based structures which were characterised as mature and functional invadopodia. While the precise mechanism leading to the formation of these structures in PI4KIIβ-depleted cells was not addressed in detail, data from this chapter is suggestive of the activation of Rac1/Cdc42 GTPases. In addition, PI4KIIβ suppresses proteolytic degradation of ECM components by regulating focal localisation of MT1-MMP to invadopodia. As a result, PI4KIIβ suppresses cellular migration in response to serum growth factors. Data from Chapter 5 describe PI4KIIβ as a negative regulator of

molecular events that precede invasion and metastasis. While exercising some caution regarding conclusions, data from this chapter give support to the hypothesis that PI4KIIβ is a suppressor of metastasis. This is supported by the oncogenomic database searches (Chapter 5) which revealed loss of heterozygosity of PI4KIIβ in some common human cancers (lung, breast, liver and pancreas). In addition, a breast carcinoma data sample from the oncogenomic databases reveal poorer patient prognosis due to PI4KIIβ under-expression. The metastatic suppressive roles of PI4KIIβ remain to be formally proven in experimental systems appropriate for the study of tumour suppressors. The notion that PI4KIIβ is linked to the development of metastatic capability is exciting and warrants further investigation. Also, unlike other suppressors of metastasis, the pathway controlled by PI4KIIβ may be druggable by targeting corresponding PI 4-phosphatases.

Appendix 1 FRAP data analysis

Required software: ImageJ, Zen 2012 blue version (Zeiss), MS excel and GraphPad Prism.

- Open confocal image series in ImageJ as a stack
- Click Edit>Selection>Specify and input the value of the bleaching area. Alternatively, use a drawing tool to highlight the bleached area. This may be inaccurate and may require readjustment.

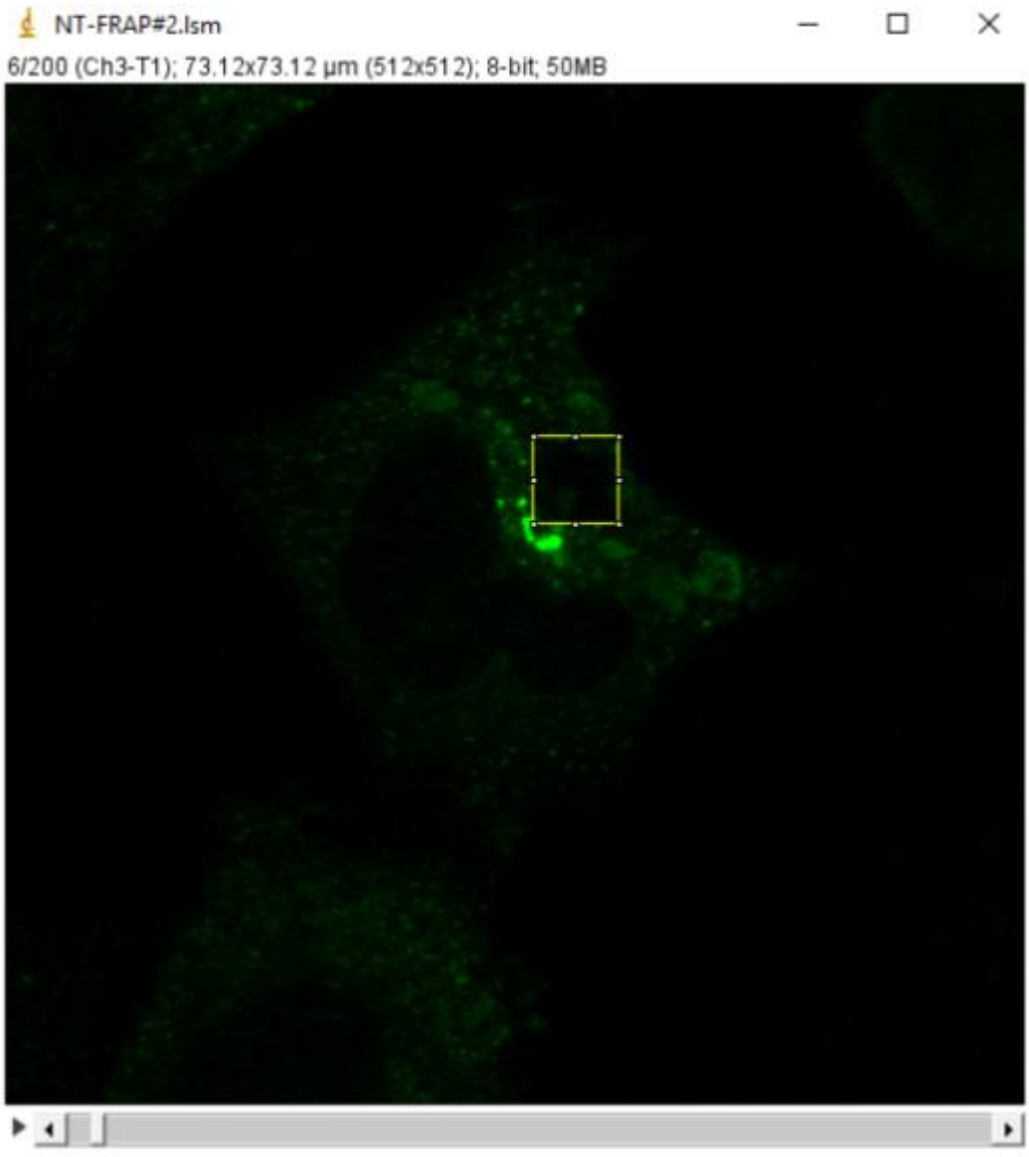

Figure A 1. Selecting the region of interest (ROI) in the image stack.

- Press ‘’T’’ to automatically save the region of interest (ROI) in the ROI manager.

- Drag and drop the selection to a non-bleached area within the cells to quantify cell fluorescence. Repeat this step for an area outside to obtain background fluorescence.
- In the ROI manager, click ‘’more’’ and then ‘’multi-measure’’ to get a result window with values for A. bleached area, B. cellular fluorescence and C. background.
- Select all values and paste in excel.
- Create a column (F) in excel for dynamic correction of the bleaching by applying the ratio: (C-E)/(D-E). This corrects the value for the background and normalise bleaching due to repetitive image acquisition.
- Add another column (G) to calculate the average values pre-bleaching fluorescence (average (F2:F6)
- Create another column (H) and compute the relative fluorescence recovery (values range from 0-1) by dividing the corrected post-bleached values by the pre-bleached average in column (G).

	A	B	C	D	E	F	G	H
1	Frame	Time Poin	Bleached	In Cell Flu	BG	DC	Mean PreB	Rel. Fluo rec
2	1	0	1555.751	818.008	22.07	1.926885	1.960668868	0.982769216
3	2	0.985	1550.529	793.836	27.802	1.987806		1.013840764
4	3	1.971	1517.016	789.512	25.008	1.951603		0.995375934
5	4	2.956	1510.672	762.832	24.192	2.012455		1.026412646
6	5	3.942	1487.378	783.576	22.376	1.924595		0.981601435
7	6	12.23	263.567	792.531	22.397	0.313153		0.159717584
8	7	13.22	277.519	784.862	23.478	0.333657		0.170175021
9	8	14.2	275.357	774.438	22.315	0.336437		0.171592969
10	9	15.19	275.969	777.845	23.07	0.335065		0.170893424
11	10	16.17	360.936	777.294	22.07	0.448696		0.228848442
12	11	17.16	350.37	750.287	23.539	0.449717		0.229369223
13	12	18.14	361.854	766.952	23.294	0.455263		0.23219782
14	13	19.13	366.729	776.376	21.152	0.457582		0.233380622
15	14	20.11	371.93	760.527	20.724	0.474729		0.242126088
16	15	21.1	405.219	760.833	18.643	0.520859		0.265653496
17	16	22.08	413.032	777.559	20.398	0.518561		0.26448157
18	17	23.07	526.984	761.567	19.704	0.683792		0.348754464
19	18	24.06	525.637	754.571	21.438	0.687732		0.350763955
20	19	25.04	598.937	778.885	21.438	0.762428		0.388861308
21	20	26.03	635.673	779.946	21.193	0.809855		0.413050429
22	21	27.01	633.49	793.184	20.969	0.7932		0.40455586
23	22	28	646.749	778.069	20.561	0.826642		0.421612291

- In GraphPad Prism, select an XY table, check ‘’start with an empty table’’ and in ‘’sub-columns’’ for replicates or error values’’ select ‘’Y’’ and enter 8 (or as many as possible) replicate values in side by side sub-columns.
- Copy timepoints from Excel column (B) and paste in X columns of Prism
- Copy relative fluorescence recovery values from Excel column (H) and paste in Y columns of Prism

	X	A							
	Time [Sec]	siRNA: Non-Targeting							
	X	A:Y1	A:Y2	A:Y3	A:Y4	A:Y5	A:Y6	A:Y7	A:Y8
1	0.000	0.982769	0.999714	1.000000	1.000000	0.993411	1.000080	0.946264	1.016897
2	0.985	1.013841	1.009666	1.006540	1.028591	0.992867	0.994394	1.004187	0.996921
3	1.971	0.995376	0.972461	1.007204	0.965912	0.999350	0.998631	1.024643	0.998945
4	2.956	1.026413	0.999490	0.989034	0.967640	1.008569	1.001386	1.028829	1.004142
5	3.942	0.981601	0.998294	0.968992	0.946359	1.005804	1.004207	0.996077	0.983094
6	12.230	0.219586	0.193242	0.133319	0.079062	0.080721	0.138200	0.019957	0.000000
7	13.220	0.232327	0.197657	0.145726	0.119980	0.094088	0.154584	0.033277	0.013626
8	14.200	0.275029	0.252800	0.200318	0.259072	0.338573	0.209133	0.280991	0.260325
9	15.190	0.273615	0.238759	0.205696	0.251720	0.346792	0.203008	0.286048	0.267760
10	16.170	0.363916	0.386507	0.317320	0.259909	0.452675	0.328778	0.396692	0.363699
11	17.160	0.369729	0.383090	0.428839	0.408562	0.437162	0.495261	0.537162	0.374173
12	18.140	0.369366	0.401362	0.433231	0.417749	0.432517	0.512769	0.532517	0.370210
13	19.130	0.368448	0.408801	0.451788	0.418583	0.440905	0.512369	0.540905	0.374652
14	20.110	0.380009	0.429588	0.457412	0.439622	0.440886	0.510256	0.540886	0.386039
15	21.100	0.403093	0.425640	0.461047	0.450153	0.440296	0.527475	0.540296	0.387310
16	22.080	0.399203	0.396319	0.460055	0.463801	0.456309	0.527497	0.556309	0.394637
17	23.070	0.417504	0.408314	0.463467	0.471253	0.459220	0.520974	0.559220	0.381730
18	24.060	0.420333	0.405385	0.460638	0.447222	0.461616	0.524845	0.561616	0.390645
19	25.040	0.388861	0.410967	0.475721	0.450958	0.474949	0.535134	0.574949	0.398585
20	26.030	0.413050	0.421684	0.462301	0.422332	0.478165	0.529042	0.578165	0.391491
21	27.010	0.404556	0.391056	0.478702	0.404843	0.490881	0.515816	0.590881	0.397005
22	28.000	0.421612	0.387481	0.488067	0.404587	0.487760	0.521729	0.587760	0.399458
23	28.980	0.429310	0.410217	0.489808	0.403569	0.491672	0.516213	0.591672	0.398253

- Click on analyse, select XY analysis, click Nonlinear regression>exponential>One-phase association. Click OK
- A table with various values of interest should appear on the left hand-side of Prism, while the recovery graph is in the ‘’Graphs’’ panel.

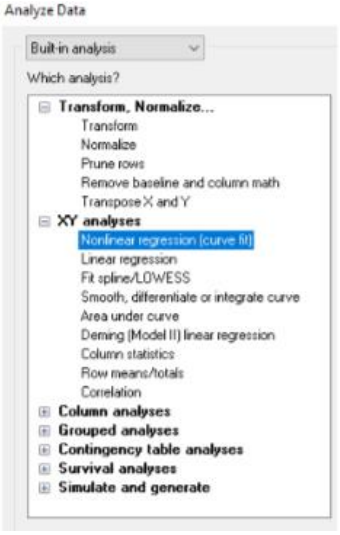

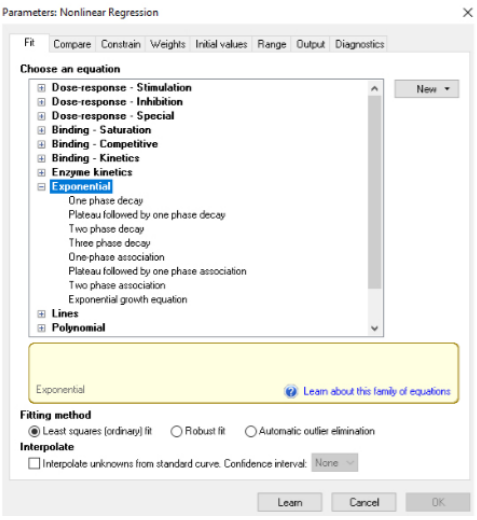

Appendix 2 Movies[19]

Movie 1

PI4KIIa-FRAP#2.wmv

PI4KIIa-FRAP#2.wmv

Movie 2

PI4KIIb-FRAP#4.wmv

PI4KIIb-FRAP#4.wmv

Movie 3

NT-FRAP#3.wmv

NT-FRAP#3.wmv

[19] Movies can be accessed on the CD-ROM attached with the hard copy.

Appendix 3 Phorbol 12-acetate 13-myristate (PMA) induces invadopodia formation in HeLa cells.

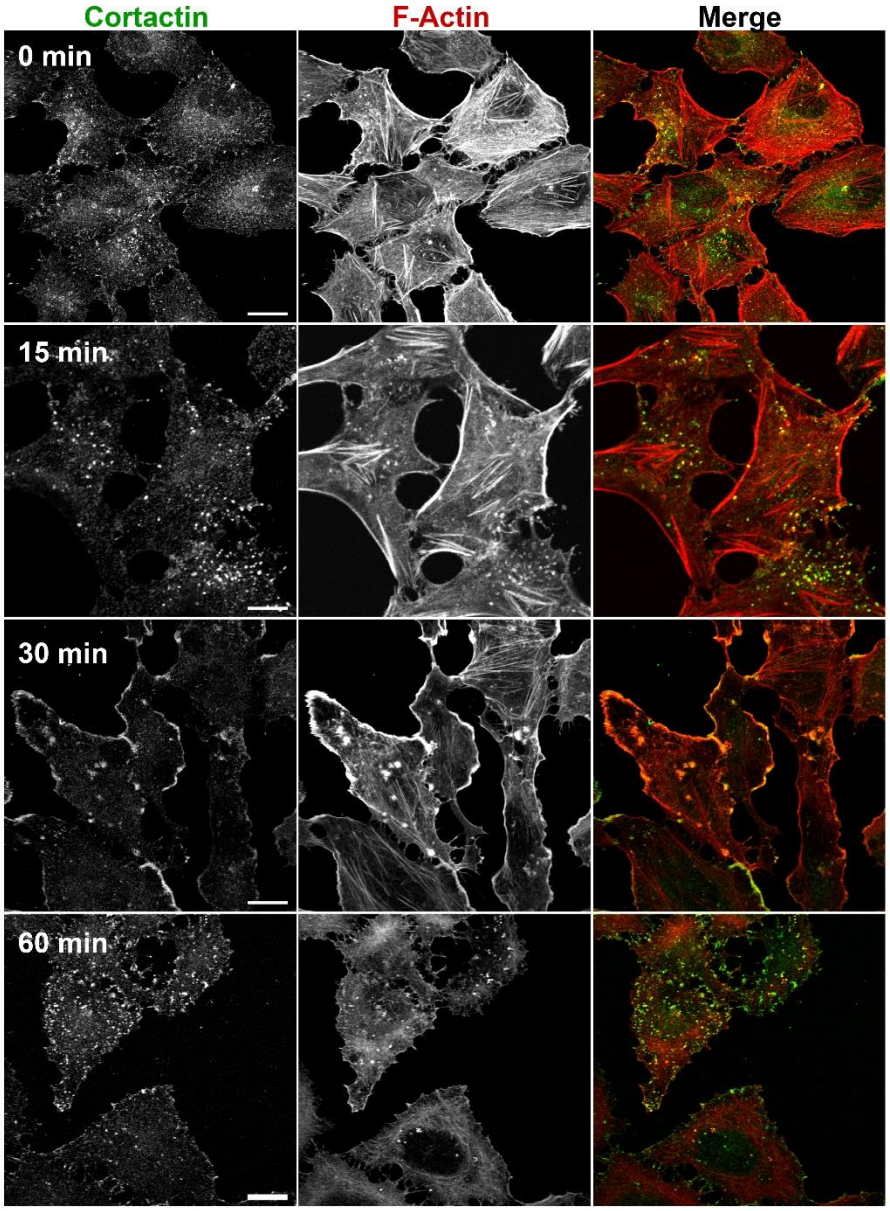

Figure A 2. PMA induces invadopodia formation in HeLa cells.

HeLa cells were treated with 50 ng/ml PMA for indicated times to induce the formation of invadopodia. Prior to treatment (0 min), stress fibres prominent in cells. However, 15-minute incubation with PMA, led to a decrease in cortical actin at the plasma membrane at the expense of cytoplasmic actin rich puncta that colocalised with invadopodia protein, cortactin. 30-minute treatment with PMA resulted in the formation of rosettes that showed co-immunostaining of F-actin and cortactin while these structures (individual invadopodia or rosettes) were almost completely

invisible after 60-minute PMA treatment; indicating a short half-life for these structures. The 15-minute timepoint served as the reference phenotype for invadopodia formation in siRNA treated cells.

Appendix 4 Publications

The following publication arose from the data presented in Chapters 3 and 5 and is appended at the back of this thesis:

Ganiyu, O. Alli-Balogun, Christina A. Gewinner, Ruth Jacobs, Janos Kriston-Vizi, Mark G. Waugh and Shane Minogue (2016). Phosphatidylinositol 4-kinase II β negatively regulates invadopodia formation and suppresses an invasive cellular phenotype. *Molecular biology of the cell*, 27(3), pp.4033–4042.

Other data from this thesis are included in manuscripts that are in preparation.

References

Agranoff, B. W. (2009). Turtles all the way: Reflections on myo-inositol. J. Biol. Chem. *284*, 21121–21126.

Alli-Balogun, G. O., Gewinner, C. A., Jacobs, R., Kriston-vizi, J., and Minogue, S. (2016). Phosphatidylinositol 4-kinase IIβ negatively regulates invadopodia formation and suppresses an invasive cellular phenotype. Mol. Biol. Cell *27*, 4033–4042.

Amatruda, J. F., Gattermeir, D. J., Karpova, T. S., and Cooper, J. A. (1992). Effects of null mutations and overexpression of capping protein on morphogenesis, actin distribution and polarized secretion in yeast. J. Cell Biol. *119*, 1151–1162.

Anderson, R. A., Boronenkov, I. V., Doughman, S. D., Kunz, J., and Loijens, J. C. (1999). Phosphatidylinositol phosphate kinases, a multifaceted family of signaling enzymes. J. Biol. Chem. *274*, 9907–9910.

Anitei, M. *et al.* (2014). A high-throughput siRNA screen identifies genes that regulate mannose 6-phosphate receptor trafficking. J. Cell Sci. *127*, 5079–5092.

Arighi, C. N., Harmell, L. M., Aguilar, R. C., Haft, C. R., and Bonifacino, J. S. (2004). Role of the mammalian retromer in sorting of the cation-independent mannose 6-phosphate receptor. J. Cell Biol. *165*, 123–133.

Audhya, A., Loewith, R., Parsons, A. B., Gao, L., Tabuchi, M., Zhou, H., Boone, C., Hall, M. N., and Emr, S. D. (2004). Genome-wide lethality screen identifies new PI4,5P_2 effectors that regulate the actin cytoskeleton. EMBO J. *23*, 3747–3757.

Auger, K. R., Serunian, L. A., Soltoff, S. P., Libby, P., Cantley, L. C., Whetton, A. D., Downes, P. C., and Cantley, L. (1989). PDGF-dependent tyrosine phosphorylation stimulates production of novel polyphosphoinositides in

intact cells. Cell *57*, 167–175.

Babst, M., Katzmann, D. J., Estepa-Sabal, E. J., Meerloo, T., and Emr, S. D. (2002a). Escrt-III: An Endosome-Associated Heterooligomeric Protein Complex Required for MVB Sorting. Dev. Cell *3*, 271–282.

Babst, M., Katzmann, D. J., Snyder, W. B., Wendland, B., and Emr, S. D. (2002b). Endosome-associated complex, ESCRT-II, recruits transport machinery for protein sorting at the multivesicular body. Dev. Cell *3*, 283–289.

Backer, J. M., Myers, M. G., Shoelson, S. E., Chin, D. J., Sun, X. J., Miralpeix, M., Hu, P., Margolis, B., Skolnik, E. Y., and Schlessinger, J. (1992). Phosphatidylinositol 3'-kinase is activated by association with IRS-1 during insulin stimulation. EMBO J. *11*, 3469–3479.

Balla, A., and Balla, T. (2006). Phosphatidylinositol 4-kinases: old enzymes with emerging functions. Trends Cell Biol. *16*, 351–361.

Balla, A., Tuymetova, G., Barshishat, M., Geiszt, M., and Balla, T. (2002). Characterization of type II phosphatidylinositol 4-kinase isoforms reveals association of the enzymes with endosomal vesicular compartments. J. Biol. Chem. *277*, 20041–20050.

Balla, A., Tuymetova, G., Toth, B., Szentpetery, Z., Zhao, X., Knight, Z. A., Shokat, K., Steinbach, P. J., and Balla, T. (2008). Design of drug-resistant alleles of type-III phosphatidylinositol 4-kinases using mutagenesis and molecular modeling. Biochemistry *47*, 1599–1607.

Balla, T. (2006). Phosphoinositide-derived messengers in endocrine signaling. J. Endocrinol. *188*, 135–153.

Balla, T. (2013). Phosphoinositides: tiny lipids with giant impact on cell regulation. Physiol. Rev. *93*, 1019–1137.

Balla, T., Downing, G. J., Jaffe, H., Kim, S., Zolyomi, a., and Catt, K. J. (1997). Isolation and Molecular Cloning of Wortmannin-sensitive Bovine Type III Phosphatidylinositol 4-Kinases. J. Biol. Chem. *272*, 18358–18366.

Ballas, L. M., and Bell, R. M. (1981). Topography of Glycerolipid Synthetic Enzymes. Biochim. Biophys. Acta *665*, 586–595.

Ballou, C. E., and Lee, Y. C. (1964). The structure of a Myoinositol mannoside from Mycobacterium tuberculosis glycolipid. Biochemistry *3*, 682–685.

Barylko, B., Gerber, S. H., Binns, D. D., Grichine, N., Khvotchev, M., Südhof, T. C., and Albanesi, J. P. (2001). A novel family of phosphatidylinositol 4-kinases conserved from yeast to humans. J. Biol. Chem. *276*, 7705–7708.

Barylko, B., Mao, Y. S., Wlodarski, P., Jung, G., Binns, D. D., Sun, H.-Q., Yin, H. L., and Albanesi, J. P. (2009). Palmitoylation controls the catalytic activity and subcellular distribution of phosphatidylinositol 4-kinase IIα. J. Biol. Chem. *284*, 9994–10003.

Baumeister, M. A., Martinu, L., Rossman, K. L., Sondek, J., Lemmon, M. A., and Chou, M. M. (2003). Loss of phosphatidylinositol 3-phosphate binding by the C-terminal Tiam-1 pleckstrin homology domain prevents in vivo Rac1 activation without affecting membrane targeting. J. Biol. Chem. *278*, 11457–11464.

Baumlova, A. *et al.* (2014). The crystal structure of the phosphatidylinositol 4 -kinase IIα. EMBO Rep. *15*, 1085–1093.

Bazenet, C. E., Ruano, A. R., Brockman, J. L., and Anderson, R. A. (1990). The human erythrocyte contains two forms of phosphatidylinositol-4-phosphate 5-kinase which are differentially active toward membranes. J. Biol. Chem. *265*, 18012–18022.

Benjamins, J. ., and Agranoff, B. W. (1969). Distribution and Properties of CDP-Diglyceride: Inositol Transferase from Brain. J. Neurochem. *16*, 513–

527.

Berditchevski, F., Tolias, K. F., Wong, K., Carpenter, C. L., and Hemler, M. E. (1997). A Novel Link between Integrins, Transmembrane-4 Superfamily Proteins (CD63 and CD81), and Phosphatidylinositol 4-Kinase. J. Biol. Chem. *272*, 2595–2598.

Berger, K. L., Kelly, S. M., Jordan, T. X., Tartell, M. A., and Randall, G. (2011). Hepatitis C virus stimulates the phosphatidylinositol 4-kinase III alpha-dependent phosphatidylinositol 4-phosphate production that is essential for its replication. J. Virol. *85*, 8870–8883.

Blangy, A., Touaitahuata, H., Cres, G., and Pawlak, G. (2012). Cofilin activation during podosome belt formation in osteoclasts. PLoS One *7*, e45909.

Blondeau, F., Laporte, J., Bodin, S., Superti-Furga, G., Payrastre, B., and Mandel, J.-L. (2000). Myotubularin, a phosphatase deficient in myotubular myopathy, acts on phosphatidylinositol 3-kinase and phosphatidylinositol 3-phosphate pathway. Hum. Mol. Genet. *9*, 2223–2229.

Bojjireddy, N. *et al.* (2014). Pharmacological and genetic targeting of the PI4KA enzyme reveals its important role in maintaining plasma membrane phosphatidylinositol 4-phosphate and phosphatidylinositol 4,5-bisphosphate levels. J. Biol. Chem. *289*, 6120–6132.

Bökenkamp, A., and Ludwig, M. (2016). The oculocerebrorenal syndrome of Lowe: an update. Pediatr. Nephrol. *31*, 2201–2212.

Bolte, S., and Cordelières, F. P. (2006). A guided tour into subcellular colocalization analysis in light microscopy. J. Microsc. *224*, 213–232.

Bonangelino, C. J., Nau, J. J., Duex, J. E., Brinkman, M., Wurmser, A. E., Gary, J. D., Emr, S. D., and Weisman, L. S. (2002). Osmotic stress-induced increase of phosphatidylinositol 3,5-bisphosphate requires Vac14p, an

activator of the lipid kinase Fab1p. J. Cell Biol. *156*, 1015–1028.

Boronenkov, I. V., and Anderson, R. A. (1995). The sequence of phosphatidylinositol-4-phosphate 5-kinase defines a novel family of lipid kinases. J. Biol. Chem. *270*, 2881–2884.

Botelho, R. J., Efe, J. A., Teis, D., and Emr, S. D. (2009). Assembly of a Fab1 Phosphoinositide Kinase Signaling Complex Requires the Fig4 Phosphoinositide Phosphatase. Mol. Biol. Cell *82*, 327–331.

Bowden, E. T., Barth, M., Thomas, D., Glazer, R. I., and Mueller, S. C. (1999). An invasion-related complex of cortactin, paxillin and PKCμ associates with invadopodia at sites of extracellular matrix degradation. Oncogene *18*, 4440–4449.

Bowden, E. T., Coopman, P. J., and Mueller, S. C. (2001). Invadopodia : Unique Methods for Measurement of Extracellular Matrix Degradation in Vitro. Methods Cell Biol. *63*, 613–627.

Braccini, L. *et al.* (2015). PI3K-C2γ is a Rab5 effector selectively controlling endosomal Akt2 activation downstream of insulin signalling. Nat. Commun. *6*, 7400.

Bravo-Cordero, J. J. *et al.* (2016). A novel high-content analysis tool reveals Rab8-driven cytoskeletal reorganization through Rho GTPases, calpain and MT1-MMP. J. Cell Sci. *129*, 1734–1749.

Bravo-Cordero, J. J., Marrero-Diaz, R., Megías, D., Genís, L., García-Grande, A., García, M. a, Arroyo, A. G., and Montoya, M. C. (2007). MT1-MMP proinvasive activity is regulated by a novel Rab8-dependent exocytic pathway. EMBO J. *26*, 1499–1510.

Bultsma, Y., Keune, W.-J., and Divecha, N. (2010). PIP4Kβ interacts with and modulates nuclear localization of the high-activity PtdIns5 *P* -4-kinase isoform PIP4Kα. Biochem. J. *430*, 223–235.

Burgess, J., Del Bel, L. M., Ma, C.-I. J., Barylko, B., Polevoy, G., Rollins, J., Albanesi, J. P., Krämer, H., and Brill, J. a (2012). Type II phosphatidylinositol 4-kinase regulates trafficking of secretory granule proteins in Drosophila. Development *139*, 3040–3050.

Byfield, M. P., Murray, J. T., and Backer, J. M. (2005). hVps34 Is a Nutrient-regulated Lipid Kinase Required for Activation of p70 S6 Kinase. J. Biol. Chem. *280*, 33076–33082.

Carlton, J. G., and Cullen, P. J. (2005). Coincidence detection in phosphoinositide signaling. Trends Cell Biol. *15*, 540–547.

Cerami, E. *et al.* (2012). The cBio Cancer Genomics Portal: An Open Platform for Exploring Multidimensional Cancer Genomics Data. Cancer Discov. *2*, 401 LP-404.

Ceresa, B. P., and Bahr, S. J. (2006). Rab7 Activity Affects Epidermal Growth Factor:Epidermal Growth Factor Receptor Degradation By Regulating Endocytic Trafficking From the Late Endosome. J. Biol. Chem. *281*, 1099–1106.

Chen, Y.-G., Wang, Z., Ma, J., Zhang, L., and Lu, Z. (2007). Endofin, a FYVE domain protein, interacts with Smad4 and facilitates transforming growth factor-beta signaling. J. Biol. Chem. *282*, 9688–9695.

Chi, S., Cao, H., Chen, J., and McNiven, M. A. (2008). Eps15 Mediates Vesicle Trafficking from the trans-Golgi Network via an Interaction with the Clathrin Adaptor AP-1. Mol. Biol. Cell *19*, 3564–3575.

Chi, S., Cao, H., Wang, Y., and McNiven, M. A. (2011). Recycling of the epidermal growth factor receptor is mediated by a novel form of the clathrin adaptor protein Eps15. J. Biol. Chem. *286*, 35196–35208.

Chowdhury, R., Diao, A., Zhang, F., Eisenberg, E., Lucocq, J., Johannes, L., Rabouille, C., Greene, L. E., and Lowe, M. (2005). Lowe Syndrome Protein

OCRL1 Interacts with Clathrin and Regulates Protein Trafficking between Endosomes and the Trans-Golgi Network. Mol. Biol. Cell *165*, 3467–3479.

Ciriello, G. *et al.* (2015). Comprehensive Molecular Portraits of Invasive Lobular Breast Cancer. Cell *163*, 506–519.

Clark, J., Anderson, K. E., Juvin, V., Smith, T. S., Karpe, F., Wakelam, M. J. O., Stephens, L. R., and Hawkins, P. T. (2011). Quantification of $PtdInsP_3$ molecular species in cells and tissues by mass spectrometry. Nat. Methods *8*, 267–272.

Clarke, J. H., Emson, P. C., and Irvine, R. F. (2008). Localization of phosphatidylinositol phosphate kinase IIγ in kidney to a membrane trafficking compartment within specialized cells of the nephron. Am. J. Physiol. Renal Physiol. *295*, F1422–F1430.

Clarke, J. H., Wang, M., and Irvine, R. F. (2010). Localization, regulation and function of Type II phosphatidylinositol 5-phosphate 4-kinases. Adv. Enzyme Regul. *50*, 12–18.

Coady, M. J., Wallendorff, B., Gagnon, D. G., and Lapointe, J. Y. (2002). Identification of a novel Na+/myo-inositol cotransporter. J. Biol. Chem. *277*, 35219–35224.

Conner, S. D., and Schmid, S. L. (2003). Differential requirements for AP-2 in clathrin-mediated endocytosis. J. Cell Biol. *162*, 773–779.

Cooke, F. T., Dove, S. K., McEwen, R. K., Painter, G., Holmes, a B., Hall, M. N., Michell, R. H., and Parker, P. J. (1998). The stress-activated phosphatidylinositol 3-phosphate 5-kinase Fab1p is essential for vacuole function in S. cerevisiae. Curr. Biol. *8*, 1219–1222.

Craige, B., Salazar, G., and Faundez, V. (2008). Phosphatidylinositol-4-Kinase Type II Alpha Contains an AP-3 – sorting Motif and a Kinase Domain That Are Both Required for Endosome Traffic. Mol. Biol. Cell *19*, 1415–1426.

Cremona, O. *et al.* (1999). Essential role of phosphoinositide metabolism in synaptic vesicle recycling. Cell *99*, 179–188.

Cullen, P., and Carlton, J. (2012). Phosphoinositides in the Mammalian Endo-lysosomal Network. In: Phosphoinositides II: The Diverse Biological Functions, ed. T. Balla, ed. M. Wymann, and ed. J. D. York, Springer Netherlands, 65–110.

Cullen, P. J., Cozier, G. E., Banting, G., and Mellor, H. (2001). Modular phosphoinositide-binding domains — their role in signalling and membrane trafficking. Curr. Biol. *11*, R882-93.

Damen, J. E., Liu, L., Rosten, P., Humphries, R. K., Jefferson, A. B., Majerus, P. W., and Krystal, G. (1996). The 145-kDa protein induced to associate with Shc by multiple cytokines is an inositol tetraphosphate and phosphatidylinositol 3,4,5-triphosphate 5-phosphatase. Proc. Natl. Acad. Sci. U. S. A. *93*, 1689–1693.

Dawson, R. M. . (1954). The measurement of ^{32}P labelling of individual kephalins and lecithin in a small sample of tissue. Biochim. Biophys. Acta *14*, 374–379.

Desrivières, S., Cooke, F. T., Parker, P. J., and Hall, M. N. (1998). MSS4, a phosphatidylinositol-4-phosphate 5-kinase required for organization of the actin cytoskeleton in Saccharomyces cerevisiae. J. Biol. Chem. *273*, 15787–15793.

Dickson, E. J., Jensen, J. B., and Hille, B. (2014). Golgi and plasma membrane pools of PI(4)P contribute to plasma membrane PI(4,5)P2 and maintenance of KCNQ2/3 ion channel current. Proc. Natl. Acad. Sci. U. S. A. *111*, E2281-90.

Dickson, E. J., Jensen, J. B., Vivas, O., Kruse, M., Traynor-Kaplan, A. E., and Hille, B. (2016). Dynamic formation of ER-PM junctions presents a lipid phosphatase to regulate phosphoinositides. J. Cell Biol. *213*, 33–48.

Dittmer, J. ., and Dawson, R. M. . (1961). The Isolation of a New Lipid , Triphosphoinositide , and Monophosphoinositide from Ox Brain. Biochem J *81*, 535–540.

Divecha, N., Truong, O., Hsuan, J. J., Hinchliffe, K. a, and Irvine, R. F. (1995). The cloning and sequence of the C isoform of PtdIns4P 5-kinase. Biochem. J. *309*, 715–719.

Dong, R. *et al.* (2016). Endosome-ER Contacts Control Actin Nucleation and Retromer Function through VAP-Dependent Regulation of PI4P. Cell *166*, 408–423.

Doughman, R. L., Firestone, A. J., and Anderson, R. A. (2003). Phosphatidylinositol phosphate kinases put PI4,5P_2 in its place. J. Membr. Biol. *194*, 77–89.

Dove, S. K., Cooke, F. T., Douglas, M. R., Sayers, L. G., Parker, P. J., and Michell, R. H. (1997). Osmotic stress activates phosphatidylinositol-3,5-bisphosphate synthesis. Nature *390*, 187–192.

Dove, S. K., McEwen, R. K., Mayes, A., Hughes, D. C., Beggs, J. D., and Michell, R. H. (2002). Vac14 controls PtdIns(3,5)P2 synthesis and Fab1-dependent protein trafficking to the multivesicular body. Curr. Biol. *12*, 885–893.

Dowler, S., Currie, R. A., Campbell, D. G., Deak, M., Kular, G., Downes, C. P., and Alessi, D. R. (2000). Identification of pleckstrin-homology-domain-containing proteins with novel phosphoinositide-binding specificities. Biochem. J. *351*, 19.

Dumas, J. J., Merithew, E., Sudharshan, E., Rajamani, D., Hayes, S., Lawe, D., Corvera, S., and Lambright, D. G. (2001). Multivalent endosome targeting by homodimeric EEA1. Mol. Cell *8*, 947–958.

Dyson, J. M., Fedele, C. G., Davies, E. M., Becanovic, J., and Mitchell, C. A.

(2012). Phosphoinositide Phosphatases: Just as Important as the Kinases. In: Phosphoinositides I: Enzymes of Synthesis and Degradation, ed. T. Balla, ed. M. Wymann, and ed. J. D. York, Dordrecht: Springer Netherlands, 215–279.

Egeblad, M., and Werb, Z. (2002). New functions for the matrix metalloproteinases in cancer progression. Nat Rev Cancer *2*, 161–174.

Elde, N. C., Morgan, G., Winey, M., Sperling, L., and Turkewitz, A. P. (2005). Elucidation of clathrin-mediated endocytosis in tetrahymena reveals an evolutionarily convergent recruitment of dynamin. PLoS Genet. *1*.

Ewald, A. J. (2015). An Arresting Story about Basement Membrane Invasion. Dev. Cell *35*, 143–144.

Falasca, M., Hughes, W. E., Dominguez, V., Sala, G., Fostira, F., Fang, M. Q., Cazzolli, R., Shepherd, P. R., James, D. E., and Maffucci, T. (2007). The role of phosphoinositide 3-kinase C2α in insulin signaling. J. Biol. Chem. *282*, 28226–28236.

Faucherre, A., Desbois, P., Nagano, F., Satre, V., Lunardi, J., Gacon, G., and Dorseuil, O. (2005). Lowe syndrome protein Ocrl1 is translocated to membrane ruffles upon Rac GTPase activation: A new perspective on Lowe syndrome pathophysiology. Hum. Mol. Genet. *14*, 1441–1448.

Fischer, A. H., Jacobson, K. A., Rose, J., and Zeller, R. (2008). Preparation of slides and coverslips for microscopy. Cold Spring Harb. Protoc. *3*, 10–13.

Flynn, D. C., Cho, Y., Vincent, D., and Cunnick, J. M. (2008). Podosomes and Invadopodia: Related structures with Common Protein Components that May Promote Breast Cancer Cellular Invasion. Breast Cancer (Auckl). *2*, 17–29.

Fortian, A., and Sorkin, A. (2014). Live-cell fluorescence imaging reveals high stoichiometry of Grb2 binding to the EGF receptor sustained during

endocytosis. J. Cell Sci. *127*, 432–444.

Gálvez, B. G., Matías-Román, S., Yáñez-Mó, M., Vicente-Manzanares, M., Sánchez-Madrid, F., and Arroyo, A. G. (2004). Caveolae are a novel pathway for membrane-type 1 matrix metalloproteinase traffic in human endothelial cells. Mol. Biol. Cell *15*, 678–687.

Gao, J. *et al.* (2013). Integrative Analysis of Complex Cancer Genomics and Clinical Profiles Using the cBioPortal. Sci. Signal. *6*, pl1.

Gary, J. D., Wurmser, A. E., Bonangelino, C. J., Weisman, L. S., and Emr, S. D. (1998). Fablp Is Essential for PtdIns (3) P 5-Kinase Activity and the Homeostasis of Vacuolar Size and Membrane Maintenance. J. Cell Biol. *143*, 65–79.

Gehrmann, T., Gulkan, H., Suer, S., Herberg, F. W., Balla, A., Vereb, G., Mayr, G. W., and Heilmeyer, L. M. G. (1999). Functional expression and characterisation of a new human phosphatidylinositol 4-kinase PI4K230. Biochim. Biophys. Acta - Mol. Cell Biol. Lipids *1437*, 341–356.

Gerber, P. P. *et al.* (2015). Rab27a controls HIV-1 assembly by regulating plasma membrane levels of phosphatidylinositol 4,5-bisphosphate. J. Cell Biol. *209*, 435–452.

Ghigo, A., Morello, F., Perino, A., and Hirsch, E. (2012). Phosphoinositide 3-Kinases in Health and Disease. In: Phosphoinositides I: Enzymes of Synthesis and Degradation, ed. T. Balla, ed. M. Wymann, and ed. J. D. York, Dordrecht: Springer Netherlands, 183–213.

Gillooly, D. J., Morrow, I. C., Lindsay, M., Gould, R., Bryant, N. J., Gaullier, J., Parton, R. G., and Stenmark, H. (2000). Localization of phosphatidylinositol 3-phosphate in yeast and mammalian cells. EMBO J. *19*, 4577 LP-4588.

Gimona, M., Buccione, R., Courtneidge, S. A., and Linder, S. (2008).

Assembly and biological role of podosomes and invadopodia. Curr. Opin. Cell Biol. *20*, 235–241.

Godi, A., Di Campli, A., Konstantakopoulos, A., Di Tullio, G., Alessi, D. R., Kular, G. S., Daniele, T., Marra, P., Lucocq, J. M., and De Matteis, M. A. (2004). FAPPs control Golgi-to-cell-surface membrane traffic by binding to ARF and PtdIns(4)P. Nat. Cell Biol. *6*, 393–404.

Griffioen, M., van der Meijden, E. D., Slager, E. H., Honders, M. W., Rutten, C. E., van Luxemburg-Heijs, S. a P., von dem Borne, P. a, van Rood, J. J., Willemze, R., and Falkenburg, J. H. F. (2008). Identification of phosphatidylinositol 4-kinase type IIβ as HLA class II-restricted target in graft versus leukemia reactivity. Proc. Natl. Acad. Sci. U. S. A. *105*, 3837–3842.

Guerriero, C. J., Lai, Y., and Weisz, O. A. (2008). Differential sorting and Golgi export requirements for raft-associated and raft-independent apical proteins along the biosynthetic pathway. J. Biol. Chem. *283*, 18040–18047.

Guillermet-Guibert, J., Bjorklof, K., Salpekar, A., Gonella, C., Ramadani, F., Bilancio, A., Meek, S., Smith, A. J. H., Okkenhaug, K., and Vanhaesebroeck, B. (2008). The p110 isoform of phosphoinositide 3-kinase signals downstream of G protein-coupled receptors and is functionally redundant with p110 . Proc. Natl. Acad. Sci. *105*, 8292–8297.

Guo, J., Wenk, M. R., Pellegrini, L., Onofri, F., Benfenati, F., and De Camilli, P. (2003). Phosphatidylinositol 4-kinase type IIα is responsible for the phosphatidylinositol 4-kinase activity associated with synaptic vesicles. Proc. Natl. Acad. Sci. U. S. A. *100*, 3995–4000.

Guo, S., Stolz, L. E., Lemrow, S. M., and York, J. D. (1999). SAC1-like domains of yeast SAC1, INP52, and INP53 and of human synaptojanin encode polyphosphoinositide phosphatases. J. Biol. Chem. *274*, 12990–12995.

Guo, Y., Sirkis, D. W., and Schekman, R. (2014). Protein sorting at the trans-

Golgi network. Annu. Rev. Cell Dev. Biol. *30*, 169–206.

Hammond, G. R. V, and Balla, T. (2014). A tail of new lipids. EMBO J., 1–2.

Hammond, G. R. V, Fischer, M. J., Anderson, K. E., Holdich, J., Koteci, A., Balla, T., and Irvine, R. F. (2012). PI4P and PI(4,5)P_2 are essential but independent lipid determinants of membrane identity. Science *337*, 727–730.

Hammond, G. R. V, Machner, M. P., and Balla, T. (2014). A novel probe for phosphatidylinositol 4-phosphate reveals multiple pools beyond the Golgi. J. Cell Biol. *205*, 113–126.

Hammond, G. R. V, Schiavo, G., and Irvine, R. F. (2009). Immunocytochemical techniques reveal multiple, distinct cellular pools of PtdIns4P and PtdIns(4,5)P_2. Biochem. J. *422*, 23–35.

Hanawa, M., Suzuki, S., Dobashi, Y., Yamane, T., Kono, K., Enomoto, N., and Ooi, A. (2006). EGFR protein overexpression and gene amplification in squamous cell carcinomas of the esophagus. Int. J. Cancer *118*, 1173–1180.

Hattula, K., Furuhjelm, J., Tikkanen, J., Tanhuanpaa, K., Laakkonen, P., and Peranen, J. (2006). Characterization of the Rab8-specific membrane traffic route linked to protrusion formation. J. Cell Sci. *119*, 4866–4877.

Hawthorne, J. N. (1955). The ethanol-insoluble phosphatides of mammalian liver. Biochem. J. *59*, 2.

Henmi, Y., Morikawa, Y., Oe, N., Ikeda, N., Fujita, A., Takei, K., Minogue, S., and Tanabe, K. (2016). PtdIns4KIIα generates endosomal PtdIns(4)P.pdf. Mol. Biol. Cell *27*, 990–1001.

Heo, W. Do, Inoue, T., Park, W. S., Kim, M. L., Park, B. O., Wandless, T. J., and Meyer, T. (2006). PI(3,4,5)P3 and PI(4,5)P2 Lipids Target Proteins with Polybasic Clusters to the Plasma Membrane. Science (80-.). *314*, 1458–1461.

Herbst, R. S., and Bunn, P. A. (2003). Targeting the Epidermal Growth Factor Receptor in Non-Small Cell Lung Cancer. Clin. Cancer Res. *9*, 5813–5824.

Herman, P. K., and Emr, S. D. (1990). Characterization of VPS34, a gene required for vacuolar protein sorting and vacuole segregation in Saccharomyces cerevisiae. Mol. Cell. Biol. *10*, 6742–6754.

Hilbi, H., Weber, S., and Finsel, I. (2011). Anchors for effectors: Subversion of phosphoinositide lipids by Legionella. Front. Microbiol. *2*, 1–8.

Hiles, I. D. *et al.* (1992). Phosphatidylinositol 3-kinase: Structure and expression of the 110 kd catalytic subunit. Cell *70*, 419–429.

Hill, E., Van Der Kaay, J., Downes, C. P., and Smythe, E. (2001). The role of dynamin and its binding partners in coated pit invagination and scission. J. Cell Biol. *152*, 309–323.

Hogan, C. *et al.* (2009). Characterization of the interface between normal and transformed epithelial cells. Nat. Cell Biol. *11*, 460–467.

Hokin, L. E. (1987). The road to the phosphoinositide-generated second messengers. Trends Pharmacol. Sci. *8*, 53–56.

Holub, B. J. (1982). The nutritional significance, metabolism, and function of myo-inositol and phosphatidylinositol in health and disease. Adv. Nutr. Res. *4*, 107–141.

Homma, K., Terui, S., Minemurall, M., Qadota, H., Anraku, Y., Kanaho, Y., and Ohya, Y. (1998). Phosphatidylinositol-4-phosphate 5-kinase localized on the plasma membrane is essential for yeast cell morphogenesis. J. Biol. Chem. *273*, 15779–15786.

Hoshino, D., Branch, K. M., and Weaver, A. M. (2013a). Signaling inputs to invadopodia and podosomes. J. Cell Sci. *126*, 2979–2989.

Hoshino, D., Kirkbride, K., Costello, K., Clark, E., Sinha, S., Grega-Larson, N., Tyska, M., and Weaver, A. (2013b). Exosome secretion is enhanced by invadopodia and drives invasive behavior. Cell Rep. *5*, 1159–1168.

Hoshino, D., Koshikawa, N., Suzuki, T., Quaranta, V., Weaver, A. M., Seiki, M., and Ichikawa, K. (2012). Establishment and validation of computational model for MT1-MMP dependent ECM degradation and intervention strategies. PLoS Comput. Biol. *8*, 1–10.

Hoshino, D., Nagano, M., Saitoh, A., Koshikawa, N., Suzuki, T., and Seiki, M. (2013c). The Phosphoinositide-Binding Protein ZF21 Regulates ECM Degradation by Invadopodia. PLoS One *8*, 1–8.

Houlihan, L. M., Christoforou, A., Arbuckle, M. I., Torrance, H. S., Anderson, S. M., Muir, W. J., Porteous, D. J., Blackwood, D. H., and Evans, K. L. (2009). A case-control association study and family-based expression analysis of the bipolar disorder candidate gene PI4K2B. J. Psychiatr. Res. *43*, 1272–1277.

Hsu, V. W., Bai, M., and Li, J. (2012). Getting active: protein sorting in endocytic recycling. Nat. Rev. Mol. Cell Biol. *13*, 323–328.

Huveneers, S., and Danen, E. H. J. (2009). Adhesion signaling - crosstalk between integrins, Src and Rho. J. Cell Sci. *122*, 1059–1069.

Ikonomov, O. C., Sbrissa, D., Fligger, J., Delvecchio, K., and Shisheva, A. (2010). ArPIKfyve regulates Sac3 protein abundance and turnover disruption of the mechanism by Sac3I41T mutation causing charcot-marie-tooth 4J disorder. J. Biol. Chem. *285*, 26760–26764.

Ikonomov, O. C., Sbrissa, D., Ijuin, T., Takenawa, T., and Shisheva, A. (2009). Sac3 Is an Insulin-regulated Phosphatidylinositol 3,5-bisphosphate phosphatase. Gain in insulin responsiveness through Sac3 down-regulation in adipocytes. J. Biol. Chem. *284*, 23961–23971.

Irvine, R. F. (2003). 20 years of Ins(1,4,5)P3, and 40 years before. Nat Rev

Mol Cell Biol *4*, 586–590.

Ishihara, H., Sasaoka, T., Hori, H., Wada, T., Hirai, H., Haruta, T., Langlois, W. J., and Kobayashi, M. (1999). Molecular Cloning of Rat SH2-Containing Inositol Phosphatase 2 (SHIP2) and Its Role in the Regulation of Insulin Signaling. Biochem. Biophys. Res. Commun. *260*, 265–272.

Itoh, T., Ijuin, T., and Takenawa, T. (1998). A novel phosphatidylinositol-5-phosphate 4-kinase (phosphatidylinositol- phosphate kinase IIγ) is phosphorylated in the endoplasmic reticulum in response to mitogenic signals. J. Biol. Chem. *273*, 20292–20299.

Itoh, Y., and Seiki, M. (2006). MT1-MMP: A potent modifier of pericellular microenvironment. J. Cell. Physiol. *206*, 1–8.

Ivaska, J., Vuoriluoto, K., Huovinen, T., Izawa, I., Inagaki, M., and Parker, P. J. (2005). PKCε-mediated phosphorylation of vimentin controls integrin recycling and motility. EMBO J. *24*, 3834–3845.

Jeschke, A. *et al.* (2015). Phosphatidylinositol 4-phosphate and phosphatidylinositol 3-phosphate regulate phagolysosome biogenesis. Proc. Natl. Acad. Sci. *112*, 201423456.

Jin, N. *et al.* (2008). VAC14 nucleates a protein complex essential for the acute interconversion of PI3P and PI(3,5)P_2 in yeast and mouse. EMBO J. *27*, 3221–3234.

Joffre, C., Barrow, R., Ménard, L., Calleja, V., Hart, I. R., and Kermorgant, S. (2011). A direct role for Met endocytosis in tumorigenesis. Nat. Cell Biol. *13*, 827–837.

Jović, M., Kean, M. J., Dubankova, A., Boura, E., Gingras, A.-C., Brill, J. a, and Balla, T. (2014). Endosomal sorting of VAMP3 is regulated by PI4K2A. J. Cell Sci. *127*, 3745–3756.

Jović, M., Kean, M. J., Szentpetery, Z., Polevoy, G., Gingras, A.-C., Brill, J. a, and Balla, T. (2012). Two phosphatidylinositol 4-kinases control lysosomal delivery of the Gaucher disease enzyme, β-glucocerebrosidase. Mol. Biol. Cell *23*, 1533–1545.

Jung, G., Barylko, B., Lu, D., Shu, H., Yin, H., and Albanesi, J. P. (2011). Stabilization of phosphatidylinositol 4-kinase type IIβ by interaction with Hsp90. J. Biol. Chem. *286*, 12775–12784.

Jung, G., Wang, J., Wlodarski, P., Barylko, B., Binns, D. D., Shu, H., Yin, H. L., and Albanesi, J. P. (2008). Molecular determinants of activation and membrane targeting of phosphoinositol 4-kinase IIβ. Biochem. J. *409*, 501–509.

Kanai, F., Liu, H., Field, S. J., Akbary, H., Matsuo, T., Brown, G. E., Cantley, L. C., and Yaffe, M. B. (2001). The PX domains of p47phox and p40phox bind to lipid products of PI(3)K. Nat Cell Biol *3*, 675–678.

Kang, M. S. *et al.* (2013). Modulation of lipid kinase PI4KIIα activity and lipid raft association of presenilin 1 underlies γ-secretase inhibition by ginsenoside (20S)-Rg3. J. Biol. Chem. *288*, 20868–20882.

Katzmann, D. J., Babst, M., and Emr, S. D. (2001). Ubiquitin-Dependent Sorting into the Multivesicular Body Pathway Requires the Function of a Conserved Endosomal Protein Sorting Complex, ESCRT-I. Cell *106*, 145–155.

Kean, M. J., Williams, K. C., Skalski, M., Myers, D., Burtnik, A., Foster, D., and Coppolino, M. G. (2009). VAMP3, syntaxin-13 and SNAP23 are involved in secretion of matrix metalloproteinases, degradation of the extracellular matrix and cell invasion. J. Cell Sci. *122*, 4089–4098.

Ketel, K., Krauss, M., Nicot, A.-S., Puchkov, D., Wieffer, M., Müller, R., Subramanian, D., Schultz, C., Laporte, J., and Haucke, V. (2016). A phosphoinositide conversion mechanism for exit from endosomes. Nature.

Kihara, A., Noda, T., Ishihara, N., and Ohsumi, Y. (2001). Two Distinct Vps34 Phosphatidylinositol 3–Kinase Complexes Function in Autophagy and Carboxypeptidase Y Sorting in Saccharomyces cerevisiae. J. Cell Biol. *152*, 519–530.

Kim, S., Kim, H., Chang, B., Ahn, N., Hwang, S., Di Paolo, G., and Chang, S. (2006). Regulation of transferrin recycling kinetics by PtdIns[4,5]P2 availability. FASEB J. *20*, 2399–2401.

Kim, W. T., Chang, S., Daniell, L., Cremona, O., Di Paolo, G., and De Camilli, P. (2002). Delayed reentry of recycling vesicles into the fusion-competent synaptic vesicle pool in synaptojanin 1 knockout mice. Proc. Natl. Acad. Sci. U. S. A. *99*, 17143–17148.

Kim, Y. J., Guzman-Hernandez, M. L., and Balla, T. (2011). A highly dynamic ER-derived phosphatidylinositol-synthesizing organelle supplies phosphoinositides to cellular membranes. Dev. Cell *21*, 813–824.

Klarlund, J. K., Rameh, L. E., Cantley, L. C., Buxton, J. M., Holik, J. J., Sakelis, C., Patki, V., Corvera, S., and Czech, M. P. (1998). Regulation of GRP1-catalyzed by Phosphatidylinositol. J. Biol. Chem. *273*, 1859–1862.

Klein, D. E., Lee, A., Frank, D. W., Marks, M. S., and Lemmon, M. A. (1998). The pleckstrin homology domains of dynamin isoforms require oligomerization for high affinity phosphoinositide binding. J. Biol. Chem. *273*, 27725–27733.

Klima, M., Baumlova, A., Chalupska, D., and Hr, H. (2015). The high-resolution crystal structure of phosphatidylinositol 4-kinase IIβ and the crystal structure of phosphatidylinositol 4-kinase IIα containing a nucleoside analogue provide a structural basis for isoform-specific inhibitor design. Acta Cryst *D71*, 1555–1563.

Kucera, A., Distefano, M. B., Berg-Larsen, A., Skjeldal, F., Repnik, U., Bakke, O., and Progida, C. (2016). Spatio-temporal resolution of Rab9 and CI-MPR

dynamics in the endocytic pathway. Traffic *17*, 211–229.

Kwiatkowska, K. (2010). One lipid, multiple functions: How various pools of PI(4,5)P2 are created in the plasma membrane. Cell. Mol. Life Sci. *67*, 3927–3946.

Kwon, H. M., Yamauchi, A., Uchida, S., Preston, A. S., Garcia-perez, A., Burg, M. B., and Handleri, J. S. (1991). Cloning of the cDNa for a Na '/ myo-Inositol Cotransporter , a Hypertonicity Stress Protein *. *267*, 1–5.

Lamia, K. A., Peroni, O. D., Kim, Y., Rameh, L. E., Kahn, B. B., and Cantley, L. C. (2004). Increased Insulin Sensitivity and Reduced Adiposity in Phosphatidylinositol 5-Phosphate 4-Kinase β-/- Mice. Mol. Cell. Biol. *24*, 5080–5087.

Lane, J., Martin, T., Weeks, H. P., Jiang, W. G., Building, H. W., and Park, H. (2014). Structure and Role of WASP and WAVE in Rho GTPase Signalling in Cancer. Cancer Genomics Proteomics *11*, 155–165.

Laporte, J., Hu, L. J., Kretz, C., Mandel, J.-L., Kioschis, P., Coy, J. F., Klauck, S. M., Poustka, A., and Dahl, N. (1996). A gene mutated in X–linked myotubular myopathy defines a new putative tyrosine phosphatase family conserved in yeast. Nat. Genet. *13*, 175–182.

de Lartigue, J., Polson, H., Feldman, M., Shokat, K., Tooze, S. a., Urbé, S., and Clague, M. J. (2009). PIKfyve Regulation of Endosome-Linked Pathways. Traffic *10*, 883–893.

Lawe, D. C., Patki, V., Heller-Harrison, R., Lambright, D., and Corvera, S. (2000). The FYVE Domain of Early Endosome Antigen 1 Is Required for Both Phosphatidylinositol 3-Phosphate and Rab5 Binding: Critical role of this dual interaction for endosomal localisation. J. Biol. Chem. *275*, 3699–3705.

Leibiger, B., Moede, T., Uhles, S., Barker, C. J., Creveaux, M., Domin, J., Berggren, P.-O., and Leibiger, I. B. (2010). Insulin-feedback via PI3K-C2α

activated PKBα/Akt1 is required for glucose-stimulated insulin secretion. FASEB J. *24*, 1824–1837.

Levin, R., Hammond, G. R. V., Balla, T., De Camilli, P., Fairn, G. D., and Grinstein, S. (2017). Multiphasic dynamics of phosphatidylinositol 4-phosphate during phagocytosis. Mol. Biol. Cell *28*, 128–140.

Li, J., Barylko, B., Johnson, J., Mueller, J. D., Albanesi, J. P., and Chen, Y. (2012). Molecular brightness analysis reveals phosphatidylinositol 4-kinase IIβ association with clathrin-coated vesicles in living cells. Biophys. J. *103*, 1657–1665.

Li, J., Lu, Y., Zhang, J., Kang, H., Qin, Z., and Chen, C. (2010). PI4KIIα is a novel regulator of tumor growth by its action on angiogenesis and HIF-1α regulation. Oncogene *29*, 2550–2559.

Li, J., Zhang, L., Gao, Z., Kang, H., Rong, G., Zhang, X., and Chen, C. (2014). Dual inhibition of EGFR at protein and activity level via combinatorial blocking of PI4KIIα as anti-tumor strategy. Protein Cell *5*, 457–468.

Lioubin, M. N., Algate, P. A., Tsai, S., Carlberg, K., Aebersold, R., and Rohrschneider, L. R. (1996). p 150 Ship , a signal transduction molecule with inositol polyphosphate-5- phosphatase activity. Genes Dev., 1084–1095.

Liu, Q., Sasaki, T., Kozieradzki, I., Wakeham, A., Itie, A., Dumont, D. J., and Penninger, J. M. (1999). SHIP is a negative regulator of growth factor receptor-mediated PKB / Akt activation and myeloid cell survival SHIP is a negative regulator of growth factor receptor-mediated PKB / Akt activation and myeloid cell survival. Genes Dev. *13*, 786–791.

Liu, Y., and Bankaitis, V. A. (2010). Phosphoinositide phosphatases in cell biology and disease. Prog. Lipid Res. *49*, 201–217.

Loijens, J. C., and Anderson, R. A. (1996). Type I phosphatidylinositol-4-phosphate 5-kinases are distinct members of this novel lipid kinase family. J.

Biol. Chem. *271*, 32937–32943.

Loijens, J. C., Boronenkov, I. V., Parker, G. J., and Anderson, R. A. (1996). The phosphatidylinositol 4-phosphate 5-kinase family. Adv. Enzyme Regul. *36*, 115–140.

Lopes da Silva, M., O'Connor, M. N., Kriston-Vizi, J., White, I. J., Al-Shawi, R., Simons, J. P., Mossinger, J., Haucke, V., and Cutler, D. F. (2016). Type II PI4-kinases control Weibel-Palade body biogenesis and von Willebrand factor structure in human endothelial cells. J. Cell Sci. *129*, 2096–2105.

López, F., Llorente, J. L., Oviedo, C. M., Vivanco, B., Marcos, C. Á., García-Inclán, C., Scola, B., and Hermsen, M. a (2012). Gene amplification and protein overexpression of EGFR and ERBB2 in sinonasal squamous cell carcinoma. Cancer *118*, 1818–1826.

Loskutov, Y. V, Kozyulina, P. Y., Kozyreva, V. K., Ice, R. J., Jones, B. C., Roston, T. J., Smolkin, M. B., Ivanov, a V, Wysolmerski, R. B., and Pugacheva, E. N. (2014). NEDD9/Arf6-dependent endocytic trafficking of matrix metalloproteinase 14: a novel mechanism for blocking mesenchymal cell invasion and metastasis of breast cancer. Oncogene, 1–14.

Lung, M., Shulga, Y. V., Ivanova, P. T., Myers, D. S., Milne, S. B., Brown, H. A., Topham, M. K., and Epand, R. M. (2009). Diacylglycerol kinase ε is selective for both acyl chains of phosphatidic acid or diacylglycerol. J. Biol. Chem. *284*, 31062–31073.

Luo, X., Wasilko, D. J., Liu, Y., Sun, J., Wu, X., Luo, Z.-Q., and Mao, Y. (2015). Structure of the Legionella Virulence Factor, SidC Reveals a Unique PI(4)P-Specific Binding Domain Essential for Its Targeting to the Bacterial Phagosome. PLOS Pathog. *11*, e1004965.

Macpherson, I. R. *et al.* (2014). CLIC3 controls recycling of late endosomal MT1-MMP and dictates invasion and metastasis in breast cancer. J. Cell Sci. *127*, 3893–3901.

Maehama, T., and Dixon, J. E. (1998). The Tumor Suppressor, PTEN/ MMAC1, Dephosphorylates the Lipid Second Messenger, Phosphatidylinositol 3,4,5-Trisphosphate. J. Biol. Chem. *273*, 13375–13378.

Malliri, A., Klooster, J. P., Olivo, C., and Collard, J. G. (2002). Determination of the Activity of Rho-Like GTPases in Cells. In: GTPase Protocols: The Ras Superfamily, ed. E. J. Manser, and ed. T. Leung, Totowa, New Jersey: Humana Press, 99–109.

Marat, A. L., Wallroth, A., Lo, W.-T., Müller, R., Norata, G. D., Falasca, M., Schultz, C., and Haucke, V. (2017). mTORC1 activity repression by late endosomal phosphatidylinositol 3,4-bisphosphate. Science (80-.). *356*, 968–972.

Marchesin, V., Montagnac, G., and Chavrier, P. (2015). ARF6 promotes the formation of Rac1 and WAVE-dependent ventral F-Actin rosettes in breast cancer cells in response to epidermal growth factor. PLoS One *10*, 1–19.

Marquer, C., Tian, H., Yi, J., Bastien, J., Dall'Armi, C., Yang-Klingler, Y., Zhou, B., Chan, R. B., and Di Paolo, G. (2016). Arf6 controls retromer traffic and intracellular cholesterol distribution via a phosphoinositide-based mechanism. Nat. Commun. *7*, 11919.

Marshall, A. J., Krahn, A. K., Ma, K., Duronio, V., and Hou, S. (2002). TAPP1 and TAPP2 are targets of phosphatidylinositol 3-kinase signaling in B cells: sustained plasma membrane recruitment triggered by the B-cell antigen receptor. Mol. Cell. Biol. *22*, 5479–5491.

Maxfield, F., and McGraw, T. (2004). Endocytic recycling. Nat. Rev. Mol. Cell Biol. *5*, 121–132.

Mazzocca, A., Liotta, F., and Carloni, V. (2008). Tetraspanin CD81-regulated cell motility plays a critical role in intrahepatic metastasis of hepatocellular carcinoma. Gastroenterology *135*, 244–256.e1.

McDermott, M. I., and Mousley, C. J. (2016). Lipid transfer proteins and the tuning of compartmental identity in the Golgi apparatus. Chem. Phys. Lipids *200*, 42–61.

Michell, R. H., Harwoot, J. L., Coleman, R., and Hawthorne, J. N. (1967). Characteristics of Rat Liver Phosphatidylinositol Kinase and its presence in the plasma membrane. Biochim. Biophys. Acta *144*, 649–658.

Milne, S. B., Ivanova, P. T., Armstrong, M. D., Myers, D. S., Lubarda, J., Shulga, Y. V., Topham, M. K., Brown, H. A., and Epand, R. M. (2008). Dramatic differences in the roles in lipid metabolism of two isoforms of diacylglycerol kinase. Biochemistry *47*, 9372–9379.

Minogue, S., Anderson, J. S., Waugh, M. G., Dos Santos, M., Corless, S., Cramer, R., and Hsuan, J. J. (2001). Cloning of a Human Type II Phosphatidylinositol 4-Kinase Reveals a Novel Lipid Kinase Family. J. Biol. Chem. *276*, 16635–16640.

Minogue, S., Chu, K. M. E., Westover, E. J., Covey, D. F., Hsuan, J. J., and Waugh, M. G. (2010). Relationship between phosphatidylinositol 4-phosphate synthesis, membrane organization, and lateral diffusion of PI4KIIα at the trans-Golgi network. J. Lipid Res. *51*, 2314–2324.

Minogue, S., and Waugh, M. G. (2012). The Phosphatidylinositol 4-Kinases: Don't Call it a Comeback. In: Phosphoinositides I: Enzymes of Synthesis and Degradation, ed. T. Balla, ed. M. Wymann, and ed. J. D. York, Dordrecht: Springer Netherlands, 1–24.

Minogue, S., Waugh, M. G., De Matteis, M. A., Stephens, D. J., Berditchevski, F., and Hsuan, J. J. (2006). Phosphatidylinositol 4-kinase is required for endosomal trafficking and degradation of the EGF receptor. J. Cell Sci. *119*, 571–581.

Miura, S. *et al.* (2000). Hgs (Hrs), a FYVE Domain Protein, Is Involved in Smad Signaling through Cooperation with SARA. Mol. Cell. Biol. *20*, 9346–

9355.

Monteiro, P. *et al.* (2013). Endosomal WASH and exocyst complexes control exocytosis of MT1-MMP at invadopodia. J. Cell Biol. *203*, 1063–1079.

Moon, R. T. (2005). Wnt/beta-catenin pathway. Sci. STKE *2005*, cm1.

Mosmann, T. (1983). Rapid colorimetric assay for cellular growth and survival: Application to proliferation and cytotoxicity assays. J. Immunol. Methods *65*, 55–63.

Mössinger, J., Wieffer, M., Krause, E., Freund, C., Gerth, F., Krauss, M., and Haucke, V. (2012). Phosphatidylinositol 4-kinase IIα function at endosomes is regulated by the ubiquitin ligase Itch. EMBO Rep. *13*, 1087–1094.

Murphy, D. a, and Courtneidge, S. a (2011). The 'ins' and 'outs' of podosomes and invadopodia: characteristics, formation and function. Nat. Rev. Mol. Cell Biol. *12*, 413–426.

Murphy, J. E., Padilla, B. E., Hasdemir, B., Cottrell, G. S., and Bunnett, N. W. (2009). Endosomes: a legitimate platform for the signaling train. Proc. Natl. Acad. Sci. U. S. A. *106*, 17615–17622.

Murray, J. T., Panaretou, C., Stenmark, H., Miaczynska, M., and Backer, J. M. (2002). Role of Rab5 in the Recruitment of hVps34/p150 to the Early Endosome. Traffic *3*, 416–427.

Myers, M. P., Pass, I., Batty, I. H., Van der Kaay, J., Stolarov, J. P., Hemmings, B. A., Wigler, M. H., Downes, C. P., and Tonks, N. K. (1998). The lipid phosphatase activity of PTEN is critical for its tumor supressor function. Proc. Natl. Acad. Sci. U. S. A. *95*, 13513–13518.

Nakatsu, F. *et al.* (2012). PtdIns4P synthesis by PI4KIIIα at the plasma membrane.pdf. J. Cell Biol. *199*, 1003–1016.

Nakatsu, F., Messa, M., Nández, R., Czapla, H., Zou, Y., Strittmatter, S. M., and de Camilli, P. (2015). Sac2/INPP5F is an inositol 4-phosphatase that functions in the endocytic pathway. J. Cell Biol. *209*, 85–95.

Nasuhoglu, C., Feng, S., Mao, J., Yamamoto, M., Yin, H. L., Earnest, S., Barylko, B., Albanesi, J. P., and Hilgemann, D. W. (2002). Nonradioactive analysis of phosphatidylinositides and other anionic phospholipids by anion-exchange high-performance liquid chromatography with suppressed conductivity detection. Anal. Biochem. *301*, 243–254.

Nielsen, E., Christoforidis, S., Uttenweiler-Joseph, S., Miaczynska, M., Dewitte, F., Wilm, M., Hoflack, B., and Zerial, M. (2000). Rabenosyn-5, a Novel Rab5 Effector, Is Complexed with hVPS45 and Recruited to Endosomes through a FYVE Finger Domain. J. Cell Biol. *151*, 601–612.

Niu, Y., Zhang, C., Sun, Z., Hong, Z., Li, K., Sun, D., Yang, Y., Tian, C., Gong, W., and Liu, J.-J. (2013). PtdIns(4)P regulates retromer-motor interaction to facilitate dynein-cargo dissociation at the trans-Golgi network. Nat. Cell Biol. *15*, 417–429.

Nola, S., Daigaku, R., Smolarczyk, K., Carstens, M., Martin-Martin, B., Longmore, G., Bailly, M., and Braga, V. M. M. (2011). Ajuba is required for Rac activation and maintenance of E-cadherin adhesion. J. Cell Biol. *195*, 855–871.

Ono, F., Nakagawa, T., Saito, S., Owada, Y., Sakagami, H., Goto, K., Suzuki, M., Matsuno, S., and Kondo, H. (1998). A Novel Class II Phosphoinositide 3-Kinase Predominantly Expressed in the Liver and Its Enhanced Expression during Liver Regeneration. J. Biol. Chem. *273*, 7731–7736.

Palamidessi, A., Frittoli, E., Garré, M., Faretta, M., Mione, M., Testa, I., Diaspro, A., Lanzetti, L., Scita, G., and Di Fiore, P. P. (2008). Endocytic Trafficking of Rac Is Required for the Spatial Restriction of Signaling in Cell Migration. Cell *134*, 135–147.

Pan, W. *et al.* (2008). Wnt3a-mediated formation of phosphatidylinositol 4,5-bisphosphate regulates LRP6 phosphorylation. Science *321*, 1350–1353.

Papadopoulos, J. S., and Agarwala, R. (2007). COBALT: constraint-based alignment tool for multiple protein sequences. Bioinformatics *23*, 1073–1079.

Paulus, H., and Kennedy, E. P. (1960). The Enzymatic Synthesis of Inositol Monophophatide. J. Biol. Chem. *235*, 1303–1311.

Paz, H., Pathak, N., and Yang, J. (2014). Invading one step at a time: the role of invadopodia in tumor metastasis. Oncogene *33*, 4193–4202.

Pellegrin, S., and Mellor, H. (2008). Rho GTPase activation assays. Curr. Protoc. Cell Biol. *38*, 14.8.1-14.8.19.

Pesesse, X., Moreau, C., Drayer, A. L., Woscholski, Y., Parker, P., and Erneux, C. (1998). The SH2 domain containing inositol 5-phosphatase SHIP2 displays. FEBS Lett. *437*, 301–303.

Pirola, L., Zvelebil, M. J., Bulgarelli-Leva, G., Van Obberghen, E., Waterfield, M. D., and Wymann, M. P. (2001). Activation loop sequences confer substrate specificity to phosphoinositide 3-kinase α (PI3Kα). Functions of lipid kinase-deficient PI3Kα in signaling. J. Biol. Chem. *276*, 21544–21554.

Pizarro-Cerdá, J., Payrastre, B., Wang, Y. J., Veiga, E., Yin, H. L., and Cossart, P. (2007). Type II phosphatidylinositol 4-kinases promote Listeria monocytogenes entry into target cells. Cell. Microbiol. *9*, 2381–2390.

Platta, H. W., and Stenmark, H. (2011). Endocytosis and signaling. Curr. Opin. Cell Biol. *23*, 393–403.

Poincloux, R., Lizárraga, F., and Chavrier, P. (2009). Matrix invasion by tumour cells: a focus on MT1-MMP trafficking to invadopodia. J. Cell Sci. *122*, 3015–3024.

Posor, Y. *et al.* (2013). Spatiotemporal control of endocytosis by phosphatidylinositol-3,4-bisphosphate. Nature *499*, 233–237.

Prenzel, N., Fischer, O. M., Streit, S., Hart, S., and Ullrich, A. (2001). The epidermal growth factor receptor family as a central element for cellular signal transduction and diversification. Endocr. Relat. Cancer *8*, 11–31.

Qin, Y., Li, L., Pan, W., and Wu, D. (2009). Regulation of phosphatidylinositol kinases and metabolism by Wnt3a and Dvl. J. Biol. Chem. *284*, 22544–22548.

Rameh, L. E. *et al.* (1997a). A Comparative Analysis of the Phosphoinositide Binding Specificity of Pleckstrin Homology Domains A Comparative Analysis of the Phosphoinositide Binding Specificity of Pleckstrin Homology Domains *. J. Biol. Chem. *272*, 22059–22066.

Rameh, L. E., Tolias, K. F., Duckworth, B. C., and Cantley, L. C. (1997b). A new pathway for synthesis of phosphatidylinositol-4,5-bisphosphate. Nature *390*, 192–196.

Ramjaun, A. R., and McPherson, P. S. (1996). Tissue-specific alternative splicing generates two synaptojanin isoforms with differential membrane binding properties. J. Biol. Chem. *271*, 24856–24861.

Reiss, S., Harak, C., Romero-Brey, I., Radujkovic, D., Klein, R., Ruggieri, A., Rebhan, I., Bartenschlager, R., and Lohmann, V. (2013). The Lipid Kinase Phosphatidylinositol-4 Kinase III Alpha Regulates the Phosphorylation Status of Hepatitis C Virus NS5A. PLoS Pathog. *9*.

Remacle, A., Murphy, G., and Roghi, C. (2003). Membrane type I-matrix metalloproteinase (MT1-MMP) is internalised by two different pathways and is recycled to the cell surface. J. Cell Sci. *116*, 3905–3916.

Ren, J., and Guo, W. (2012). ERK1/2 Regulate Exocytosis through Direct Phosphorylation of the Exocyst Component Exo70. Dev. Cell *22*, 967–978.

Reverter, M. *et al.* (2014). Cholesterol Regulates Syntaxin 6 Trafficking at trans-Golgi Network Endosomal Boundaries. Cell Rep. *7*, 883–897.

Rhodes, D. R., Yu, J., Shanker, K., Deshpande, N., Varambally, R., Ghosh, D., Barrette, T., Pandey, A., and Chinnaiyan, A. M. (2004). ONCOMINE: A Cancer Microarray Database and Integrated Data-Mining Platform1. Neoplasia *6*, 1–6.

Rivas, M. P., Kearns, B. G., Xie, Z., Guo, S., Sekar, M. C., Hosaka, K., Kagiwada, S., York, J. D., and Bankaitis, V. A. (1999). Pleiotropic alterations in lipid metabolism in yeast sac1 mutants: relationship to 'bypass Sec14p' and inositol auxotrophy. Mol. Biol. Cell *10*, 2235–2250.

Robinson, D. *et al.* (2015). Integrative Clinical Genomics of Advanced Prostate Cancer. Cell *161*, 1215–1228.

Robinson, J. W., Leshchyns'ka, I., Farghaian, H., Hughes, W. E., Sytnyk, V., Neely, G. G., and Cole, A. R. (2014). PI4KIIα phosphorylation by GSK3 directs vesicular trafficking to lysosomes. Biochem. J. *464*, 145–156.

Rojas, M., Yao, S., and Lin, Y.-Z. (1996). Controlling Epidermal Growth Factor (EGF)-stimulated Ras Activation in Intact Cells by a Cell-permeable Peptide Mimicking Phosphorylated EGF Receptor. J. Biol. Chem. *271*, 27456–27461.

Rossé, C. *et al.* (2014). Control of MT1-MMP transport by atypical PKC during breast-cancer progression. Proc. Natl. Acad. Sci. U. S. A. *111*, E1872-9.

Rozenvayn, N., and Flaumenhaft, R. (2001). Phosphatidylinositol 4,5-bisphosphate mediates Ca^{2+}-induced platelet α-granule secretion. Evidence for type II phosphatidylinositol 5-phosphate 4-kinase function. J. Biol. Chem. *276*, 22410–22419.

Rozenvayn, N., and Flaumenhaft, R. (2003). Protein kinase C mediates translocation of type II phosphatidylinositol 5-phosphate 4-kinase required for

platelet α-granule secretion. J. Biol. Chem., 8126–8134.

Rusch, V., Klimstra, D., Venkatraman, E., Pisters, P. W. ., Lagenfeld, J., and Dmistrovsky, E. (1997). Overexpression of the Epidermal Growth Factor Receptor and Its Ligand Transforming Growth Factor α is frequent in resectable Non-Small Cell Lung Cancer but does not predict tumour progression. Clin. Cancer Res. *3*, 515–523.

Rusk, N., Le, P. U., Mariggio, S., Guay, G., Lurisci, C., Nabi, I. R., Corda, D., and Symons, M. (2003). Synaptojanin 2 Functions at an Early Step of Clathrin-Mediated Endocytosis. Curr. Biol. *13*, 659–3.

Saarikangas, J., Zhao, H., and Lappalainen, P. (2010). Regulation of the actin cytoskeleton-plasma membrane interplay by phosphoinositides. Physiol. Rev. *90*, 259–289.

Sahai, E., and Marshall, C. J. (2003). Differing modes of tumour cell invasion have distinct requirements for Rho/ROCK signalling and extracellular proteolysis. Nat. Cell Biol. *5*, 711–719.

Salazar, G., Craige, B., Wainer, B. H., Guo, J., De Camilli, P., and Faundez, V. (2005). Phosphatidylinositol-4-kinase type II α is a component of adaptor protein-3-derived vesicles. Mol. Biol. Cell *16*, 3692–3704.

Sanz-Moreno, V. *et al.* (2011). ROCK and JAK1 Signaling Cooperate to Control Actomyosin Contractility in Tumor Cells and Stroma. Cancer Cell *20*, 229–245.

Sasaki, T., Takasuga, S., Sasaki, J., Kofuji, S., Eguchi, S., Yamazaki, M., and Suzuki, A. (2009). Mammalian phosphoinositide kinases and phosphatases. Prog. Lipid Res. *48*, 307–343.

Sato, H., Takino, T., and Miyamori, H. (2005). Roles of membrane-type matrix metalloproteinase-1 in tumor invasion and metastasis. Cancer Sci. *96*, 212–217.

Sbrissa, D., Ikonomov, O. C., Fenner, H., and Shisheva, A. (2008). ArPIKfyve Homomeric and Heteromeric Interactions Scaffold PIKfyve and Sac3 in a Complex to Promote PIKfyve Activity and Functionality. J. Mol. Biol. *384*, 766–779.

Schenck, A., Goto-Silva, L., Collinet, C., Rhinn, M., Giner, A., Habermann, B., Brand, M., and Zerial, M. (2008). The endosomal protein Appl1 mediates Akt substrate specificity and cell survival in vertebrate development. Cell *133*, 486–497.

Schlame, M., and Haldar, D. (1993). Cardiolipin Is Synthesized on the Matrix Side of the Inner Membrane in Rat Liver Mitochondria. J. Biol. Chem. *268*, 74–79.

Schu, P., Takegawa, K., Fry, M., Stack, J., Waterfield, M., and Emr, S. (1993). Phosphatidylinositol 3-kinase encoded by yeast VPS34 gene essential for protein sorting. Science (80-.). *260*, 88–91.

Schulze, H., Korpal, M., Hurov, J., Kim, S. W., Zhang, J., Cantley, L. C., Graf, T., and Shivdasani, R. A. (2006). Characterization of the megakaryocyte demarcation membrane system and its role in thrombopoiesis. Blood *107*, 3868–3875.

Seelan, R. S., Lakshmanan, J., Casanova, M. F., and Parthasarathy, R. N. (2009). Identification of myo-Inositol-3-phosphate Synthase Isoforms: CHARACTERIZATION, EXPRESSION, AND PUTATIVE ROLE OF A 16-kDa γc ISOFORM. J. Biol. Chem. *284*, 9443–9457.

Shin, H.-W., and Nakayama, K. (2004). Dual control of membrane targeting by PtdIns(4)P and ARF. Trends Biochem. Sci. *29*, 513–515.

Shisheva, A., Sbrissa, D., and Ikonomov, O. (1999). Cloning, characterization, and expression of a novel Zn 2+ - binding FYVE finger-containing phosphoinositide kinase in insulin- sensitive cells. Mol. Cell. Biol. *19*, 623–634.

Shulga, Y. V., Topham, M. K., and Epand, R. M. (2011). Study of arachidonoyl specificity in two enzymes of the PI cycle. J. Mol. Biol. *409*, 101–112.

Silhankova, M., Port, F., Harterink, M., Basler, K., and Korswagen, H. C. (2010). Wnt signalling requires MTM-6 and MTM-9 myotubularin lipid-phosphatase function in Wnt-producing cells. EMBO J *29*, 4094–4105.

Simons, J. P. *et al.* (2009). Loss of phosphatidylinositol 4-kinase 2α activity causes late onset degeneration of spinal cord axons. Proc. Natl. Acad. Sci. U. S. A. *106*, 11535–11539.

Sinha, R. K., Bojjireddy, N., Kulkarni, D., Ratheesh, A., Chiplunkar, S. V., Gude, R., and Subrahmanyam, G. (2013). Type II phosphatidylinositol 4-kinase β is an integral signaling component of early T cell activation mechanisms. Biochimie *95*, 1560–1566.

Snoek-van Beurden, P., and Von den Hoff, J. (2005). Zymographic techniques for the analysis of matrix metalloproteinases and their inhibitors. Biotechniques *38*, 73–83.

Song, E., Luo, N., Alvarado, J. A., Lim, M., Walnuss, C., Neely, D., Spandau, D., Ghaffarieh, A., and Sun, Y. (2017). Ocular Pathology of Oculocerebrorenal Syndrome of Lowe: Novel Mutations and Genotype-Phenotype Analysis. Sci. Rep. *7*, 1442.

Sorkin, A., and von Zastrow, M. (2009). Endocytosis and signalling: intertwining molecular networks. Nat. Rev. Mol. Cell Biol. *10*, 609–622.

Stack, J. H., and Emr, S. D. (1994). Vps34p required for yeast vacuolar protein sorting is a multiple specificity kinase that exhibits both protein kinase and phosphatidylinositol-specific PI 3-kinase activities. J. Biol. Chem. *269*, 31552–31562.

Stauffer, T. P., Ahn, S., and Meyer, T. (1998). Receptor-induced transient

reduction in plasma membrane PtdIns(4,5)P_2 concentration monitored in living cells. Curr. Biol. *8*, 343–346.

Stenmark, H., Aasland, R., Toh, B. H., and D'Arrigo, A. (1996). Endosomal localization of the autoantigen EEA1 is mediated by a zinc- binding FYVE finger. J. Biol. Chem. *271*, 24048–24054.

Strahl, T., and Thorner, J. (2007). Synthesis and function of membrane phosphoinositides in budding yeast, Saccharomyces cerevisiae. Biochim. Biophys. Acta - Mol. Cell Biol. Lipids *1771*, 353–404.

Sun, Y., Hedman, A. C., Tan, X., Schill, N. J., and Anderson, R. A. (2013). Endosomal Type Iγ PIP 5-Kinase Controls EGF Receptor Lysosomal Sorting. Dev. Cell *25*, 144–155.

Szentpetery, Z., Várnai, P., and Balla, T. (2010). Acute manipulation of Golgi phosphoinositides to assess their importance in cellular trafficking and signaling. Proc. Natl. Acad. Sci. U. S. A. *107*, 8225–8230.

Takino, T., Miyamori, H., Kawaguchi, N., Uekita, T., Seiki, M., and Sato, H. (2003). Tetraspanin CD63 promotes targeting and lysosomal proteolysis of membrane-type 1 matrix metalloproteinase. Biochem. Biophys. Res. Commun. *304*, 160–166.

Tan, J., and Brill, J. a (2014). Cinderella story: PI4P goes from precursor to key signaling molecule. Crit. Rev. Biochem. Mol. Biol. *49*, 33–58.

Tan, X., Sun, Y., Thapa, N., Liao, Y., Hedman, A. C., and Anderson, R. A. (2015). LAPTM4B is a PtdIns(4,5)P_2 effector that regulates EGFR signaling , lysosomal sorting , and degradation. EMBO J. *34*, 1–17.

Tatin, F., Varon, C., Génot, E., and Moreau, V. (2006). A signalling cascade involving PKC, Src and Cdc42 regulates podosome assembly in cultured endothelial cells in response to phorbol ester. J. Cell Sci. *119*, 769–781.

Taub, N., Teis, D., Ebner, H. L., Hess, M. W., and Huber, L. A. (2007). Late Endosomal Traffic of the Epidermal Growth Factor Receptor Ensures Spatial and Temporal Fidelity of Mitogen-activated Protein Kinase Signaling □. *18*, 4698–4710.

Taylor, G. S., Maehama, T., and Dixon, J. E. (2000). Myotubularin, a protein tyrosine phosphatase mutated in myotubular myopathy, dephosphorylates the lipid second messenger, phosphatidylinositol 3-phosphate. Proc. Natl. Acad. Sci. U. S. A. *97*, 8910–8915.

Teis, D., Wunderlich, W., and Huber, L. A. (2002). Localization of the MP1-MAPK Scaffold Complex to Endosomes Is Mediated by p14 and Required for Signal Transduction. Dev. Cell *3*, 803–814.

Teo, H., Gill, D. J., Sun, J., Perisic, O., Veprintsev, D. B., Vallis, Y., Emr, S. D., and Williams, R. L. (2006). ESCRT-I Core and ESCRT-II GLUE Domain Structures Reveal Role for GLUE in Linking to ESCRT-I and Membranes. Cell *125*, 99–111.

Thapa, N., Choi, S., Hedman, A., Tan, X., and Anderson, R. a (2013). Phosphatidylinositol phosphate 5-kinase Iγi2 in association with Src controls anchorage-independent growth of tumor cells. J. Biol. Chem. *288*, 34707–34718.

Thapa, N., Sun, Y., Schramp, M., Choi, S., Ling, K., and Anderson, R. A. (2012). Phosphoinositide Signaling Regulates the Exocyst Complex and Polarized Integrin Trafficking in Directionally Migrating Cells. Dev. Cell *22*, 116–130.

Toker, A. (2012). Phosphoinositide 3-Kinases---A Historical Perspective. In: Phosphoinositides I: Enzymes of Synthesis and Degradation, ed. T. Balla, ed. M. Wymann, and ed. J. D. York, Dordrecht: Springer Netherlands, 95–110.

Tokuda, E., Itoh, T., Hasegawa, J., Ijuin, T., Takeuchi, Y., Irino, Y., Fukumoto,

M., and Takenawa, T. (2014). Phosphatidylinositol 4-phosphate in the Golgi apparatus regulates cell-cell adhesion and invasive cell migration in human breast cancer. Cancer Res. *74*, 3054–3066.

Tomlinson, R. V., and Ballou, C. E. (1961). Complete characterization of the myo-inositol polyphosphates from beef brain phosphoinositide. J. Biol. Chem. *236*, 1902–1906.

Traynor-Kaplan, A., Kruse, M., Dickson, E. J., Dai, G., Vivas, O., Yu, H., Whittington, D., and Hille, B. (2017). Fatty-acyl chain profiles of cellular phosphoinositides. Biochim. Biophys. Acta - Mol. Cell Biol. Lipids *1862*, 513–522.

Treyer, A., Pujato, M., Pechuan, X., and Musch, A. (2016). Iterative sorting of apical and basolateral cargo in Madin-Darby canine kidney cells. Mol. Biol. Cell *27*, 2259–2271.

Uldry, M., Ibberson, M., Horisberger, J. D., Chatton, J. Y., Riederer, B. M., and Thorens, B. (2001). Identification of a mammalian H+-myo-inositol symporter expressed predominantly in the brain. EMBO J. *20*, 4467–4477.

Ungewickell, A., Ward, M. E., Ungewickell, E., and Majerus, P. W. (2004). The inositol polyphosphate 5-phosphatase Ocrl associates with endosomes that are partially coated with clathrin. Proc. Natl. Acad. Sci. U. S. A. *101*, 13501–13506.

Várnai, P., and Balla, T. (2008). Live cell imaging of phosphoinositides with expressed inositide binding protein domains. Methods *46*, 167–176.

Varnai, P., Thyagarajan, B., Rohacs, T., and Balla, T. (2006). Rapidly inducible changes in phosphatidylinositol 4,5-bisphosphate levels influence multiple regulatory functions of the lipid in intact living cells. J. Cell Biol. *175*, 377–382.

Vicinanza, M. *et al.* (2011). OCRL controls trafficking through early

endosomes via PtdIns4,5P_2-dependent regulation of endosomal actin. EMBO J. *30*, 4970–4985.

Vieira, A. V, Lamaze, C., and Schmid, S. L. (1996). Control of EGF receptor signaling by clathrin-mediated endocytosis. Science (80-.). *274*, 2086–2089.

Waguri, S., Dewitte, F., Le Borgne, R., Rouille, Y., Uchiyama, Y., Dubremetz, J.-F., and Hoflack, B. (2003). Visualization of TGN to Endosome Trafficking through Fluorescently Labeled MPR and AP-1 in Living Cells. Mol. Biol. Cell *14*, 142–155.

Wang, H., Sun, H.-Q., Zhu, X., Zhang, L., Albanesi, J., Levine, B., and Yin, H. (2015). GABARAPs regulate PI4P-dependent autophagosome:lysosome fusion. Proc. Natl. Acad. Sci. *112*, 7015–7020.

Wang, J., Gambhir, A., Hangyás-Mihályné, G., Murray, D., Golebiewska, U., and McLaughlin, S. (2002). Lateral sequestration of phosphatidylinositol 4,5-bisphosphate by the basic effector domain of myristoylated alanine-rich C kinase substrate is due to nonspecific electrostatic interactions. J. Biol. Chem. *277*, 34401–34412.

Wang, J., Sun, H., Macia, E., Kirchhausen, T., Watson, H., Bonifacino, J. S., and Yin, H. L. (2007). PI4P Promotes the Recruitment of the GGA Adaptor Proteins to the Trans -Golgi Network and Regulates Their Recognition of the Ubiquitin Sorting Signal. Mol. Biol. Cell *18*, 2646–2655.

Wang, Y. J., Wang, J., Sun, H. Q., Martinez, M., Sun, Y. X., Macia, E., Kirchhausen, T., Albanesi, J. P., Roth, M. G., and Yin, H. L. (2003). Phosphatidylinositol 4 Phosphate Regulates Targeting of Clathrin Adaptor AP-1 Complexes to the Golgi. Cell *114*, 299–310.

Watanabe, T., Wang, S., Noritake, J., Sato, K., Fukata, M., Takefuji, M., Nakagawa, M., Izumi, N., Akiyama, T., and Kaibuchi, K. (2004). Interaction with IQGAP1 links APC to Rac1, Cdc42, and actin filaments during cell polarization and migration. Dev. Cell *7*, 871–883.

Waugh, M. G., Chu, K. M. E., Clayton, E. L., Minogue, S., and Hsuan, J. J. (2011). Detergent-free isolation and characterization of cholesterol-rich membrane domains from trans-Golgi network vesicles. J. Lipid Res. *52*, 582–589.

Waugh, M. G., Minogue, S., Anderson, J. S., Balinger, A., Blumenkrantz, D., Calnan, D. P., Cramer, R., and Hsuan, J. J. (2003). Localization of a highly active pool of type II phosphatidylinositol 4-kinase in a p97 / valosin-containing-protein-rich fraction of the endoplasmic reticulum. Biochem J *373*, 57–63.

Waugh, M. G., Minogue, S., Chotai, D., Berditchevski, F., and Hsuan, J. J. (2006). Lipid and peptide control of phosphatidylinositol 4-kinase IIα activity on Golgi-endosomal Rafts. J. Biol. Chem. *281*, 3757–3763.

van Weering, J. R., Verkade, P., and Cullen, P. J. (2010). SNX-BAR proteins in phosphoinositide-mediated, tubular-based endosomal sorting. Semin Cell Dev Biol *21*, 371–380.

Wei, Y. J., Sun, H. Q., Yamamoto, M., Wlodarski, P., Kunii, K., Martinez, M., Barylko, B., Albanesi, J. P., and Yin, H. L. (2002). Type II phosphatidylinositol 4-kinase β is a cytosolic and peripheral membrane protein that is recruited to the plasma membrane and activated by Rac-GTP. J. Biol. Chem. *277*, 46586–46593.

Wenk, M. R., Lucast, L., Di Paolo, G., Romanelli, A. J., Suchy, S. F., Nussbaum, R. L., Cline, G. W., Shulman, G. I., McMurray, W., and De Camilli, P. (2003). Phosphoinositide profiling in complex lipid mixtures using electrospray ionization mass spectrometry. Nat. Biotechnol. *21*, 813–817.

Whitman, M., Kaplan, D., Robertst, T., and Cantley, L. (1987). Evidence for two distinct phosphatidylinositol kinases in fibroblasts. Implications for cellular regulation. Biochem J *247*, 165–174.

Wieffer, M. *et al.* (2013). PI4K2β/AP-1-Based TGN-Endosomal Sorting

Regulates Wnt Signaling. Curr. Biol. *23*, 2185–2190.

Wiesner, C., El Azzouzi, K., and Linder, S. (2013). A specific subset of RabGTPases controls cell surface exposure of MT1-MMP, extracellular matrix degradation and three-dimensional invasion of macrophages. J. Cell Sci. *126*, 2820–2833.

Williams, K. C., and Coppolino, M. G. (2011). Phosphorylation of membrane type 1-matrix metalloproteinase (MT1-MMP) and its vesicle-associated membrane protein 7 (VAMP7)-dependent trafficking facilitate cell invasion and migration. J. Biol. Chem. *286*, 43405–43416.

Williams, K. C., McNeilly, R. E., and Coppolino, M. G. (2014). SNAP23, Syntaxin4, and vesicle-associated membrane protein 7 (VAMP7) mediate trafficking of membrane type 1-matrix metalloproteinase (MT1-MMP) during invadopodium formation and tumor cell invasion. Mol. Biol. Cell *25*, 2061–2070.

Wymann, M. (2012). PI3Ks---Drug Targets in Inflammation and Cancer. In: Phosphoinositides I: Enzymes of Synthesis and Degradation, ed. T. Balla, ed. M. Wymann, and ed. J. D. York, Dordrecht: Springer Netherlands, 111–181.

Wymann, M. P., Bulgarelli-Leva, G., Zvelebil, M. J., Pirola, L., Vanhaesebroeck, B., Waterfield, M. D., and Panayotou, G. (1996). Wortmannin inactivates phosphoinositide 3-kinase by covalent modification of Lys-802, a residue involved in the phosphate transfer reaction. Mol. Cell. Biol. *16*, 1722–1733.

Xie, Z., Fang, M., and Bankaitis, V. A. (2001). Evidence for an intrinsic toxicity of phosphatidylcholine to Sec14p-dependent protein transport from the yeast Golgi complex. Mol. Biol. Cell *12*, 1117–1129.

Xu, Y., Hortsman, H., Seet, L., Wong, S. H., and Hong, W. (2001). SNX3 regulates endosomal function through its PX-domain-mediated interaction

with PtdIns(3)P. Nat Cell Biol *3*, 658–666.

Yamamoto, A., DeWald, D. B., Boronenkov, I. V, Anderson, R. A., Emr, S. D., and Koshland, D. (1995). Novel PI(4)P 5-kinase homologue, Fab1p, essential for normal vacuole function and morphology in yeast. Mol. Biol. Cell *6*, 525–539.

Yoo, S. H., Huh, Y. H., Huh, S. K., Chu, S. Y., Kim, K. D., and Hur, Y. S. (2014). Localization and projected role of phosphatidylinositol 4-kinases IIα and IIβ in inositol 1,4,5-trisphosphate-sensitive nucleoplasmic Ca^{2+} store vesicles. Nucleus *5*, 341–351.

Yu, J. W., Mendrola, J. M., Audhya, A., Singh, S., Keleti, D., DeWald, D. B., Murray, D., Emr, S. D., and Lemmon, M. A. (2004). Genome-wide analysis of membrane targeting by S. cerevisiae pleckstrin homology domains. Mol. Cell *13*, 677–688.

Zheng, H.-T., Jiang, L.-X., Lv, Z.-C., Li, D.-P., Zhou, C.-Z., Gao, J.-J., He, L., and Peng, Z.-H. (2008). Are there tumor suppressor genes on chromosome 4p in sporadic colorectal carcinoma? World J. Gastroenterol. *14*, 90–94.

Zhong, Y., Wang, Q. J., Li, X., Yan, Y., Backer, J. M., Chait, B. T., Heintz, N., and Yue, Z. (2009). Distinct regulation of autophagic activity by Atg14L and Rubicon associated with Beclin 1-phosphatidylinositol-3-kinase complex. Nat Cell Biol *11*, 468–476.

Zhou, B., Cai, Q., Xie, Y., and Sheng, Z.-H. (2012). Snapin recruits dynein to BDNF-TrkB signaling endosomes for retrograde axonal transport and is essential for dendrite growth of cortical neurons. Cell Rep. *2*, 42–51.

Zhou, Q. *et al.* (2014). Molecular insights into the membrane-associated phosphatidylinositol 4-kinase IIα. Nat. Commun. *5*, 3552.

Zhu, X. F., Liu, Z. C., Xie, B. F., Li, Z. M., Feng, G. K., Yang, D., and Zeng, Y. X. (2001). EGFR tyrosine kinase inhibitor AG1478 inhibits cell proliferation

and arrests cell cycle in nasopharyngeal carcinoma cells. Cancer Lett. *169*, 27–32.

Zhuang, G., Hunter, S., Hwang, Y., and Chen, J. (2007). Regulation of EphA2 receptor endocytosis by SHIP2 lipid phosphatase via phosphatidylinositol 3-kinase-dependent Rac1 activation. J. Biol. Chem. *282*, 2683–2694.

Zoncu, R., Efeyan, A., and Sabatini, D. M. (2011). mTOR: from growth signal integration to cancer, diabetes and ageing. Nat Rev Mol Cell Biol *12*, 21–35.

Zoncu, R., Perera, R. M., Balkin, D. M., Pirruccello, M., Toomre, D., and De Camilli, P. (2009). A phosphoinositide switch controls the maturation and signaling properties of APPL endosomes. Cell *136*, 1110–1121.

Zurzolo, C., and Simons, K. (2016). Glycosylphosphatidylinositol-anchored proteins: Membrane organization and transport. Biochim. Biophys. Acta - Biomembr. *1858*, 632–639.